The Role of VAMP proteins in K^+ Channel Regulation

Ben Zhang

B.Sc., M.Med.

Thesis submitted for the degree of Doctor of Philosophy

College of Medical, Veterinary and Life Sciences

Institute of Molecular, Cell and Systems Biology

University of Glasgow

January 2015

Abstract

SNARE (soluble N-ethylmaleimide-sensitive factor protein attachment protein receptor) proteins drive vesicle traffic, delivering membrane and cargo to target sites within the cell and at its surface. They contribute to cell homeostasis, morphogenesis and pathogen defense. A subset of SNAREs, including the *Arabidopsis* SNARE SYP121, are known also to coordinate solute uptake via physical interactions with K^+ channels and to moderate their gating at the plasma membrane.

R-SNAREs, also known as vesicle-associated membrane proteins (VAMPs), are most commonly associated with trafficking vesicles. In guard cells of *Arabidopsis*, ABA-dependent stomatal closure was inhibited when the expression of VAMP71 family genes were suppressed by an antisense VAMP711 construct. Such results reveal that VAMPs play an important role in plant response to stress, especially in the regulation of stomatal closure under ABA treatment. Two R-SNAREs, VAMP721 and VAMP722, are known to assemble in SNARE core complexes with SYP121 and with its closest homolog SYP122, which raises the question whether the channel interaction might extend to the R-SNAREs leading to VAMP regulating channel gating.

To answer this question, I investigated the interaction between the VAMP7 proteins with KC1 and KAT1 K^+ channels by mating based Split-Ubiquitin System (mbSUS) assay, and verified these interactions by ratiometric bimolecular fluorescence complementation (rBiFC) assay. I found VAMP721 and VAMP722, but not VAMP723, interacted with the channels. The selective binding was associated with the VAMP longin domain, notably with Tyr^{57}.

What is the effect of the VAMP-K^+ channel interaction on transmembrane ion transport and vesicle traffic? I found VAMP721

affected K^+ channel gating and suppressed the K^+ current within the physiological voltage range by electrophysiological analysis in *Xenopus* oocytes and in VAMP over-expression wild type *Arabidopsis*. The effect of VAMP721 on K^+ channel regulation was opposite to the action of SYP121 on K^+ channel. From localization, interaction and electrophysiological studies, I was able to show that Tyr^{57} is a key residue required both for VAMP-dependent gating of the K channels and for localization of the VAMPs at the plasma membrane. For vesicle traffic, I found overexpression of full length VAMP721 in *Arabidopsis* seedlings blocked the secretion of secYFP while coexpressing with KC1 K^+ channel rescued the traffic block, demonstrating a potential action of VAMP-K^+ channel interaction on secretory traffic. These results add to understanding the interaction between SNARE and K^+ channels that link membrane traffic with osmotically active solute transport in the plant.

Table of contents

List of Tables

List of Figures

List of Abbreviations

ABA	amino acid	KDEL	Lys-Asp-Glu-Lue
Ade; A	adenine	LB	Luria-Bertani medium
Asp; D	Aspartic acid	Leu; L	leucine
Asn; N	Asparagine	mbSUS	mating based split ubiquitin system
ALMT	Al^{3+}-activated malate transporter	MS	Murashige and Skoog basal medium
ATP	adenosine triphosphate	Met; M	Methionine
B	Boron	MOPS	3-(N-morpholino) propanesulfonic acid
BAK1	BRI1-Associated receptor Kinase 1	NPR1	Non-expressor of Pathogenesis-Related Gene 1
BRI1	Brassinosteroid Insensitive 1	NTP	Deoxynucleotide
BiFC	bimolecular fluorescence complementation	NSF	N-ethylmaleimide-sensitive factor
$[Ca^{2+}]_i$	Cytosolic-free Ca^{2+}	Nub	N-terminal half of ubiquitin
CaM	calmodulin	PAGE	polyacrylamide gel electrophoresis
CBL	calmodulin-binding-like	paGFP	photoactivatable green fluorescent protein
CDPKs	Ca^{2+}-dependent protein kinases	PCR	polymerase chain reaction
CDS	coding sequence	PEN1	Penetration 1
CFP	cyan fluorescent protein	Phe, F	Phenylalanine
CIPKs	CBL-interacting protein kinases	PIPs	Plasma membrane intrinsic proteins
CPCs	coat proteins complexes	PLV	ProteinA-LexA-VP16
cRNA	complementary RNA	PM	plasma membrane
CSM	Synthetic Complete Medium	PP2C	Protein phosphatase 2C
Cub	C-terminal half of ubiquitin	ROS	reactive oxygen species
Cys; C	cysteine	RNA	Ribonucleic acid
DEPC	diethyl pyrocarbonate	RFP	red fluorescent protein
DMSO	dimethyl sulfoxide	SDS	sodium dodecyl sulphate

DNA	deoxyribonucleic acid	Ser; S	Serine
DRPs	dynamin-related GTPases	SM	Sec1/Munc18
DTT	dithiothreitol	SNARE	soluble NSF attachment protein receptor
ER	endoplasmic reticulum	SNAP	Soluble NSF Attachment Protein
EDTA	ethylenediaminetetraacetic acid	TAE	tris acetate EDTA
FRET	fluorescence resonance energy transfer	TGN	trans-Golgi network
FLS2	Flagellin Sensitive 2	TEVC	two-electron-voltage clamp
GFP	green fluorescent protein	Y2H	yeast two-hybrid system
GDP	guanosine diphosphate	Try; T	tryptophan
GLRs	glutamate receptor homologs	Tyr; Y	tyrosine
Gln; Q	Glutamine	Ura; U	uracil
Gly; G	Glycine	VAMP	vesicle-associated membrane protein
CNGCs	cyclic nucleotide-gated channel homologs	Val; V	Valine
GTP	Guanosine-5'-triphosphate	YNB	yeast nitrogen base
His; H	histidine	YFP	yellow fluorescent protein
HA	hemagglutinin		
HDEL	His-Asp-Glu-Lue		

Acknowledgment

First and foremost, I have to thank my supervisor, Prof. Mike Blatt. Without his continuing support and willingness to help with every problem throughout the process, this thesis would have never been accomplished.

I would like to thank Dr. Christopher Grefen, who I am indebted to for teaching me molecular biology and everything about yeast experiment.

I would like to thank Dr. Rucha Karnik for teaching me biochemistry and giving me lots of suggestions.

I would like to thank Dr. Yizhou Wang for helping me do the electrophysiological analysis in plants.

I would like to thank Dr. Cecile Lefoulon, Dr. Annegret Honsbein, and Dr. Vijay Gutla for teaching me how to do electrophysiological analysis.

My study in Glasgow would have meant nothing without the support and friendship of everyone in Stevenson lab: Anna Amtmann, Carla Minguet, Sakharam Waghmare, Emily Larson, Giorgio Perella, Mary-Ann Madsen, Maria Papanatsiou, Amparo Asensi, Wijitra Horaraung, Cornelia Eisenach, Fabian Kellermeier, Ema Sani, Christin Alderhold ne Sturm, Amparo Ruiz-Pardo, Naomi Donald, Adrian Hills, Craig Carr, George Boswell and all the people from Bower Building.

I would also like to thank Jia Zhao, Min Hou, Menglin Cao, Yongxu Lu, Dong Li and other friends, without their help and support, I can not achieve as much as I have.

Finally, and most importantly, I would like to thank my parents for their love, support and encouragement. None of this could have happened without them. I also want to thank all other family members; thank you for your understanding and support. I dedicate my thesis to all of them.

I would also like to thank China Scholarship Council for funding me.

Author's Declaration

I hereby declare that all the works presented in this thesis is my own, with the following exceptions: the K^+ current of *Arabidopsis* root epidermal cells were recorded under voltage clamp by Dr. Yizhou Wang.

Part of this work has been submitted (See Appendix II, pp 267).

Ben Zhang

23rd January 2015

Chapter 1. Introduction

1.1 Membrane vesicle traffic and its roles in plant development and defence

There are a large number of membrane-bounded organelles in eukaryotic cells, such as the endoplasmic reticulum (ER), Golgi apparatus, trans-Golgi network, endosomes, and vacuoles. Because most proteins and oligosaccharides are produced in one organelle (like the ER) and need be transported to their final destination, these organelles need a membrane trafficking system to connect with each other. During the membrane trafficking, the transport vesicles loaded with cargo molecules bud from the donor organelle, deliver to the destination organelle, touch the target membrane, and discharge the cargo molecules (Fujimoto and Ueda, 2012).

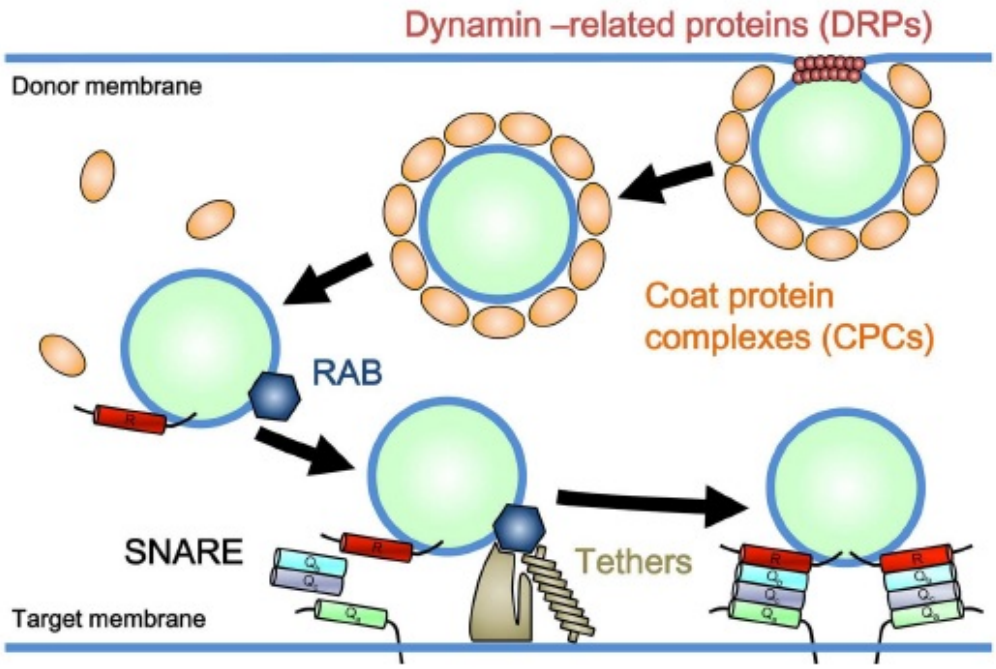

Figure 1-1. A general model of the mechanism of membrane trafficking

Images were adapted from previous publication (Fujimoto and Ueda, 2012).

As shown in Figure 1-1, there are many proteins involved in the membrane trafficking system. The coat proteins complexes and dynamin-related GTPases are used in the formation of traffic vesicles. The former has a role in cargo selection and membrane deformation, while the latter takes part in the scission of donor membrane. The Rab GTPases with other proteins like exocyst are involved in tethering the traffic vesicles to the target membrane. Finally, the SNARE proteins will form a SNARE complex and drive the membrane fusion, under help of other proteins like Sec1/Munc18 proteins (Fujimoto and Ueda, 2012).

In plant cells, the membrane trafficking system can be classified as three major modalities (Uemura and Ueda, 2014):

1. The biosynthetic-secretory modality (or exocytosis modality), in which the synthesized proteins are delivered from the ER to the plasma membrane (PM) or cell exterior via the Golgi apparatus and the TGN (Jurgens and Geldner, 2002).
2. The endocytic modality, in which the PM components or some components from extracellular are delivered to some organelles in the cell. Some of these components will be recycled back to the PM and others will be delivered to the vacuole for degradation (Saito and Ueda, 2009).
3. The third modality is the vacuolar transport modality. There is still no clear information about this modality. Several proteins synthesized at the ER can be transported to the vacuole through the Golgi apparatus, TGN, and multivesicular endosomes (MVE; Viotti 2014). Some other proteins are directly transported from ER to the vacuole and stored there (Hara-Nishimura et al. 1998).

The membrane trafficking system plays very important roles in not only basic cellular activities but also a number of physiological functions

that including plant development, signalling and plant defence. Plant cells are able to elongate up to 200 times of their original length, which requires transport of membrane material to the PM (Cosgrove, 1997). The growth of root hairs and pollen tubes depends on delivery of transport vesicles to their tips (Hepler et al. 2001). In normal leaf development, the polar flow of auxin, which depends on membrane trafficking system, is very important. For example, the phenotypes of *syp22* mutants, like wavy leaves, semi-dwarfism, and abnormal leaf vascular tissues, were thought to be caused by a defect in polar transport of auxin (Shirakawa et al., 2009). In 2012, Ebine et al. (2012) have linked membrane trafficking with the flowering time of *Arabidopsis thaliana*. The late flowering phenotype they found was due to elevated expression of FLOWERING LOCUS C, a negative regulator of flowering, in *syp22* mutants or *doc1-1* mutant. In the latter mutant, there is defect of a Calossin-like protein, BIG, which affected the vacuolar/endosomal trafficking.

As an example of trafficking in defence, in *Arabidopsis*, after addition of a peptide of bacterial flagellin, fig22, the fusion protein Flagellin Sensitive 2 (FLS2) with GFP was found to rapidly accumulate in intracellular vesicles (Robatzek et al., 2006). FLS2 is a Leu-rich repeat transmembrane receptor kinase which interacts and recognizes flg22 (Felix et al., 1999; Chinchilla et al., 2006). Penetration 1 (PEN1), originally identified as SYR1, and its barley ortholog ROR2 also take part in the immunity of non-host plant to pathogens (Collins et al., 2003). They accumulate at fungal entry sites and the resistance function depending on a SYP121-SNAP33-VAMP721/VAMP722 SNARE complex formation (Kwon et al., 2008) which I discuss below. Kalde et al. (2007) reported that the exocytosis of vesicles containing antimicrobial pathogenesis-related proteins is dependent on SYP132. In their research, SYP132 was found to be phosphorylated in response to pathogen elicitor treatment and required for PR-1 secretion.

Like proteins, the biosynthesis and secretion of many plant secondary metabolites depend on vesicle trafficking system. In *Arabidopsis* and Lisianthus (*Eustoma grandiflorum*), phytochemicals like anthocyanins are synthesized in the ER and accumulate in the central vacuole, a process which is dependent on the transport of flavonoid-containing vesicles (Markham et al., 2000; Zhang et al., 2006a). Artemisinin is a potent antimalarial drug and in plants it is an allelopathic herbicide that can inhibit the growth of other plants. The biosynthesis of the artemisinin precursor depends on two different pathways, which are isolated in different organelles of plant cells (Towler and Weathers, 2007). Isotope tracer techniques have shown that there is crosstalk between these two pathways, which controls the biosynthesis of artemisinin (Towler and Weathers, 2007; Schramek et al., 2010). This finding suggests vesicle trafficking might be a important rate-limited step of Artemisinin biosynthesis. The release of artemisinin to environment is also through the exocytosis modality in leaves and roots (Jessing et al., 2013).

1.2 SNARE proteins

Since the 1980s, when SNARE (soluble N-ethylmaleimide-sensitive factor attachment protein receptor) proteins were first characterized (Novick et al., 1980; Balch et al., 1984), rapid progress has been made identifying SNAREs as key elements in membrane fusion. SNAREs are generally small proteins of 100-300 amino acids in length. They contain an SNARE motif of roughly 60 amino acid residues. This domain consists of the heptad repeat forming a coiled-coil structure (Rehman and Sansebastiano, 2014). In the C terminus of most SNAREs, there is a transmembrane domain that usually anchors the proteins in the membrane. Some SNAREs like SNAP-25-like SNARE protein (Qb+c-SNARE) just have two SNARE motifs and no transmembrane

domain. Many SNAREs also have a N terminal domain, which can fold independently and regulate the membrane fusion reactions (Dietrich et al.. 2003).

SNAREs have been classified as t (target)- and v (vesicle)-SNAREs, reflecting their functional localization, and as Q (glutamine)- and R (arginine)- SNAREs, based on the conserved amino acid contributed to the central layer of the core complex (Fasshauer et al., 1998; Sollner et al., 1993). Q-SNAREs can be further classified to four types, Qa-, Qb-, Qc-, and Qb+c-SNAREs, based on their positions within the assembled four-helix bundle. Qa-SNAREs were originally described in their role in synaptic exocytosis, so they are called as syntaxins (Bennett et al., 1992). The Qb+c-SNAREs are similar as the neuronal SNARE SNAP-25, which constitute a special class with both Qb- and Qc-SNARE motifs. The other class of SNAREs are R-SNAREs which are also called as vesicle associated membrane proteins (VAMPs). The five different groups of plant SNARE subfamilies are shown in Figure 1-2.

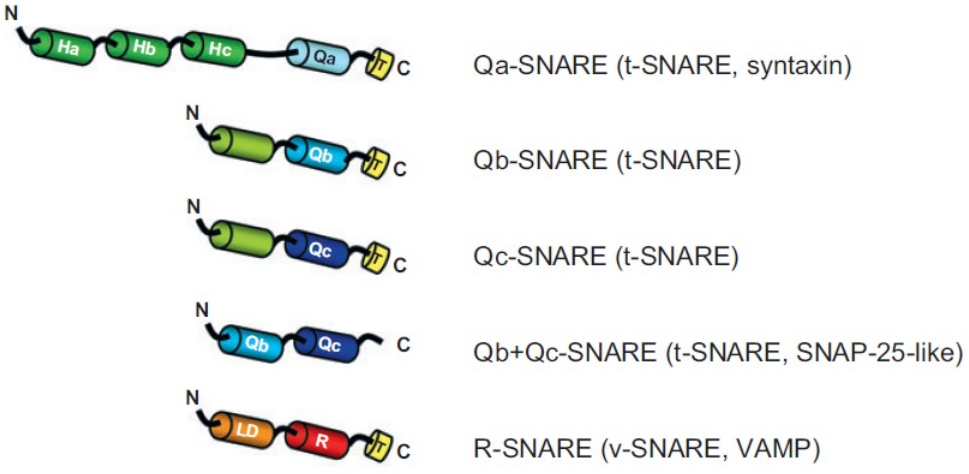

Figure 1-2. Scheme of the general domain organization of plant SNARE proteins

Image was adapted from previous publication (Lipka et al., 2007).

Q-SNAREs are generally localized to the target membrane. Most of them include an N terminal autoregulatory domain, a linker, the SNARE motif, and a C terminal transmembrane domain. In Qa-SNAREs, there are three helices which are called the Ha, Hb, and Hc (or jointly H_{abc}) domains, and these domains are folded into three helical bundles which mimics the parallel four-helix bundle of the SNARE complex (Rehman and Sansebastiano, 2014). This set of folded N terminal domains interacts with the SNARE domain in the close conformation to prevent promiscuous interactions with cognate partners before activation and with other SNARE proteins (Munson et al. 2000). Qb- and Qc-SNAREs also contain an N terminal domain which has a coiled-coil structure similar to Qa-SNARE (Hong, 2005). In animals, SNAP-25 can attach to the PM by palmitoylation (Veit et al., 1996), but there is no conserved palmitoylation site in plant Qb+c-SNAREs (Lipka et al., 2007). Nevertheless, the SNAP33, one of Qb+c-SNAREs, has been reported to localize at the PM in *Arabidopsis* by a unknown mechanism (Wick et al., 2003).

VAMPs are normally localized to the vesicle membrane. Like other SNAREs, VAMPs have three regions, the N terminal domain, a SNARE motif, and the transmembrane domain. According to whether they contain a short or a long longin domain, VAMPs can be subdivided into two groups: short VAMPs or ‘brevins’ (from the Latin word brevis, meaning short) and long VAMPs or ‘longins’ (Rossi et al., 2004). Longin domain of ‘longins’ is 120-140 amino acids length. Interestingly, only longins are found in plants. These proteins can be divided between three groups that have homologies to their counterparts in yeast and animals, namely the Sec22-, YKT6- and VAMP7-like R-SNAREs. Of the twelve VAMP7-like R-SNAREs in model plant *Arabidopsis*, the four VAMP71 group proteins show the greatest similarity to mammalian VAMP7 and are involved primarily in endosomal trafficking; the remaining VAMPs, comprising the VAMP72 subgroup, appear specific to green plants and,

with few exceptions, are thought to be responsible primarily for secretion at the PM (Uemura et al., 2007; Sanderfoot, 2007).

In *Saccharomyces cerevisiae*, there are 25 proteins that belong to the SNARE family while in humans they number 36 (Jahn and Scheller, 2006). Plant cells have many more SNAREs than animals and fungi. There are 57 SNAREs in monocotyledonous *Oryza sativa* (International Rice Genome Sequencing Project 2005), and 69 SNAREs in the *Populus trichocarpa* (Tree black cottonwood: Tuskan et al., 2006). As shown in Table 1-1, there are 63 SNAREs are known in *Arabidopsis* (Bassham et al., 2008 a). A comparable numbers of SNAREs within each subgroup are found in all known land plant genomes, which suggest that the larger number of SNAREs number is not related to a particular plant lifestyle or habitat but related to an essential aspect of plant biology (Sanderfoot et al., 2000). Most appear to have originated from a series of early endoduplication events that coincided with the colonization of land. Only a few SNAREs appear truly unique: the novel plant-specific SNAREs (NPSN) and the SYP7 Qc-SNAREs (Sanderfoot et al., 2000; Lipka et al., 2007).

Table 1-1. *Arabidopsis* SNARE Proteins

Protein	Locus No.	Protein	Locus No.	Protein	Locus No.
Qa-SNAREs (Syntaxin)		MEMB12	At5g50440	**Qb+c-SNAREs (SNAP25)**	
SYP81	At1g51740	GOS11	At1g15880	SNAP33	At5g61210
SYP31(AtSED6)	At5g05760	GOS12	At2g45200	SNAP29	At5g07880
SYP32	At3g24350	VTI11 (ZIG1/VTI1a)	At5g39510	SNAP30	At1g13890
SYP41(AtTLG2a)	At5g26980	VTI12 (ZIP1/VTI1b)	At1g26680	**R-SNAREs (VAMPs)**	
SYP42(AtTLG2b)	At4g02195	VTI13	At3g29100	SEC22	At1g11890
SYP43(AtTLG2c)	At3g05710	VTI14	At5g39630	YKT61	At5g58060
SYP21(AtPEP12)	At5g16830	NPSN11	At2g35190	YKT62	At5g58180
SYP22 (SGR3/aTvam3)	At5g46860	NPSN12	At1g48240	VAMP711	At4g32150
SYP23 (AtPLP)	At4g17730	NPSN13	At3g17440	VAMP712	At2g25340
SYP24	At1g32270	**Qc-SNAREs**		VAMP713	At5g11150
KNOLLE (SYP111)	At1g08560	USE11	At1g54110	VAMP714	At5g22360
SYP112	At2g18260	USE12	At3g55600	VAMP721	At1g04750
PEN1 (SYP121/SYR1)	At3g11820	BET11 (BS14a)	At3g58170	VAMP722	At2g33120
SYP122 (Synt4)	At3g52400	BET12 (BS14b)	At4g14445	VAMP723	At2g33110
SYP123	At4g03330	SFT11	At4g14600	VAMP724	At4g15780
SYP124	At1g61290	SFT12	At1g29060	VAMP725	At2g32670
SYP125	At1g11250	SYP51	At1g16240	VAMP726	At1g04760
SYP131	At3g03800	SYP52	At1g79590	VAMP727	At3g54300
SYP132	At5g08080	SYP61 (OSM1)	At1g28490	VAMP728	At3g24890
Qb-SNAREs		SYP71	At3g09740	TYN11 (Tomosyn)	At5g05570
SEC20	At3g24315	SYP72	At3g45280	TYN12	At4g35560
MEMB11	At2g36900	SYP73	At3g61450		

The name and locus number of 63 known SNAREs in *Arabidopsis* (Bassham et al.. 2008 a) are listed in the table. They are classified to four subgroups, Qa-, Qb-, Qc-, Qb+c-SNAREs and R-SNAREs, based on their positions within the assembled four-helix bundle.

In 2004, Uemura et al. (2004) performed a extensive analysis of the subcellular location of 54 SNAREs in *Arabidopsis*. They found almost all of these SNAREs are expressed through out all tissues examined. They also located 38 SNAREs to single compartment, 7 to two compartments,

and 3 that appeared in three compartments. Their results are shown in Figure 1-3. In total, 17 SNAREs localized at the plasma membrane, 6 SNAREs at the ER, 9 SNAREs at Golgi apparatus, 4 SNAREs at trans-Golgi network, 2 SNAREs were found in endosomes, 7 in both the prevacuolar compartment and vacuoles, 2 SNAREs were found in trans-Golgi network/prevacuolar compartment/vacuoles, and 1 SNARE in trans-Golgi network/late endosome/prevacuolar compartment /PM (Uemura et al., 2004).

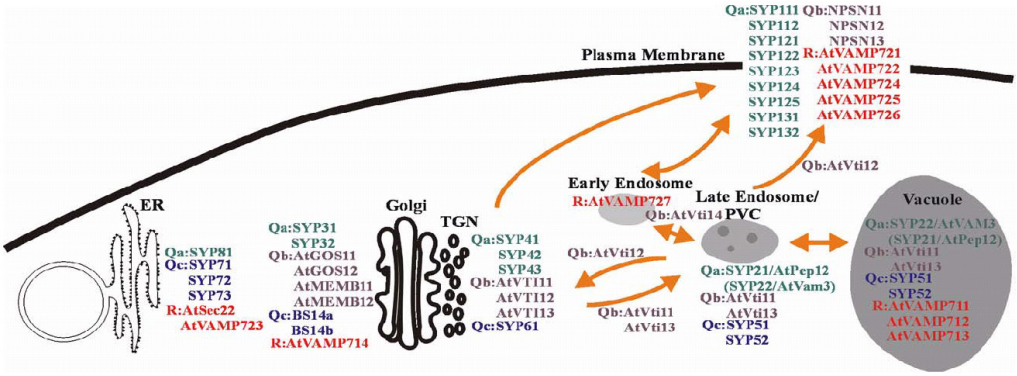

Figure 1-3. The subcellular location of SNAREs in *Arabidopsis*.

Images were adapted from previous publication (Uemura et al., 2004)

1.3 The functions of SNAREs in plants

The canonical role of SNAREs is to perform the final step of membrane fusion. They can form a SNARE complex to bring the two membrane surfaces together. Figure 1-4 shows the mechanics of vesicle fusion and the SNARE cycle. There are two kinetic modes for membrane fusion in plants and animals. One is the “Kiss and run” mode, in which the SNARE complex is formed and disassembles quickly. The vesicles release their cargo but are not fully integrating with the target membrane. The other one is the fully fusion mode, in which the SNARE complex assembles stable and completely. But to complete membrane fusion requires help from additional proteins (Pratelli et al., 2004).

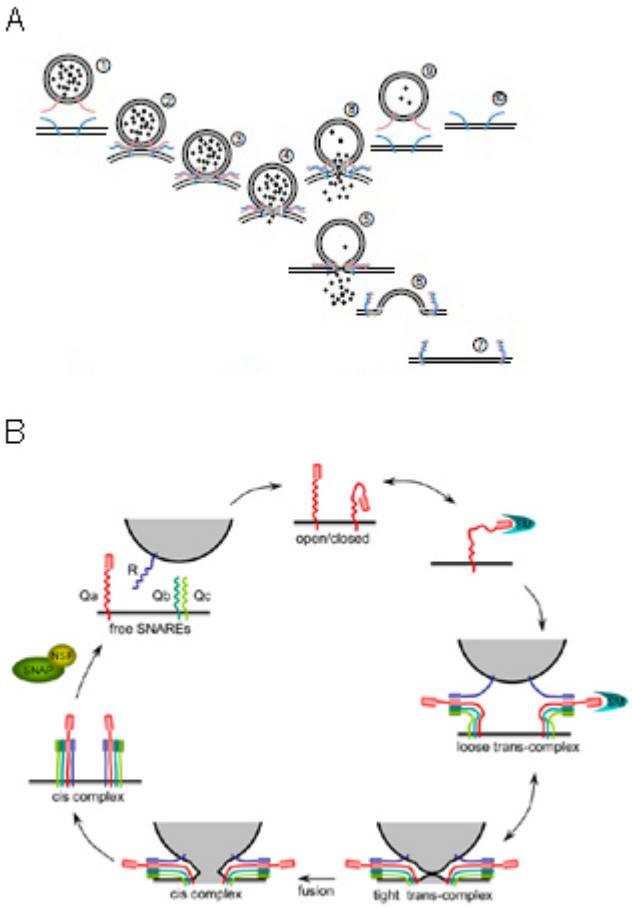

Figure 1-4. The mechanics of vesicle fusion and the SNARE cycle.

A: Two membrane fusion modes: SNARE proteins at the vesicle (dark pink) and target (blue) membranes interact to bring the two membrane surfaces together. Hemifusion follows with adjacent lipid monolayers conjoined either by rearrangement of phospholipid acylchains or by insertion of hydrophobic molecules into intramembraneous areas. Final fusion (and release of the vesicle contents as indicated) occurs with the merging of the two trans-lipid layers into a continuous fusion pore. Kiss-and-run release of vesicle contents without intercalation of the membrane faces arises from tethering and a short-lived fusion before the bilayers disengage.

B: The SNARE cycle: SNARE components as indicated: red, R-SNARE; blue, Qa-SNARE; yellow, Qb- and Qc-SNAREs

Images were adapted from previous publications (Pratelli et al. 2004; Bassham and Blatt, 2008)

In general the SNARE cycle of membrane fusion (as shown in Figure 1-4 B) begins with new SNAREs produced in ER and delivered to their hosting compartment by vesicle traffic. The next step is the release of the Q-SNARE closed conformation. This step depends on Sec1/Munc18-like proteins binding to the H_{abc} domain to expose the Q-SNARE motif. The resulting exposition of the Qa SNARE helix allows association with helices provided by the membrane-associated Qb- and Qc-SNAREs and an R-SNARE, which form a SNARE complex. Many studies have confirmed that three Q-SNAREs and one R-SNARE are required to form one complex (Katz and Brennwald, 2000; Ossig et al., 2000; Graf et al., 2005). Association in the trans-complex - that is, between the unfused vesicle and target membrane SNAREs - is accompanied by a large increase in core α-helical structure, which drives the transition to the cis-complex with membrane fusion, and the release of vesicle cargo into the acceptor compartment. After energy-dependent disassembly and recycling of the individual complex units, the SNARE cycle can restart (Lipka et al., 2007； Bassham and Blatt 2008). Table 1-2 summarizes the composition of SNARE complex in *Arabidopsis* from previous reports.

Table 1-2. The composition of SNARE complex in *Arabidopsis*

Qa-SNARE	SYP111	SYP111	SYP121	SYP121	SYP121
Qb-SNARE		NPSN11			VTI11
Qc-SNARE		SYP71		SYP51	
Qb+c-SNARE	SNAP33		SNAP33		
R-SNARE	VAMP721/722	VAMP721/722	VAMP721/722		
Reference	1, 2	2	3	4	4

Qa-SNARE	SYP121	SYP122	SYP132	SYP132	SYP21
Qb-SNARE				NPSN11	
Qc-SNARE					SYP51
Qb+c-SNARE		SNAP33	SNAP33		
R-SNARE	VAMP722	VAMP721/722	VAMP721/722		
Reference	5	6	7, 16	8	4

Qa-SNARE	SYP22	SYP22	SYP23	SYP31	SYP41
Qb-SNARE	VTI11		VTI11	MEMB1	
Qc-SNARE	SYP51		SYP51	BET1	SYP61
Qb+c-SNARE					
R-SNARE	VAMP727	VAMP711		SEC22	
Reference	9	10	11	12	4

Qa-SNARE	SYP41	SYP41	SYP42	SYP43	SYP121
Qb-SNARE	VTI12	VTI12		VTI11/VTI12/ NSNP11	
Qc-SNARE	SYP61	SYP61	SYP61		SYP61
Qb+c-SNARE					
R-SNARE		YKT61/62			
Reference	13	14	4	10	15

Reference in the table:

1	Mayer and Jürgens, 2004	7	Bednarek et al. 2010	13	Bassham et al., 2000
2	Ei Kasmi et al., 2013	8	Wang et al., 2014	14	Chen et al., 2005
3	Kwon et al., 2008	9	Ebine et al., 2008	15	Hachez et al., 2014
4	Sanderfoot et al., 2001	10	Fujiwara et al., 2014	16	Yun et al., 2013
5	Kato et al., 2010	11	Shirakawa et al., 2010		
6	Kato and Bai, 2010	12	Hong., 2005		

A functional SNARE complex requires three Q-SNAREs and one

R-SNARE to generate a fusogenic complex (Katz and Brennwald, 2000; Ossig et al., 2000; Graf et al., 2005). In this table, the existence of SNAREs in each complex according to previous reports are listed. Each column shows know composition of one SNARE complex with its reference. However, this table does not rule out the existence of additional SNAREs in each complex.

Beyond the canonical role in membrane fusion, SNARE proteins contribute to other physiological activities, including disease resistance (Collins et al., 2003), gravitropism (Kato et al., 2002; Surpin et al., 2003; Yano et al., 2003), cell plate formation (Lukowitz et al., 1996), arbuscule and nodule tissue formation (Mai et al., 2006; Ivanov et al., 2012). Most likely, SNARE proteins act in these processes through their roles in SNARE complex assembly and vesicle traffic.

How many SNAREs are needed to maintain membrane trafficking? There are around 4000 SYP121 molecules/μm^2 at the cell surface (Grefen et al., 2010b; Gall et al., 2010). One guard cell of *Vicia faba* has surface area around 4000 μm^2 (Shope et al., 2003), so there will be more than $1.6x10^7$ SYP121 molecules in a guard cell. In coleoptiles, one of the fastest growing tissues in plants, growth speed is 3.8 $\mu m/s$ and the vesicle delivery rate is 0.15 μm^2 at 0.2 vesicles/s (Phillips, et al. 1988; Sutter et al., 2000), which means there are no more than 130 membrane fusion events per second needed to maintain surface expansion. In guard cell, the speed is slower, the surface area are just increases at a rate near 0.1 $\mu m^2/s$ in bean (Meckel et al., 2005). Han et al. (2004) suggested 5-8 complexes are involved in the formation of a putative fusion pore. Using single-molecule fluorescence microscopy, the number of SNARE complexes required for docking of liposomes to deposited bilayers was only one per docked liposome (Bowen et al., 2004). If we predict four SNARE complexes are used for one fusion site, then there will be only 520 SNARE complexes or 2080 SNARE proteins used for membrane fusion at the same time in a cell. Compared to the total number of SNARE proteins in one cell, this is a small number and

suggests that most of the SNARE proteins are not activated for membrane fusion. Previous reports have indicated that the Q-SNAREs are occurred in clusters by self-organization based on simple physical principles in cell membranes, which is called as 'icebergs' model (Sieber et al., 2007; Murray and Tamm, 2009). This model can be used to explain the reason why so many SNAREs expressed in cells. The other potential explanation is that a few SNARE proteins are known also to interact with ion channels and affect their regulation, a point which will be introduced in a later section.

1.4 Other proteins involved in vesicle fusion

In vesicle membrane trafficking, SNAREs only take part in membrane fusion, the targeting, tethering and docking of these vesicles require many other proteins, including Rab-GTPases, exocyst, and Sec1/Munc18-like proteins.

1.4.1 Exocyst

The exocyst is a tethering complex mediating the first contact between secretory vesicles and the target membrane. They can interact with cytoskeletal proteins, Rab GTPases, and some other proteins (Zarsky et al., 2013). In yeast and mammalian cells, each exocyst subunit is encoded by a single gene (Zhang et al., 2010; Elias et al., 2008), while in plants they have multiple genes for one subunit, which suggests exocyst may have different functions in different plant tissues or species. In yeast, the exocyst is composed of eight distinct subunits, referred to as Sec3p, Sec5p, Sec6p, Sec8p, Sec10p, Sec15p, Exo70p, and Exo84p (TerBush et al., 1996). In *Arabidopsis*, there are two highly similar genes homologous to Sec3 and Sec5, one homologue of Sec6, Sec8 and Sec10 each, two paralogues related to Sec15, three copies of

a putative Exo84, and 23 potential *Arabidopsis* genes related to Exo70 (Elias et al., 2003; Synek et al., 2006).

The exocyst is essential for plant survival. In *Arabidopsis*, *sec5 exo70A1* and *sec6 exo70A1* double mutant lines have shown a synergistic defect in etiolated hypocotyl elongation. Mutants in exocyst subunits SEC5, SEC6, SEC8, and SEC15a showed defective pollen germination and pollen tube growth phenotypes (Hala et al., 2008). The *Arabidopsis* mutant exo*84b* was severely dwarfed and had compromised leaf epidermal cell and guard cell division. During cytokinesis, GFP-tagged exocyst subunits Sec6, Sec8, Sec15b, Exo70A1, and Exo84b exhibited distinctive localization maxim at cell plate initiation and cell plate maturation (Fendrych et al., 2010). These results suggests that exocyst is involved in secretory processes during cytokinesis, especially in the cell plate initiation, the cell plate maturation, and the formation of new primary cell wall.

The *Arabidopsis* genome encodes a large number of Exo70 subunits, yet several of these are critical for plant development. For example, an Exo70A mutation disturbed the polar growth of root hairs and stigmatic papillae (Synek et al., 2006), suggesting that Exo70 is involved in cell-specific exocytosis within differentiating plant tissues. A recent study showed that Exo70b1 interacted with Sec5 and Exo84 to form an exocyst complex involved in autophagy-related and Golgi-independent membrane traffic to the vacuole (Kulich et al., 2013). These studies suggest that Exo70 is needed for several different exocytosis/trafficking pathways, even within a single cell. Exo70 proteins are also involved in stress-related responses. Transcription of Exo70b2 and Exo70h1 have been shown to be up-regulated by treatment of plants with a bacterial elicitor peptide, and *Arabidopsis* plants mutated in these two genes were more sensitive to plant pathogens (Pecenkova et al., 2011). Exo70b2 acted as a target of the plant U-boxtype ubiquitin ligase 22, which was a negative regulator of pathogen associated molecular

patterns triggered responses (Stegmann et al., 2012). Silencing of Exo70 genes in rice roots has also been shown to disrupt trafficking associated with Cu-induced ROS production in the presence of the heavy metal (Lin et al., 2013).

1.4.2 Rab GTPases

Rab GTPases are members of the superfamily of small regulatory GTPases. Rab GTPases function as molecular switches and cycle between GTP-bound and GDP-bound states. The binding of Rab GTPases with their specific effector depends on this cycle. In the GDP-bound state, Rab GTPases are inactive and bind to a Rab disassociation inhibitor in the cytoplasm. The Rab Guanine Exchange Factor activates Rab GTPases and exchanges GDP with GTP to activate Rab GTPases for association with the target membrane. The activated Rab GTPases can further bind to their specific effectors which further mediate the membrane trafficking. Rab effectors include tethering factors, enzymes of phosphatidyl-inositiol metabolism, myosins, kinesins and regulators of SNARE protein assembly (Woollard and Moore, 2008). In vesicle formation, Rab9 binds with its effector tail-interacting protein, which recycles mannose 6-phosphate receptors and helps to transport vesicle within Rab9 from trans-Golgi network to late endosomes (Carroll et al., 2001). In vesicle tethering, for example, vesicle-associated protein p115 and a Golgi-residing GM130- and GRASP65-containing complex are thought to be effectors of Rab1. Rab1 binding activates these proteins and tether ER-derived vesicles to the Golgi (Allan et al., 2000; Mayer et al., 2001). In membrane fusion, most evidence indicates Rabs indirectly regulate SNARE function. One example is about early endosome fusion, Rab5 interacts with its effector early endosome antigen 1, which further binds with syntaxin-13 (Mcbride et al., 1999).

There are 11 Rab GTPases have been identified in yeast and more

than 60 in mammalian cells (Schultz et al., 2000). They can be classified into eight groups according to the particular vesicle trafficking pathway. In *Arabidopsis*, there are 57 Rab GTPases which also divide between these eight groups (Bassham et al., 2008). Rab GTPases in RabD and RabB groups are involved in early secretory traffic. Proteins in the RabF1 and RabF2 subgroups of RabF GTPases are involved in biosynthetic traffic to the vacuole. RabA, RabE and RabF are active in post-Golgi secretory traffic. Information is scarce on members of the RabC, RabG and RabH groups and on some subclasses within the large RabA group (Woollard and Moore, 2008).

1.4.3 Sec1/Munc18-like Proteins

Sec1/Munc18-like (SM) proteins are composed of a conserved set of domains, comprising a total of around 600 amino acids, and form a structure that folds into an arch-shaped “clasp” structure (Misura et al., 2000). The genomes of *Saccharomyces cerevisiae* contain 4 SM family genes, while humans have 7 SM proteins (Toonen and Verhage, 2003). *Arabidopsis* has 6 members of the SM proteins and other plants have similar numbers (Sanderfoot et al., 2007).

Much research in yeast and animal cells, and more recently in plants, indicate up to three different modes about the binding between SM proteins and SNARE proteins:

1. SM proteins bind with closed stage Qa-SNARE proteins in which the H_{abc} domain folds back onto the SNARE motif to block assembly in the SNARE complex. Munc13 and Munc18 SM proteins effectively clasp these SNARE protein to stabilize this closed (or occluded) conformation (Betz et al., 1997; Fernandez et al., 1998).
2. SM proteins bind with N terminal domain of SNARE proteins in both open or closed stages. The SM protein Vps45p and Sly1p interacted with N-terminal motif of Q-SNARE proteins (Dulubova et al., 2002; Yamaguchi

et al., 2002). The latter even binds with a short, evolutionarily conserved N-terminal peptide (Yamaguchi et al., 2002).

3. SM proteins bind with SNARE complex. The SM protein Sec1p in yeast only interacted with syntaxin Sso1p in SNARE complex instead of directly interacted with Sso1p, even it was in closed stage (Carr et al., 1999).

In short, SM proteins have multiple roles when they are bound with SNARE proteins. In the first mode, the SM protein acts as a negative regulator of SNARE complex formation and prevents promiscuous interactions with other SNARE proteins. The other modes are associated in various stages of priming and assembly of the SNARE complex, effectively indicating that SM proteins have the opposite effect on vesicle traffic. Both roles of SM proteins are most likely evolutionary adaptations to prevent SNARE proteins binding with non-cognate syntaxins and to promote SNARE assembly for rapid trafficking requirements (Toonen and Verhage, 2003). In plant cells, SM proteins can interact with Qa-SNARE proteins and change the SNAREs from closed to open, which allows them to assemble the SNARE complex. Mutagenesis and biophysical studies have indicated that the SM proteins also interact with VAMPs in the SNARE complex (Shen et al., 2007).

There are several studies about SM proteins in plants that relate to their specificity and functions. VPS45 was localized to the trans Golgi network, early endosomes, and vacuole in *Arabidopsis* and interacted with different SNARE proteins which showed that VPS45 plays a distinct role in plant cells (Bassham et al., 2000; Zouhar et al., 2009). VPS33 was found on late endosomes and the vacuole in *Arabidopsis*, and it seemed to be part of a so-called “Class-C-Complex” (Rojo et al., 2005). There are three genes belong to the SM proteins at the PM, SEC11, SEC1a (=SEC12), and SEC1b (=SEC13). Only SEC11 (or KEULLE) has been investigated thoroughly. SEC11 interacts with Qa-SNARE SYP111 during cytokinesis and both proteins were originally described to be important

for cell division (Waizenegger et al., 2000; Assaad et al., 2001). However, mutation of SEC11 gives a phenotype of absent root hairs, while SYP111 knock out seedlings still could grow root hairs (Assaad et al., 2001), which suggests SEC11 has role in independent of SYP111. Karnik et al. (2013) have reported that SEC11 binds with SYP121; they also have shown there are two modes of the binding, one directly interacts with SYP121, the other one was dependent on assembly of a complex with VAMP721 and SNAP33.

1.5 The role of SNARE proteins in regulating transport by vesicle trafficking

A number of studies over the past decade have highlighted a wide range of physiological processes that depend on SNARE-mediated vesicle traffic. Here I review a few of the best documented of these examples.

1.5.1 Boron transporters and PIN proteins traffic

Endocytic membrane trafficking is a key mechanism for controlling the amount of proteins at the PM and therefore has an important role of plant signalling, in part through protein transfer from the PM to endosomal compartments and degradation in the vacuole. Again, SNARE proteins are involved in the turnover of integral membrane proteins.

One example of such a role is traffic of the PIN proteins. PIN proteins are auxin efflux carriers. They are involved in the asymmetrically distribution of auxin across adjacent cells, which regulates plant growth and development. The polarized localization of PIN proteins depends on membrane vesicle trafficking and has been associated with several SNARE proteins. Surpin et al. (2003) have analysed the phenotype of

Arabidopsis mutants *vti11-1* and *zig-1,* the latter gene encodes R-SNARE VTI11 (Kato et al., 2002). These mutants have defects in vascular patterning and auxin transport, which suggests that the SNARE VTI11 plays a role in proper PIN proteins localization (Surpin et al., 2003). Endosidin 1 is a chemical compound which can be used to block the traffic of some PM auxin transporters. The endosidin 1 treatment induced the rapid aggregation of PIN2 and AUX1 into some distinct endomembrane bodies. Because SYP61-CFP fluorescence signal was present in the same bodies, the trafficking of PIN2 and AUX1 might be through the pathway involving SYP61 (Robert et al., 2008). SYP22 (or VAM3) is one of the Qa-SNARE proteins that localizes to the (pre-) vacuolar compartment. SYP22 deficiency caused abnormal distribution of auxin in leaf cells. Further research has shown that the proper expression pattern of PIN1 depended on SYP22 (Shirakawa et al., 2009). In a study of the SYP4 subgroup SNARE proteins, the *syp42/syp43* mutant impaired PIN2 protein accumulation in vacuole, which means SYP43 and SYP42 are likely to be important for PIN proteins transport (Uemura et al., 2012).

Boron (B) is one of the important trace elements in plant, but excess of B is toxic to plant cell. Thus, plants respond to different levels of B by regulating the number of B transporter at the PM. Traffic of B transporters requires SNAREs to drive this process. Takano et al. (2005) found that BOR1 B_{in} transporter was removed from the PM to vacuole for degradation in the presence of high B concentration. BOR4 is a BOR1 paralogue in *Arabidopsis* and functions as a B efflux transporter. It is also located at the PM but, as Miwa et al. (2007) have shown, its population at the plasma membrane did not decrease under high B concentration treatment. Clearly, the different cycling characteristics of BOR1 and BOR4 form a system which can help the plant meet the B stress.

1.5.2 K^+ channel cycling and ABA signalling

Stomata are pores formed by a pair of guard cells in most higher plants. The guard cells open the stoma to allow the entry of CO_2 into leaf for photosynthesis and they close stomata to help retain water by preventing transpiration. The stomatal movement depends on the change in cell volume of the guard cells. Ion accumulation forms a major part of the osmotic pressure change during stomata movement. For example, during stomata opening, K^+ and other ions are transported into the guard cells, which increases the osmotic pressure and leads to an increase in guard cell volume to open the stoma. These processes are regulated, in part through activity changes in K^+ channel activity and through cycling of the K^+ channels between the PM and endosomal membrane pool.

Recent work has verified the role of SNARE proteins in K^+ channel trafficking under ABA treatment (Sutter, et al. 2007). These studies showed a tight and dynamic control of the population of K^+ channel like KAT1 at the PM by ABA. KAT1 K^+ channel assembled in punctate at the PM. ABA treatment triggered the endocytosis of KAT1 proteins from the PM, sequestration in an endosomal pool, and over several hours KAT1 proteins could recycle back to the PM after ABA washout. The cycling of KAT1 is dependent on Q-SNARE SYP121. In tobacco and *Arabidopsis*, the truncated SYP121, so-called Sp2 fragment, prevented stomatal movement under ABA treatment by interfering with the Ca^{2+}, K^+, and Cl^- channels. This Sp2 fragment lacks the C terminal transmembrane domain and affects the function of native SYP121 (Leyman et al., 1999). Further research has shown that the Sp2 fragment of SYP121 suppresses the delivery of KAT1 K^+ channel to the PM and changes the distribution of the channels (Sutter et al., 2006). Finally, a recent study has shown in *syp121* mutant *Arabidopsis* that the recycling of KAT1 is slow compared to wild type plants (Eisenach et al., 2012). These results clearly indicate that SYP121 is involved in KAT1 K^+ channel traffic and

cycling in plant cells.

The role of VAMPs in stomatal movement under ABA treatment has also been reported. Under ABA treatment, the protein levels of VAMP721 and VAMP722 were down regulated (Yi et al., 2012). In antisense plants in which the expression of VAMP711 was suppressed, Leshem et al. (2010) found that ABA treatment induced ROS production as in the wild-type plants, but the stomata failed to close. ROS distribution was also affected in antisense plants, suggesting a close connection to signalling events known to be associated with ABA.

1.5.3 Aquaporin traffic

Aquaporins are water channel that facilitates the transport of both water and small neutral molecules. Plasma membrane intrinsic proteins (PIPs) are plant aquaporins which regulate the root and leave hydraulic conductivity and are situated at the PM. There is now substantial evidence to indicate that aquaporin traffic is important for plant homeostasis and survival under water stress conditions. The function of PIPs depends on transcriptional control of expression, activity change, and the modulation of PIPs trafficking (Hachez et al., 2013). SNARE proteins contribute to the regulation of PIPs traffic in plant cells. Besserer et al. (2012) found that both maize and *Arabidopsis* SYP121 interacted directly with PIP2;5 in maize (*Zea mays*). The expression of the Sp2 fragment of SYP121 in maize mesophyll protoplasts or epidermal cells led to a decrease in the delivery of PIP2;5 to the PM. The activity of PIP2;5 was also negatively affected by Sp2 fragment (Besserer et al., 2012) and was ascribed to the reduction in PIP population at the PM.

In *Arabidopsis*, the *syp61* mutant showed a strong sensitivity to osmotic stress (Zhu et al., 2002), and SYP61 co-localized and co-purified with SYP121 in *Arabidopsis* (Drakakaki et al., 2012), suggesting the role of SYP61 in aquaporin traffic. Hachez et al. (2014) found that the plant

aquaporin PIP2;7 colocalized with SYP121 and SYP61 and directly interacted with both two Q-SNAREs. In the same research, the authors also provided eveidence for the interaction between SYP121 and SYP61. The proper delivery of PIP2;7 to the PM was dependent on the SNARE complex formed by these two SNARE proteins.

1.5.4 Plant immunity and pathogen receptor traffic

SNARE proteins are involved in plant immunity and plant interactions with other organisms in a number of settings. Early studies indicated that the Qa-SNARE SYP121 in *Arabidopsis* and ROR2, which encoded the functionally homologous syntaxin in barley, were required for basal penetration resistance against barley powdery mildew (Collins et al., 2003). In response to fungal attack, both Qa-SNAREs formed a binary SNARE complex with SNAP33 which was used to mark the membrane site targeted by the pathogen. Furthermore, vesicles containing antimicrobial compounds were found to carry VAMP721/722. These two VAMPs formed a SNARE complex with SYP121 and SNAP33 in the PM (Kwon et al., 2008) and facilitated to the membrane fusion.

SNARE proteins are equally important for symbiotic interactions of plants. During the process of establishing symbiosis, it is often the case that the the host forms a specialized membrane to surround the symbiont. This membrane then forms the heart of endosymbiotic junction. A case in point is the symbiosis formed between *Medicago truncatula* and arbuscular micorhyzal fungi. In this case, two members of the VAMP72 group, MtVAMP721d and MtVAMP721e, were located at the site of symbiosome and silencing of these two genes blocked symbiosome and arbuscule formation (Ivanov et al., 2012). Plants can respond to microbial attack by the synthesis of several pathogenesis-related (PR) proteins. These PR proteins are synthesized in the ER and transported to the PM or vacuole by vesicle trafficking. Wick et al. have shown that the

expression level of SNAP33 was increased after inoculation with some pathogens (Wick et al., 2003). PR genes were under control of Non-expressor of Pathogenesis-Related genes (NPR1), NPR1 also regulated transcription of SNAP33. After mutation analysis, SNAP33 was found to be involved in the secretory pathway of PR1 (Wang et al., 2005). The other SNARE protein associated with PR secretion is SYP132. Kalde et al. (2007) have used virus to induce NbSYP132 silencing in *Nicotiana benthamiana.* In these silenced plants, the accumulation of PR1a in the cell wall was affected, the inoculated bacterial growth was enhanced, and more disease symptoms formation could be observed. Similarly, Wang, et al. (2014) found in wheat (*Triticum aestivum*) that TaSYP132 could interact with TaNPSN11. The resistance of wheat to pathogen attack was reduced by knocking-down *TaNPSN11,* and in the wild-type plants TaNPSN11 was mainly distributed in cell membrane facing the attacked membrane site (Wang et al., 2014). These results suggest that the transport of vesicles containing PR might depend on a SNARE complex of SYP132, SNAP33, and NPSN11.

1.5.5 BRI1 traffic

Brassinosteroids are phytohormones that play a crucial role in plant growth and development. They are involved in promotion of cell expansion and cell elongation (Clouse and Sasse, 1998; Nemhauser et al., 2004), in promotion of vascular differentiation (Cano-Delgado et al., 2004), in formation of pollen tube (Szekeres et al., 1996; Clouse and Sasse, 1998), and in seed germination (Leubner-Metzger, 2001; Steber and McCourt, 2001). Brassinosteroid Insensitve 1 (BRI1; He et al., 2000) encodes a key receptor for this class of molecules and has been shown to localize to the PM as well as endosomal structures. BRI1 is regulated by its co-receptor BRI1-Associated receptor Kinase 1 (BAK1). BAK1 can interact with BRI1 and co-expression of these two proteins in protoplasts

leads to increased internal accumulation of BRI1 (Russinova et al., 2004). Interestingly, the accumulation of BRI1 in endosomes enhanced BR signalling (Geldner et al., 2007), an observation suggesting that the endocytosis is important for the function of BRI1. Robert et al. (2008) found that after blocking the endocytosis by endosidin 1, fluorescence analysis of GFP-tagged BR1 showed the receptor was expressed in large intracellular endosidin bodies in *Arabidopsis* seedlings, whereas BRI1-GFP was found at the PM and in endosomes without endosidin 1 treatment. The fluorescence of SYP61-CFP and BRI1-GFP could be found in the same bodies after endosidin 1 treatment, indicating endosidin 1 affected the endocytosis and sorting of BRI1 by impacting a pool of early endosomes defined by SYP61 (Robert et al., 2008). These results suggests SYP61 is involved in the trafficking of BRI1 in plant cells.

1.6 Ion channels

1.6.1 General introduction

The plasma membrane and internal membranes of all plant cells form a hydrophobic barrier to diffusion and therefore serve to regulate the inward and outward transport of selected molecules and ions. These biological membranes contain transport proteins which facilitate the transport of selected ions and molecules through membrane.

Generally, transport proteins can be divided between three main categories: pumps, carriers, and channels (Taiz and Zeiger, 2010). An overview of the transport proteins located at the PM and tonoplast are shown in Figure 1-6. Pumps transport solutes against the electrochemical gradient for the transported ion(s) and therefore use additional energy, usually from ATP hydrolysis, for this purpose. Hence, these processes are often referred to as primary active transport. Carrier

proteins bind the transported molecule on one side of the membrane and then undergo a confirmation change that releases it on the other side. Transport through carriers can be either passive or secondary active. The transport via a passive carrier is sometimes called “facilitated diffusion”, which is primarily found in bacteria. Secondary active carriers transport solute across membrane against their gradient of electrochemical potential by coupling the uphill transport of one solute to the downhill transport of another. In plants, most carriers that are secondary active couple transport with H^+ and use energy indirectly from the H^+-ATPase (Taiz and Zeiger, 2010).

Ion channels are transmembrane proteins that function as selective pores through which ions can transit across the membrane by simple diffusion. The size of a channel pore and the density and nature of surface charges on its interior lining determine the ion specificity. As long as the channel pore is open, solutes that can penetrate the pore diffuse through it very rapidly, often at rates of 10^8 ions per second through each channel. Transport through ion channels is passive and is driven only by the electrochemical gradient on the permeant ion (Taiz and Zeiger, 2010). Thus, the thermodynamic behavior of an ion channel is defined by the Nernst equation:

$$\Delta E = \frac{RT}{zF}\left(\ln\frac{[X]_o}{[X]_i}\right)$$

where E is the equilibrium or Nernst potential of the ion X, $[X]_o$ and $[X]_i$ are its extra- and intracellular concentrations, R is the gas constant (8.314 J/K mol), T is the absolute temperature in degrees Kelvin, z is the charge on ion X and F is Faraday’s constant (9.648 $x10^4$ C/mol). This equation can be further simplified for a univalent cation at 25 °C:

$$\Delta E = 59mV \log \frac{[X]_O}{[X]_i}$$

Where $[X]_o$ and $[X]_i$ are its extra- and intracellular concentrations. According to this equation, a tenfold difference in concentration across membrane corresponds to a Nernst potential 59 mV, which means that a membrane potential of 59 mV can maintain tenfold concentration difference for the permeant ion (Taiz and Zeiger, 2010).

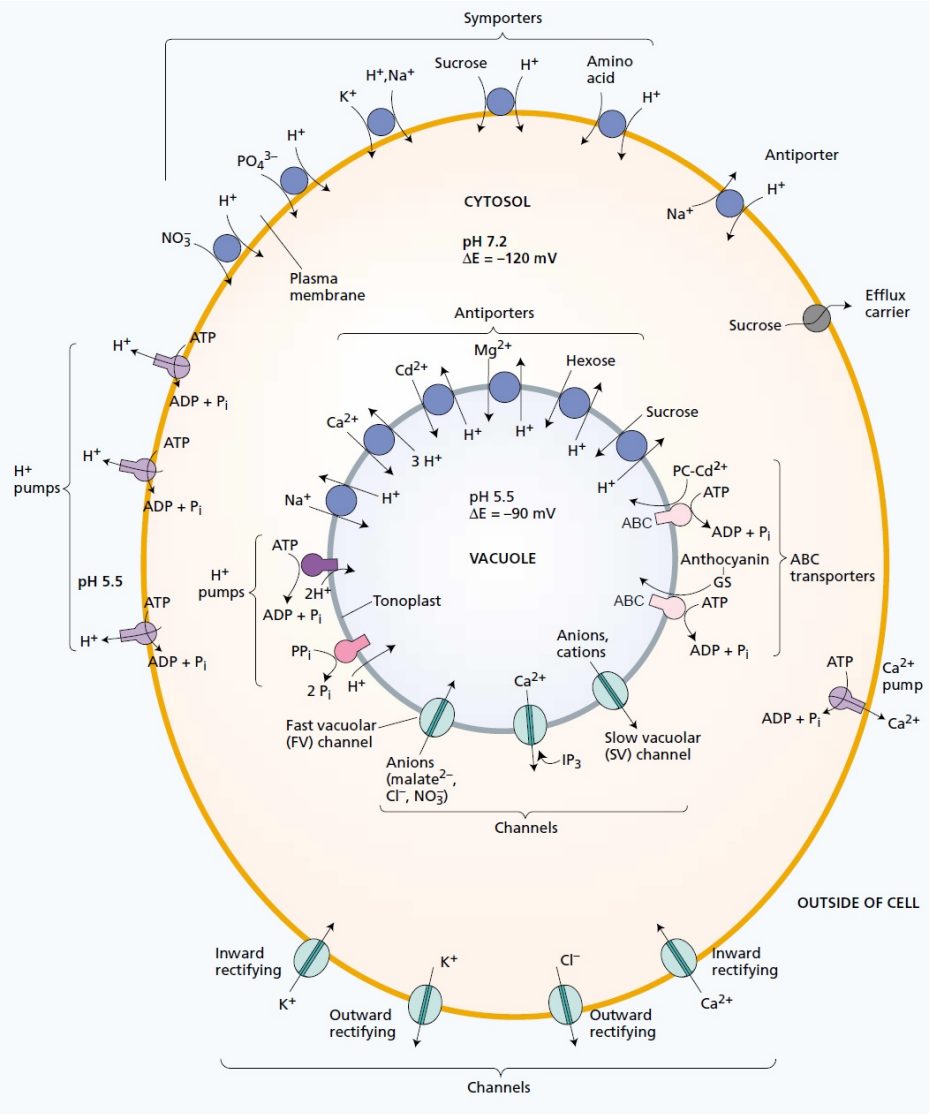

Figure 1-5. Overview of the pumps, transporters, and channels in the PM and major tonoplast of plant cells

Image was adapted from previous publication (Taiz and Zeiger, 2010)

Most ion channels are not open all the time. Indeed, tight control of ion channel activity is essential for the survival of most cells. The very large ion fluxes possible through an ion channel means that they could easily deplete a cell of important ions in a very short time period. To control their activity, channels usually include molecular structures that enable the channel to “gate” open and to rapidly close the channel pore. In many cases, external and internal signals serve to control this gating process. These signals include membrane potential changes, ligands that may bind to the channels, hormones, light, as well as post-translational modifications such as phosphorylation of the channel protein (Taiz and Zeiger, 2010).

Ion channels can be classified according to which chemical or physical modulator controlling their gating activity. In plants, voltage-gated channels are controlled by a change in membrane potential, mechanosensitive channels are controlled by osmotic pressure or membrane curvature, and second messenger gated channels respond to nucleotides. The other way to classify ion channels is based on which ions they carry, like K^+, Ca^{2+}, Cl^-, and the organic anion $malate^{2-}$. But it should be noted that ion channels generally do not have a high selectivity for a specific ion when compared to pumps and carriers. For example, most Cl- channels can also carry NO^{3-} and $malate^{2-}$ (Hedrich et al., 1994; Schmidt and Schroeder, 1994), while many Ca^{2+} channels are equally permeable to Ba^{2+} (Gelli and Blumwald, 1997; Hamilton et al., 2000). In the following sections, three major ion channel groups will be introduced, Ca^{2+} channels, anion channels, and K^+ channels.

1.6.2 Plant calcium channels

The usage of free calcium ions (Ca^{2+}) as secondary messengers is one of the signal transduction pathways in both plant and animal cells. The huge difference of Ca^{2+} concentrations between cytoplasmic (around

100 nM) and non-cytoplasmic solutions (mM) enables the generation of calcium signals by fast changes of cytosolic free Ca^{2+} concentration ($[Ca^{2+}]_i$) via membrane-localized Ca^{2+}-permeable channels (Stael et al., 2012). Plants react to changing environmental conditions through this immediate signal pathway. Specific changes in Ca^{2+} levels in plants can be evoked by several signals, including abiotic, biotic, and developmental stimuli, which are further recognized by Ca^{2+} sensor proteins and lead to a variety transcriptional and metabolic responses.

Voltage-dependent calcium currents have been found in all plant cell types examined (Demidchik et al., 2002; Stoelzle et al., 2003; Verret et al., 2010). But genome analyses show that plants lack genes homologous to the voltage-dependent calcium channels of animals (Hedrich et al., 2012). In vacuolar membrane, there is one channel which named the slow-activating vacuolar channel which is known to carry Ca^{2+}. In the PM, 20 glutamate receptor homologs (GLRs) and a family of 20 cyclic nucleotide-gated channel homologs (CNGCs) have been found as candidate plasma membrane Ca^{2+} channel genes.

The slow-activating (SV) vacuolar channel contains two homologous domains. Each domain contains six transmembrane helices and one pore domain. In *Arabidopsis*, there is only one SV channel, encoded by the gene Two-Pore Channel 1 (TPC1; Furuichi et al., 2001). TPC1 has a role in seed germination and stomatal guard-cell closure in response to external Ca^{2+} (Peiter et al., 2005). A knockout mutant of this channel shows Ca^{2+} current lost in guard cells, suggesting that the SV channel functions as conductance for Ca^{2+} release (Peiter et al., 2005). In rice (*O. sativa*), wheat (*Triticum aestivum*), and tobacco (*N. tabacum*), there are two TPC genes (Wheeler and Brownlee, 2008).

Of the channels at the PM, Tapken and Hollmann (2008) found *Arabidopsis* AtGLR1.1 and AtGLR1.4 have functional Na^+, K^+, and Ca^{2+} permeable ion pore domains. Michard et al. (2011) reported that GLRs facilitated Ca^{2+} influx across the plasma membrane, modulated apical

$[Ca^{2+}]_i$ gradient, and consequently affected pollen tube growth and morphogenesis. Heterologous expression of *Arabidopsis* CNGC18 in *Escherichia coli* resulted in a time- and concentration-dependent accumulation of more Ca^{2+} (Frietsch et al., 2007).

1.6.3 Plant anion channels

Plant anion channels allow the efflux of anions from cells. Patch-clamp studies on plant cells identified two prominent anion currents classified into S-type and R-type/Al-sensitive channels (Hedrich et al., 2012).

In plant guard cells, anion channels play important role in stomatal movement. The Slow Anion Channel-associated 1 (SLAC1) channel was the first identified gene for an anion channel in plants and encodes the S-type anion channels in *Arabidopsis*. SLAC1 is expressed in guard cells where it serves as a pathway for anion efflux for stomatal closure; in the *slac1* mutation the stomata do not close fully in response to closing signals, including ABA, Ca^{2+}, and NO, and environmental stimuli such as CO_2, darkness, humidity, and ozone (Negi et al., 2008; Vahisalu et al., 2008; Saji et al., 2008).

In *Xenopus* oocytes, heterologous expression of SLAC1 currents requires phosphorylation by the protein kinase OST1 (Geiger et al., 2009; Lee et al., 2009), suggesting that this post-translational modification is important for its activity in the plant. Functional expression of SLAC1 shows a higher permeability for nitrate than for chloride and give a channel that is also weakly permeable to malate (Schmidt and Schroeder, 1994; Geiger et al., 2009). In plant cells, the OST1-dependent phosphorylation for SLAC1 activation was verified by analysis in *ost1-2* mutant (Geiger et al., 2009). Furthermore, multiple sites in both N terminus and C terminus of SLAC1 are phosphorylated by OST1 (Lee et al., 2009; Vahisalu et al., 2010).

The first gene encoding R-type anion channel in *Arabidopsis* is AtALMT12, which has similar sequence as ALMT1. Extracellular Al^{3+} treatment did not stimulate AtALMT12-dependent anion currents in oocytes, so it was renamed as quickly activating anion channel 1, QUAC1 (Meyer et al., 2010). In *Arabidopsis*, QUAC1 was expressed at the PM of guard cells and required for stomatal closure. Patch-clamp studies found reduced R-type currents in *Arabidopsis* mutants lacking QUAC1, but remaining R-type currents in this mutant suggested the exist of other gene encode additional QUAC (Meyer et al., 2010; Sasaki et al., 2010).

S-type anion channels are also expressed in other plant tissues. In addition to SLAC1, there are four SLAC1 homologues, S-type anion channel 1-4 (SLAH1-4) in *Arabidopsis*. SLAH1-3 were located at the PM. SLAH1 and SLAH2 were expressed in roots and SLAH3 was expressed in whole plant (Negi et al., 2008). Investigation of SLAH3 showed that it could form an S-type anion channel and the channel activation was dependent on phosphorylation by CPK21 (Geiger et al., 2011).

Plant anion channels are also involved in tolerance to salinity (Kollist et al., 2011). Al^{3+} is highly toxic to plant growth. In response to Al^{3+}, tolerant plant can secreted Al^{3+}-chelating organic anions, such as malate and citrate at the root surface (Delhaize et al., 1993; Pineros and Kochian, 2001; Delhaize et al., 2007). A family of membrane proteins known as Al^{3+}-activated malate transporters (ALMTs) were identified (Sasaki et al., 2004; Hoekenga et al., 2006). ALMTs have 6-8 predicted membrane domains. Expression of individual ALMT in *Xenopus oocytes* was sufficient to mediate Al^{3+}-induced malate currents and the reversal potential shifts showed Nernstian behavior correlating with the malate gradient suggesting ALMTs encoded anion channels (Hoekenga et al., 2006).

1.6.4 Plant potassium channels

Potassium (K^+) is the most important inorganic ion in plant cells and can comprise up to 10% of the total plant dry weight. Plant cells use this cation primarily as a compatible osmotic solute to maintain turgor and drive cell expansion. Potassium is also important for enzyme activation, stabilization of protein synthesis, neutralization of negative charges on proteins, and the control of membrane polarization (Lebaudy et al., 2007; Dreyer and Uozumi, 2011). K^+ uptake from the soil and translocation throughout the plant depends on a network of transport pathways which includes K^+ channels and coupled K^+ transporters. In *Arabidopsis*, there are 35 genes that contribute to K^+ transport. They divide between 3 families of channels and 3 families of transporters, for a total of 15 and 20 genes, respectively (Maser et al., 2001). Here I focus on the K^+ channels.

In plant cells, K^+ channels can be subdivided into two channel classes: non-voltage-gated and voltage-gated K^+ channels. The K^+ channels in *Arabidopsis* are shown in Table 1-3.

Table 1-3. The K^+ channels in *Arabidopsis*

Channel class	Sub-family	Channel name	Locus No.
Voltage-gated K^+ channels (Shaker/Kv K^+ channels)	K_{in}	KAT1	At5g46240
		KAT2	At4g18290
		AKT1	At2g26650
		AKT5	At4g32500
		SPIK	At2g25600
	K_{weak}	AKT2	At4g22200
	K_{silent}	KC1	At4g32650
	K_{out}	SKOR	At3g02850
		GORK	At5g37500
Voltage-independent K^+ channels	Tandem-pore K^+ channels	TPK1	At5g55630
		TPK2	At5g46370
		TPK3	At4g18160
		TPK4	At1g02510
		TPK5	At4g01840
		KCO3	At5g46360

Adapted from Dreyer and Uozumi (2011).

As shown in Figure 1-6A and Figure 1-7, a functional K^+ channel is formed by several K^+ channel subunits. For example, four Shaker/Kv K^+ channel subunits come together with the pore at the centre (See Figure 1-6 A). Their pore-forming regions dip into the membrane, forming a K^+ selective finger region at the outer part of the pore. The structure of different K^+ channel subunits are showed in Figure 1-6 C to F. Each subunit contains the transmembrane domains and the pore regions.

The voltage-independent K^+ channels consist of six members, five tandem-pore channels (TPK1-TPK5) and a single K_{ir}-like K^+ channel subunit (KCO3). In a TPK subunit, there is a tandem repeat structure of 'transmembrane-pore-transmembrane', while there is only one in KCO3 (See Figure 1-6 D and E). In the C terminus of TPK channel, there are two Ca^{2+} binding domain, which suggests Ca^{2+} binding can directly activate the channel (Gobert et al., 2007). A functional K^+ channel is formed by two TPK subunits. The voltage-independent K^+ channels are expressed on tonoplast and other organelle membranes, except for TPK4 that is expressed on the PM in pollen (Becker et al., 2004; Gobert et al., 2007; Isayenkov et al., 2011).

In plant cells, there are some non-selective cation channels which also contribute to K^+ current. In the vacuole membrane of *Arabidopsis* guard cells, fast vacuolar (FV) channels have been found. FV channels are voltage dependent and open at membrane potentials close to 0 mV (Hedrich et al., 1987; Pei et al., 1999). Elevated vacuolar K^+ concentration and resting $[Ca^{2+}]_i$ can activate this channel, while elevated $[Ca^{2+}]_i$, polyamines, and Mg^{2+} inhibit the channel (Hedrich et al., 1987; Pei et al., 1999; Pottosin and Muniz 2002). The gene encoding FV channel is still unknown.

The "Shake" K^+ channels are voltage-gated K^+ channels. The name "shaker" comes from that of the first member of this family, initially cloned from *Drosophila,* which gives rise to a shaking phenotype in the fly. Now these channels are called Kv K^+ channels. Each subunit of a Kv K^+

channel is built of six transmembrane α-helices, S1-S6, with both N- and C-termini situated on the cytosolic side of the membrane (Figure 1-6 C; Uozumi et al., 2008). The pore region is located between S5 and S6 α-helices. Functional Kv K^+ channels are formed by four subunits. The structures of the Kv K^+ channel subunit and the functional K^+ channel are shown in Figure 1-6 A-C.

The gating of Kv K^+ channels is directly regulated by voltage. As shown in Figure 1-6 C, the S1 to S4 helices form the voltage-sensing module, while S5-pore region-S6 form the selective pore. The model of Kv channel gating is showed in Figure 1-6 B (side view) and Figure 1-7 (two potential mechanisms). Changes in membrane potential rearranges the structure of voltage-sensing module, which causes the structure of the central pore to change and leads the channel to close or open.

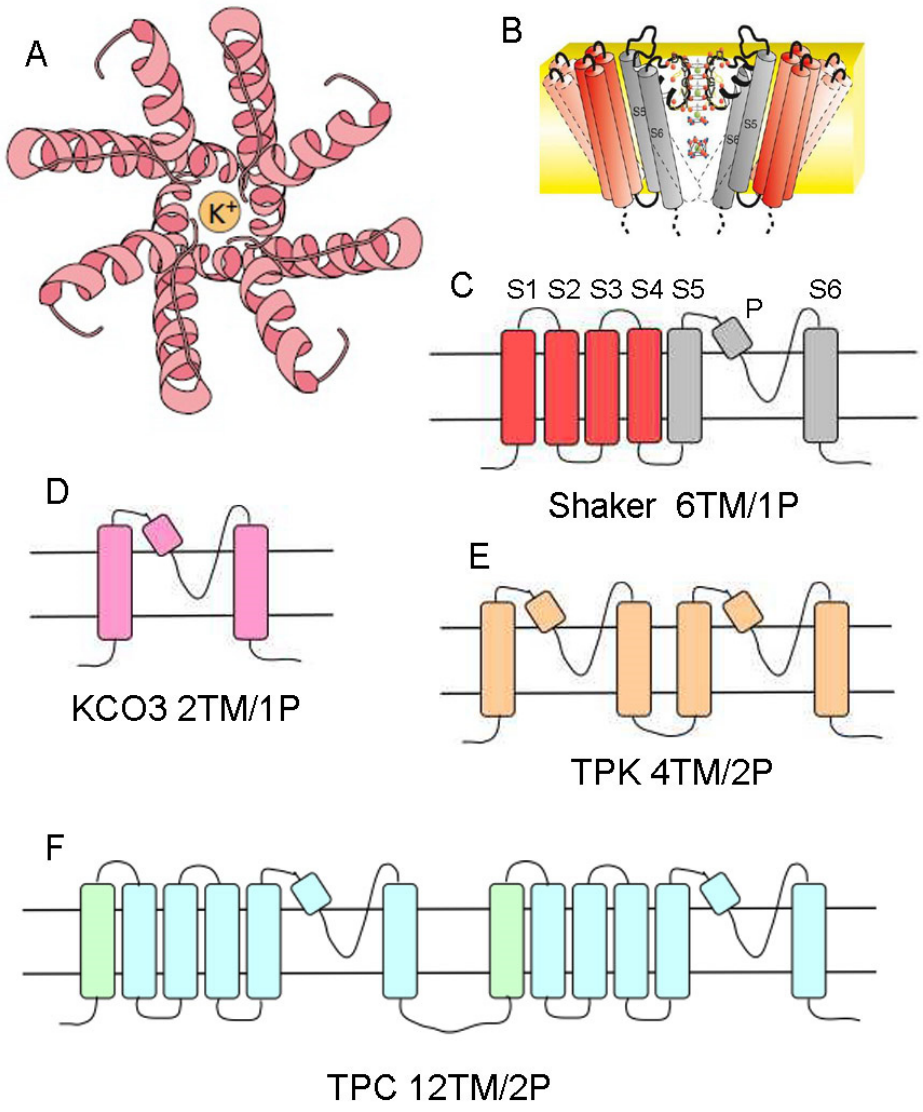

Figure 1-6. The model of K^+ channels in plants

(A) Top view of function K^+ channels in plant cells, looking through the pore of the channel. This figure is adapted from Leng et al (2002).

(B) The model of Shaker K^+ channel forming. The pore-forming modules of all four subunits contribute equally to the central permeation pathway (here just two subunits are displayed). The narrowest part of the pore is formed by the K^+ channel signature motif TxGYG. Polar oxygen atoms of all four subunits (red spheres) assemble four K^+ coordination sites (between the five dashed circles) with an electrostatic environment mimicking the inner hydration shell of a K^+ ion in solution (K^+ ion, green; water molecules, red/blue). A K^+ ion entering the lowest of these four sites exerts a repulsive electrostatic force on the K^+ ion residing in the neighbouring K^+ coordination site; the second K^+ ion will then hop one site further and exert the repulsive force on its neighbour, and so on. The permeation pathway can be occluded by structural rearrangements at the cytosolic end of the pore-forming module (the so-called S6 gate; segments in dashed lines). This figure is adapted from Dreyer and Blatt

(2009).
(C-F) Side view of the Shaker/Kv K^+ channel, the tandem-pore channels (TPK), and KCO3 (K_{ir}-like) K^+ channel. TM, transmembrane domain; P, pore region. For Shaker K^+ channels (as shown in C),each subunit comprises six transmembrane domains (S1-S6) and a Pore region between S5 and S6. Helices S1 to S4 form the voltage-sensing module (red) and helices S5 and S6 form the lining of the pore and its selectivity filter (grey).

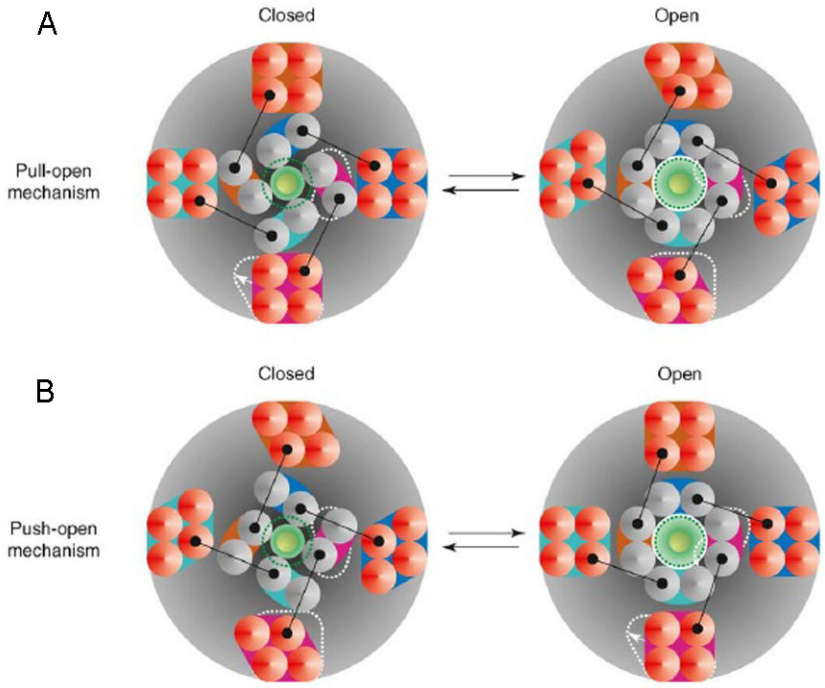

Figure 1-7. The model of Kv K^+ channel gating

Two potential mechanisms, a 'Pull-open' mechanism (A) and a 'Push-open' mechanism (B), can be used to explain the relationship between change of voltage-sensing module and channel gating. Structural rearrangements within the outer ring formed of the voltage-sensing modules (S1-S4, red) cause structural changes in the inner ring formed of the pore modules (S5-S6, grey). Rotation of the outer ring against the inner ring either opens or obstructs the permeation pathway for the hydrated K^+ ion (green) at the cytosolic vestibule of the channel. Positive-going voltage causes a clockwise rotation of the outer ring relative to the inner ring in both cases (left to right in A; right to left in B). Differences in coupling between the rings might account for the opposite gating characteristics of the inward- and outward-rectifying channels. In a 'pull-open' mechanism (outward-rectifiers), the conformational change of the voltage-sensing module associated with this rotation (from square to rhombus as shown) results in channel

opening (A), whereas in a 'push-open mechanism' (inward-rectifiers), it results in channel closure (B).
Adapted from Dreyer and Blatt (2009).

The voltage-dependence of channel gating can be described by Boltzmann function:

$$I_K = g_{\max} \frac{V - E_K}{1 + e^{\delta \frac{V - V_{\frac{1}{2}}}{RT}}}$$

Where g_{max} is the conductance maximum, E_K is the equilibrium voltage for K^+, $V_{1/2}$ is the voltage yielding half-maximal conductance, δ is the apparent gating charge or voltage-sensitivity coefficient (Dreyer and Blatt, 2009), V is the membrane voltage, and R and T have their usual meanings. In this function, there are three free parameters: the gating charge δ, the half-maximal activation voltage $V_{1/2}$, and the conductance maximum g_{max}. In a current-voltage (I-V) plot, δ determines the steepness of the curve while change of $V_{1/2}$ moves the location of the whole curve. Curves with different values of g_{max}, δ and $V_{1/2}$ are shown in Figure 1-8 as a example.

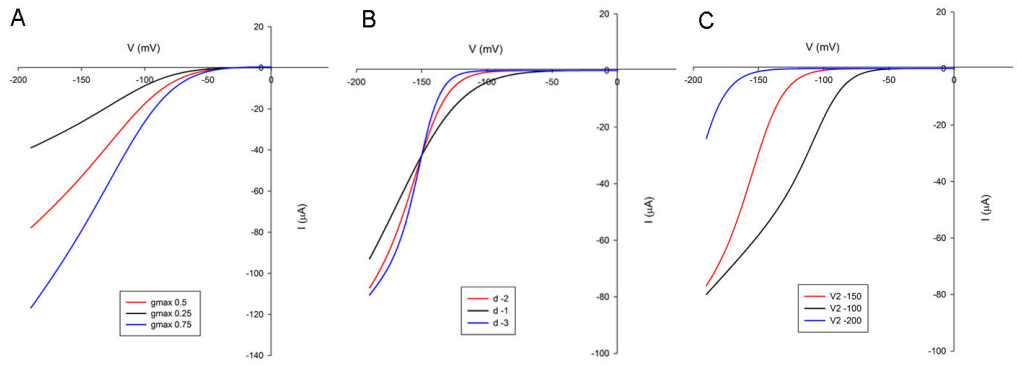

Figure 1-8. The effects of different value of g_{max}, δ, and $V_{1/2}$ on I-V curves

A: The effect of g_{max}. Keep $V_{1/2}$ and δ in common (150 mV and -2), only change the value of g_{max} from 0.25 to 0.75 mS.
B: The effect of δ. Keep $V_{1/2}$ and g_{max} in common (-150 mV and 0.5 mS), only change the value of δ from -3 to -1.
C: The effect of $V_{1/2}$. Keep δ and g_{max} in common (-2 and 0.5 mS), only change the value of $V_{1/2}$ from -200 mV to -100 mV.

All Kv K^+ channels are located to the PM. According to their function, shaker K^+ channels can be subdivided among four groups, inward-rectifying (K_{in}), silent (K_{silent}), weakly rectifying (K_{weak}) and outward-rectifying (K_{out}) K^+ channels. The current characteristics of each group K^+ channels are shown in Figure 1-9.

Members of the K_{in} channel group facilitate K^+ uptake into the cell. These channels typically open at voltages negative of -80 to -100 mV and this threshold is not sensitive to the K^+ ion concentration outside the cell (Dreyer and Blatt, 2009). In *Arabidopsis*, the K_{in} group includes AKT1, AKT5, KAT1, KAT2, and SPIK. AKT1 is mainly expressed in root; AKT5 and SPIK are expressed in flower and pollen tube; KAT1 and KAT2 are found in guard cells and also several other tissues (Gambale and Uozumi, 2006; Lebaudy et al., 2007). K_{silent} channels do not form functional channels alone, but only when assembled with other K_{in} channel subunits and thereby regulate channel gating. In *Arabidopsis*, only KC1 belongs to the K_{silent} group. KC1 is expressed in root epidermis, but is also found in other cell types, including guard cells. It preferentially assembles with K_{in} subunit AKT1 and affects channel gating by moving activation to more negative voltages compared to AKT1 alone (Reintanz et al., 2002; Duby et al., 2009). In plant roots, the AKT1-KC1 channel has a more negative value of activation compared to AKT1 alone, which can help plant to avoid K^+ ion loss through the channel at intermediate voltages and under K^+-limiting conditions (as shown in Figure 1-9 b).

The third group of Kv K^+ channel is that of the K_{weak} channels. These channel subunits may assemble with K_{in} channel subunits like K_{silent} but do not affect the activation threshold of the heterotetramer. Instead, after coexpression of K_{weak} and K_{in} channel subunits, the channel shows two current modes in different range of voltages (Marten et al., 1999; Dreyer et al., 2001; Xicluna et al., 2007). As shown in Figure 1-9 c, the first mode leads to gating analogous to that of the K_{in} channels; the second mode

gives a channel that is a little open over the entire physiological voltage range. There is only one K_{weak} channel subunit AKT2 in *Arabidopsis*. K_{in}, K_{weak} and K_{silent} subunits are able to mediate K^+ influx, and they can assemble heteromeric channels with one another (Obrdlik et al., 2004; Xicluna et al., 2007; Lebaudy et al., 2008).

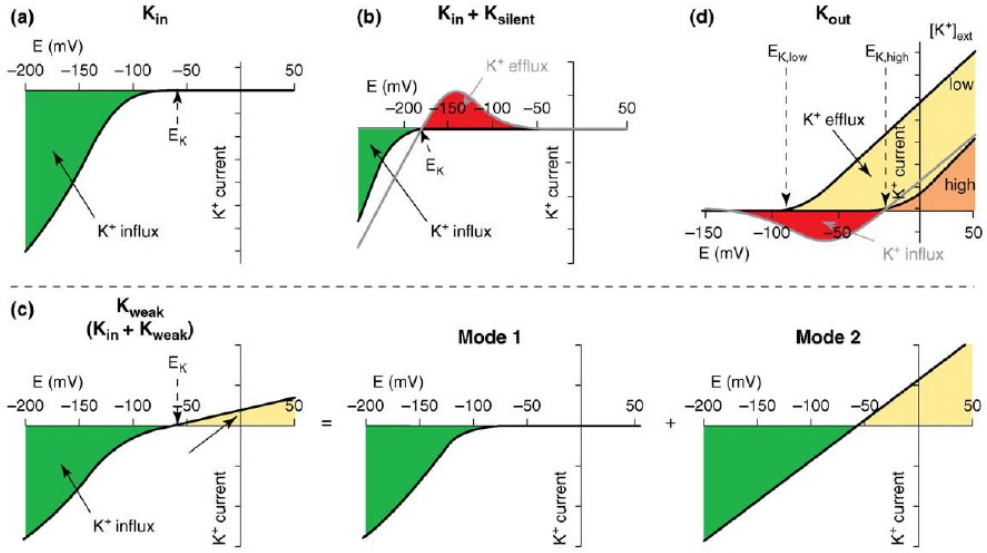

Figure 1-9. Current characteristics of voltage-gated K^+ channels from plants

(a) K_{in} channels mediate K^+ influx.
(b) K_{silent} subunits assemble with K_{in} subunits and modify their gating properties to displace channel gating (opening) to more negative voltages. A normal K_{in} channel would open at moderate negative voltages (grey curve), resulting in K^+ loss through the channel assembly at intermediate voltages (red shading) and very negative E_K.
(c) K_{weak} channels or heteromeric channels between K_{weak} and K_{in} subunits show a bimodal gating behaviour (Mode 1 and Mode 2).
(d) K_{out} channels mediate K^+ efflux. Unique to these channels, voltage-dependent gating adjusts with the extracellular K^+ concentration (shift of the black curves in high and low K^+). Without this K^+-sensitivity, these channels would provide a shunt pathway for K^+ influx when the external K^+ concentration is high (gray curve, red shading).
Images were adapted from previous publication (Dreyer and Blatt, 2009).

The last group is that of the K_{out} channels. These channels open with membrane depolarization and permit K^+ ion efflux. They give an outwardly rectifying current as shown in Figure 1-9 d. The gating of K_{out}

channels is sensitive to both membrane voltage and extracellular alkali cation concentration (Blatt and Gradmann, 1997; Johansson et al., 2006). The K_{out} channel subunits do not assemble with K_{in}, K_{weak} and K_{silent} subunits (Dreyer et al., 2004). In *Arabidopsis*, GORK and SKOR are the only K_{out} channel subunits. SKOR is mainly expressed in root stellar tissue and contribute to solute loading of the xylem (Gaymard et al., 1998). GORK is expressed strongly in guard cells where it facilitates K^+ loss from guard cells during stomatal closure (Hosy et al., 2003). It is also expressed in root epidermal cells and root hairs (Ache et al., 2000; Ivashikina et al., 2001). In an analysis of fluorescence-tagged GORK in guard cells, Eisenach et al. (2014) found GORK could assemble in puncta in the PM of guard cells like KAT1, and it dissociated in response to external K^+. This redistribution had close relationship with GORK channel gating, but is not associated with endocytic traffic.

1.6.5 The regulation of Kv K^+ channels

Kv K^+ channels are affected by a number of stimuli, including hormones such as ABA and auxin, metabolites, and pathogen elicitors. The stimuli related to channel regulation include transcription/translational processes, post-translational modification, ligand and voltage regulation, and membrane trafficking.

In general, over the longer term K^+ channels are regulated at the transcriptional and translation levels. Pilot et al. (2003) have shown that K^+ deficiency decreased the mRNA level of AKT2 in shoot and SKOR in root, while Shin and Schachtman (2004) find KC1 level was up regulated under K^+ starvation. Salt stress also induced KC1 transcription and decreased the level of AKT2 mRNA after 7 days treatment (Pilot et al., 2003). Transcription and translation were also affected by various endogenous signals. ABA treatments were found to decrease KC1 and SKOR mRNA levels; the auxin antagonist 2,4-D strongly reduced

transcript accumulation of KC1, AKT1, and SKOR; and 6-Benzylaminopurine treatment inhibited the transcription of SKOR and decreased the transcription of AKT1 and KC1 (Pilot et al., 2003). In maize, auxin treatment enhanced the mRNA level of ZMK1, a Kv like K_{in} channel in *Zea mays* (Philippar et al., 1999).

Kv K^+ channel assembly also constitutes a mode of regulation. In general, Kv channels are assembled of four polypeptides, each consisting of the six transmembrane domains with the last two α-helices contributing $1/4^{th}$ of the pore. As mentioned before, K_{in}, K_{weak}, and K_{silent} subunits all can form functional channels when assembled with one another. For example, guard cells commonly assemble functional channels as heterotetramers of KAT1 and KAT2, although AKT1, AKT2, and KC1 are expressed at low levels (Szyroki et al., 2001; Lebaudy et al., 2008). When heterologously expressed in *Xenopus* oocytes, none of these genes alone formed a channel that fully matching the properties of native K^+ current in plant (Bruggemann et al., 1999), consistent with the idea that the native channels need to be composed of a combination of subunits. The functional K^+ channels were assembled in plant in homomeric way (Lebaudy et al., 2008). Electrophysiological analyses have provided evidence that heteromeric shaker channels can be formed on co-expression of AKT2 with KAT1 (Baizabal-Aguirre et al., 1999), KAT1 with KAT2 (Pilot et al., 2001; Lebaudy et al., 2008), AKT2 with KAT2 (Xicluna et al., 2007), and AKT1 with KC1 (Reintanz et al., 2002). In the case of AKT1 and KAT1, Dreyer et al. (1997) reported that coexpression of AKT1 and a Ca^{2+} sensitive KAT1 mutant in oocytes altered the Ca^{2+} sensitivity of the K^+ current . As noted previously, KC1 also serves as a regulator to shift the voltage dependence of the K^+ current formed with AKT1 and prevents net K^+ efflux through these channels. Only for K_{out} channel is the evidence consistent with their assembly of four homologous subunits, either GORK or SKOR (Dreyer et al., 2004).

Other proteins contribute to the regulation of channel activity, generally through post-translational modification and/or interactions. One example is the regulation by 14-3-3 proteins. These proteins are known for their role in the control of ion transport across plasma and vacuolar membrane through interaction with the plasma membrane H^+-ATPase and the tonoplast VH^+-ATPase. It also directly interacts with KAT1 (van den Wijngaard et al., 2005). Furthermore, Sottocornola et al. (2006) have shown that injecting recombinant plant 14-3-3 protein into oocytes displaces the KAT1 conductance-voltage curve to more positive voltages.

Post-translational regulation of Kv K^+ channels commonly depends on small molecular intermediates, like reactive oxygen species (ROS), cytosolic-free Ca^{2+}, pH, as well as direct modifications of the channel proteins through protein phosphorylation. ROS are important signals in plant cells. They are produced in response to a number of stimuli, including major biotic and abiotic stresses (Apel and Hirt, 2004). ROS include singlet O_2, hydroxyl radical ($\cdot OH$), hydrogen peroxide (H_2O_2), superoxide radical ($\cdot O_2^-$; Wang and Jiao, 2000). In plant cells, they are essential for development, stress signalling, pathogen defence, and other physiological processes (Grant and Loake, 2000; Gapper and Dolan, 2006; Zhang et al., 2013). ROS can modify directly the primary sequences of many proteins and thereby alter the structure and activity of protein (Stone and Yang, 2006). Exogenous ROS (H_2O_2) enhanced current amplitude and activation kinetics of SKOR, and the effects were reversed by the reducing agent dithiothreitol. By further mutating the 11 cysteine residues of SKOR, a single residue, Cys^{168}, located within the S3 α-helix of the voltage sensor complex, was found to be the target of ROS in SKOR (Garcia-Mata et al., 2010). ROS also regulates the other K_{out} channel GORK. The primary sequences of the two channels are extremely close, and all of the relevant Cys residues are conserved, so it is likely that GORK is regulated by ROS the same way as SKOR is.

GORK is also regulated by ROS on transcription level. Exposure to ozone induces ROS burst in *Arabidopsis* and activates K^+ outward-rectifying currents related to GORK; these effects are associated with up-regulation of the mRNA level of GORK (Tran et al., 2013). Shin and Schachtman (2004) reported that K^+ deficiency induced ROS burst in root could active K^+ uptake, suggesting ROS also regulated K_{in} channels.

Cytosolic-free Ca^{2+} is another important messenger in plant cells as noted before. Resting $[Ca^{2+}]_i$ in plants, as in all living cells, is normally very low, typically held at about 100 nM. It may be elevated to micromolar concentrations briefly under some circumstances and can mediate the downstream responses including the regulation of Kv K^+ channels (Blatt, 2000). For example, in guard cells, increasing $[Ca^{2+}]_i$ inhibits K_{in} channels at the PM, which leads to a fall in turgor of guard cells and stomatal closure. Some K^+ channels may be activated directly by Ca^{2+}. As mentioned above, some of the TPK channels contain two Ca^{2+}-binding EF-hands in the C-terminal domain (Latz et al., 2007; Becker et al., 2004), which may couple them to directly Ca^{2+} signals.

Other K^+ channels are regulated by Ca^{2+} through their interaction with proteins that serve as Ca^{2+} sensors. Among the Ca^{2+} binding proteins known to regulate channel activities, three families have been identified in plant cells. The first family is that of calmodulin (CaM) and CaM-related proteins, which contain four Ca^{2+} binding domains (Snedden and Fromm, 2001; Luan et al., 2002); the second family is that of the Ca^{2+}-dependent protein kinases (CDPKs) which have CaM-like Ca^{2+}-binding domains and a kinase domain (Harmon et al., 2000); and the third is that of the calcineurin B-like (CBL) proteins that are similar to both the regulatory B-subunit of calcineurin and the neuronal Ca^{2+} sensor in animals (Kudla et al., 1999; Luan et al., 2002).

Calcium-dependent protein kinases were first identified in plant in 1991 (Harper et al., 1991). CDPK proteins contain a variable N-terminal

domain, a catalytic domain, a junction domain containing an autoinhibitory segment, and a C terminal end of the kinase catalytic domain, which is fused to a regulatory calmodulin-like domain that contains four functional Ca^{2+}-binding EF-hands (Takahashi and Ito, 2011). They are activated upon Ca^{2+} binding to the four EF hands in C terminus, which makes them effective switches for the transduction of Ca^{2+} signals (Harper and Harmon, 2005). In guard cell of *Vicia faba*, micromolar $[Ca^{2+}]_i$ has been shown to activate CDPKs and stimulate phosphorylation of several proteins (Li et al., 1998). In the same report about *V. faba*, after incubating the in vitro-translated KAT1 with CDPK, the phosphorylation of KAT1 was shown by adding [γ-^{32}P]ATP in autoradiography. Coexpression of CDPK with KAT1 in oocytes has also been shown to alter the kinetics and magnitude of induced K^+ currents (Berkowitz et al., 2000), which supports a model of Ca^{2+} dependent K^+ channel regulation mediated by CDPK.

Kv K^+ channels in plants are also regulated through a network of calmodulin-binding-like (CBL) proteins that interact with specialized protein kinases, the so-called Calcineurin B-like molecule interacting protein kinase (CIPKs). CBLs can be found only in higher plants, suggesting they may function in plant-specific signalling processes. In *Arabidopsis*, there are at least ten CBLs (Kohler et al., 1999; Kim et al., 2000) and at least 25 genes for putative CIPKs (Luan et al., 2002). CBLs, like CaM, have several EF-hand domains, which bind with Ca^{2+}. CBLs interact with CIPKs and activate their kinase activity under micromolar level of $[Ca^{2+}]_i$ (Wu et al., 2010). The CBL-interacting domain of CIPKs may allow block of the kinase active site, and after Ca^{2+} dependent interaction, the kinase domain of CIPK could be released for substrate access (Guo et al., 2001). Some CBLs, like CBL1, 4, and 9, are located to membrane. CBL1 and CBL9 can target CIPK1 and CIPK23 to the PM (Ishitani et al., 2000; D'Angelo et al., 2006; Xu et al. 2006), which suggests these proteins may be positioned to phosphorylate membrane

associated proteins like K^+ channels. A screening for *Arabidopsis* mutants sensitive to low K^+ led to the isolation of *lks1* which harbored a mutation in the gene encoding the CIPK23. CIPK23 was strongly up-regulated in response to low K^+ and the *lks1* mutation reduced K^+ uptake and caused growth inhibition (Xu et al. 2006). Xu et al. (2006) have suggested that low-K^+ stress signals could trigger $[Ca^{2+}]_i$ elevation, which would lead to the binding between CBL1 and CBL9 with CIPK23. CIPK23 directly interacts and phosphorylates the AKT1 in plant. The interaction between CIPK23 and AKT1 was shown to involve the kinase domain of CIPK23 and the ankyrin repeat domain of AKT1 (Xu et al., 2006). In *cipk23* mutant plants, the role of CBL1/9-CIPK23 in root K^+ uptake via phosphorylation of AKT1 was confirmed (Cheong et al. 2007). Furthermore, it was shown that dephosphorylation of AKT1 by the PP2C phosphatase inactivated AKT1 (Lee et al., 2007). The experiment in *Xenopus* oocytes supports this result. K^+ current of AKT1 required coexpression with CBL1 and CIPK23 in oocytes (Honsbein et al., 2009). Lan et al. (2011) found CBLs physically interacted with and inactivate PP2C phosphatases to recover the CIPK-dependent AKT1 channel activity in oocytes, suggesting there was a signaling network consisting of CBL–CIPK–PP2C interactions in the activation of the AKT1 channel.

Finally, channel trafficking is involved in the Kv K^+ channel regulation. As mentioned before, KAT1 is localized at the PM in puncta from which ABA has been shown to trigger its endocytosis; recycling to the plasma membrane is also dependent on SYP121 (Sutter et al., 2006; Sutter et al., 2007). The traffic of channel proteins is dependent on SNAREs related membrane fusion, the role of SNARE-ion channel interaction in plants will be introduced in next section.

1.6.6 Ion channel interaction with SNARE proteins

The Qa-SNARE protein SYP121 (=SYR1/PEN1) of tobacco (*N.*

tocacum) and *Arabidopsis* was first identified by the Blatt group in a search for the ABA receptor (Leyman et al., 1999). Like other Qa-SNAREs, SYP121 contains a three-fold domain (H_{abc}) with a high probability for forming coiled-coil structures in protein-protein interactions, a SNARE motif which is important for SNARE complex formation, and a transmembrane domain at the C terminus (See Figure 1-2). Initial studies showed that SYP121 was found throughout the plant and located to the PM (Leyman et al., 2000). More recently, SYP121 has been identified with traffic also at the trans-Golgi network, possibly indicating a cycling of the Qa-SNARE itself or suggesting additional roles for the Qa-SNARE in membrane vesicle cycling between the PM, early endosomes and the Golgi (Drakakaki et al., 2012). ABA treatment, salt stress, and wounding induced SYP121 expression in plant, while cold stress and other hormones including auxin, kinetin, and gibberellic acid did not (Leyman et al., 2000). These findings supported the idea that SYP121 is involved in a subset of abiotic stress responses, especially associated with ABA signalling. Leyman, et al. (1999) introduced the Sp2 fragment as a soluble truncated version of SYP121 lacking the C-terminal membrane anchor. The Sp2 fragment was shown to interfere with SYP121 function by competing with SYP121 for its binding partners (Geelen et al., 2002). Expressing the Sp2 fragment under control of an inducible promoter also altered leaf development, suppressed the root growth, and blocked the transport of a secreted YFP to the apoplast, suggesting that SYP121 was involved in SNARE-mediated secretory vesicle traffic (Geelen et al., 2002; Sutter et al., 2006; Tyrrell et al., 2007). Subsequent studies have taken advantage of mutants of SYP121 and its close homologue SYP122. The *syp121* and *syp122* single mutants normally have no visible phenotype, indicating that these proteins have overlapping functions; only the *syp121/syp122* double mutant shows phenotypes of dwarfing, abberant development and severe necrosis (Zhang et al., 2007). However, phenotypes specific for both SYP121 and SYP122 are

known (Eisenach et al., 2012; Nuhse et al., 2003).

In 2003, the role of SYP121 in plant disease resistance was found. In response to 'non-host' pathogen attack, SYP121 and its functionally homologue in barley, ROR2, were shown to form a binary SNARE complex with Qb+c SNARE HvSNAP-34 and facilitated the exocytosis (Collins et al., 2003). In 2008, the SNARE complex containing Qa-SNARE SYP121/SYP122, Qb+c SNARE SNAP33, and R-SNARE VAMP721/722 were found in *Arabidopsis* immune response to non-adapted powdery mildew fungi such as *Blumeria graminis* and *Erysiphe pisi* (Kwon et al., 2008). It was worth to mention that the function of SYP121 in penetration resistance remains enigmatic. It is hard to visualize how a secreted SNARE can mediate the membrane fusion in apoplast, so the accumulation of SYP121 may play a role as a papillary marker without direct effect on penetration resistance (Nielsen and Thordal-Christensen, 2013).

Zhang et al. (2008) found 365 genes were at least two fold up-regulated in *syp121/syp122* double mutant compared to wild type *Arabidopsis*, most of these genes were also up-regulated during expression of pathogen defense, this result suggested that SYP121 and SYP122 appeared to avoid over stimulation of some defences. They also reported that the salicylic acid level was dramatically elevated and the jasmonic acid signalling marker, PDF1.2, was also highly upregulated in syp121/syp122 double mutant, indicating these two Qa-SNAREs functioned as a negative regulator of some biotic stress induced defence pathways.

The evidence outlined above is largely consistent with roles for the Qa-SNAREs in traffic. However, a number of observations also were inconsistent with such an interpretation, especially for SYP121. As noted before, SYP121 was first discovered in ABA-dependent regulation of stomata closure. Disrupting function of SYP121 by cleavage with *Clostridium botulinum* type C Toxin or competition with a soluble

truncated version of the protein (Sp2 fragment) suppressed ABA-dependent regulation of the K^+ and Cl^- channel currents in tobacco guard cells (Leyman et al., 1999). Further research reported that the Sp2 fragment could shift the activation voltage of Ca^{2+} channels in the guard cells to more negative voltages and affect the voltage-evoked $[Ca^{2+}]_i$ (Sokolovski et al., 2008). These studies suggest SYP121 can regulate the activity of ion channels. What is the regulation mechanism?

Previous reports (Sutter et al., 2006; Sutter et al., 2007) have answered this question in relation to vesicle trafficking. KAT1 was tagged with hemagglutinin (HA) epitopes and a photoactivatable green fluorescent protein (paGFP) to monitor the channel distribution and trafficking dynamics in tobacco leaves. The results showed that KAT1 is located in discrete puncta at the PM. Under ABA treatment, KAT1 transferred from the PM to an endosomal membrane pool and after ABA washout, KAT1 could recycle back to the PM. Coexpression of tagged KAT1 and Sp2 fragment of SYP121 suppressed KAT1 traffic and affected the channel distribution in puncta in the PM. Subsequently, Eisenach et al. (2012) linked KAT1 traffic with its function in K^+ uptake and stomatal movements. These studies indicated that traffic of the channels was largely dependent on SYP121, not SYP122, and that the channels were recycled to the PM following ABA-evoked endocytosis. In the *syp121* mutant, traffic was suppressed, which led to a slowing of stomata reopening. These results show that ion channel regulation is dependent on SNARE-mediated vesicle trafficking. However, these studies also show that recycling/traffic of channels is 10-fold slower than the SNARE-dependent changes in channel activity observed with ABA, which suggests there are other channel regulation pathways possibly invovling direct interaction with SNAREs.

Honsbein et al. (2009) were first to report that a plant SNARE could interact with Kv K^+ channels and regulate channel gating. They used yeast mating-based split-ubiquitin system (mbSUS),

co-immunoprecipitation, and bimolecular fluorescence complementation (BiFC) assays to confirm the directly interaction between SYP121 and KC1. Fluorescence recovery after photobleaching (FRAP) and fluorescence loss in photobleaching (FLIP) experiments showed that this interaction did not affect the distribution and transport of AKT1-KC1 K^+ channels. After coexpression of AKT1, KC1, and SYP121 in oocytes, they found SYP121 could rescue the AKT1-KC1 K^+ current. In *Arabidopsis* roots, KC1 and AKT1 form the functional K^+ channel which transports K^+. The *kc1*, *akt1*, and *syp121* mutant *Arabidopsis* seedlings showed similar suppressed growth in low K^+-medium with NH_4^+ (in which the K^+ transporters were blocked and the K^+ uptake was only dependent on K^+ channel; Honsbein et al., 2009). In conclusion, KC1, AKT1, and SYP121 appear to assemble a tripartite protein complex for K^+ uptake in root and SYP121 promotes the AKT1-KC1 K^+ channel gating. This research has shown SNARE-mediated ion channel regulation independent of vesicle trafficking. In other words, the complex among AKT1-KC1-SYP121 serves as a molecular governor, keep channel-mediated uptake of the osmotically active K^+ in check and coordinate its transport with changes in cell volume (Grefen and Blatt, 2008).

Qa-SNAREs like SYP121 include a number of protein domains that are important for SNARE complex formation (Brunger et al., 2005). If the SNARE-ion channel interaction mentioned above is not related to vesicle trafficking or signalling, then it raises the question whether the K^+ channels bind with the same domain of SYP121 which is used for vesicle trafficking. KC1 interacted with SYP121, but not its closest homolog SYP122 (Honsbein et al., 2009). Therefore, Grefen et al. (2010 a) prepared chimeras by exchanging N terminal domains between SYP121 and SYP122. They found residues within the N terminal first 12 amino acids were essential for SYP121 interaction with KC1 by mbSUS and BiFC. Using single mutants of SYP121, they then showed that a minimal

sequence motif FxRF was essential for KC1 binding. Electrophysiology in oocytes and in wild type or *syp121* mutant *Arabidopsis* complemented with the mutant forms of SYP121 identified this FxRF motif was the minimal requirement for the channel gating regulation (Grefen et al., 2010 a). SYP121 also interacted with KAT1 and such interactions depended on the same motif (Honsbein et al., 2011), suggest KAT1 may be regulated by SYP121 through both trafficking dependent and independent pathways. So, unlike the interaction between Q-SNARE with channels in animals (Michaelevski et al., 2003; Cui et al., 2004), SYP121 binds with K^+ channels dependent on a novel FxRF motif in N terminus, not the SNARE motif. The N terminus of Qa-SNARE is important in regulating SNARE complex formation and vesicle traffic. Thus, K^+ channel binding to SYP121 may occupy the same sites as other proteins, and the interaction may this way affect vesicle trafficking. Recently, the channel binding site on SYP121 in *Arabidopsis* was found to overlap with that for the SM protein SEC11 (Karnik et al., 2013 a), which highlights the possible role for the K^+ channels to initiate a handover with SEC11 binding at this site and release SYP121 for SNARE assembly. These results mentioned above present a different way to support the idea that SNARE-ion channel interaction that coordinates membrane traffic with osmotically active solute transport in the plant.

SNAREs have been shown interact with ion channels In mammalian cells. For example, the voltage-gated K^+ channel Kv1.1 interacts with Syntaxin 1A, a neuronal form of syntaxin, similar to SYP121 in *Arabidopsis* (Sanderfoot et al., 2000). Syntaxin 1A binds the N terminus of Kv1.1, increasing the extent of inactivation of the channel and affecting the current amplitude (Fili et al., 2001; Michaelevski et al., 2002). Kv2.1 is a slow-inactivating delayed rectifier Kv channel. In neuroendocrine cells, Kv2.1 interacts both with syntaxin 1A and SNAP-25 (Michaelevski et al., 2003; Tsuk et al., 2008). Coexpression of Kv2.1 with these two SNARE

proteins in oocytes, affected the activation of the channel. Coimmunoprecipitation analysis showed that SNAP-25 alone bound weakly to Kv2.1 and syntaxin 1A enhanced the binding of SNAP25 with Kv2.1 (Michaelevski et al., 2003). At least one R-SNARE protein also interacts with mammalian channels. Mammalian VAMP2 is the cognate partner of Syntaxin 1A. VAMP2 and Syntaxin 1A form a SNARE complex with SNAP25 for transmitter and hormone release by exocytosis (Sudhof, 1995). VAMP2 also binds with the Kv2.1 channel in vitro and enhances the channel inactivation when expressed in oocytes (Lvov et al., 2008). This interaction is lost on assembly of the SNARE core complex in vitro (Tsuk et al., 2008), suggesting that the channel bound with the SNARE motif of VAMP2.

Finally, SNAREs in animals have been shown to interact with Ca^{2+} channels and affect their gating. Syntaxin 1A was shown early on to bind with voltage-gated Ca^{2+} channels (Catterall, 1999; Bezprozvanny et al., 2000). Again, the channel binding site of Syntaxin 1A is associated with the SNARE motif of the Qa-SNARE (Bezprozvanny et al., 2000; Cui et al., 2004; Tsuk et al., 2005), which assembles with the cognate SNARE proteins to form the core complex during vesicle fusion. These reports shown SNARE proteins can interact with ion channel and affect their electrophysiological properties in mammalian, all of which depend on the SNARE motif.

1.7 Aim of the thesis

In guard cells of *Arabidopsis*, Leshem et al. (2010) found that the ABA-dependent stomatal closure was suppressed when the expression of VAMP71 family genes were suppressed by an antisense VAMP711 construct. Such results reveals that VAMP proteins play an important role in plant response to stress, especially in the regulation of stomatal closure under ABA treatment. Some VAMPs (like VAMP721 and

VAMP722) can form SNARE complex with SYP121 at the PM (Kwon et al., 2008), and of course SYP121 can interact and regulate KC1 and KAT1 K^+ channels at the PM (Honsbein et al., 2009; Honsbein et al., 2011). These findings raise the question whether the VAMPs also can interact with K^+ channels and regulate their channel gating.

The first goal of this study was to answer the question whether there is interaction between the VAMP7 group proteins and one or more K^+ channels. I investigated the interaction between the VAMP7 proteins with different K^+ channels (KC1 and KAT1, which are shown to interact with SYP121) by mating based Split-Ubiquitin System assay, and verify these interactions by ratiometric bimolecular fluorescence complementation assay. Then the interacting and non-interacting VAMPs (VAMP721 and VAMP723) were chosen for further research.

A second goal of this study was to identify the domain of VAMP721 required for the SNARE-ion channel interaction. Some VAMP7 proteins show a very high homology; in the VAMP72 subfamily, VAMP721, 722, and 723 have 83% amino acids that are similar in sequence. I prepared domain exchanged chimeras to isolate the important domain for interaction. After that, I identified the minimal sequence requirement for the VAMP-channel interaction.

The previous work described above links vesicle trafficking and ion channel activity by SNARE-ion channel interactions (Honsbein et al., 2009; Grefen et al., 2010). Thus, the third goal of this study was to investigate the functional meaning of the VAMP-channel interactions. I performed electrophysiological research using *Xenopus* oocytes and *Arabidopsis* to show the effect of VAMP on K^+ channel gating. Finally, in order to investigate the effect of VAMP-channel interaction on trafficking, the traffic rescue analysis in vivo was performed and the results quantified on the confocal microscope.

Chapter 2: Material and Methods

2.1 General Material and Methods

All chemicals were purchased from Sigma Aldrich (Poole, UK), VWR International (Poole, UK), and Fisher Scientific (Southampton, UK) unless otherwise stated. Enzymes for molecular biology were purchased from Invitrogen (Life Technologies, Paisley, UK), New England Biolabs (NEB, Hitchin, UK), and Promega (Madison, USA). All primers were purchased from Invitrogen.

PCR

All primers used in the experiments are listed in the Appendix Table 1 (pp 230). Calculation of primers' annealing temperature was performed with the NetPrimer Analysis Software (http://www.premierbiosoft.com/netprimer), which analyzed primer melting temperature using the nearest neighbor thermodynamic theory to ensure accurate melting temperature prediction. Primers were stored in a concentration of 100 μM. The dNTP mixture (2 mM of each NTP) and $MgSO_4$ solution (25 mM) were provided with the KOD Hot Start DNA Polymerase (Novagen, USA) .

PCR reaction were prepared in 0.2 ml standard thin-walled PCR tubes. As a general rule, the PCR reaction mix was prepared and kept on ice until the lid of the Thermal Cycler (PTZ-200, MJ Research) was preheated to 104 °C. Then the program was paused until insertion of the tube of PCR reactions mix. This step can minimise template degradation by 3'-5' exonuclease activity of the DNA Polymerase.

For the purpose of amplifying the DNA of VAMPs from *Arabidopsis* genomes template or cloning PCR products into plasmids, the PCR reaction was carried out with the KOD Hot Start DNA Polymerase

(Novagen, USA) as follows in the first table below. The typical cycling conditions used for gateway-clone system (Life Technologies, Paisley, UK) are given in the second table below.

Table 2-1. Set-up of PCR reaction

component	μl added/reaction
10x Reaction Buffer	5
dNTP mix (2mM each)	5
$MgSO_4$ (25 mM)	5
primers (10 μM)	1.5 forward and reverse
template plasmid (100 ng/μl) or plant genome	1
KOD	1
distilled water	to 50

Table 2-2. Setting of PCR reaction

frequency	step	temperature (°C)	duration (sec)
1x	initial denaturation	95	120
10x	denaturation	95	10
	primer annealing	individual + 3	10
	primer extension	72	20
15x	denaturation	95	10
	extension	72	20
1x	final extension	72	120
1x	Final temperature	4	∞

DNA quantification and sequencing

DNA was quantified by measuring the absorbance (in optical density units) of a suitable dilution in distilled water at 260 nm. A 50 μl UVette 220-1600 nm single sealed cuvette (Eppendorf, Germany) was used in combination with the Eppendorf BioPhotometer plus (Eppendorf, Germany). The absorbance value, corrected against a distilled water blank, was multiplied with the dilution factor 50 (40) to obtain DNA (RNA) concentration in ng/μl. DNA sequencing was carried out by GATC Biotech (Cologne, Germany). Sequencing data were analysed with the SeqMan (part of the DNASTAR software).

Restriction enzyme digests

PCR products and plasmids were digested with restriction enzymes that were obtained from NEB. All digests were carried out in a volume of 20 µl at 37 °C for 1 hours as follows in the table below. Reaction buffer were added according to the manufacturer's instructions. After digestion, the samples were generally separated on agarose gels, the desired DNA bands excised and eluted from the gel as described above. A double digest was performed with two enzymes that were able to work efficiently in the reaction buffer according to the Double Digest Finder of NEB (https://www.neb.com/tools-and-resources/interactive-tools/double-digest-finder).

Table 2-3. Set-up of a standard restriction digest reaction

component	µl added/reaction
restriction enzyme	0.25 (~5 unites)
DNA	1 (~1 ㎎)
10X buffer	2
distilled water	to 20

DNA ligation reactions

All ligation reactions of cohesive and blunt DNA ends were carried out with T4 DNA ligase (NEB, Hitchin, UK). Reactions were set up according to the introduction from the manufacturer. The 10x Ligase buffer was stored in small aliquots to avoid degradation of its ATP content. The insert:vector ratio of 6:1 and 9:5 were used. In general, the incubations were at 4 °C overnight. The ligation reaction product was used for CCDB *E.coli* transformation.

Agarose gel electrophoresis and gel purification

PCR products or restriction enzyme digests were resolved by agarose gel electrophoresis after appropriate addition of 6x loading buffer (0.25 % bromophenol blue, 0.25 % xylene cyanol, 15% Ficoll) to achieve a final 1x dilution. In general, for expected fragments of 400-3000 bp, a 1.5 % agarose gel was used: 1.5 % agarose powder dissolved in 1 x TAE and 50 µl/l ethidium bromide solution (50x TAE stock solution: 2 M Tris, 5.7 % acetic acid, 50 mM EDTA). Separation of DNA bands was performed in 1x TAE buffer by application of 100-150 V for approx. 15- 30 min. DNA bands were visualised under UV light on a GelDoc 2000 scanner (Bio-Rad). Where necessary, DNA bands were

excised under UV light. DNA was extracted from the agarose with the PureLink™ Quick Gel Extraction and PCR Purification Combo Kit (Life Technologies, Paisley, UK) according to the manufacturer's instructions. Elution was always performed with distilled water.

Preparation of chemical-competent *E.coli*

One tube of TOP10 *E.coli* cell was cultured as seed in 5 ml LB medium (10 g/l NaCl, 10 g/l Tryptone, and 5 g/l Yeast Extract. The media were used in sterile conditions after autoclaving. For plates, 10 g/l Agar was added) with streptomycin (10 mg/l). The seed culture were incubated at 37 °C 180 rpm overnight. Then added the seed culture into 500 ml LB medium with streptomycin (10 mg/l) and cultured for around 3 h at 37 °C until the OD600 was 0.3-0.4. Before harvesting the cells at 4000 g (Multifuge 3 S-R, Heraeus), 5 min, 4 °C, they were incubated for 10 min on ice. All the following steps were performed on ice as well. Cells were washed by resuspension in 100 ml pre-cooled sterile 100 mM $MgCl_2$ and spun down at 4000 g, 5 min, 4 °C. The cell pellet was resuspended in 50 ml pre-cooled sterile 100 mM $CaCl_2$ and centrifugate as above. The final cell pellet was resuspended in 10 ml pre-cooled sterile TB solution (100 mM $CaCl_2$ and 15% Glycerol). After that, the *E.coli* cells were aliquoted (100 μl) into Eppendorf tubes by filling them quickly with a multipette. The aliquots were stored at -80 °C.

Calculating Transformation Efficiency

The transformation efficiency of competent cells were calculated according to the protocal from Invitrogen (Life Technologies, Paisley, UK). The pUC19 DNA was transformed into one tube (100 μl) of TOP10 competent cells (see below). Then used the following formula to calculate the transformation efficiency.

Transformation efficiency (# transformants/μg DNA) =

$$\frac{\#\text{ of colonies}}{10\text{ pg pUC19 DNA}} * \frac{10^6\text{ pg}}{\mu\text{g}} * \frac{100\ \mu\text{l total volume}}{50\ \mu\text{l plated}} * 10$$

The competent cells with transformation efficiency more than $1*10^8$ were used in the experiment.

Transformation of chemical-competent *E.coli*

Transformation of chemical-competent TOP10 *E.coli* was performed with the following heat shock procedure:

1. Take competent cells out of -80°C and thaw on ice (approximately 20-30min).
2. Mix 1 to 5 μl of DNA (usually 10 pg to 100 ng) into 100μL of competent cells in a microcentrifuge or falcon tube. Gently mix by flicking the bottom of the tube with finger.
3. Place the competent cell/DNA mixture on ice for 30min.
4. Heat shock each transformation tube by placing the tube into a 42°C water bath for 30 seconds.
5. Put the tubes back on ice for 2 min.
6. Add 200 μl LB media without antibiotic and grow in 37°C shaking incubator for 1 h.
7. Plate some or all of the transformation onto a LB agar plate containing the appropriate antibiotic (see table below).
8. Incubate plates at 37°C overnight.

Table 2-4. The antibiotics used in this research

antibiotic	final concentration (mg/l)
ampicillin	100
kanamycin	25
spectinomycin	100
gentamycin	20

Plasmid minipreps

Single colonies were picked with a sterile toothpick and inoculated into 4 ml liquid sterile LB medium containing antibiotics as required. The cultures were grown on a shaker at 37 °C (TOP10 *E.Coli*) or 28 °C (*Agrobacterium*), 180 rpm overnight. Cells were harvested by centrifugation at maximum speed in a microcentrifuge for one minute at room temperature. The plasmids were extracted with the following protocol.

Table 2-5. The buffer used for plasmid minipreps

Buffer 1	50 mM Tris-Cl pH 8.0, 10 mM EDTA, 10 μg/ml RNAse A, 10 μg/ml Lysozyme
Buffer 2	200 mM NaOH, 1 % SDS
Buffer 3	3 M K acetate, adjust pH to 5.5 by acetic acid
TE buffer	10 mM Tris-HCl pH 8.0, 1 mM EDTA

1. Transfer overnight culture to a 2 ml Eppendorf tube, and spin down cell culture at high speed for 1 min at room temperature.
2. Discard the supernatant. To remove the liquid completely by upside down tube onto a piece of paper towel for a few seconds.

3. Add 400 μl of Buffer 1 into each tube, and vortex to completely resuspend cell pellet.

4. Add 400 μl of Buffer 2 and mix by gently inverting the tube 5-6 times.

5. Add 400 μl of Buffer 3 and mix by inverting the tubes several times.

6. Centrifuge the tubes at high speed at room temperature for 10 min.

7. Carefully transfer the supernatant to a new labeled 2 ml Eppendorf tube and add same volume of Chloroform:isoamylalcohol solution (24:1). Mix well and centrifuge the tubes at high speed at room temperature for 5 min.

8. Transfer the supernatant (~850 μl) to a new labeled 2 ml Eppendorf tube and add same vulome of ice-cold isopropanol (850 μl). Invert several times to mix solution well.

9. Centrifuge full speed for 20 min at 4 °C. Pour off supernatant.

10. Add 500 μl ice-cold 70% ethanol to each tube.

11. Centrifuge full speed for 10 min at 4 °C. Pour off supernatant.

12. Place opened tubes upside down over a tissue paper to soak the remaining ethanol.

13. Dry pellet in speed vac.

14. Dissolve the pellet in 100 μl TE buffer. Place tubes in a 65 °C heat block for 10 min.Vortex shortly and store at 4 °C.

Glycerol stocks

For yeast, 750 μl cultured cells were mixed with 250 μl sterile 80% glycerol stock solution to obtain the final glycerol concentrations at 20%. The mixed culture stored in -80 °C.

For *E.coli* and *Agrobacterium*, 930 μl cultured cells were mixed with 70 μl. The mixed culture stores in -80 °C.

Preparation of chemical-competent *Agrobacterium*

One tube of *Agrobacterium* (GV3101PMP90) was cultured as seed in 20 ml LB medium with Rifampicin (50 mg/l) and Gentamycin (20 mg/l). The seed culture were incubated at 28 °C 180 rpm overnight. Then added the seed culture into 500 ml LB medium with Rifampicin (50 mg/l) and Gentamycin (20 mg/l) and cultured for around 5 h at 28 °C until the OD600 was 0.5-0.7. Before harvesting the cells at 4000 g (Multifuge 3 S-R, Heraeus), 5 min, 4 °C, they were incubated for 10 min on ice. All the following steps were performed on ice as well. Cells were washed by resuspension in 100 ml pre-cooled sterile 150 mM NaCl and spined down at 4000 g, 5 min, 4 °C. The cell pellet was resuspended in 10 ml pre-cooled sterile 20 mM $CaCl_2$. After that, the *Agrobacterium* were aliquoted (200 μl) into Eppendorf tubes by filling them quickly with a multipette. The aliquots were stored at -80 °C.

Transformation of *Agrobacterium*

Transformation of chemical-competent TOP10 E.coli was performed with the following heat shock procedure:

1. Take competent cells out of -80 °C and thaw at room temperature for around 5 min.
2. Mix 5μl of DNA into 200 μL of competent cells in a microcentrifuge or falcon tube. Gently mix by flicking the bottom of the tube with finger.
3. Incubate the tube on ice for 5 min.
4. Incubate the tube in liquid nitrigen for 5 min.
5. Incubate the tube at 37 °C for 5 min.
6. Add 800 μl LB media without antibiotic and grow in 28 °C shaking incubator for 2 h.
7. Plate some or all of the transformation onto a LB agar plate containing Rifampicin (50 mg/l) and Gentamycin (20 mg/l).
8. Incubate plates at 28 °C for 72 h.

SDS-PAGE

Protein samples were separated by SDS-PAGE. A 8 or 10% separation gel with a 5% stacking gel was used. The different SDS gel parts were prepared as given in the table below:

Table 2-6. The gel preparation of SDS-PAGE

Component	8 % separation gel	10 % separation gel	5 % stacking gel
Acrylamide (30%)	13.6 ml	17 ml	8.3 ml
1 M Tris-HCl pH 6.8	-	-	6.3 ml
1.5 M Tris-HCl pH 8.8	12.5 ml	12.5 ml	-
10% SDS	0.5 ml	0.5 ml	0.5 ml
H_2O	to 50 ml	to 50 ml	to 50 ml

The separation gel was poured first and covered with isopropanol during the polymerization time of around 30 min. After removing the isopropanol, the stacking gel with an appropriate comp was added. After another polymerisation time of about 30 min, the gel was loaded with the protein samples of interest. These samples were prepared before loading by adding one volume of 2x sample loading buffer (10 mM DTT, 5% SDS, 2 mM EDTA, 0.1% Triton X-100, 10% Glycerol, 50 mM Tris-HCl pH 6.8, 0.001% Bromophenol blue). In order to avoid possible aggregation of membrane proteins, the protein samples were incubated 37 °C for 1 h before loading. Remaining samples were stored at -20 °C.

Typically, 5-10 μg of sample proteins were loaded per lane. 3 μl of PageRuler Plus Prestained Protein Ladder (Thermo fisher scientific, USA) was loaded as molecular weight standard. Gels were run in SDS Running Buffer (3.02 g/l Tris, 14.25 g/l Glycine, 10 g/l SDS) at 120 V.

Western Blot analysis

Table 2-7. The buffer used for Western blot analysis

Buffer and solution	Composition
Bjerrums buffer	6.1 g/l Tris, 2.4 g/l Glycine, 20% Methanol
Ponceau S solution	2 g/l Ponceau S in 5 % acetic acid
TBS solution	8 g/l NaCl, 0.2 g/l, 3 g/l Tris, adjust pH to 7.4 by HCl
Blocking solution	5 % milk powder (Marvel, Iceland, UK) in TBS slution, 0.02 % NaN_3
Antibody solution	antibody, TBS solution, 2.5 % milk powder, 0.02 % NaN3

A semi-dry blotting system (Perfect Blue Semi-Dry Electro Blotter, paqlab, Germany) was used for the transfer of proteins from the gel to the membrane. Blotting paper (Blotting Pad 707, VWR, USA) and transfer membrane (BioTrace^{TM} NT Nitrocellulose Transfer Membranes, Pall Life Sciences, USA) were cut to match the size of the gel and saturated in cold Bjerrums buffer. SDS gels were briefly rinsed in distilled water and equilibrated in cold Bjerrums buffer. To assembling the gel sandwich, a piece of blotting paper was put in the centre of the base of the blotting system first. Then a prepared blotting membrane of same size was put on top of the blotting paper. After that the gel was placed on top of the membrane. Finally another piece of blotting paper was put on top. A pipette or test tube could be used to roll bubbles out of layers. After the gel sandwich was assembled, the safety lid containing the cathode plate could get closed. Then the lid was fixed using the screwing knobs. Unless stated otherwise, the blotting conditions were 10 V for 1 h.

After blotting, the membrane was incubated in Ponceau S for 5 min

at room temperature with gentle shaking to detect transferred proteins. Excess stain was washed off with distilled water, and the stained membrane was scanned.

The membrane was then placed into Blocking solution and incubated for 1 h at room temperature with slow movement on a horizontal shaker. After the blocking step, the membrane was transferred into primary antibody solution and Incubated either 3 h at room temperature or overnight at 4 °C. Then unbound antibody was removed by washing three times in TBS solution (5 min each time at RT with fast movement). After subsequent incubation with the secondary antibody solution as described for the primary antibody, these wash steps were repeated. the secondary antibody was either an anti-rabbit HRP (1:20000; Goat Anti-Rabbit IgG - Horseradish Peroxidase, G21234, GE Healthcare, USA) or an anti-rat HRP (1:20000; Rabbit Anti-Rat IgG H&L (HRP), ab6734, Abcam, UK) conjugate depending on the animal species the primary antibody was used.

Detection was generally by a chemiluminescent signal from a substrate for the HRP enzyme (SuperSignal West Femto Chemiluminescent Substrate, Thermo Fisher Scientific, USA). The chemiluminescent signal was caught on a imaging platform (Fusion spectra, Vilber Lourmat, France) according to the manufacturer's instructions.

2.2 Molecular Biology Methods

Construction of Oocytes expression vector with N terminal HA tag

The available vectors for Oocytes protein expression and electrophysiology analysis came from Chen et al. 2011. In order to create a vector which allowed protein expression in Oocytes could be verified by western blot, a HA tag was added in the N terminal of Gateway cassette

by PCR amplification, restriction endonucleases, and DNA ligation. The backbone without Gateway expression cassette was amplified from pGT-Dest (Chen et al., 2011) with primers CG-S-pGT-HpaI and CG-A-pGT-SnaBI, thereby adding an HpaI site at the 3' and a SnaBI site at the 5' termini of the expression cassette. The Gateway sequence of vector pNX35-Dest (Grefen and Blatt, 2012) was amplified using primers BZ-S-PmeI-2xHA and BZ-A-HpaI-GW. T4 DNA ligase (NEB, Hitchin, UK) was used to carry out blunt-end ligation and subsequent transformation and selection was in ccdB-survival *E.coli* cells (Life Technologies, Paisley, UK). The vector sequence was verified by restriction endonuclease digestion and sequencing (GATC, Konstanz, Germany).

The Oocytes protein expression vector, pGT-myc-Dest (Zhang et al., unpublished), which contained C terminal myc tag was created by a former post-doc of Prof. Blatt's group, Dr. Christopher Grefen.

Preparation of VAMPs and K^+ channels clones

Gateway® Technology (Life Technologies, Paisley, UK) was used to create clones used for yeast mating based split-ubiquitin assays (mbSUS) and ratiometric Bimolecular Fluorescence Complementation (rBiFC) analysis. Gateway system is a universal technology to clone DNA sequences for functional analysis and expression in multiple systems. It is based on the bacteriophage lambda site-specific recombination system which facilitates the integration of lambda into the *E. Coli* chromosome and the switch between the lytic and lysogenic pathways (Ptashne, 1992). In the Gateway® Technology, the components of the lambda recombination system are modified to improve the specificity and efficiency of the system (Bushman et al., 1985). All primers used in this study were shown in Table 1.

As mentioned in the user manual, the creation of an insert of interest for in vivo cloning required only a PCR product that includes the B

recombination sites, no restriction enzyme digest was needed. Attachment of the B1 site (5'-3': ggggacaagtttgtacaaaaaagcaggct) or B3 site (5'-3': ggggacaactttgtataataaagttg) was mediated as overhanging sequence in the respective forward primer and attachment of the B2 site (5'-3': ggggaccactttgtacaagaaagctgggt) or B4 site (5'-3': ggggacaactttgtatagaaaagttgggt) as an overhang in the respective reverse primer. In order to fuse the PCR product in frame with an N-terminal tag, the forward primer must include two additional nucleolus to maintain the proper reading frame. Depending on the destination vector, a stop-codon was needed in the reverse primer or provided by the vector itself. The table below shows the primers used for the amplification of VAMPs and K^+ channels. Template for these PCRs were *Arabidopsis* cDNA library created by Dr. Christopher Grefen.

Table 2-8. The primer pairs used for K^+ channels and VAMPs amplification

Coding sequence		Forward		Reverse	
		attB1	attB3	attB2 with stop	attB4 w/o stop
KC1	At4g32650	39	-	40	42
KAT1	At5g46240	37	-	38	41
VAMP711	At4g32150	5	-	6	-
VAMP712	At2g25340	7	-	8	-
VAMP713	At5g11150	9	-	10	-
VAMP714	At5g22360	11	-	12	-
VAMP721	At1g04750	13	29	14	-
VAMP722	At2g33120	15	-	16	-
VAMP723	At2g33110	17	30	18	-
VAMP724	At4g15780	19	-	20	-
VAMP725	At2g32670	21	-	22	-
VAMP726	At1g04760	23	-	24	-
VAMP727	At3g54300	25	-	26	-
VAMP728	At3g24890	27	-	28	-

The clones containing AKT1, SYP121, CBL1, and CIPK23 were created by Dr. Christopher Grefen.

Preparation of the chimeric VAMP clones

VAMP721 and VAMP723 were divided into three regions comprising the longin domain (L), the SNARE domain (S), and the transmembrane domain (M), with two breaks in the VAMP sequences at the $D^{124}H^{125}$ and the $R^{196}K^{197}$ junctions. The Entry clones containing corresponding

VAMPs were used as template for PCR.

Chimeric clones of VAMPs were constructed using overlap extension PCR which contained two steps of PCR. In the first PCR step, the fragments which used to make up the chimeric gene were amplified. The Primers possessed a 5' extension which was complementary to the the other gene. For example, primer 47 (5’-3’ AAGATAAAACTCATTGTCCTTGCAATT) contained specific sequence of VAMP723 and a extension sequence of VAMP721 (underline). Different fragments were fused together in a second PCR step using the primers containing the Gateway site. The table below shows the primers used for the chimeric clones construction. The Entry clones containing VAMP were used as template for these PCR.

Table 2-9. The primer pairs used for the preparation of VAMP chimeric clones

1st round PCR

No.	Fragment	Primer
A	VAMP721L	13, 43
B	VAMP721S	46, 44
C	VAMP721M	48, 14
D	VAMP723 L	17, 43
E	VAMP723 S	46, 45
F	VAMP723 M	47, 18
G	VAMP721 LS	13, 44
H	VAMP721 SM	46, 14
I	VAMP723 LS	17, 45
J	VAMP723 SM	46, 18

2nd round PCR

PCR product	Template	Primer
721L723SM	A+J	13, 18
721S723LM	B+D+F	17, 18
721M723LS	C+I	17, 14
723L721SM	D+H	17, 14
723S721LM	E+A+C	13, 14
723M721LS	F+G	13, 18

Preparation of VAMP longin domain chimeric clones

In order to isolate the binding domain within the longin domain of VAMP721, a similar strategy of chimeric constructs was used. The longin

domain of two VAMPs were divided into three equal parts: L_A (residues 1-40), L_B (residues 41-80), and L_C (residues 81-124). The overlap extension PCR was used for longin domain exchange clones preparation. These segments were swapped using the VAMP721 sequence to provide the backbone for the remainder of the VAMP assembly. The table below shows the primers used for the chimeric clones construction.

Table 2-10. The primer pairs used for the preparation of VAMP longin domain chimeric clones

1st round PCR

No.	Fragment	Primer
a	VAMP721L_A	13, 51
b	VAMP721L_B	50, 55
c	VAMP721L_C	54, 14
d	VAMP723L_A	17, 52
e	VAMP723L_B	49, 56
f	VAMP723L_C	53, 43
g	VAMP721L_{AB}	13, 55
h	VAMP721L_{BC}	50, 14
i	VAMP723L_{AB}	17, 56
j	VAMP723L_{BC}	49, 43
k	VAMP721SM	46, 14

2nd round PCR

PCR product	Template	Primer
721L_A723$L_B$$L_C$	a+j+k	13, 14
721L_B723$L_A$$L_C$	b+d+f+k	17, 14
721L_C723$L_A$$L_B$	c+i	17, 14
723L_A721$L_B$$L_C$	d+h	17, 14
723L_B721$L_A$$L_C$	e+a+c	13, 14
723L_C721$L_A$$L_B$	f+g+k	13, 14

Preparation of VAMP mutant clones

Point mutant clones of VAMP were generated by one of site-directed mutagenesis (SDM) methods, QuickChange™ (Stratagene, La Jolla, USA) method. In this method, two overlapping primers were directly used in a PCR reaction using a plasmid-based gene as template. Simple transformation of the resulting PCR product in *E.coli* allows isolation of the mutated DNA. Prior to transformation in *E.coli*, the amount of wild type template was digested with DpnI (NEB, Hitchin, UK), an enzyme that degrades methylated DNA (Karnik et al., 2013a). The primers used in preparation of point mutant clones were designed by a web-based software, SDM-Assist (http://psrg.org.uk/sdm-assist). This software allows the user to generate and choose primers for SDM that contain a unique restriction site identity allowing for highly efficient identification of 'mutated clones' by a simple restriction digest. introduce a restriction site through silent mutations in the primer sequence (Karnik et al., 2013 a).

For the VAMP double mutant clones preparation, the Entry clone of VAMP721^{Y57A} was used as the template. The second mutant was added using the same SDM method.

The primer pairs used in mutant clone preparation was shown in the first table below.

Table 2-11. The primer pairs used for the preparation of VAMP single or double mutants

Mutant clone	Primer Pair	Mutant clone	Primer Pair
VAMP721 Y57A	57, 58	VAMP721 Y57A T54A	81, 82
VAMP721 D61A	63, 64	VAMP721 Y57A F55A	83, 84
VAMP721 Q76A	67, 68	VAMP721 Y57A N56A	85, 86
VAMP721 S80A	71, 72	VAMP721 Y57A L58A	87, 88
VAMP721 Y57D	58, 60	VAMP721 Y57A V59A	89, 90
VAMP721 Y57F	61, 62	VAMP721 Y57A E60A	91, 92
VAMP721 D61N	65, 66	VAMP721 Y57A G62A	93, 94
VAMP721 Q76E	69, 70	VAMP721 Y57A F63A	95, 96
VAMP723 D57Y	107, 108	VAMP721 Y57A T64A	97, 98
VAMP721 Y57A C50A	73, 74	VAMP721 Y57A Y65A	99, 100
VAMP721 Y57A D51A	75, 76	VAMP721 Y57A C66A	101, 102
VAMP721 Y57A G52A	77, 78	VAMP721 Y57A V67A	103, 104
VAMP721 Y57A H53A	79, 80	VAMP721 Y57A V68A	105, 106

The PCR reaction was set up in two individual reactions one for each primer (0.3 μM final concentration). The reactions were set up in KOD system as described before. The amplification was carried out as followed table.

Table 2-12. Set-up of the 2-step PCR reaction for site-directed mutagenesis

Frequency	Step	Temperature (°C)	Duration
1x	initial denaturation	95	2 min
12x	denaturation	95	30 s
	primer annealing	56	1 min
	primer extension	72	6 min (one minute per kbp)
two individual reactions were pooled toghter			
15x	denaturation	95	30 s
	extension	72	7 min

After PCR reaction, the products were digested by 2 µl (around 4000 units) of DpnI (NEB, Hitchin, UK) at 37°C overnight. 5 µl of the PCR reaction were subsequently transformed in *E.coli* strain Top10. Five colonies per plate were isolated and analysed via restriction digest and sequencing (GATC Biotech, Konstanz, Germany).

Preparation of Destination clones

Subsequent these PCR products were inserted by BP reactions in pDONR207, pDONR221-P3P2 and pDONR221-P1P4 (Life Technologies, Paisley, UK) yielded Entry clones that were verified via sequencing. Gateway Destination clones were generated using LR Clonase II (Life Technologies, Paisley, UK) by LR reaction according to the manufacturer's instructions.

For rBiFC analysis, the 2in1 Gateway-compatible cloning system was used. This 2in1 rBiFC system can ensure equal gene dosage, and the inclusion of an internal fluorescence marker allows for expression

control and ratiometric quantification (Grefen and Blatt, 2012). There were two different expression cassettes on the same vector backbone (pBiFCt-2in1-NC; as shown in Chapter 3, Figure 3 and Figure 4). I mixed two Entry clones with gateway sites (L3L2 for VAMPs and R1R4 for K^+ channels), then performed the single-step LR reaction to transfer two independent genes into the vector.

The Destination vector used in this study were shown in the table below.

Table 2-13. The destination vectors used in this research.

Vector name	Gateway site	Comments	Reference
pMetYC-Dest	R1, R2	Yeast expression vector (bait)	Grefen et al., 2009
pNX35-Dest	R1, R2	Yeast expression vector (pray)	Grefen et al., 2012
pUBN-GFP-Dest	R1, R2	Plant expression vector with N terminal GPF tag (location check)	Grefen et al., 2010b
pBiFCt-2in1-NC	R3, R2 and R1, R4	2-in-1 Plant BiFC vector	Grefen and Blatt, 2012
pGT-cMyc-Dest	R1, R2	Oocyte expression vector with C terminal myc tag (Oocytes electrophysiology)	Zhang et al., unpublished
pGT-nHA-Dest	R1, R2	Oocyte expression vector with N terminal HA tag (Oocytes electrophysiology)	Zhang et al., unpublished
pUB-Bic-Dest	R1, R2	Plant expression vector (Plant electrophysiology)	Chen et al., 2011
pTecG-2in1-NC	R3, R2 and R1, R4	2-in-1 traffic rescue analysis Vector	Karnik et al., 2013b

2.3 Mating Based Split-Ubiquitin Assays

The mating based split-ubiquitin (mbSUS) assay is a alternative method to the classical yeast two-hybrid system. The mbSUS assay relies on the ubiquitin-degradation pathway as a sensor for protein-protein interactions. Two different yeast strains were used for mbSUS assays: THY.AP4 for bait (contain X-CubPLV by vector pMetYC-Dest) and THY.AP5 for prey (contain NubG-X or NubI by vector pNX35-Dest).

To study the protein-protein interaction by mbSUS assay, several points need to be considered. Firstly, the bait protein should not be soluble or nuclear-localized. These bait proteins will lead to background activity or false positive results. Because the lexA transcriptional regulator would activate reporter genes without being cleaved by the ubiquitin specific proteases (USPs). The second point is the topology of proteins. The Cub-PLV at C terminal end of bait and NubG at N terminal end of prey should be in the cytosol. Because the interaction between Cub and Nub only happened in the cytosol where USPs can recognize the reconstituted ubiquitin (Grefen et al., 2009). For all of above reasons, VAMPs were cloned into pNX35-Dest which fused NubG on N terminus of R-SNARE and K^+ channels were cloned into pMetYC-Dest.

Table 2-14. The yeast strains used in mbSUS assay

Name	Organism	Genotype	Function
THY.AP4	*S. cerevisae*	MATα; ade2 − , his3 − , leu2 − , trp1 − , ura3 − ; lexA::ADE2, lexA::HIS3, lexA::lacZ	Used for transformation of Cub-clones
THY.AP5	*S. cerevisae*	MATα; ade2 − , his3 − , leu2 − , trp1 −	used for transformation of Nub-clones

All media were listed in the table below and used in sterile conditions

after autoclaving or filter sterilization.

Table 2-15. The buffers and media used for yeast transformation

Buffer and medium	Composition
YPD media	2% peptone, 2% glucose, 1% yeast extract, 2% agar (pH = 6.0)
1 M and 0.1 M LiAc solution	dissolve lithium acetate in de-ionized water. Adjust the pH to 7.5 with acidic acid, and sterilize by filtration.
ssDNA	dissolve 10 mg/ml ssDNA in de-ionized water, sonicate and/or boil for 5 min following cooling on ice before use.
PEG solution	dissolve PEG 3350 in de-ionized water to a final concentration of 50% (w/v), sterilize by filtration and avoid water loss during storage as this significantly decreases the transformation efficiency.
SC-minimal medium	1.7 g/l yeast nitrogen base (without amino acids), 5 g/l ammonium sulphate, 20 g/l glucose, 1.5 g/l of SC-dropout mix; adjust pH to 6.0– 6.3 with KOH; add 20 g/l agar if solid medium is needed

Individual dropout-mixes were obtained from BIO-101 (www.qbiogene.com/products/bio101) and contained all amino acids apart from the desired selective one(s). Oxoid agar was obtained from Oxoid (Basingstoke, Hampshire, England, # LP0011). Chemicals for auxotrophy selection were prepared by dissolving each amino acids in 100 ml of water and sterilized by filtration and stored in darkness at 4°C:

ADE: 0.4 g of adenine sulphate (add 5ml per litre media)

URA: 0.4 g of uracile (add 5 ml per litre media)

LEU: 2.0 g of L-leucine (add 5 ml per litre media)

TRP: 0.4 g of L-tryptophane (add 5 ml per litre media)

HIS: 0.4 g of L-histidine (add 5 ml per litre media)

MET: 1.5 g of L-methionine (equals a 0.1 M stock solution, add appropriate amount to obtain 5, 50 and 500 μM final concentrations)

The SC-auxotrophy selection medium were prepared by adding appropriate auxotrophy selection chemical into the SC-minimal media as shown below:

Table 2-16. The medium used for mbSUS assay

Medium	Comment
CSM_{-TUM} medium	transformation of Nub-clones in THY.AP5.
CSM_{-LM} medium	transformation of Cub-clones in THY.AP4.
CSM_{-LTUM} medium	yeast mating checking
$CSM_{-LTUMAH}$ medium with Met	yeast growth checking; different methionine concentrations can help to increase the signal-to-noise ratio

Yeast transformation

Yeast were transferred according to the methods reported by Gietz et al. (1995) and Grefen et al. (2009). Competent yeast were prepared freshly before every time transformation. The yeast transformation was performed according to the protocol below:

1. Inoculate THY.AP4 and AP5 in 5 ml YPD each and incubate, shaking overnight at 180 rpm, 28 °C.
2. After culture overnight, transfer the pre-culture in fresh 45 ml YPD and incubate shaking for 3–5 h until OD_{600} 0.6–0.8.
3. Harvest cells by centrifugation (10 min at 2000 g), and discard supernatant.
4. Wash with 20 ml of sterile water and centrifuge again and discard

supernatant.

5. Resuspend the cells with 1 ml of 0.1 M LiAc and transfer to a 2 ml Eppendorf tube, spin down (2 min at 2000 g) and discard supernatant.

6. Add appropriate amount of 0.1 M LiAc (multiply number of transformation with 20 µl) and incubate at room temperature for 30 min.

7. Meanwhile prepare sterile PCR tubes with 10 µl of ssDNA and 5 µl of plasmid DNA for each transformation.

8. Prepare mastermix: mix 70 µl of PEG solution, 10 µl of 1 M LiAc, and 20 µl of competent yeast for each transformation.

9. Mix the mastermix with the DNA mixture from step 7.

10. Incubate at 30°C for 30 min using a PCR-cycler and Heat shock cells at 43°C for 15 min.

11. Spin down yeast at 2000 g for 2 min, and discard supernatant using a pipette.

12. Wash cells with 100 µl of sterile water, spin down and discard supernatant.

13. Resuspend cells in 50 µl of sterile water and plate on appropriate SC-plate. Incubate for 72 h at 28 °C.

mbSUS assay

The yeast mbSUS assay was performed according to the protocol of Grefen et al. (2009):

1. Pick one single colony of prey yeast and inoculate in 5 ml SC_{-TUM} medium. Grow overnight at 180 rpm, 28 °C.

2. Pick one single colony of bait yeast and inoculate in 5 ml SC_{-LM} medium. Grow overnight at 180 rpm, 28 °C.

3. Harvest remaining cells and resuspend them in YPD (for each mating 20 µl of YPD should be calculated).

4. Mix 20 µl of each bait and prey in sterile PCR tube and immediately drop 4 µl of each mating onto a YPD plate. Incubate overnight at 28 °C.

5. Transfer yeast from the YPD plate to a SC_{-LTUM} medium plate by sterile toothpick. Grow overnight at 180 rpm, 28 °C.

6. Pick the mating yeast colony of each sample and incubate in 3 ml SC_{-LTUM} medium overnight at 180 rpm, 28 °C.

7. Harvest 2 ml of the mating cells and deep-freeze it for later Western Blot analysis.

8. Harvest 100 μl remaining cells and dilute them to OD 1.0 and 0.1 respectively in sterile water.

9. A 4 μl aliquot of each dilution was spotted on SC_{-LTUM} medium plate and $SC_{-LTUMAH}$ medium with different methionine concentrations (0, 50, and 500 μM). Check for growth after 3 days.

Yeast protein extraction for Western Blot analysis

For total protein extraction, 2 ml of yeast culture (or use deep-frozen aliquots as mentioned above in mbSUS assay) was harvested by centrifugation at full speed for 1 min in a microcentrifuge. After remove the supernatant, 50 μl acid-washed glass beads and 150 μl of “Lyse & Load” buffer (50 mM Tris-HCl (pH 6.8), 4% SDS, 8 M urea, 30% glycerol, 0.1 M DTT, 0.005% bromophenol blue; store at −20°C) was added. Then done the vortex mixing for 1 min at the highest setting. After that, incubated for 10 min at 65 °C. Finally, Spin down and transfer supernatant in a fresh tube. Then the sample could be used in western blot analysis.

2.4 Ratiometric Bimolecular Fluorescence Complementation (rBiFC) analysis and VAMP localization analysis

Agrobacterium Preparation

Table 2-17. The medium and buffer used for *Agrobacterium* transformation

Medium and buffer	Comment
MS medium	0.05× MS salts without organics or added vitamins, pH 7.0-7.2, and filter sterilize
AS buffer	10 mM $MgCl_2$, 10 mM MES-KOH, pH 5.6, 150 mM acetosyringone
Transformation buffer	0.05× MS media, 150 μM acetosyringone, 0.003 % Sylwet-77, and filter sterilize

1. Pick a single colony of transformed *Agrobacteria* that contains the plasmid of sample. Grow them overnight at 180 rpm, 28 °C in 5 m LB medium with antibiotics (In this study, rifampicin 50 μg/ml, gentamicin 20 μg/ml, and the specific antibiotic for the plasmid were used).
2. Add 200 μl of the overnight seed culture to 4.8 ml of fresh LB-Rif, Gent, antibiotic media and grow for 4–5 h at 180 rpm, 28 °C to an OD of approximately 0.6.
3. Centrifuge *Agrobacteria* at 4000 g for 10 min at 4 °C and wash the pellet twice with 5 ml of 4 °C cold sterile water.
4. Resuspend either in 4 °C cold AS media for *Nicotiana* transformation or 4 °C cold transformation buffer for *Arabidopsis* transformation. Adjust to a final OD of 0.2-0.4.
5. Incubate at least 2 h on ice before proceeding with the transformation steps.

Sometimes an *Agrobacterium* colony does not contain the plasmid, yet carries the plasmid-borne resistance. Plasmid copy numbers in *Agrobacterium* are at low levels, hence the DNA concentration obtained directly from host cells is too low for restriction analysis (Blatt and Grefen, 2014). Therefore, the transformed *Agrobacterium* should be verified via plasmid rescue in *E.coli* and restriction digest before using in plant transformation.

Tobacco leaf transformation

For *Nicotiana tabacum* leaf infiltration, plants were grown in a growth chamber (Sanyo FitoTron) for 4-6 weeks in long day conditions (16 h light, light intensity ~200 μmol m^{-2} s^{-1}, 26 °C/22 °C day/night, 60%/70% day/night relative humidity). A plant in 5-7 leaf stage was chosen.

1. 4-6 h before infiltration, the plant need to be well watered.
2. The epidermis on the underside of 2nd to 4th youngest leaf was grazed by a sharp tool.
3. The *Agrobacterium* suspension was injected into the abaxial epidermis of leaf by pressing the opening of a 1 ml syringe firmly to the wound. The infiltrated area could be visible by changing to a darker colour.
4. The plant was well watered and returned back to the growth chamber.
5. Expression could be analysed in 48 h or 72 h after infiltration, depending on the promotor used for the protein expression.

Transient *Arabidopsis* seedling root transformation

Before transformation, the seed need to be sterilised. At first, around 100-500 seed were suspended in 1 ml sterilisation solution (10 ml fresh

10% $NaHClO_3$ with one drop of Triton X-100) in a Eppendorf tube. After 8-10 min, the seed were washed as least 5 times with sterile distilled water by pipetting off the suspending solution and replacing it with fresh sterile distilled water. Then the seed were stored at 4 °C in the dark for more than 2 days. Seed that germinated in the tube were discarded (usually after 4-6 weeks).

Arabidopsis seed were sowed in sterile 0.05x MS medium (In a 6-well sterile plate, 4 ml MS medium per well). The seed were added by using 1 ml filter pipette tip, 30 seed per well and the plate was sealed by parafilm. *Arabidopsis* seedlings for co-incubation with *Agrobacterium tumefaciens* were grown for 3-4 days for germination under sterile conditions in long day condition (16 h light, light intensity ~180 μmol m^{-2} s^{-1}, 22 °C).

When the cotyledons had opened free of the seedcoat and the root was around 1-2 mm long, the seedling transformation could be performed. Firstly, the growth medium was removed from the well using a sterile filter 1 ml pipette tip by slowly aspirating solution from different position of the well to avoid any mechanical disturbance to the seedlings. The seedlings were kept wet during the whole process. Then 4 ml of the *Agrobacterium* suspension was added to the well. The plate was resealed again and returned to the growth chamber. After 3-4 days co-cultivation, expression could be analysed.

Confocal imaging

At first, the microscope slides were prepared by adding lines of silicon-based, pressure-sensitive adhesive (355 Medical Adhesive, Dow Corning, USA) to hold the coverslip.

For analysis of *N. tabacum* leaf, a ~1 cm^2 piece was excised using a sharp razor blade. To reduce background fluorescence due to air pockets, excised leaf samples were vacuum infiltrated with distilled water

in a 50 ml syringe. At first, the tip of the syringe was blocked by a finger and water and the leaf sample were added from the back. The plunger was replaced, the finger removed and the remaining air pressed out of the syringe. With a finger over the opening tip, the plunger was then pulled back to generate a vacuum in the syringe, and the vacuum was released slowly to refill air spaces in leaf with water. This last step was repeated 2-3 times untill the leaf was full of water. The leaf sample was then removed and placed on the slide with lower epidermis up. A coverslip was placed over the leaf, pressing the edges of the coverslip down on the adhesive gently.

For analysis of *Arabidopsis* seedlings, a drop of water was placed on the slide and fine forceps were used to transfer 3-6 seedlings to the drop. Then a coverslip was placed over the seedlings, pressing the edges of the coverslip down on the adhesive gently.

Confocal imaging was performed on a Zeiss CLSM510 inverted confocal microscope (Jena, Germany). All images were taken with standardized confocal settings: pinhole set to 1 airy unit, image size set to 512 x 512 pixels, line scan with collection set to average 8 scans, and z-stacks with 14-16 slices with intervals set to approximately 0.6x of the z-resolution depth.

For BiFC analysis, the images were taken with a Plan neofluar 20x/0.5 objective and with the following setting:

Table 2-18. The setting of confocal microscope for rBiFC analysis

	YFP	RFP
Excitation wavelength	514 nm	543 nm
Emission filter settings	BP 535-590 nm	BP 560-615 nm
Dichroic filter settings	HFT 458/514	HFT 488/543

For VAMP location analysis, the images were taken with a Plan

neofluar 40x/1.3 Oil DIC objective and with the following setting:

Table 2-19. The setting of confocal microscope for VAMP localization analysis

Excitation wavelength	488 nm
Emission filter settings	BP 505-550 nm
Dichroic filter settings	HFT 488/543

Plant protein extraction and Western sample preparation

1. For Western analysis, four pieces of ~1 cm^2 piece of *N. tabacum* leaf or 10-20 *Arabidopsis* seedlings are collected on dry ice or stored in -80 °C.
2. The samples are ground in dry ice.
3. Add 200 μl of HB buffer (50 mM Tris-HCl pH 7.4, 500 mM sucrose, 10% glycerol, 20 mM EDTA, 20 mM EGTA, 50 mM NaF, 10 mM ascorbic acid, and 5 mM DTT), well mix by vortex, and keep on ice for 1 h.
4. Spin down at 3000 rpm, 4 °C for 30 sec. Take all supernatant and transfer to a 2 ml eppendorf tube.
5. Add 1 ml of chilled acetone and keep at -20 °C for 3-5 h.
6. Spin down at maximun speed, 4 °C for 20 min.
7. Discard supernatant and add 500 μl 70% chilled ethanol.
8. Spin down at maximun speed, 4 °C for 5 min. Dry for until the ethanol is gone.
9. Add 100 μl dye (8% SDS, 30% Glycerol, 50 mM Tris-HCl (pH6.8) 0.005% bromophenol blue, and 0.1 M DTT; store at -20 °C) and sonicate. Put the sample at 70 °C for 10 min. And spin down full speed for 2 min. The supernatant can be used for Western analysis.

2.5 Electrophysiology analysis in *Xenopus laevis* oocytes

cRNA preparation

The AKT1, CIPK23 and CBL1 constructs that provided the template for in vitro transcription were kindly supplied by the authors of a previous publication (Xu et al., 2006). KAT1 and KC1 were cloned into the oocyte expression vector pGT-myc-Dest, which added a myc tag in the C terminus of the expressed protein. VAMP721, VAMP723, chimeric VAMPs, and mutant VAMPs were cloned into the oocyte expression vector pGT-nHA-Dest, which added a 2xHA tag in the N terminus of the expressed protein.

DNA plasmids were linearized by restriction digestion at 37 °C for 5-7 h, as shown in table below. The linearization site is behind the CDS and its following 3'UTR of *Xenopus laevis* β-globin. The β-globin sequences enhance translation efficiency of heterologous mRNA transcripts in oocytes (Krieg & Melton, 1984). The unique right size band was checked by loading 1 μl of DNA on a gel, and the linearized DNA was purified by PureLink™ Quick Gel Extraction and PCR Purification Combo Kit (Life Technologies, Paisley, UK).

Table 2-20. Set-up of the linearization of DNA plasmids

Component	μl added/reaction
DNA	20
restriction enzyme	4
10X buffer	5
Water	to 50

In vitro transcription was performed by using mMESSAGE

mMACHINE T7 kit (Ambion, Life Technologies, Paisley, UK) according to the manufacturer's protocol. The frozen reagents of the kit (RNA Polymerase Enzyme, 2X NTP/CAP, 10X Reaction Buffer) were thawed on the ice at first and kept the 10X Reaction Buffer at room temperature until assembling the reaction. The transcription reaction was assembled at room temperature as shown in the table below. After that the tube was gently flicked to mix reagents in the reaction well and microfuged briefly to collect the reaction mixture at the bottom of the tube. The tube was incubated at 37°C overnight.

Table 2-21. Set-up of in vitro transcription reaction

Component	μl added/reaction
2X NTP/CAP	10
10X Reaction Buffer	2
linear template DNA	0.1-1 μg
Enzyme Mix	2
nuclease-free water	to 20

In order to purify cRNA, a LiCl precipitation method was used. This method is a convenient and effective way to remove unincorporated nucleotides and most proteins. However, it does not precipitate transfer RNA and may not efficiently precipitate RNAs smaller than 300 nucleotides. Also, the concentration of RNA should be at least 0.1 μg/μL to assure efficient precipitation. At first, the reaction was stopped by adding 30 μL nuclease-free water and 30 μL LiCl precipitation solution (provided in the kit). Then all reagents in the tube were mixed well and stored in -20 °C for more than 30 min. Centrifugation was followed for 15 min at maximum speed, 4 °C to pellet the RNA. Then the supernatant was carefully removed and the pellet was washed once with ~1 mL

70% ethanol (prepared by nuclease-free water). Finally, the 70% ethanol was removed carefully. The cRNA was resuspended in a nuclease-free water and determined the RNA concentration and stored frozen at -80°C.

Quantitation of cRNA

The quantitation of cRNA was checked by two different methods.

Firstly, the concentration of cRNA was determined by a UV/Vis photometer (BioPhotometer plus, Eppendorf, Germany). This method required that the quantity of RNA was large enough to use 1 μl in 79 μl nuclease-free water. The concentration should be more than 800 ng/μl and the OD260/OD280 should be 1.8 to 2.0.

Secondly, the quality was checked by denaturating agarose gel electrophoresis. Gel-running equipment was cleaned by incubation in 1M NaOH/ 0.1 % SDS for 2-3 h and rinsed thoroughly with DEPC-H_2O to remove Rnase. Before pouring the gel, 1.5% Agarose was melted in DEPC-H_2O in a microwave, cooled down in a pre-heated 60 °C water bath and mixed with pre-warmed 10x MOPS (11.2 ml) and Formaldehyde (20 ml) under the fume hood. The gel running buffer was 1x MOPS in DEPC-H_2O. A denaturating mastermix was prepared (as shown below) and 11.7 μl of this mastermix was mixed with 1 μg cRNA and incubated in a preheated water bath at 65 °C for 15 min before cooling on ice. Samples were loaded in total together and 2 μl of a RNA ladder (Millennium Size Marker, Ambion, Applied Biosystems, # 7150) was used as molecular weight marker. The gel was run as described in 2.1 for DNA agarose gels. There should be one clear band with a little smear for good quality cRNA.

Table 2-22. The buffer used for cRNA quantitation

Buffer	Composition
DEPC-H_2O	1 ml DEPC (Sigma, # 32490) per 1 l distilled water, stirred for several hours, autoclaved twice.
10x MOPS	200 mM MOPS, 50 mM sodium acetate, 10 mM EDTA, adjust to pH7 with NaOH (stored at 4 °C in the dark)
Denaturation mix	for 10 samples: 10 μl DEPC-H2O, 10 μl 10xMOPS, 35 μl Formaldehyde, 100 μl Formamide, 20 μl RNAse free loading buffer (provided in the kit), 1 μl EtBr

Oocytes isolation and Injection

Table 2-23. The buffer used for oocytes culture

Buffer	Composition
ND96 w/o Ca^{2+}	96 mM NaCl, 2 mM KCl, 1 mM $MgCl_2$, 10 mM HEPES-NaOH pH 7.4
ND96 with Ca^{2+}	1 mM $CaCl_2$, 96 mM NaCl, 2 mM KCl, 1 mM $MgCl_2$, 10 mM HEPES-NaOH pH 7.4

Ovary lobes were surgically removed from anaesthetised female frogs by semi-sterile procedures. The oocytes were filled in the ovary lobes. The mechanically very stable follicle is surrounded by a collagenase-resistant network of fibrils, called the vitelline layer, by several layers of follicle cells and by connective tissue containing blood vessels. For procedures that require direct contact with the plasma

membrane such as patch clamping, the vitelline layer has to be removed (Sigel, 2010). So the follicular cell layer was digested for 30 min and gentle shaking with 2 mg/ml Collagenase from *Clostridium histolyticum* (type 1A; Sigma, # C9891) dissolved in sterile filtered ND96 w/o Ca^{2+}. Following digest the oocytes were washed in a 50 ml Falcon tube several times with large volumes of sterile filtered ND96 with Ca^{2+} for the calcium ions to inactivate the collagenase. Gentamycin (5 mg/l) was added into the buffer to Inhibit the growth of contaminated bacteria. Mature oocytes, stage V or VI oocytes, were identified by their dark animal hemispheres and their yellowish vegetal hemispheres (Keiper, 2003). They were selected under a binocular (10x objective). The oocytes could be stored at 18 °C in sterile filtered ND96 with Ca^{2+} and 5 mg/l Gentamycin for no more than 1 week (The buffer replaced everyday).

For injection, oocytes were immobilised on openings of a nylon mesh glued to the bottom of a Petri dish. Oocytes were kept immersed in the ND96 with Ca^{2+} and 5 mg/l Gentamycin buffer at all stages of the injection. The Injection of cRNA was performed with a 3-D micromanipulator (Drummond, ‘Nanoject’) to give standard volumes of 20 nl/oocytes are released by the injector. A horizontal automatic pipette puller was used to pull the thin glass tubes used for injection into fine tips. The different cRNAs were prepared in the ratios as described in the results.

Electrophysiological recording

Table 2-24. The buffer used for electrophysiological recording

Buffer and dye	Composition
Bath solution	30 mM KCl, 66 mM NaCl, 1.8 mM $MgCl_2$, 1.8 mM $CaCl_2$, and 10 mM HEPES-NaOH, pH 7.2
RIPA buffer	1 M Tris-HCl pH 7.4, 10% SDS, 10% NP-40, 1 M NaCl, 500 mM EDTA, 500 mM NaF, 200 mM PMSF
Oocytes Loading Dye	10% SDS, 2% Triton X-100, 20% Glycerol, 100 mM Tris-HCl pH 6.8, 4 M Urea, 4 mM EDTA

After injection, oocytes were incubated in ND96 with Ca^{2+} and 5 mg/l Gentamycin at 18 °C for 3 d with daily buffer changes before electrophysiological recordings. Whole-cell currents were recorded under voltage clamp using an Axoclamp 2B two-electrode clamp circuit (Axon Instruments). The clamping protocols are described in the results. Data were analyzed with the HENRY III software (Adrian Hills, University of Glasgow) and Sigmaplot v11.2 software (SPSS software, Portsmouth, UK). Measurements were performed under continuous perfusion with bath buffer.

Oocytes that yielded currents were harvested separately immediately after the measurements, stored briefly on ice and frozen separately at -20 °C. Following data analysis, the respective oocytes were pooled for membrane protein extraction. For each oocyte, 20 μl of RIPA buffer were added before thawing. Homogenisation of oocytes in this buffer was achieved by pipetting with a 100 μl tip and vortexing. Then the RNase and DNase were added (2.5u each/oocyte), mixed well, and kept on ice. After 30 min, the mixture was spin down at 2000 rpm, 4 °C for 5 min. Then the supernatent was transfered to a new clean 1.5 ml

Eppendorf tube and mixed with same volume of Oocyte Loading Dye. Finally, the sample was put at 37 °C for 1 h, and spun down at full speed for 2 min. The upper supernatant was used for Western analysis.

2.6 Electrophysiology analysis in *Arabidopsis* root epidermal cells

The overlap extension PCR was used to link an HA tag at N terminus of VAMPs. The 2xHA tag was amplified from pNX35-Dest using the primer pair 110 and 111, which adding the overlapping VAMP721 sequence at 3' end and an attB1 gateway site as 5' end of HA sequence. The VAMPs with overlap HA part at 5' end and attB2 gateway site at 3 'end were amplified from Entry clones containing VAMP721, VAMP723, and VAMP721 Y57D. The primer pair 109 and 14 was used for VAMP721, while 109 and 18 was used for VAMP723. Then these two fragments were used as templates in the 2nd round PCR. Primer pair 111 and 14 was used for VAMP721, while 111 and 18 was used for VAMP723. The final PCR product contained attB1-B2 gateway sites and a 2xHA tag at the N terminus after expression. After BP and LR reactions as described in 2.2, the HA-VAMPs were introduced into the Destination vector pUB-Bic-Dest (Chen et al., 2011).

The *Arabidopsis* seedlings were grown and transferred as described in 2.4. Recordings from *Arabidopsis thaliana* Col-0 root epidermal cells were carried out on 6-8 d-old seedlings 3-5 d after transforming by co-cultivation with Agrobacterium. Seedlings were bathed in solutions of 10 mM KCl with 5 mM Ca^{2+}-MES, pH 6.1 (adjusted with $Ca(OH)_2$, free [Ca^{2+}] = 1 mM) and voltage clamp recordings made use of standard, two-electrode methods (Meharg et al., 1994; Chen et al., 2011). Measurements were carried out on mature epidermal cells in cell files lacking root hairs to avoid electrical coupling and clamp‐current dissipation by root hairs and between cells as described previously. All recordings were analyzed and leak currents subtracted using HENRY III

software (Adrian Hills, University of Glasgow). Expression was verified on a cell-by-cell basis using the co-expressed GFP marker (Chen et al., 2011). Plant proteins were extracted as described in 2.4 and used for Western analysis.

2.7 Traffic rescue analysis

In plant cells, the vesicle trafficking plays a central role in plant development and cell differentiation and mediating the responses to biotic and abiotic stress. In order to investigate the plant vesicle trafficking pathways, researchers will meet several challenges. At first, the trafficking system comprised a lot of organelles that are in constant flux. Secondly, the plasma membrane cargoes traffic inequality. Third, some endosomal domains are too small to be visualized directly by light microscopy techniques (Otegui, 2014). In resent years, many techniques have successfully been used for analysis of vesicle trafficking in plant, including analysis by dyes, by fluorescent protein, and by some labeled compounds in vesicle (Otegui, 2014). In my research, I investigated vesicle traffic by the traffic rescue analysis. The VAMPs and K^+ channels were cloned in tetracistronic vector pTecG-2in1-NC (Karnik et al., 2013b). Then I used secretory marker secYFP in this vector to examine the impact of channel interaction on traffic to the plasma membrane. When expressed, secYFP is normally secreted to the apoplast (Richter et al., 2009); only with secretory block does secYFP accumulate within the secretory pathway and give rise to a pronounced intracellular YFP signal. The vector pTecG-2in1-NC is also incorporates expression cassettes for GFP-HDEL (Karnik et al., 2013b), which I will introduce below.

In animal cells, fusion a neuroendocrine secretory protein on C terminus of GFP, the florescent protein can be used to image the secretory pathway and the mobility of Golgi transferases (Kaether and

Gerdes, 1995; Cole et al., 1996). In plant, fused GFP with patatin, a 23 amino acids length peptide from potato tuber storage, can target GFP to the ER (Stiekema et al., 1988). To ensure the retention of GFP in the ER, the sequence of KDEL (Lys-Asp-Glu-Leu) signal and seven upstream amino acids from the C terminus of an HSP90 homologue from *Catharanthus roseus* are fused to GFP. Expression of this peptide-GFP-KDEL can result florescent signal in ER of tobacco leaf (Boevink et al. 1996). A similar approaching is expression of the recombinant protein peptide-GFP-HDEL in *Arabidopsis* roots and imaging the retention signal in ER (Haselo and Amos, 1995). Further research has shown that GFP with patatin peptide but without KDEL can target ER and direct secrete to apoplast in tobacco leaves (Boevink et al., 1999). Thus, in pTecG-2in1-NC vector, the signal of GFP-HDEL is used as an transformation marker and ratiometric reference in this vector (Karnik et al., 2013b). Then the ratio of secYFP/GFP-HDEL can be used to measure secretory traffic and its block.

The *Agrobacterium* Preparation, transient tobacco leaf transformation, transient *Arabidopsis* seedling root transformation, plant protein extraction and Western sample preparation were performed according to the protocol in 2.4.

For traffic rescue analysis, the confocal images were taken with Planapo 20x/0.75 objective and with the following setting:

Table 2-25. The setting of confocal microscope for traffic rescue analysis

	YFP	GFP
Excitation wavelength	514 nm	458 nm
Emission filter settings	BP 530-600 nm	BP 475-525 nm
Dichroic filter settings	NFT 635 VIS	NFT 545 nm

2.8 Statistics

Statistical analysis of independent experiments is reported as means ± SE as appropriate with significance determined by Student's t-test. Joint, nonlinear least-squares fittings were performed using a Marquardt-Levenberg algorithm (Marquardt et al., 1963) as implemented in SigmaPlot v.11.2 (SPSS software, Portsmouth UK).

Chapter 3. Identifying VAMP interactions and the key binding sites by mating based Split-Ubiquitin System assay

3.1 Introduction

In addition to their canonical roles in vesicle traffic, a few SNARE proteins are known to interact with ion channels and affect their regulation independent of SNARE complex formation. In the model plants tobacco (*Nicotiana tabacum*) and *Arabidopsis thaliana*, Prof. Blatt's group have found that the SNARE SYP121 (=SYR1/PEN1) contributes to abscisic acid (ABA) regulation of Ca^{2+}, Cl^-, and K^+ channels in guard cells (Leyman et al., 1999; Leyman et al., 2000; Sokolovski et al., 2008). These SNARE proteins appear to regulate channel function directly through physical interactions with channels present at the membrane. Key support for this idea came from studies showing that SYP121 interacts directly with the regulatory K^+ channel subunit KC1 and forms a tripartite complex with a second K^+ channel subunit, AKT1 (Honsbein et al., 2009). Subsequent research showed that the interaction of SYP121 with KC1 is associated with a novel FxRF motif situated within the first 12 residues of the SNARE sequence (Grefen et al., 2010a). These data clearly show that the interaction site is not associated with the SNARE motif which is essential for SNARE complex assembly, but it does not explain whether such assembly is important for channel binding.

R-SNAREs, also known as vesicle-associated membrane proteins (VAMPs), are most commonly associated with trafficking vesicles. They are divided between three groups that have homologies to their counterparts in yeast and animals, namely the Sec22-, YKT6- and VAMP7-like R-SNAREs. Of the twelve VAMP7-like R-SNAREs in the

plant model *Arabidopsis*, the four VAMP71 proteins show the greatest similarity to mammalian VAMP7 and are involved primarily in endosomal trafficking; the remaining VAMPs, comprising the VAMP72 subgroup, appear specific to green plants and, with few exceptions, are thought to be responsible primarily for secretion at the PM (Uemura et al., 2007; Sanderfoot, 2007). Uemura et al. (2005) reported the subcellular location of the GFP fused VAMP7 proteins following expression in protoplasts. Their studies indicated that VAMP711, VAMP712 and VAMP713 are targeted to the vacuolar membrane, and VAMP714, VAMP723 and VAMP727 are located on the Golgi apparatus, the endoplasmic reticulum and the endosome, respectively; VAMP721, VAMP722, VAMP724, VAMP725 and VAMP726 are mainly localized at the PM.

During membrane fusion, VAMPs form SNARE complexes with other SNAREs. Kwon et al. (2008) found that the closely related VAMPs VAMP721 and VAMP722 assemble in complex with SNAP33 and SYP121 at the PM. Thus, the juxtaposition with the non-canonical functions of SYP121 raises the possibility that these VAMPs interact with the same K^+ channels that bind SYP121. The aim of the work presented in this chapter was to investigate the interaction between these VAMP7 proteins and the KC1 and KAT1 K^+ channels that interact with SYP121. The mating based Split-Ubiquitin System (mbSUS) assay was used for this purpose. I found VAMP721 and VAMP722, but not VAMP723, interacted with these K^+ channels. Then after exchange different domains between VAMP721 and VAMP723, additional SUS results showed that the longin domain has an essential role in interaction between VAMP721 and K^+ channels, and identified the Tyr residue at position 57 in longin domain of VAMP721 as critical for this interaction.

3.2 Results

3.2.1 The interaction between VAMPs with K^+ channels

The mating-based split-ubiquitin system in yeast is a method that relies on the ubiquitin-degradation pathway as a sensor for protein-protein interactions. The first step of the mbSUS assay is the transformation of bait and prey constructs into two different haploid *Saccharomyces cerevisiae* strains, THY.AP4 and THY.AP5, respectively. Both strains are unable to synthesize the amino acids Leu, Trp, His, and Ade. In addition, THY.AP4 can not produce Ura (The genotypes of these two strains are shown in table 2-14). After transformation, the vector of bait (pMetYC-Dest) gives THY.AP4 strain the ability of Leu synthesis. Similarly, the THY.AP5 strain gets the ability to produce Trp from prey vector pNX35-Dest (Grefen et al., 2009; Grefen et al., 2012). So after mating, the diploid yeast can grow on the medium without Leu, Try, and Ura (CSM_{-LTUM} medium. The ability of diploid yeast to produce Ura is got from the genome of the THY.AP5 strain). Leu and Trp synthesis are restored by the presence of bait and prey vector backbone, respectively. In THY.AP4, there are also reporter genes which restore the capacity for Ade and His production. These genes are under control of the split-ubiquitin system. Ubiquitin is split into two halves (Nub and Cub). The isoleucine at position 13 of Nub is mutated to glycine to avoid spontaneous reassembling (NubG). The diploid yeast get NubG from THY.AP5 and Cub from THY.AP4. If two proteins, which interact with each other, are fused to NubG and Cub respectively, their re-assembly gives a functional ubiquitin in the diploid yeast. The synthetic transcription factor, protein A-LexA-VP16 (PLV), at the C terminus of Cub is then released, leading to activation of lexA-driven reporter genes ADE2, HIS3 and lacZ in the nucleus (Obrdlik et al., 2004; Grefen et al., 2009). As shown in table 2-14, the diploid yeast get these lexA-driven reporter genes from THY.AP4. NubG from THY.AP5 is used as negative control, while wild-type Nub (NubI) is used as positive control. Finally, in the pMetYC-Dest vector, the expression of the bait-Cub fusion protein is

under control of the *met25* promoter, which enables reducing the level of bait protein expression and helps to increase the signal-noise ratio. Note that the bait protein is VP16-tagged while the prey is HA-tagged, so the expression of bait and prey proteins in yeast may be verified by Western blot analysis.

In the mbSUS assay of this chapter, the coding sequences of KC1, KAT1, and VAMPs were amplified by PCR and analyzed via restriction digest and sequencing (GATC Biotech, Konstanz, Germany). Then they were inserted into expression vector by Gateway cloning technology (Life Technologies, Paisley, UK). The NubG-VAMP fused proteins were used as prey while K^+ channel-CubPLV fusions were used as bait. All mbSUS assays were repeated three times to confirm interactions. Only one of each of these independent experiments is shown in figures below.

Interaction between each of the VAMP7 proteins and the KAT1 K^+ channel is shown in Figure 3-1. From left to right, the first column was the the photo of yeast growth on CSM_{-LTUM} medium taken 24 h after yeast dropping, which was used to verify the successful mating. The other columns are photos of growth on $CSM_{-AHLTUM}$ medium and were used to estimate the comparative protein-protein interactions. These photos were taken 72 h after yeast dropping. Different concentrations of methionine (0, 50 μM for KAT1 and 0, 500 μM for KC1) were used in $CSM_{-AHLTUM}$ medium to confirm the presence of interaction. In each column, two dilutions (OD_{600} 1.0 and 0.1) were used to make sure the difference of yeast growth was not related to the drop size. The diploid yeast containing NubG as prey served as a negative control while the yeast carrying NubI as prey (wild type N terminus of ubiquitin) was the positive control. To confirm the expression of bait and prey proteins, the Western blot results are shown in right lane.

In VAMP71 group, the diploid yeast grew well when carrying KAT1 K^+ channel with all four proteins. When dropped on plates with 50 μM Met, the yeast growth of VAMP711 was not as strong as the others,

which meant the interaction between VAMP711 and the KAT1 K^+ channel was weak. In the VAMP72 group, there was strong growth with VAMP721, VAMP722, VAMP724, and VAMP726, while weaker growth was recovered with the Nub-VAMP727 fusion. No growth was observed in $CSM_{-AHLTUM}$ medium when KAT1 mated with VAMP723, VAMP725, and VAMP728.

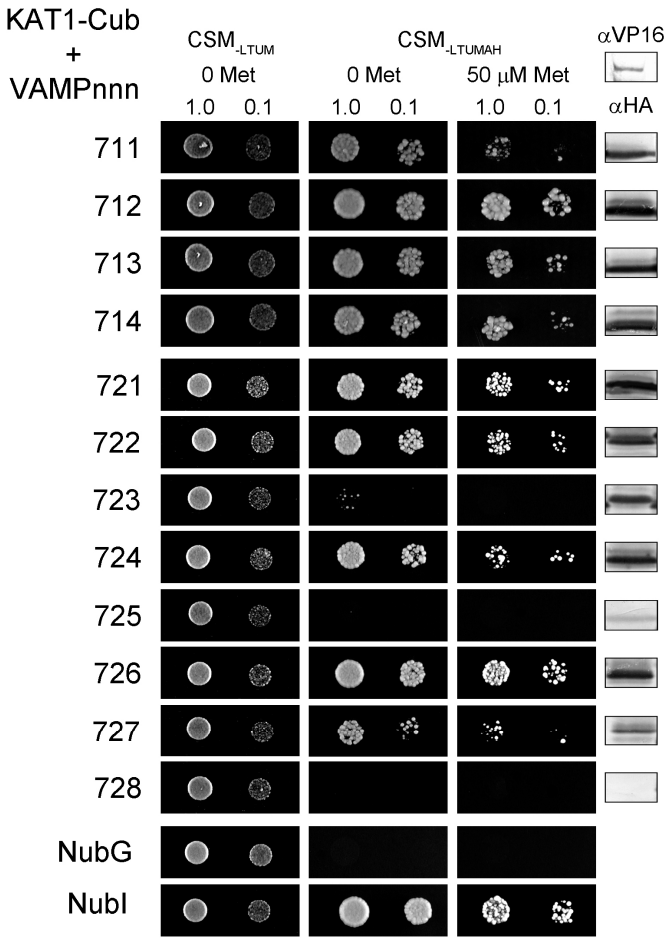

Figure 3-1. mbSUS assay for interaction between VAMPs and KAT1

Diploid yeast expressing KAT1-Cub as bait with NubG-X fusions of VAMP7 proteins and controls (negative: NubG; positive: NubI) as prey were spotted onto different media as indicated. CSM_{-LTUM}: Complete Synthetic medium (CSM) without leucine (Leu, L), tryptophan (Try, T), uracil (Ura, U), and Methionine (Met, M) was used to verify the presence of both bait and prey vectors. $CSM_{-LTUMAH}$: CSM without L, T, U, M, Adenine (Ade, A), and Histidine (His, H) was used to verify Ade- and His-independent growth. The addition of 50 μM Met to CSM-LTUMAH was used to verify interaction when K^+ channels-Cub expression was suppressed. Diploid yeast were dropped at 1.0 and 0.1 OD_{600} in each case. Incubation time was 24 h for CSM-LTUM plate and 72 h for

CSM-LTUMAH plates. Western blot analysis (5 μg total protein/lane) of the haploid yeast used in mating (right) was carried out with commercial HA antibody for the VAMP fusions and VP16 antibody for the K^+ channel fusions.

The actual expression of VAMPs and KAT1 was verified by Western blot analysis. For NubG-VAMP expression analysis, total protein from the same diploid yeast was used. For bait analysis, I used THY.AP4 yeast carrying K^+ channel CubPLV construct before mating. For Western blots, HA and VP16 epitopes were used as noted above. Anti-HA-Rat antibody (1:10000) and anti-VP16-Rabbit antibody (1:10000) were used as the primary antibodies in Western blotting. As shown in the right lane of Figure 3-1, all of the VAMPs showed similar expression levels, except VAMP725 and VAMP728. These two VAMPs failed to express in yeast. VAMP723 was expressed but showed little evidence of interaction with the KAT1 K^+ channel.

Figure 3-2 shows similar experiments carried out using the KC1-Cub fusion protein as bait. Again, the successful yeast mating was verified by colony growth on CSM_{-LTUM} medium. In this case, all diploid yeast showed similar growth on $CSM_{-LTUMAH}$ without Met, which indicated a high level of background noise and is probably related to the much higher expression of the KC1-Cub protein, compared to KAT1 expression in Figure 3-1. Western blot analysis also supported this protein expression difference. The band corresponding to KC1 was much more stronger than that of KAT1 with the same volume of sample loaded on the gel. The addition of a higher concentration Met (500 μM) in $CSM_{-LTUMAH}$ plates suppressed the expression level of KC1-Cub, uncovering a difference in yeast growth between the VAMPs. All of the VAMP71 proteins showed some interaction with KC1 K^+ channel. In the VAMP72 group, VAMP721, VAMP722, VAMP724, and VAMP726 showed growth, and hence stronger interaction with KC1, while VAMP723 and VAMP727 showed little or no growth. Again, VAMP725 and VAMP728

failed to express and no conclusion can be drawn for these proteins therefore.

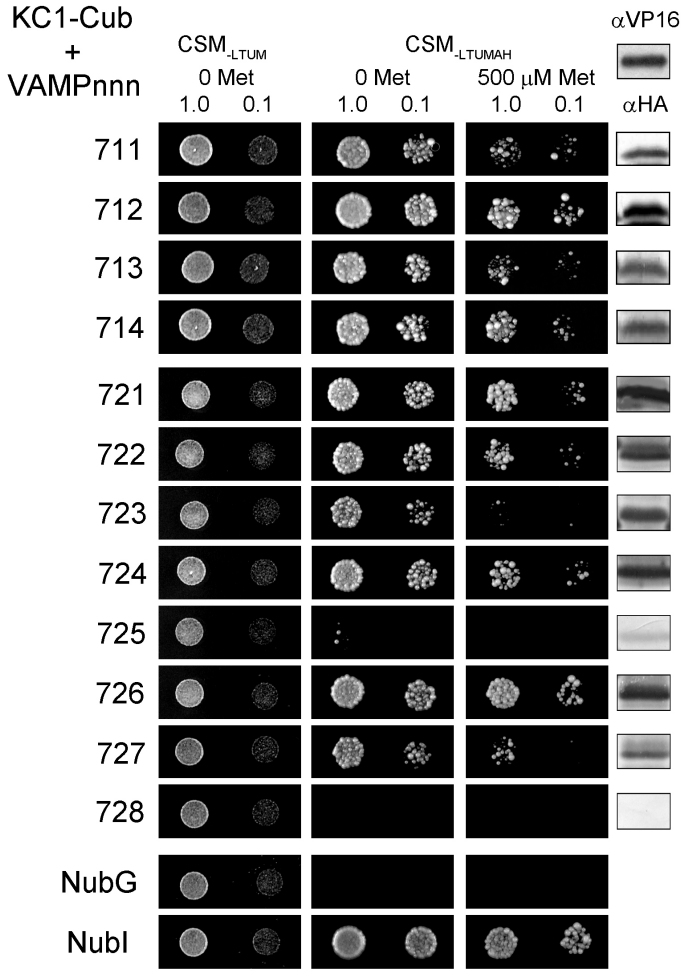

Figure 3-2. mbSUS assay for interaction between VAMPs and KC1

Diploid yeast expressing KC1-Cub as bait with NubG-X fusions of VAMP7 proteins and controls (negative: NubG; positive: NubI) as prey were spotted onto different media as indicated. CSM_{-LTUM}: Complete Synthetic medium (CSM) without leucine (Leu, L), tryptophan (Try, T), uracil (Ura, U), and Methionine (Met, M) was used to verify the presence of both bait and prey vectors. $CSM_{-LTUMAH}$: CSM without L, T, U, M, Adenine (Ade, A), and Histidine (His, H) was used to verify Ade- and His-independent growth. The addition of 500 μM Met to $CSM_{-LTUMAH}$ was used to verify interaction when K^+ channels-Cub expression was suppressed. Diploid yeast were dropped at 1.0 and 0.1 OD_{600} in each case. Incubation time was 24 h for CSM_{-LTUM} plate and 72 h for $CSM_{-LTUMAH}$ plates. Western blot analysis (5 μg total protein/lane) of the haploid yeast used in mating (right) was carried out with commercial HA antibody for the VAMP fusions and VP16 antibody for the K^+ channel fusions.

Two general conclusions can be drawn from these results. First, it appeared that both of the channel proteins are able to interact to some extent with members of the VAMP71 subgroup of R-SNAREs. I return to this point in the Discussion. Second, among the VAMP72 subgroup the results indicated consistent and selective interactions of the PM-localized VAMP721 and VAMP722 with both KC1 and KAT1 K^+ channels, by contrast with VAMP723 that has been localized to the ER. VAMP721 and VAMP722 are greater than 97% sequence identical. Double homozygous *vamp721/vamp722* mutant seedlings show lethal and dwarf phenotypes (Kwon et al., 2008; Zhang et al., 2011; El Kasmi et al., 2013). During SNARE complex formation, VAMP721 and VAMP722 appear functionally redundant in vivo (As shown in Table 1-2, either VAMP721 or 722 can be used to form SNARE complex with other SNARE proteins). Therefore, I focused on the interaction of the channels with VAMP721 and used VAMP723 as a control for further investigation.

3.2.2 The longin domain of VAMP721 is essential for K^+ channel interaction

VAMPs contain three protein domains, namely a so-called longin domain at the N terminus, the SNARE motif, and the transmembrane domain at the C terminus. A comparison of the protein sequences for VAMP721, VAMP722 and VAMP723 showed a substantial degree of identity with few regions of divergence between these VAMP72 proteins (See Figure 3-3, with grey shadow). It offered few clues to any possible K^+ channel binding sites. Therefore, to isolate residues associated with channel binding, I undertook a series of domain-swapping experiments

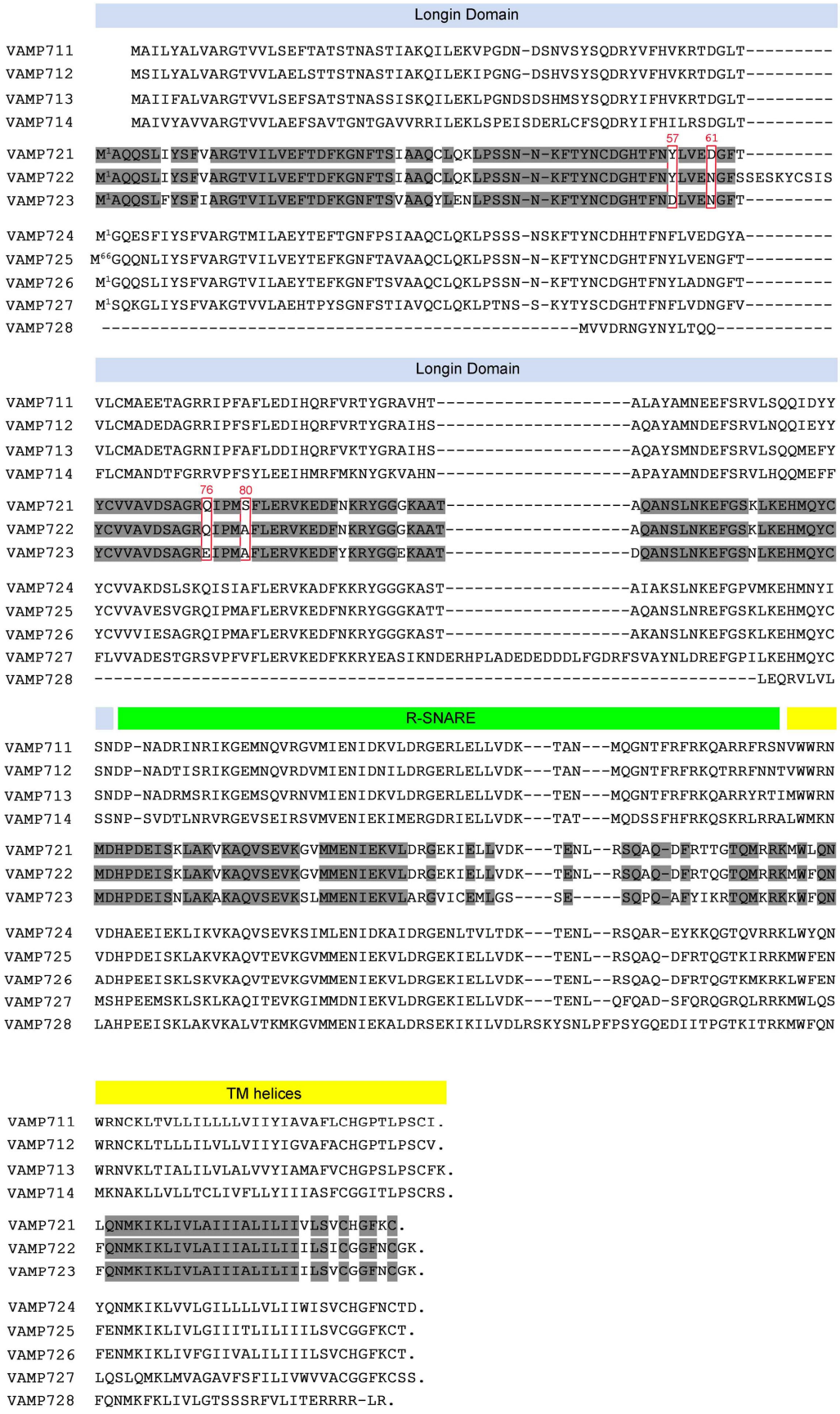

Figure 3-3. Alignment of VAMPs protein sequences

For domain swapping, VAMP721 and VAMP723 were divided into three regions: the amino acid sequence from 1 to 123, corresponding to the longin domain of VAMP721; the residues from 124 to 185, corresponding to R-SNARE motif; and the sequences from 186 to 220 that form the transmembrane domains. In Figure 3-3, they are shown in different colours: the longin domain region (residues 1-123, L) in blue, the R-SNARE motif (residues 124-185, S) in green, and the transmembrane domain (residues 186-220, M) in yellow. For the transmembrane domain, Uemura et al. (2005) chose the amino acid residues from 193 to 220 which included the transmembrane domain and intra vesicular tail. In my work, I chose amino acid residues from 186 to 220 as the transmembrane domain of VAMP721 which thus contained seven more residues. As described in Chapter 2, I used the overlap extension PCR to prepare the entry clones in which the three domains, L, S, and M of VAMP721 and VAMP723 were exchanged. Six non-redundant chimera clones were generated. Then these VAMP chimeras were transferred into the destination vector pNX35-Dest by LR reaction and performed the mbSUS assay using these constructs as prey and KC1 or KAT1 K^+ channel as bait.

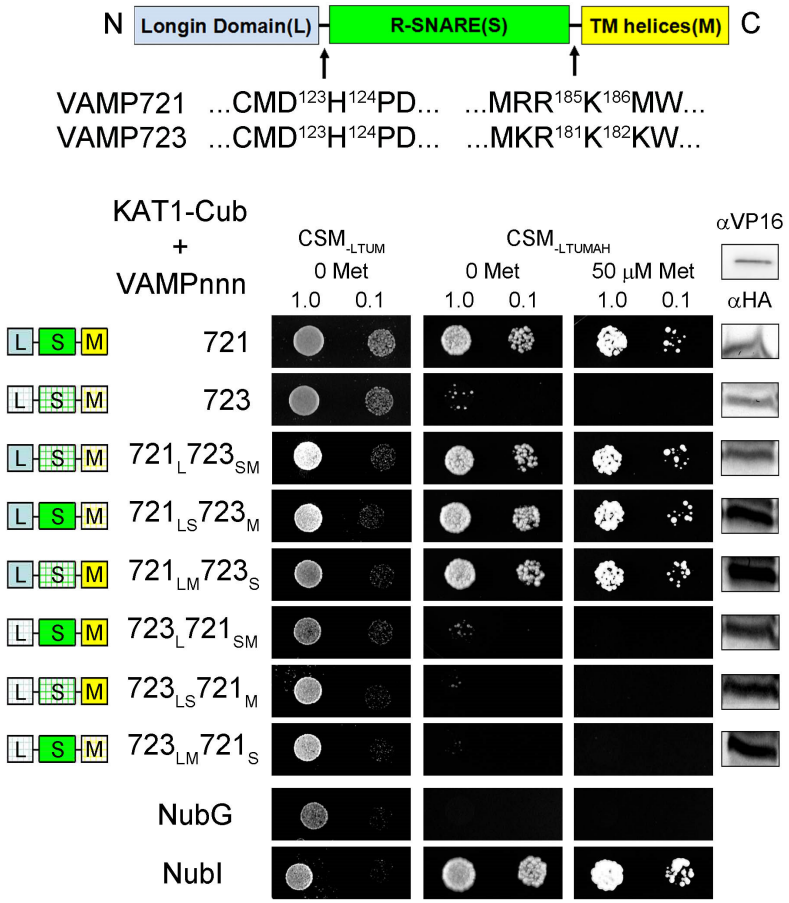

Figure 3-4. Interaction of KAT1 K^+ Channel Requires the VAMP721 longin domain

The longin domain (L, blue), the SNARE domain (S, green), and the transmembrane domain (M, yellow), with two breaks in the VAMP sequences at the $D^{123}H^{124}$ and the $R^{185}K^{186}$ junctions are shown at the top (for VAMP723, the secon break was at $R^{181}K^{182}$ as shown in Figure 3-3). Different chimeras are shown as colour cartoons on the left (VAMP721: solid colour; VAMP723: dotted-line filling). Diploid yeast expressing KAT1-Cub as bait with NubG-X fusions of VAMP721-723 chimeras or controls (negative: NubG; positive: NubI) as prey were spotted onto different media as indicated. CSM_{-LTUM} was used to verify the presence of both bait and prey vectors. $CSM_{-LTUMAH}$ was used to verify Ade- and His-independent growth. The addition of 50 μM Met to $CSM_{-LTUMAH}$ was used to verify interaction with lower K^+ channel-Cub expression. Diploid yeast was dropped at 1.0 and 0.1 OD_{600} in each case. Incubation time was 24 h for CSM_{-LTUM} and 72 h for $CSM_{-LTUMAH}$. Western blot analysis (5 μg total protein/lane) of the haploid yeast used for mating (right) using commercial HA antibody for the VAMP fusions and VP16 antibody for the K^+ channel fusions.

Figure 3-4 summarizes the mbSUS results for interaction between the VAMP chimeras and KAT1, including both the positive and negative controls of the full-length VAMP721 and VAMP723 constructs. Diploid yeast growth was only recovered when the preys contained the longin domain from VAMP721 (as $721_{L}723_{SM}$, $721_{LS}723_{M}$, and $721_{LM}723_{S}$). Interaction was retained, in each case, in the presence of 50 μM Met which suppressed the expression of the bait construct. However, in every case, chimeras incorporating the longin domain of VAMP723 failed to yield yeast growth, even if it contained the R-SNARE motif and the transmembrane domain from VAMP721 (as $723_{L}721_{SM}$). The expression of all VAMP chimeras and KAT1 was verified by Western blot analysis as shown on the right side of the figure. Similar results with supporting Western blot analysis were obtained in interaction tests between KC1 and VAMP chimeras, as shown in Figure 3-5. Again, with the higher expressing KC1-Cub construct the difference in yeast growth was seen only in present of 500 μM Met. In conclusion, the mbSUS assays indicated that the interaction of VAMP721 with KC1 and KAT1 K^{+} channels was dependent on the longin domain of the R-SNARE.

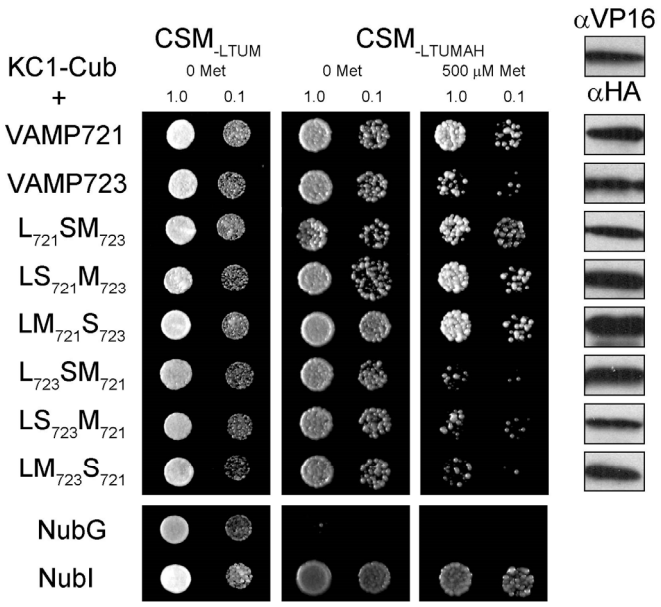

Figure 3-5. Interaction of KC1 K^+ Channel Requires the VAMP721 longin domain

Diploid yeast expressing KC1-Cub as bait with NubG-X fusions of VAMP7 proteins and controls (negative: NubG; positive: NubI) as prey were spotted onto different media as indicated. CSM_{-LTUM}: Complete Synthetic medium (CSM) without leucine (Leu, L), tryptophan (Try, T), uracil (Ura, U), and Methionine (Met, M) was used to verify the presence of both bait and prey vectors. $CSM_{-LTUMAH}$: CSM without L, T, U, M, Adenine (Ade, A), and Histidine (His, H) was used to verify Ade- and His-independent growth. The addition of 500 μM Met to $CSM_{-LTUMAH}$ was used to verify interaction when K^+ channels-Cub expression was suppressed. Diploid yeast were dropped at 1.0 and 0.1 OD_{600} in each case. Incubation time was 24 h for CSM_{-LTUM} plate and 72 h for $CSM_{-LTUMAH}$ plates. Western blot analysis (5 μg total protein/lane) of the haploid yeast used in mating (right) was carried out with commercial HA antibody for the VAMP fusions and VP16 antibody for the K^+ channel fusions.

3.2.3 The central Longin sequence of VAMP721 is essential for K^+ channel interaction

In the second round of chimeric construction, I divided the longin domains of VAMP721 and VAMP723 into three, roughly equal segments, L_A (residue 1-39), L_B (residue 40-81), and L_C (residue 82-123), as shown in Figure 3-6. I exchanged these three segments between the two VAMPs and used VAMP721 R-SNARE motif and transmembrane domain as backbone for the remainder of the VAMP assembly. Six non-redundant chimeras were generated from the longin $L_AL_BL_C$ segments of VAMP721 and VAMP723 by overlap extension PCR as described in Chapter 2. Each of these chimeras was tested in mbSUS assays again for interaction with the KAT1 and KC1 K^+ channels and was validated with supporting Western blot analysis.

Figure 3-6 shows the interaction between these longin domain chimeras and KAT1. VAMP721 and VAMP723 were included again for comparison. Interaction with the KAT1 K^+ channel was indicated for constructs that incorporated the L_B part of VAMP721 by the rescue of yeast growth on $CSM_{-LTUMAH}$ and in the presence of 50 μM Met (as $721L_{AB}723L_C$, $721L_{BC}723L_A$, and $721L_B723L_{AC}$). Replacing the central L_B segment of longin domain of VAMP721 with that of VAMP723 (as $721L_{AC}723L_B$) was enough to inhibit the interaction with KAT1 K^+ channel in the mbSUS assay. The same results were obtained with KC1 as bait (Figure 3-7). These results indicated that the L_B segment of VAMP721 was important for the interaction with K^+ channels.

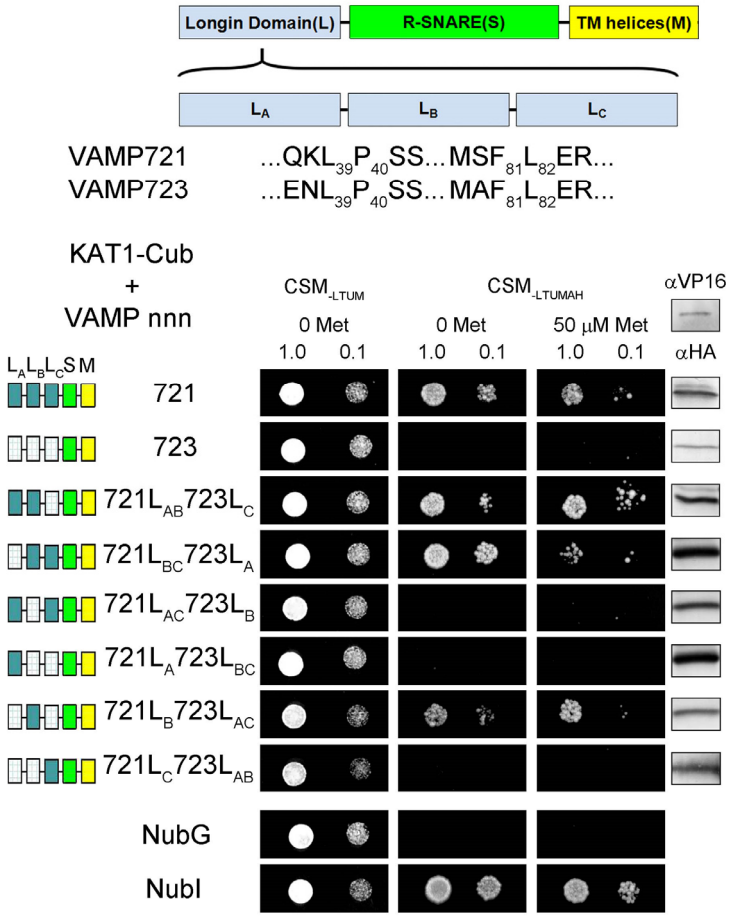

Figure 3-6. The central section L_B of the longin domain is essential for the Interaction between VAMP721 and KAT1

The longin domain (L, blue) was divided into three segments with two breaks in the VAMP sequences at the L^{39}P^{40} and the F^{81}L^{82} junctions as shown on the top. Different chimeras were shown as colour cartoon in left (VAMP721: solid colour; VAMP723: dotted-line filling). Diploid yeast expressing KAT1-Cub as bait with NubG-X fusions of VAMP721-723 longin domain chimeras or controls (negative: NubG; positive: NubI) as prey were spotted onto different media as indicated. VAMP721 and VAMP723 as preys were included for comparison. CSM$_{-LTUM}$ was used to verify the presence of both bait and prey vectors. CSM$_{-LTUMAH}$ was used to verify Ade- and His-independent growth. The addition of 50 μM Met to CSM$_{-LTUMAH}$ was used to verify interaction when K^+ channel-Cub expression was suppressed. Diploid yeast were dropped at 1.0 and 0.1 OD_{600} in each case. Incubation time was 24 h for CSM$_{-LTUM}$ plate and 72 h for CSM$_{-LTUMAH}$ plates. Western blot analysis (5 μg total protein/lane) of the haploid yeast used in mating (right) was carried out with commercial HA antibody for the VAMP fusions and VP16 antibody for the K^+ channel fusions.

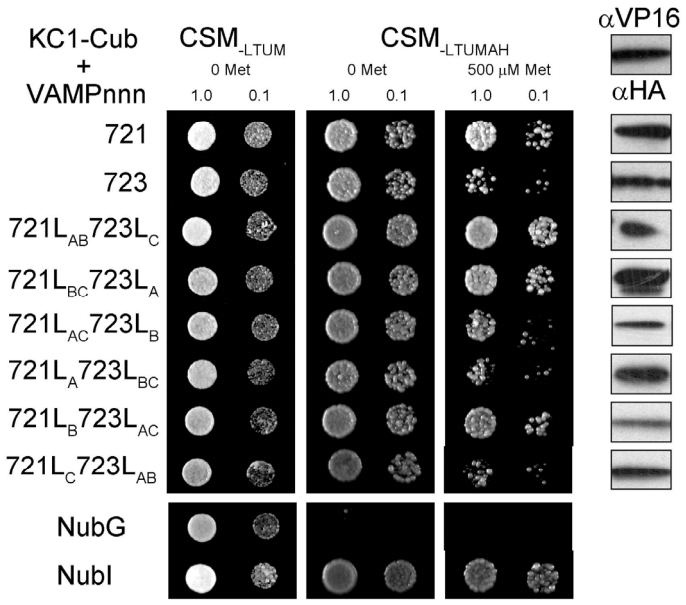

Figure 3-7. The central section L_B of the longin domain is essential for the Interaction between VAMP721 and KC1

Diploid yeast expressing KC1-Cub as bait with NubG-X fusions of VAMP721-723 longin domain chimeras or controls (negative: NubG; positive: NubI) as prey were spotted onto different media as indicated. VAMP721 and VAMP723 as preys were included for comparison. CSM_{-LTUM} was used to verify the presence of both bait and prey vectors. $CSM_{-LTUMAH}$ was used to verify Ade- and His-independent growth. The addition of 500 μM Met to $CSM_{-LTUMAH}$ was used to verify interaction when K^+ channel-Cub expression was suppressed. Diploid yeast were dropped at 1.0 and 0.1 OD_{600} in each case. Incubation time was 24 h for CSM_{-LTUM} plate and 72 h for $CSM_{-LTUMAH}$ plates. Western blot analysis (5 μg total protein/lane) of the haploid yeast used in mating (right) was carried out with commercial HA antibody for the VAMP fusions and VP16 antibody for the K^+ channel fusions.

3.2.4 Tyr^{57} of VAMP721 is a key residue in K^+ channel interaction

Within the L_B segment of the VAMP721 longin domain there are four amino acids that differ from VAMP723, namely Tyr^{57}, Asp^{61}, Gln^{76}, and Ser^{80}. The alignment of this part of the VAMPs can be found in Figure 3-3 and Figure 3-8, in which the important residues are highlighted by red squares or in red font.

Tyrosine (Tyr, Y) is a uncharged polar amino acid which has a phenolic hydroxyl group as its R group. Aspartic acid (Asp, D) is a charged polar acidic amino acids with a β-carboxyl group (CH_2COO^-) as the R group. Glutamine (Gln, Q) has an acetamino sidechain as its R group which makes it an uncharged polar amino acid. Serine (Ser, S) is also an uncharged polar amino acid with the small hydroxyl group as R group. In order to investigate their roles in VAMP-K^+ channel interaction, each of these residues in VAMP721 was substituted in turn with Ala by the QuickChange™ (Stratagene, La Jolla, USA) method as described in Chapter 2. Each single-site mutant was tested by mbSUS assay for interaction with K^+ channels.

Figure 3-8 shows the results of mbSUS interaction tests between VAMP single-site mutants and KAT1. As before, VAMP721 and VAMP723 were included for comparison. After dropping on selective media, yeast growth was recovered with preys VAMP721^{D61A}, VAMP721^{Q76A}, and VAMP721^{S80A}. However, yeast growth of VAMP721^{Y57A} was slightly reduced in the presence of 50 μM Met, suggesting that this residue was important for interaction with the channel. In VAMP723, the corresponding residue 57 is Asp, which is a charged amino acid. Therefore I replaced Tyr^{57} in VAMP721 with Asp and also undertook the reverse mutation in VAMP723 to generate VAMP721^{Y57D} and VAMP723^{D57Y}. The VAMP721^{Y57D} substitution eliminated yeast growth, even in the absence of Met. Remarkably, the complementary mutation VAMP723^{D57Y} yielded strong growth of the

diploid yeast, indicating the interaction between VAMP723^{D57Y} and KAT1. Western blot analysis showed that these single site mutants did not affect VAMP expression in yeast.

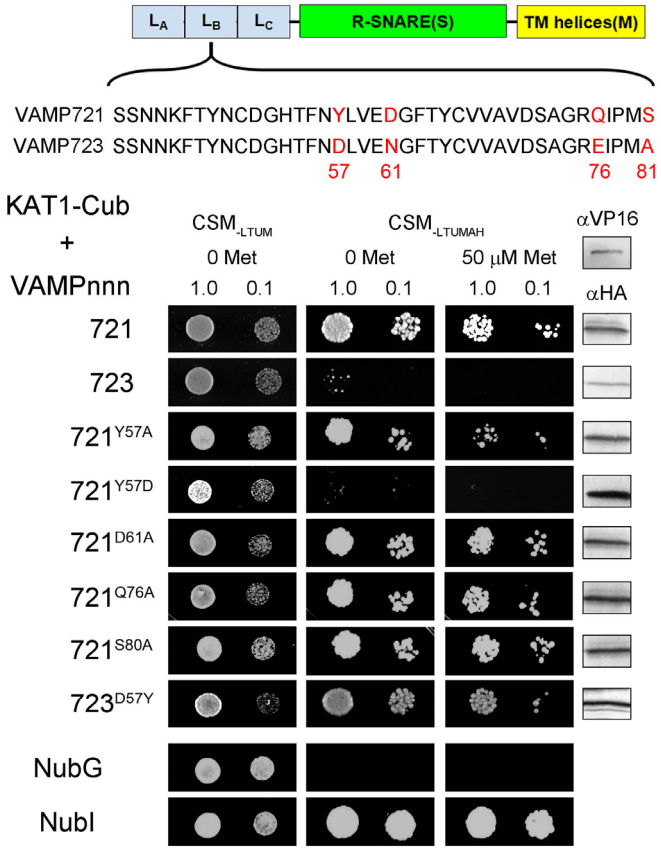

Figure 3-8. VAMP721 Interaction with the KAT1 K⁺ Channel Depends on Residues Tyr^{57}

The alignment of L_B longin domain amino acid sequences of VAMP721 and VAMP723 indicated for reference. Diploid yeast expressing KAT1-Cub as bait with NubG-X fusions of VAMP721 mutants, VAMP723 mutant or controls (negative: NubG; positive: NubI) as prey were spotted onto different media as indicated. VAMP721 and VAMP723 as preys were included for comparison. CSM$_{-LTUM}$ was used to verify the presence of both bait and prey vectors. CSM$_{-LTUMAH}$ was used to verify Ade- and His-independent growth. The addition of 50 μM Met to CSM$_{-LTUMAH}$ was used to verify interaction when K⁺ channel-Cub expression was suppressed. Diploid yeast were dropped at 1.0 and 0.1 OD_{600} in each case. Incubation time was 24 h for CSM$_{-LTUM}$ plate and 72 h for CSM$_{-LTUMAH}$ plates. Western blot analysis (5 μg total protein/lane) of the haploid yeast used in mating (right) was carried out with commercial HA antibody for the VAMP fusions and VP16 antibody for the K⁺ channel

fusions.

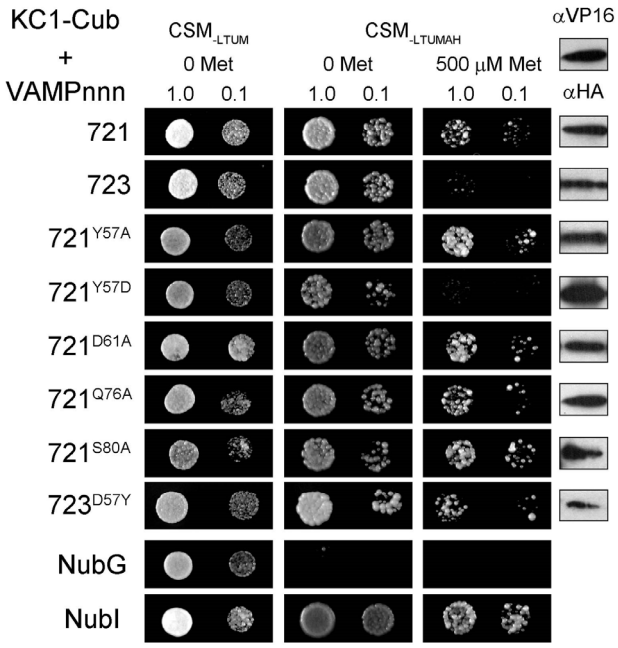

Figure 3-9. VAMP721 Interaction with the KC1 K^+ Channel Depends on Residues Tyr^{57}

Diploid yeast expressing KC1-Cub as bait with NubG-X fusions of VAMP721 mutants, VAMP723 mutant or controls (negative: NubG; positive: NubI) as prey were spotted onto different media as indicated. CSM_{-LTUM} was used to verify the presence of both bait and prey vectors. VAMP721 and VAMP723 as preys were included for comparison. $CSM_{-LTUMAH}$ was used to verify Ade- and His-independent growth. The addition of 500 μM Met to $CSM_{-LTUMAH}$ was used to verify interaction when K^+ channel-Cub expression was suppressed. Diploid yeast were dropped at 1.0 and 0.1 OD_{600} in each case. Incubation time was 24 h for CSM_{-LTUM} plate and 72 h for $CSM_{-LTUMAH}$ plates. Western blot analysis (5 μg total protein/lane) of the haploid yeast used in mating (right) was carried out with commercial HA antibody for the VAMP fusions and VP16 antibody for the K^+ channel fusions.

I repeated these experiments using KC1 as the bait in mbSUS assays. As shown in Figure 3-9, $VAMP721^{Y57D}$ strongly suppressed diploid yeast growth when expression of bait was reduced in the present of 500 μM Met. Growth was not affected by any of the other mutants and the complementary $VAMP723^{D57Y}$ mutant was sufficient to rescue growth.

Thus I concluded that the interaction between VAMP721 and KC1 or KAT1 K^+ channels depended on the Tyr residue at position 57.

In order to rule out the roles of other amino acids in VAMP-K^+ channel interaction, I performed mbSUS assay using VAMP721^{D61N} or VAMP721^{Q76E} as preys, thus exchanging these other residues of VAMP721 to their corresponding residues in VAMP723. For residue Ser^{80}, the corresponding residue in VAMP723 is Ala, so I did not prepare any mutant for this residue. The results are shown in Figure 3-10 and confirms that these mutants were not of primary importance for K^+ channel interaction.

I carried more residue exchanges to investigate this site, in particular to test whether Tyr^{57} might serve as a site for phosphorylation of the protein. These mbSUS results are shown in Figure 3-10. Phenylalanine (Phe, F) is an amino acid with polar R group. Compared to Tyr, Phe has a phenyl group instead of phenolic hydroxyl group and is more strongly hydrophobic. Exchange residue 57 of VAMP721 from Tyr to Phe had no effect on diploid yeast growth, indicating that missing of the -OH in residue was not important for the interaction. Asparagine (Asn, N) is a uncharged polar amino acid. It has an acylamino group as the R group and is often used as a control for phosphomimetic substitutions (Lee et al., 2005; Cameron et al., 2009; Shi et al., 2013). The diploid yeast of VAMP721^{Y57N} did not grow, even in CSM$_{-LTUMAH}$ plate without Met, like VAMP721^{Y57D}. This result suggested that the charge brought by R group of Tyr^{57} is probably not important for the interaction and, therefore, that phosphorylation of the site is less likely to be important in regulating the interaction. In conclusion, Tyr^{57} of VAMP721 was essential for the interaction between VAMP721 and K^+ channel, but its group size rather than charge is more important in the interaction.

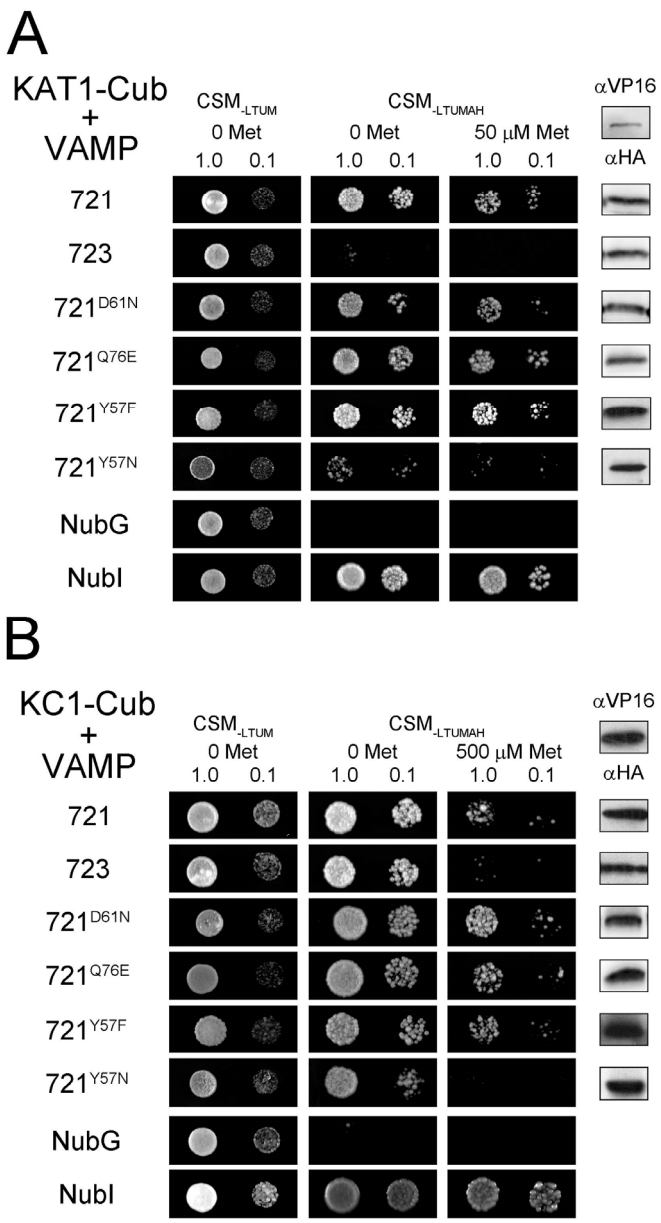

Figure 3-10. The effect of VAMP721 Single-Site Mutant D61N, Q76E, Y57F and Y57N on the interaction with K^+ channels

Diploid yeast expressing KAT1-Cub as bait (A) or KC1-Cub as bait (B) with NubG-X fusions of VAMP721 mutants or controls (negative: NubG; positive: NubI) as prey were spotted onto different media as indicated. VAMP721 and VAMP723 as preys were included for comparison. CSM_{-LTUM} was used to verify the presence of both bait and prey vectors. $CSM_{-LTUMAH}$ was used to verify Ade- and His-independent growth. The addition of Met to $CSM_{-LTUMAH}$ (500 μM for KC1 and 50 μM for KAT1) was used to verify interaction when K^+ channel-Cub expression was suppressed. Diploid yeast were dropped at 1.0 and 0.1 OD_{600} in each case. Incubation time was 24 h for CSM_{-LTUM} plate and 72 h for $CSM_{-LTUMAH}$ plates. Western blot analysis (5 μg total protein/lane) of the haploid yeast used in mating (right) was carried out with commercial HA

antibody for the VAMP fusions and VP16 antibody for the K^+ channel fusions.

3.2.5 The role of residues around VAMP721 Tyr^{57} in K^+ channel interaction

The importance of VAMP721 residue Tyr^{57} in binding with the channels does not rule out contributions from other residues within the longin domain or elsewhere in VAMP721 sequence. To investigate the role of other residues, I prepared a series of double-mutant VAMP clones. Because VAMP721^{Y57A} had a weak effect in suppressing the VAMP-K^+ channel interaction, Y57A was chose as one of the mutations. For the other mutant sites, the amino acid residues around Tyr^{57} (from Cys^{50} to Val^{68}) were changed sequentially to Ala. Again, as described in Chapter 2, I used the QuickChange™ (Stratagene, La Jolla, USA) method to add the second-site mutations starting with VAMP721^{Y57A} as the template in the PCR reactions. mbSUS assays were performed using these VAMP double-sites mutants as preys and the KC1 and KAT1 K^+ channels as baits.

Similar results were obtained with the two channels and are shown in Figure 3-11 and Figure 3-12 with supporting Western blot analysis. Compared with VAMP723, I found the double-site mutants did not completely suppress yeast growth except the one of Tyr^{65}. However, the weak diploid yeast growth in $CSM_{-LTUMAH}$ with Met had provided some information about the contribution of residues around Tyr^{57}. Addition of mutations at some residues, including Gly^{52} to Asn^{56}, Leu^{58} to Glu^{60}, Gly^{62}, Tyr^{65}, Val^{67} and Val^{68}, affected growth and therefore must have suppressed the interaction between VAMP721 and the K^+ channels. As shown in Figure 3-3, the residues around Tyr^{57}, from Cys^{50} to Glu^{60} were highly conserved among VAMP72 group proteins, suggested they might play a role in basic function of the R-SNARE protein. The mbSUS assay

results clearly showed that these conserved residues of VAMP721 (Gly^{52} to Asn^{56}, Leu^{58} to Glu^{60}) were also involved in the interaction with K^+ channel. Other important residues like Gly^{62}, Val^{67} and Val^{68} were also conserved among VAMP72 group proteins. For Tyr^{65}, when mutated it to Ala, the double mutant diploid yeast growth were completely suppressed, suggested it was involved in VAMP-channel interaction.

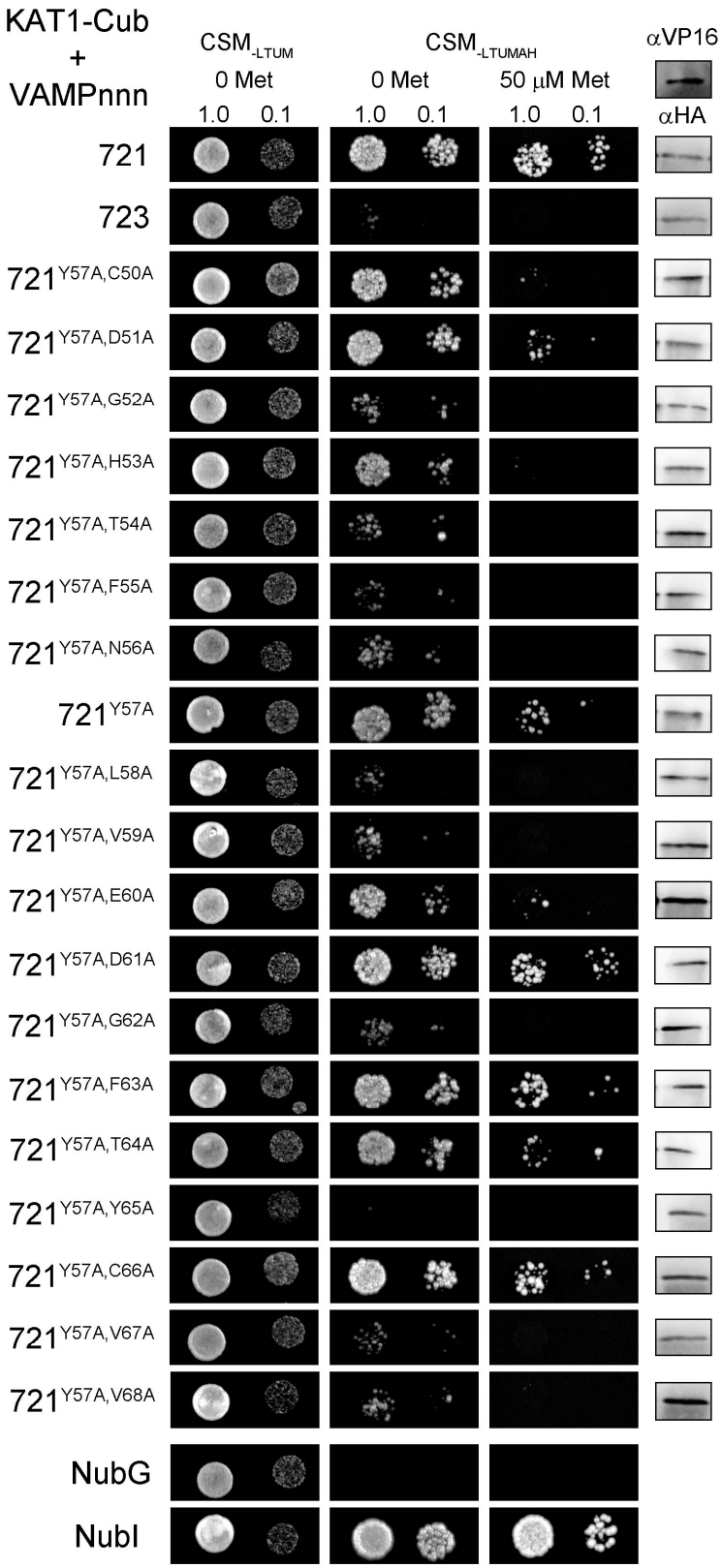

Figure 3-11. The contribution of other residues around Tyr[57] for VAMP721-KAT1 interaction

Diploid yeast expressing KAT1-Cub as bait with NubG-X fusions of VAMP721 double mutants or controls (negative: NubG; positive: NubI) as

prey were spotted onto different media as indicated. VAMP721 and VAMP723 as preys were included for comparison. CSM_{-LTUM} was used to verify the presence of both bait and prey vectors. $CSM_{-LTUMAH}$ was used to verify Ade- and His-independent growth. The addition of 50 μM Met to $CSM_{-LTUMAH}$ was used to verify interaction when K^+ channel-Cub expression was suppressed. Diploid yeast were dropped at 1.0 and 0.1 OD_{600} in each case. Incubation time was 24 h for CSM_{-LTUM} plate and 72 h for $CSM_{-LTUMAH}$ plates. Western blot analysis (5 μg total protein/lane) of the haploid yeast used in mating (right) was carried out with commercial HA antibody for the VAMP fusions and VP16 antibody for the K^+ channel fusions.

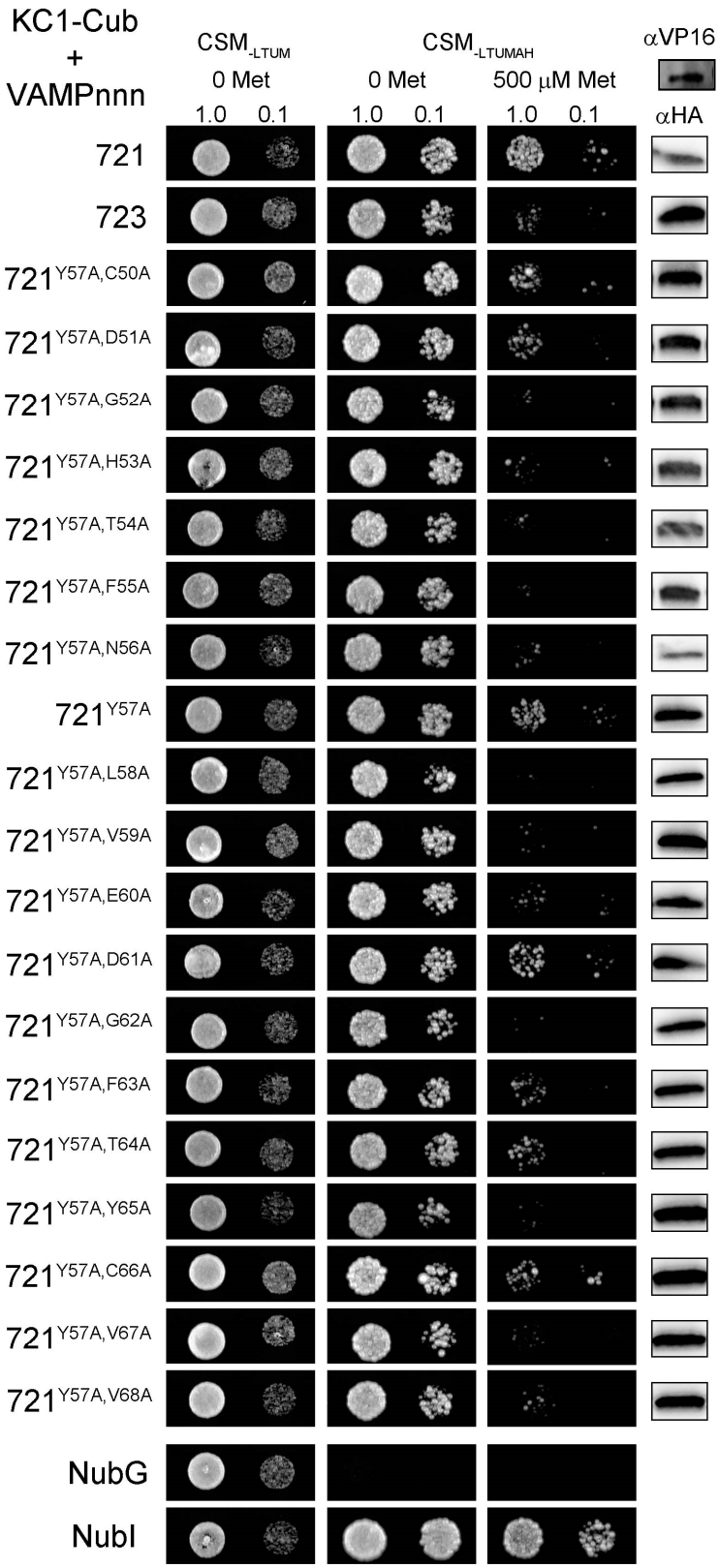

Figure 3-12. The contribution of other residues around Tyr[57] for VAMP721-KC1 interaction

Diploid yeast expressing KC1-Cub as bait with NubG-X fusions of VAMP721 double mutants or controls (negative: NubG; positive: NubI) as

prey were spotted onto different media as indicated. VAMP721 and VAMP723 as preys were included for comparison. CSM_{-LTUM} was used to verify the presence of both bait and prey vectors. $CSM_{-LTUMAH}$ was used to verify Ade- and His-independent growth. The addition of 500 μM Met to $CSM_{-LTUMAH}$ was used to verify interaction when K^+ channel-Cub expression was suppressed. Diploid yeast were dropped at 1.0 and 0.1 OD_{600} in each case. Incubation time was 24 h for CSM_{-LTUM} plate and 72 h for $CSM_{-LTUMAH}$ plates. Western blot analysis (5 μg total protein/lane) of the haploid yeast used in mating (right) was carried out with commercial HA antibody for the VAMP fusions and VP16 antibody for the K^+ channel fusions.

3.3 Discussion

In this Chapter, the interaction of *Arabidopsis* VAMPs with two PM K^+ channels was examined using the mbSUS assay. This method is an alternative to the classical yeast two-hybrid system. The mbSUS assay relies on the ubiquitin-degradation pathway as a sensor for protein-protein interactions. Ubiquitin tagged proteins are normally degraded by 26S proteasomes (Zwickl et al., 2001). When ubiquitin is fused with a reporter protein, it is recognised by ubiquitin specific proteases (UBPs). UBPs cleave the reporter protein linked to the C terminus of ubiquitin (Johnsson et al., 1994). For mbSUS, ubiquitin is genetically divided between amino acids 34 and 35 of the 76-residue protein to make the N terminal (Nub) and C terminal (Cub) ubiquitin fragments. These fragments are able to reassemble ubiquitin and be recognised by the UBPs to release the reporter protein. So this split-ubiquitin approach can be used to detect the interaction of protein pairs with cellular concentrations below 700 nM (Muller and Johnsson, et al., 2008). In the mbSUS system, the N-terminal half of ubiquitin is mutated at position 13 (which generates NubG) which prevents spontaneous reassembling of the two halves of ubiquitin. The C-terminal half of ubiquitin is then fused with transcription reporter complex PLV (ProteinA-LexA-VP16). As a result, the fusion of a bait protein to the

CubPLV co-expressed with a prey fusion with NubG gives a pair of fragments derived from ubiquitin which are able to switch on reporter gene activity if the fused components interact (Grefen et al., 2009). The method is useful for cytosolic and membrane-bound proteins, which facilitates the testing of proteins that might otherwise be mislocalized or truncated, as they would be in the yeast two-hybrid (Y2H) system which requires nuclear localization for reporter gene expression (Grefen et al., 2009). The mbSUS system is not based on a transcriptional readout as the conventional Y2H system. Therefore, it is suitable for the analysis of strong transcription factors, which may interfere with the readout in conventional Y2H system (Wellhausen and Lehming, 1999; Fields and Song, 1989). Furthermore, the UBPs are present in both cytosol and nucleus. So mbSUS system is suitable for detection of membrane protein-protein interaction in their native environment (Lehming, 2002).

I found that both the KC1 and KAT1 K^+ channels could interact with VAMP71 subgroup proteins (Figure 3-1 and Figure 3-2) as well as several of the VAMP72 subgroup proteins. The VAMP71 group proteins have similar sequence to mammalian VAMP7 members which are known to facilitate endosomal traffic (Sanderfoot et al., 2007). In plant cells, VAMP711 mediates the transport of H_2O_2-containing vesicles to the vacuole (Leshem et al., 2006). Silencing of VAMP711 in *Arabidopsis* by RNAi disturbed the distribution of ROS in plant cells and suppressed the stomatal closing under ABA treatment (Leshem et al., 2010). The interaction between VAMP711 and K^+ channels was the weakest of the four VAMP71 proteins. Stronger interaction readouts were observed with VAMP712, VAMP713, and VAMP714 as preys. When GFP-tagged, VAMP712 and VAMP713 have been recovered at the vacuole and VAMP714 at the Golgi, but functional roles for these three R-SNAREs remains uncertain, and a question remains over their localization, especially in light of the analysis based on overexpression in protoplasts (Uemura et al., 2004). The alignment between VAMP711 and VAMP721

shows only 38% sequence similarity (as shown in Figure 3-3). How significant these interactions are is therefore difficult to say.

Of the eight VAMP72 subgroup proteins, VAMP721, VAMP722, VAMP724, and VAMP726 interacted strongly with both KC1 and KAT1 K^+ channels (Figure 3-1 and Figure 3-2). All of these VAMPs associate with secretory traffic at the PM. By contrast, no substantive interaction was observed with VAMP723 which has been localized at the ER, and mbSUS assays indicated only a weak interaction with VAMP727 which has been associated with traffic between early endosomes and the PM (Uemura et al., 2004; Uemura et al., 2007). The homologs VAMP721 and VAMP722 are known to assemble SNARE core complexes with SYP121 to drive vesicle fusion at the PM in *Arabidopsis* (Kwon et al., 2008; Karnik et al., 2013b). VAMP721 and VAMP722 are greater than 97% sequence identical and appear functionally redundant in vivo (Kwon et al., 2008; Zhang et al., 2011; El Kasmi et al., 2013). VAMP723 has 83% sequence similarity with VAMP721, yet it did not interact with the K^+ channels. Thus I focused on the interaction with VAMP721 and used VAMP723 as a control for further investigation to resolve the interacting domains.

It is worth noting that the expression level of SNAREs in diploid yeast containing KC1 was higher than that of diploid yeast containing KAT1 (one example of such a difference can be found in Figure 3-10). Bruggemann et al. (1999) reported KAT1 expression could rescue the growth of yeast mutant lacking K^+ transporters in low-K^+ medium, which suggests KAT1 forms functional K^+ channel in yeast. I suspect that the relative low level of expression in diploid yeast containing KAT1 generally was attributed to the KAT1 K^+ channel activity which could have affected the solute balance of the yeast. By contrast, KC1 does not form functional K^+ channels by itself and is therefore less likely to have had a similar effect on yeast growth. To reveal the effect of K^+ channel activity on yeast protein expression, more work will need to be done in the future.

The mbSUS assays using VAMP domain chimeras as prey showed

the key domain for VAMP-K^+ channel interaction was localized to the VAMP longin domain and conferred specificity in the K^+ channel interactions (Figure 3-4 and Figure 3-5). The N terminal binding domain of VAMP721 paralleled the finding from SYP121. Previous reports have shown that SYP121 interacts with KC1 and KAT1 K^+ channels through its N terminal FxRF motif, which is also removed from the SNARE motif of this Qa-SNARE (Grefen et al., 2010a; Honsbein et al., 2011).

Several SNAREs have been identified to interact directly with K^+ and Ca^{2+} channels in animals, interactions that have been proposed to underpin potentiation in neuronal signaling (Bezprozvanny et al., 1995; Bezprozvanny et al., 2000; Ji et al., 2002; Cui et al., 2004). Notably the principle Qa-SNARE syntaxin 1A, which mediates in traffic at the neuronal PM, will bind with Kv2.1 K^+ channels in vitro and has been shown to subtly modulate channel activity when expressed in *Xenopus* oocytes (Tsuk et al., 2005). Mammalian VAMP2 is the cognate partner of syntaxin 1A. It also binds with the Kv2.1 channel in vitro and enhances channel inactivation when expressed in oocytes (Lvov et al., 2008). However, channel binding by syntaxin 1A is associated with the SNARE motif of the Qa-SNARE (Bezprozvanny et al., 2000; Cui et al., 2004; Tsuk et al., 2005). Kv2.1 binding to VAMP2 is lost on assembly of the SNARE core complex in vitro (Tsuk et al., 2008), suggesting that the channel also binds with the SNARE motif of this R-SNARE in animal cells.

By contrast, in the second round mbSUS assay which using VAMP longin domain chimeras as preys, my results identified a key part of the binding site of VAMP721 to the central part of longin domain (as shown in Figure 3-6 and Figure 3-7). Most important, this site is different from the SNARE motif which has previously been shown to be very ‘sticky’ and interacts with many different proteins (Bezprozvanny et al., 2000; Cui et al., 2004; Xu et al., 2010). Interestingly, in the central L_B region of the longin domains, there are only four amino acids that differ between VAMP721 and VAMP723. I found that the single residue Tyr^{57} was

essential for the VAMP721 binding when expressed in yeast. In VAMP723, the residue at position 57 is Asp. The exchange of this amino acid between VAMP721 and VAMP723 generated VAMP mutants VAMP721^{Y57D} and VAMP723^{D57Y} (Figure 3-8 and Figure 3-9). The former strongly inhibited the interaction with KC1 and KAT1 K^+ channels, while the latter was sufficient to engineer channel interaction in this, otherwise non-interacting VAMP. These findings underlined the central importance of this residue to the interaction. One intriguing question arising from these data relates to the implicit re-localization of the mutant VAMPs - at least of VAMP723^{D57Y} - and their distributions at the PM. To answer this question, the subcellular location of GFP fused VAMPs was examined and these results are presented in the next chapter.

It is of interest that Tyr^{45} of the neuronal Tl-VAMP/VAMP7 (Vivona et al., 2010) plays a crucial role in maintaining the VAMP in a closed conformation and unavailable for binding in a SNARE core complex with syntaxin 1A and SNAP25. The residue is phosphorylated by the c-Src kinase in vitro and in vivo. The phosphomimetic Tl-VAMP^{Y45E} mutant activates exocytosis and increases the VAMP binding affinity with the cognate SNAREs (Burgo et al., 2013). So it was worth considering if Tyr^{57} of VAMP721 in plants is a potential phosphorylation site and that phosphorylation may contribute to the binding with the K^+ channel. In the amino acid Tyrosine, there is a phenolic hydroxyl group as the R group. Is the size of the R group important for VAMP721-K^+ channel interaction? I exchanged this uncharged amino acid to Phe and Asn to further investigate the role of residue Tyr^{57} in VAMP721-K^+ channel interaction. The VAMP721^{Y57F} had no effect on K^+ channel binding, which suggested there was role of the residue conjugation or physical size in VAMP-K^+ channel interaction. VAMP721^{Y57N} suppressed the interaction like VAMP721^{Y57D}, especially in the CSM$_{-LTUMAH}$ with Met medium (See Figure 3-10), suggesting that the negative charge introduced by Asp at this location was not the key to VAMP- K^+ channel binding. According to

these results, it is still difficult to be sure whether Tyr^{57} is a phosphorylation site. More work like mutating Tyr^{57} to glutamate and serine needs to be done in the future.

What are the contributions from other residues around Tyr^{57}? To answer this question, I performed mbSUS assay using double mutants of VAMP721 as preys and KC1 or KAT1 as baits. I found conserved residues around Tyr^{57}, including Gly^{52} to Asn^{56}, Leu^{58} to Glu^{60}, Gly^{62}, Tyr^{65}, Val^{67} and VAl^{68} were involved in the VAMP-channel interaction, but their contributions were only evident in the double mutants. When mutated to Ala together with the Y57A mutation, I found diploid yeast growth was suppressed in the present of Met in each of these cases, suggesting these residues around Tyr^{57} played roles in channel binding. In other words, the interaction between VAMP721 and K^+ channels might depend on a special protein structure containing Tyr^{57} and residues around it.

To investigate the protein structure of VAMP721, I performed structure prediction by the Protein Homology/analogY Recognition Engine V 2.0 (Phyre2; Kelley and Sternberg, 2009). Phyre2 is a web-based service which predicts the three-dimensional structure of a protein based on the fact that different homologous protein sequences often adopt remarkably similar structures. Thus, given a protein sequence of interest, one may compare this sequence to the sequences of proteins with experimentally determined structures. If a homologue can be found, an alignment of the two sequences can be generated and used to build a three-dimensional model of the sequence of interest (Bennett-Lovsey et al., 2008). The Phyre2 service predicts the protein structure using the principles and techniques of this homology modelling mentioned above. The work process of Phyre2 server is described below:

At first, the Phyre2 service carries out a Blast search among the submitted protein sequences of interest with protein sequences from a library of known protein structures taken from the Structural

Classification of Proteins database. Secondly, the secondary structure is predicted by three programs, including Psi-Pred (McGuffin et al., 2000), SSPro (Pollastri et al., 2002), and JNet (Cuff et al., 1999). In the third step, the Phyre2 service will combine the information from last two steps and carry out an analysis using a protein-protein alignment algorithm, which is detailed in Bennett-Lovsey et al. (2008). This alignment process returns a score on which the alignments are ranked. Finally, the top ten highest scoring alignments are then used to construct full 3D models of the submitted protein.

The protein structures of SEC22, YKT6, and VAMP7 in humans have been reported (Gonzalez et al., 2001; Tochio et al., 2001; Kent et al., 2012). Based on these structures, I performed Phyre2 analysis for VAMP721 (Job ID: 72d4b19fce88aabd). From this analysis, 209 residues (95% of the sequence) could be modelled at more than 90% confidence using the multiple templates. As shown in figure 3-13, the longin domain of VAMP721 was folded back (colored from dark blue to yellow). The important residues around it (Gly^{52} to Glu^{60}) formed a beta-strand which was inside the longin domain structure (as shown in Figure 3-13 B yellow part), and Tyr^{57} was positioned in the center of longin domain (as shown by white arrow). Such a beta-strand might be an important structure for the binding to the channels. The exchange of residue 57 between Tyr and Asp, might affect how longin domain form a special 3D structure, which then finally decides the VAMP-channel interaction. The double mutants of Tyr^{57} with Tyr^{65} completely suppressed yeast growth.

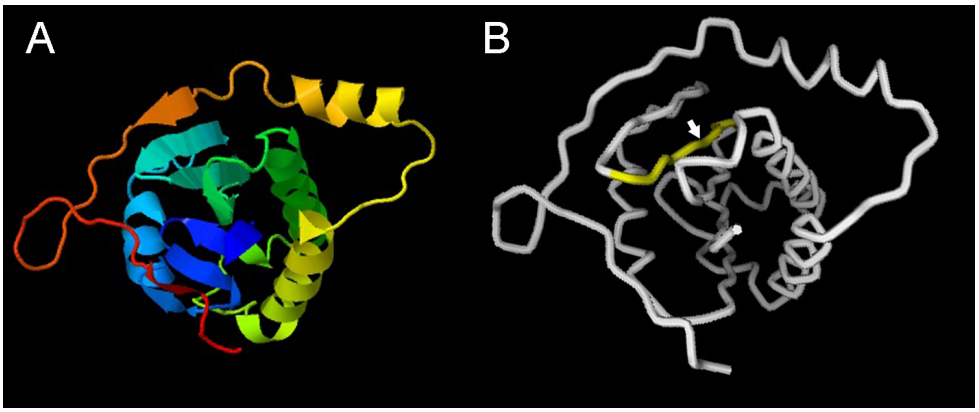

Figure 3-13. The predicted structure of VAMP721

The prediction was performed by Phyre2.
A: The 3D view was performed by JSmol. The protein were coloured from N to C terminus according to the order of rainbow (from blue to red). The longin domain were folded back (coloured from dark blue to yellow).
B: The protein structure was analysis by 3D Molecular Viewer. The residue Gly^{52} to Glu^{60} formed a beta-strand (as shown in yellow). The residue Tyr^{57} was in center of this beta-strand (white arrow).

Compared to other methods, the mbSUS assay in yeast is inexpensive and fast. However, each of the protein-protein interaction detection methods has its own strengths and weaknesses. The mbSUS system in yeast may produce false positive and negative results (Lehming, 2002). So in next chapter, the main interaction discovered by mbSUS assay were verified by BiFC analysis, combined with the investigation about the role of residue 57 in VAMP localization.

Chapter 4. Tyr^{57} of VAMP721 is essential for VAMP subcellular location and K^+ channel interaction in vivo

4.1 Introduction

In 2005, Uemura et al. (2005) performed the experiment to investigate the subcellular targeting mechanism of *Arabidopsis* R-SNAREs. They used the vacuolar localized VAMP711, the endosomal localized VAMP727, and the PM localized VAMP721 as backbones, and made the GFP-tagged chimeric proteins by exchanging different domains among these VAMP proteins. Their results showed that the transmembrane domain was not relevant for the vacuolar targeting, while the longin domain was essential for the vacuolar and PM targeting. In Chapter 3, the mbSUS assay results indicated Tyr^{57} in longin domain of VAMP721 was essential for VAMP-K^+ channel interaction and the exchange between VAMP721 and VAMP723 of the residues at position 57 was enough to determine K^+ channel binding. Considering KC1 and KAT1 K^+ channels are expressed at the PM but VAMP723 is normally localized to the endoplasmic reticulum, these results raised a question whether the residue at position 57 could affect the subcellular location of the VAMPs and finally determine the VAMP-channel interaction. To answer this question was the first aim of this chapter.

There are many methods to investigate protein-protein interactions. Each methods has its own strengths and weaknesses. Using only one technique inevitably suffers the potential for false (positive, but also negative) results compared to that occurring in reality. To resolve this problem, a combination of techniques is necessary to validate protein interactions. In Chapter 3, I performed mbSUS assays to investigate VAMP-K^+ channel interactions. Usually, an interaction detected needs to be verified by two different experiments. So the second aim of the work presented in this chapter was to verify VAMP-K^+ channel interactions

identified in Chapter 3 by different methods.

Here I reported experiments tagging VAMP721, VAMP723, VAMP721^{Y57D}, and VAMP723^{D57Y} with GFP for transient expression in *Arabidopsis* seedlings to explore the localization of VAMP. For protein-protein interaction confirmation, I used ratiometric bimolecular fluorescence complementation (rBiFC) analysis to validate the VAMP-K^+ channel interactions.

4.2 Results

4.2.1 The single-site mutant of residue 57 affect the localization of VAMP721 and VAMP723.

In order to investigate the subcellular location of VAMPs, the entry clones containing VAMP721, VAMP723, VAMP721^{Y57D}, and VAMP723^{D57Y} were used to make destination clones by LR reaction with the destination vectors pUBN-GFP-Dest (Grefen et al., 2010b) as described in Chapter 2. pUBN-GFP-Dest are a Gateway-compatable vectors with fluorescent tags incorporating the UBQ-10 promoter of *Arabidopsis*. Because the C terminus of the VAMPs comprise transmembrane domains, I fused GFP to the N termini. I transferred these destination clones into *Arabidopsis* seedlings by *Agrobacterium tumefaciens*-mediated gene transfer using cocultivation and analyzed the fluorescence distribution by confocal microscopy using standardized recording parameters as described in Chapter 2.

In *Arabidopsis* seedlings, the localization differences between endomembrane, the tonoplast and the PM is distinguishable by labeling at the root hair tips and around the nucleus. Expression of GFP tagged proteins at the PM normally shows fluorescence only to the outside of the nucleus on the cell wall side and around the edge of the root hair tip; labeling in the endoplasmic reticulum and other endomembrane

compartments is generally found surrounding the nucleus both on the cell wall and internal sides, and commonly fills the hyaline zone of the root hair tip; localization at the tonoplast shows up as labeling only on the internal side of the nucleus and to the inside of the root hair tip.

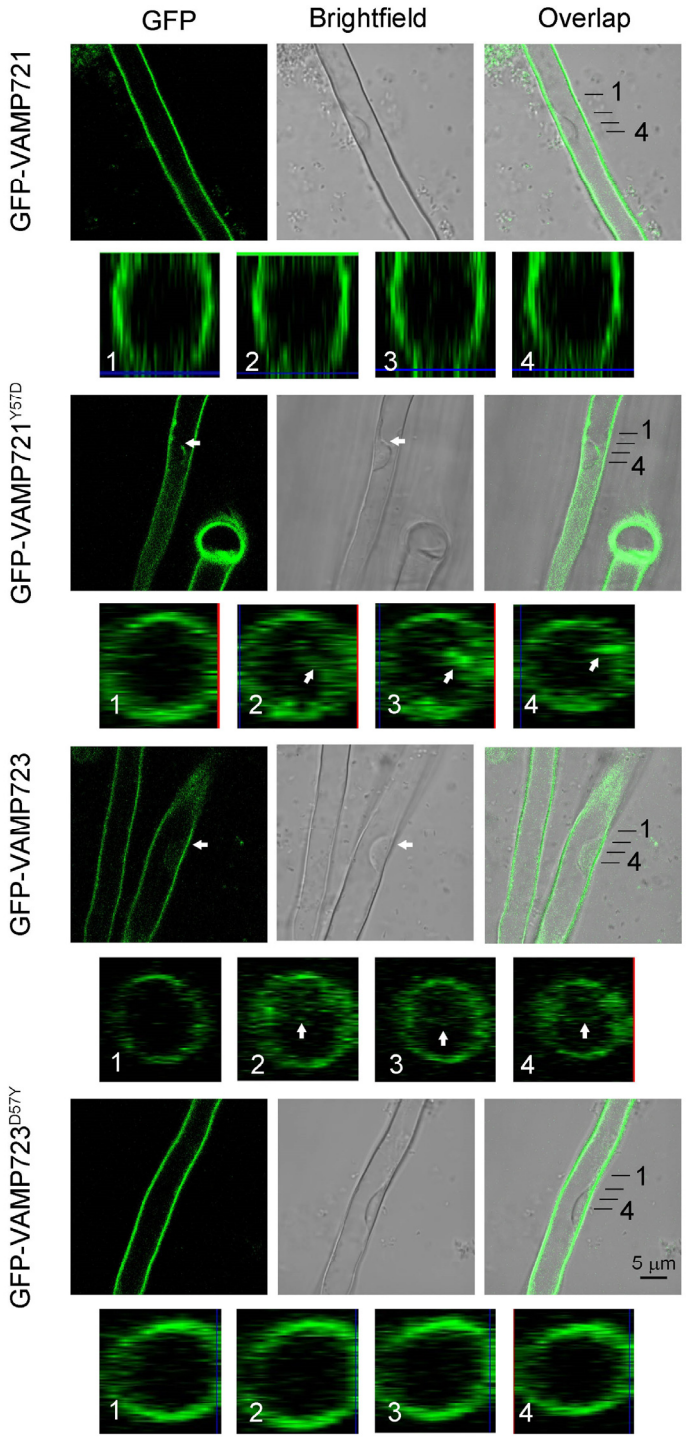

Figure 4-1. The single-site mutants VAMP721^{Y57D} and VAMP723^{D57Y} affect the localization of the R-SNAREs

Images showing (left to right) optical sections through *Arabidopsis* root hairs with GFP fluorescence, bright-field and overlay, and with Z-axis transects (panels 1-4) for GFP-tagged constructs of VAMP721, VAMP721^{Y57D}, VAMP723, and VAMP723^{D57Y}. The GFP-VAMP constructs were transiently transformed in *Arabidopsis* seedlings and images collected 3 days post-transformation. Transects were taken through the

root hair nucleus at positions marked in the overlap images (1-4 from top to bottom) in each example. Scale bar: 5 μm.

Figure 4-1 showed the GFP signal of root hairs and the Z-axis transects of GFP-tagged constructs of VAMP721, VAMP721^{Y57D}, VAMP723, and VAMP723^{D57Y}. Uemera et al. (2004) reported that VAMP721 is targeted to the PM while VAMP723 is found in the endoplasmic reticulum. My results supported these finding. There was no GFP signal observed on the cytosol side of the nucleus for GFP-VAMP721, indicating its subcellular location at the PM. For GFP-VAMP723, there was some fluorescence visible around nucleus, as indicated by white arrow in GFP fluorescence and brightfield images. In the transect images of all samples, image 1 was shown as a control which was cut the root hair avoiding nucleus. No GFP signal was visible beyond the cell periphery. In image 2-4, some internal fluorescence structure was visible also inside the cell (white arrow), which suggested labeling of the endoplasmic reticulum or other endomembrane compartments. For GFP-VAMP723^{D57Y}, the GFP signal distributed in a way similar to that of VAMP721, which indicated the peripheral location of this VAMP723 mutant. For GFP-VAMP721^{Y57D}, the signal around nucleus was like that of VAMP723, indicating that the mutation of Tyr^{57} to Asp changed the localization of VAMP721. In conclusion, the residue 57 of VAMP721 and VAMP723 appear important for the localization of VAMPs.

4.2.2 VAMP721, but not VAMP723, interacts with KAT1 and KC1 K^+ Channels in vivo

To assess VAMP-K^+ channel interactions, I cloned the coding sequences of VAMP721 and VAMP723 into the 2in1 vector system (Grefen, 2012) for transient transformation, expression, and ratiometric

bimolecular fluorescence complementation (rBiFC).

As shown in Figure 4-2, The 2in1 rBiFC vector incorporates a set of independent, Gateway-compatible cassettes, each with a 35S promoter and either the N or C terminal half of YFP. The 2in1 vector also includes a third 35S promoter-driven cassette with the coding sequence for soluble RFP which provides a control for transformation and a reference for ratiometric quantification of BiFC. In order to perform the Western blot analysis, an HA epitope is included between nYFP and the first Gateway cassette (R3R2), while a Myc epitope is included between the second Gateway cassette (R1R4) and cYFP. The VAMPs incorporate a C-terminal membrane anchor, hence, when labeled at this end of the protein any tag would be localized on the extracytosolic side of the membrane. Thus, I generated VAMPs tagged on the N-terminus with the N terminal half of YFP (nYFP-HA-VAMPnnn) and I tagged the K^+ channels at their C terminus with the C-terminal half of YFP (K^+ channel-Myc-cYFP).

KAT1 expresses well in and is correctly targeted to the PM when expressed in tobacco (Sutter et al., 2006; Sutter et al., 2007). For reasons that are still unclear, KC1 is poorly mobilized from the ER in tobacco and becomes localized at the PM only when expressed in *Arabidopsis* (Duby et al., 2008; Honsbein et al., 2009). Therefore, I carried out transient transformations with KAT1 and the VAMPs in tobacco leaves, and I transformed *Arabidopsis* seedlings to test interactions with KC1. YFP and RFP fluorescence was analyzed by confocal microscopy using standardized recording parameters as described in Chapter 2, and rBiFC ratios were determined after subtraction of background fluorescence recorded from untransformed tissues in each case. For Western blot analysis, anti-HA (1:10000) and anti-Myc (1:5000) antibodies were used as the primary antibodies.

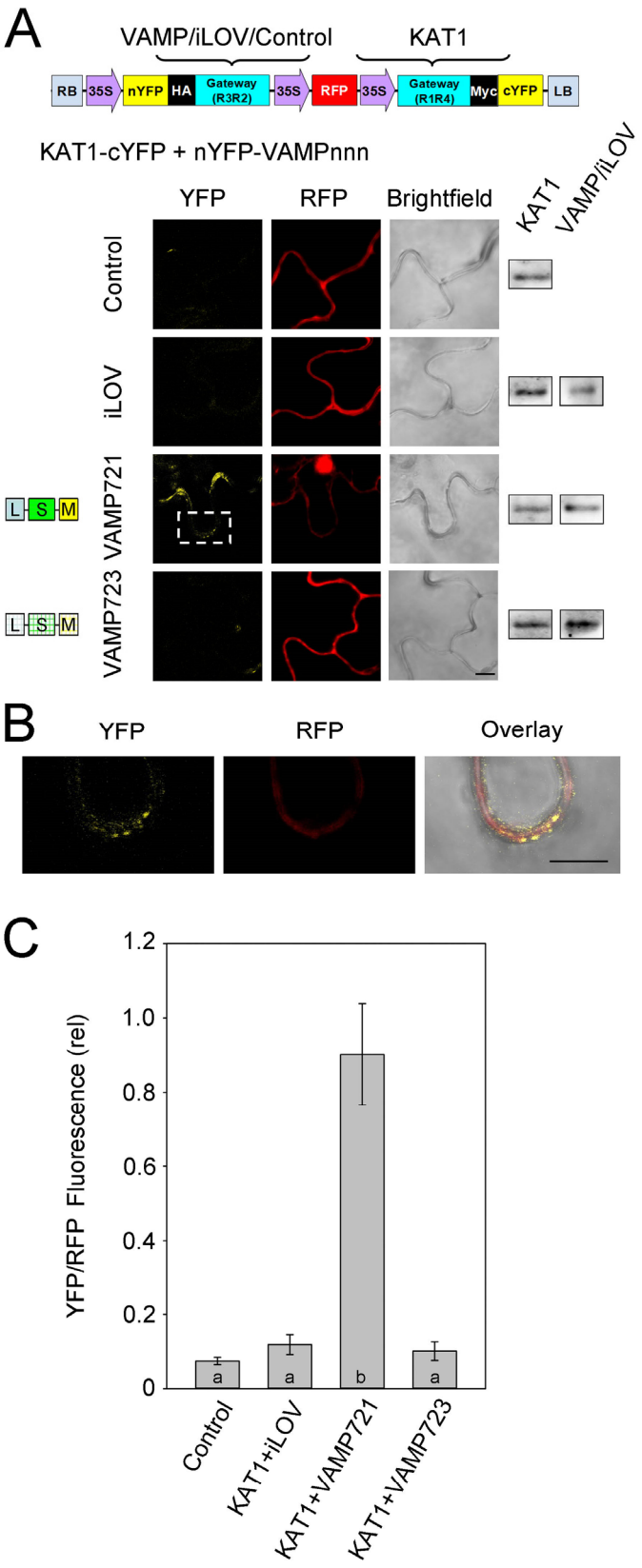

Figure 4-2. VAMP721 interacts with KAT1 in vivo while VAMP723 does not

(A) Ratiometric Bimolecular Fluorescence Complementation (rBiFC) analysis of YFP and RFP fluorescence collected from tobacco transformed using the pBiFCt-2in1-NC (Grefen, 2012) 2in1 vector (schematic *above*). Images are (*left* to *right*) YFP (BiFC) fluorescence, RFP fluorescence, and brightfield. Constructs (*top* to *bottom*) included coding sequences for KAT1-Myc-cYFP with either the empty cassette (control) or nYFP-HA-X fusions with iLOV, VAMP721 and VAMP723. Scale bar, 10 μm. Western blot analysis using αHA and αmyc antibodies to verify fusion protein expression are shown (*right*).
(B) Expanded view of the image region denoted by the white box in (A) for nYFP-VAMP721 co-expressed with KAT1-cYFP. Images are (*left* to *right*) YFP fluorescence, RFP fluorescence, and brightfield. Scale bar: 10 μm.
(C) rBiFC fluorescence signals from three independent experiments. Each bar represents the mean ±SE of fluorescence intensity ratios from 10 images taken at random over the leaf surface. rBiFC signals were calculated as the mean fluorescence intensity ratio determined from each image set after subtracting the background fluorescence determined from an equivalent number of images taken from non-transformed tissues. Significance is indicated by letters at $P < 0.01$.

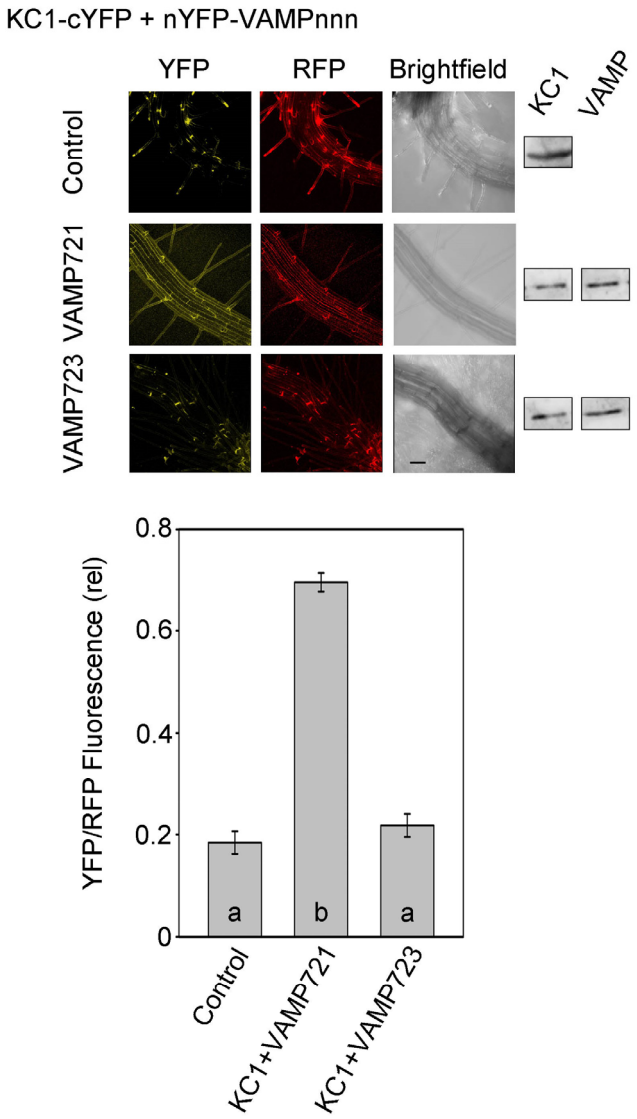

Figure 4-3. VAMP721, but not VAMP723, interacts with the KC1 K^+ channel in vivo

rBiFC analysis of nYFP-HA-VAMPnnn fusions of VAMP721 and VAMP723 and their interaction with KC1-Myc-cYFP. Images were collected from *Arabidopsis* roots epidermal cells transiently transformed as described in chapter 2. Three-dimensional projections were derived from confocal image stacks and the projections were analysed for YFP and RFP fluorescence intensities after background subtraction. Images are (left to right) YFP (BiFC) fluorescence, RFP fluorescence as a cell marker, and the corresponding mid-plane brightfield image. The images correspond to constructs (top to bottom) including the coding sequences for KC1-cYFP with the empty cassette (control), VAMP721, and VAMP723. Scale bar: 10 μm. Western blot analysis using αHA and αmyc antibodies to verify fusion protein expression are shown (*right*). Mean ± SE for rBiFC ratios (YFP/RFP fluorescence, *below*) comprise data from

three independent experiments, each including images (n>10) taken from randomly selected roots. rBiFC fluorescence ratios were calculated from the mean fluorescence intensities determined from each YFP/RFP image pair after background subtraction. Significance is indicated by letters ($P < 0.01$).

Figure 4-2 summarized representative images from one of three experiments in which KAT1 was co-expressed with the VAMPs, and it included statistical rBiFC analysis for all three experiments. As controls, I expressed KAT1-myc-cYFP on its own and with nYFP-tagged iLOV in the 2in1 vector. iLOV is a soluble phototropin unrelated to the VAMPs and is expressed constitutively in *Arabidopsis* (Chapman, 2008). The RFP fluorescence of each sample indicated the successful transformation. Consistent with the mbSUS assays, KAT1 co-expression with VAMP721 gave a strong rBiFC signal. YFP fluorescence was clearly evident in puncta distributed around the cell periphery (Figure 4-2B), consistent with the characteristic localization of the KAT1 channel at the PM in previous reports (Sutter et al., 2006; Sutter et al., 2007). Coexpression with VAMP723 yielded a low rBiFC ratio that was indistinguishable from the background signals observed on expressing KAT1-cYFP alone and together with nYFP-iLOV. The expression of VAMPs or iLOV and KAT1 K^+ channels in rBiFC analysis were verified by Western blot analysis. The results were shown in the right lane. In Figure 4-3, a similar pattern in rBiFC ratios was observed using KC1 as the partner for interactions.

In conclusion, VAMP721 normally interacted with the K^+ channels, while VAMP723 did not.

4.2.3 The longin domain of VAMP721 is essential for K^+ channel interaction in vivo

To validate the role of longin domain in VAMP721-KAT1 K^+ channel

interaction in vivo, I introduced chimeras incorporating the VAMP721 and VAMP723 longin domains, $VAMP721_{L}723_{SM}$ and $VAMP723_{L}721_{SM}$, into the rBiFC 2in1 vector system (as shown in Figure 4-2 A above) and used the constructs to transiently transform in tobacco leaves. Figure 4-4 showed the images and statistical analysis of rBiFC fluorescence ratios from three independent experiments together with measurements from tissues expressing the vector with KAT1 alone and with iLOV as the negative controls. The results demonstrated a highly significant rBiFC signal above the negative controls when KAT1 was co-expressed with $VAMP721_{L}723_{SM}$ that included the VAMP721 longin domain, but not with the complementary $VAMP723_{L}721_{SM}$ chimera that included the VAMP723 longin domain. The expression of VAMP chimeras or iLOV and KAT1 K^{+} channels in rBiFC analysis were verified by Western blot data.

Thus, I concluded that longin domain of VAMP721 was a primary determinant of the physical interaction between VAMP721 and KAT1.

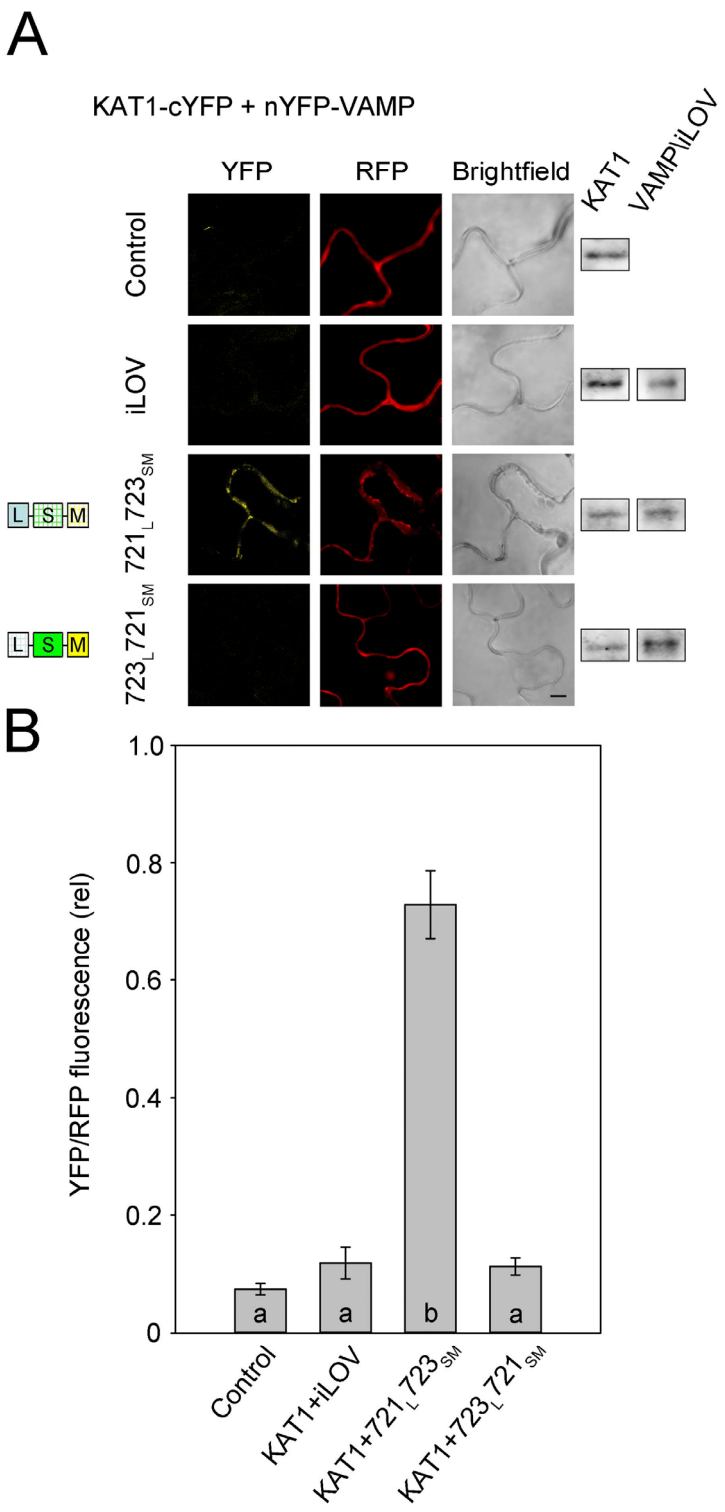

Figure 4-4. VAMP721 interaction with KAT1 K^+ channel Depends on the longin domain

(A) Ratiometric Bimolecular Fluorescence Complementation (rBiFC) analysis of YFP and RFP fluorescence collected from tobacco transformed using the pBiFCt-2in1-NC 2in1 vector. Images are (left to right) YFP (BiFC) fluorescence, RFP fluorescence, and brightfield. Constructs (top to bottom) included coding sequences for

KAT1-Myc-cYFP with either the empty cassette (control) or nYFP-HA-X fusions of iLOV, VAMP721 longin domain with VAMP723 R-SNARE and TM helices ($VAMP721_L723_{SM}$), and VAMP723 longin domain with VAMP721 R-SNARE and TM helices ($VAMP723_L721_{SM}$). Scale bar = 10 μm. Western blot analysis using αHA and αmyc antibodies to verify fusion protein expression are shown (*right*).
(B) rBiFC fluorescence signals from three independent experiments. Each bar represents the mean ± SE of fluorescence intensity ratios from 10 images taken at random over the leaf surface. rBiFC signals were calculated as the mean fluorescence intensity ratio determined from each image set after subtracting the background fluorescence determined from an equivalent number of images taken from non-transformed tissues. Significance is indicated by letters at $P < 0.01$.

4.2.4 Tyr^{57} of VAMP721 is essential for K^+ channel interaction in vivo

In Chapter 3, I indicated that Tyr^{57} of VAMP721 was essential for VAMP-K^+ channel interaction. To validate these findings in vivo, again I incorporated the corresponding single-site substitutions in the 2in1 vector carrying KAT1-Myc-cYFP for transient transformation of tobacco and carrying KC1-Myc-cYFP for transient transformation of *Arabidopsis* seedlings.

Figure 4-5 summarized images and rBiFC analysis collected from tobacco in which KAT1-Myc-cYFP and nYFP-HA-VAMP single site mutants coexpressed. Strong rBiFC signals were recovered with $VAMP721^{D61A}$, $VAMP721^{Q76A}$, and $VAMP721^{S80A}$, indicating that these single mutants had no effect on the interaction with KAT1. Although variable, a comparable rBiFC signal was also recovered with the $VAMP721^{Y57A}$ mutant. However, when the fusions of KAT1 and $VAMP721^{Y57D}$ were co-expressed, the rBiFC signal was statistically indistinguishable from the background of the negative controls expressing the KAT1 fusion on its own and with the complementary iLOV fusion. Co-expression of the rBiFC fusions of KAT1 with $VAMP723^{D57Y}$ also yielded a strong signal. The fusion protein expression of KAT1 and VAMP mutants were verified by Western blot analysis.

The interaction between VAMP721 single mutants and KC1 K^+ channel were also validated by rBiFC analysis in *Arabidopsis* seedlings. As shown in Figure 4-6, only VAMP721^{Y57D} suppressed the rBiFC signal, while VAMP723^{D57Y} mutant gave a strong rBiFC signal. Altogether, these rBiFC results supported my finding that the exchange between Tyr and Asp in the residue at position 57 could affect the VAMP localization, especially for VAMP723^{D57Y}. In each case, a strong BiFC fluorescence signal was found between VAMP723^{D57Y} and KC1 or KAT1, suggested this mutant must have relocated to the PM, as I showed before (Figure 4-1).

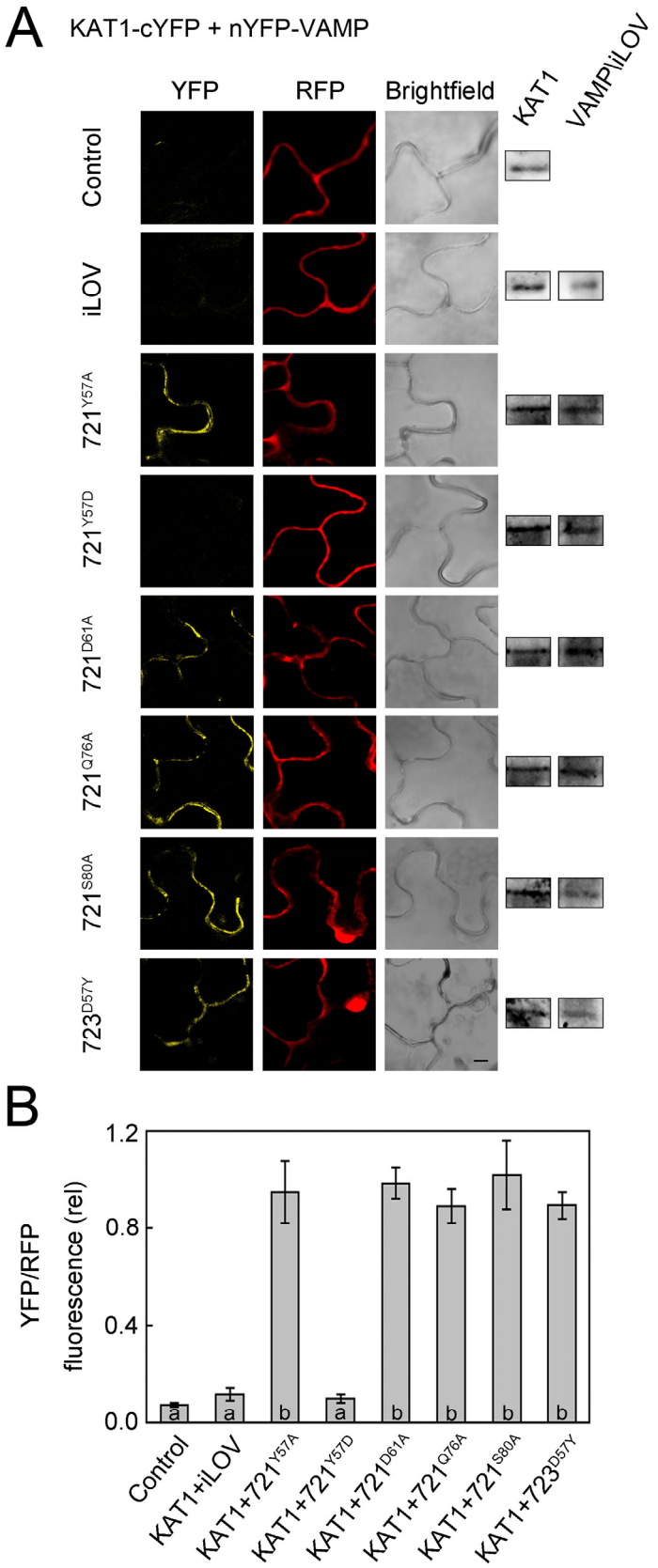

Figure 4-5. Interaction of KAT1 In Vivo Depends on VAMP721 Residue Tyr^{57}

(A) Ratiometric Bimolecular Fluorescence Complementation (rBiFC) analysis of YFP and RFP fluorescence collected from tobacco transformed using the pBiFCt-2in1-NC 2in1 vector. Images are (*left* to *right*) YFP (BiFC) fluorescence, RFP fluorescence, and brightfield. Constructs (*top* to *bottom*) included coding sequences for KAT1-Myc-cYFP alone and with nYFP-HA-X fusions of iLOV, VAMP721^{Y57A}, VAMP721^{Y57D}, VAMP721^{D61A}, VAMP721^{Q76A}, VAMP721^{S80A}, and VAMP723^{D57Y}. Scale bar: 10 μm. Western blot analysis using αHA and αmyc antibodies to verify fusion protein expression are shown (*right*).
(B) rBiFC fluorescence signals from three independent experiments. Each bar represents the mean ± SE of fluorescence intensity ratios from 10 images taken at random over the leaf surface. rBiFC signals were calculated as the mean fluorescence intensity ratio determined from each image set after subtracting the background fluorescence determined from an equivalent number of images taken from non-transformed tissues. Significance is indicated by letters at $P<0.01$.

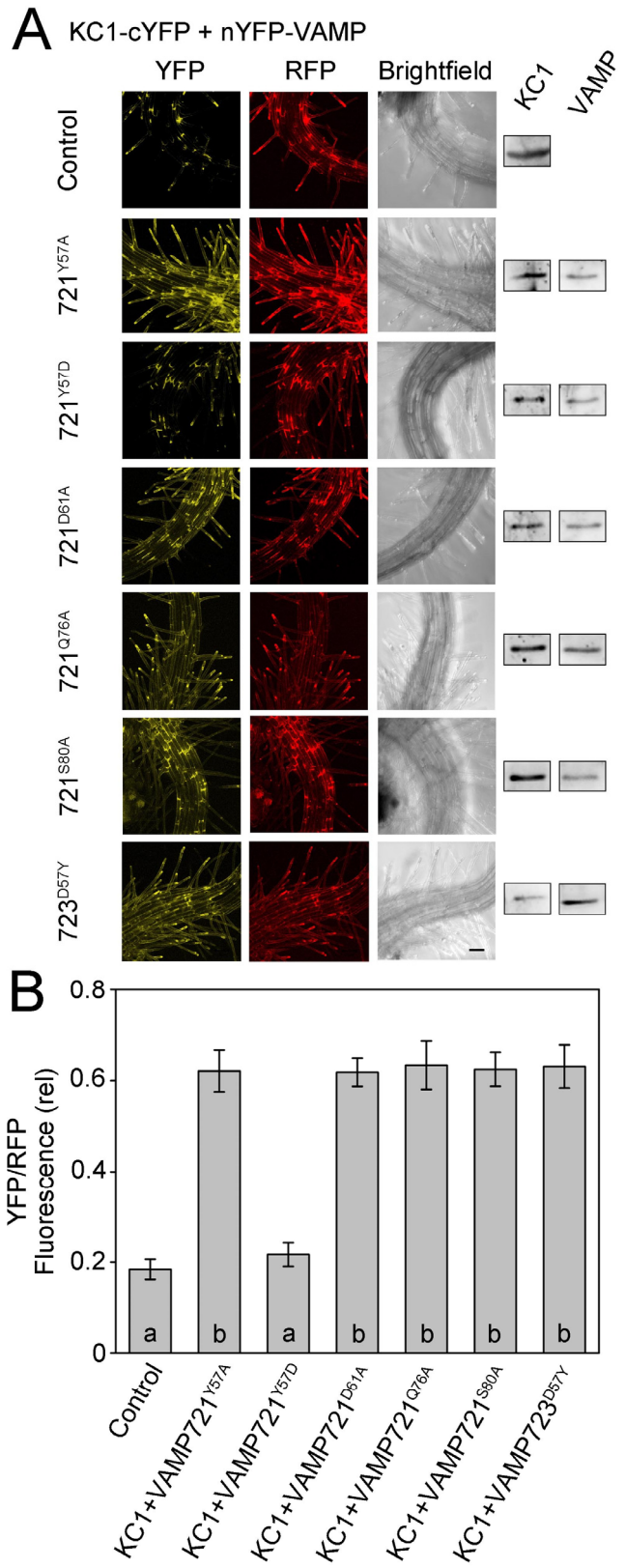

Figure 4-6. Interaction of KC1 In Vivo Depends on VAMP721 Residue Tyr^{57}

(A) Ratiometric Bimolecular Fluorescence Complementation (rBiFC) analysis of YFP and RFP fluorescence collected from *Arabidopsis* roots

epidermal cells transiently transformed as described in chapter 2. Three-dimensional projections were derived from confocal image stacks and the projections were analysed for YFP and RFP fluorescence intensities after background subtraction. Images are (left to right) YFP (BiFC) fluorescence, RFP fluorescence as a cell marker, and the corresponding mid-plane brightfield image. Images are (left to right) YFP (BiFC) fluorescence, RFP fluorescence, and brightfield. Constructs (top to bottom) included coding sequences for KC1-Myc-cYFP alone and with nYFP-HA-X fusions of iLOV, VAMP721^{Y57A}, VAMP721^{Y57D}, VAMP721^{D61A}, VAMP721^{Q76A}, VAMP721^{S80A}, and VAMP723^{D57Y}. Scale bar: 10 μm. Western blot analysis using αHA and αmyc antibodies to verify fusion protein expression are shown (*right*).
(B) rBiFC fluorescence signals from three independent experiments. Each bar represents the mean ± SE of fluorescence intensity ratios from 10 images taken at random over the leaf surface. rBiFC signals were calculated as the mean fluorescence intensity ratio determined from each image set after subtracting the background fluorescence determined from an equivalent number of images taken from non-transformed tissues. Significance is indicated by letters at $P<0.01$.

4.3 Discussion

In Chapter 3, I found VAMP721 interacted with K^+ channels while VAMP723 did not. The residue at position 57 was important for the VAMP-K^+ channel binding. The mutant VAMP721^{Y57D} inhibited the interaction while the complementary VAMP723^{D57Y} mutation was enough to allow this non-interacting VAMP to bind with the K^+ channels. These findings on one hand indicate a selective physical interaction between the VAMPs and the K^+ channels. On the other hand, the findings raise the question whether the exchange of residue 57 between VAMP721 and VAMP723 might affect the subcellular localization of the VAMPs. To answer this question, I cloned VAMP721, VAMP723, VAMP721^{Y57D}, and VAMP723^{D57Y} into a Gateway-compatible vectors with fluorescent tags (pUBN-GFP-Dest; Grefen et al., 2010b) to determine the location of the constructs without the rBiFC fluorophores which might affect VAMP localization through their annealing. The results strongly suggest that channel binding and PM localization are equally dependent on the

residue at position 57.

In plants, *A. tumefaciens*-mediated gene transfer has been widely used for generating both the stable and transient transformations. I performed the transient transformation according to the protocol from previous reports (Campanoni et al., 2007; Blatt and Grefen, 2014), as described in Chapter 2. For VAMP localization analysis, the *Arabidopsis* seedlings were transient transferred and the GFP signal in root hairs were imaged.

As reported before (Uemura et al., 2004), VAMP721 was targeted at the PM while VAMP723 was in the endoplasmic reticulum. My results supported this finding (Figure 4-1). The fluorescence around nucleus at least indicated that VAMP721 and VAMP723 located to different subcellular locations. For VAMP721^{Y57D}, the GFP signal around nucleus membrane in the cytosol side as that of VAMP723 clearly showed this mutant could change the expression location. Some or all protein might target to some endomembrane organelles, like the endoplasmic reticulum. By contrast, there was no signal around nucleus membrane on the cytosolic/vacuolar side that could be found from the VAMP723^{D57Y} mutant, suggested this mutated Asp to Tyr redirected the protein to the PM.

Residue at position 57 of VAMPs is situated in the center of the longin domain. In plants, the longin domains of VAMPs have been reported to determine the protein expression location (Uemura et al., 2005). In mammals, VAMP7/TI-VAMP is one of R-SNAREs which has 120 residues length longin domain. VAMP7 delivery to its target, the late endosomal compartments, was via interaction with AP3 which bound the longin domain of VAMP7 (Martinez-Arca et al., 2003; Pryor et al., 2008). AP3 is one of the family of heterotetrameric clathrin adaptors, which is thought to be involved in the transport of proteins to late endosomes/lysosomes (Dell' Angelica et al., 1999; Le Borgne et al., 1998). Further protein structure research revealed that the interaction

between VAMP7 and AP3 required the R-SNARE motif to be engaged in SNARE complex formation, which released the longin domain from a folded back stage (Kent et al., 2012), so AP3 transported VAMP7 when it was part of a cis-SNARE complex. These results suggest the longin domain of VAMPs might be the binding site of some trafficking proteins which deliver these R-SNAREs to their targets. From my results, it appears that residue 57 of the VAMPs was essential for R-SNARE location. It is possible that this site is a potential binding site for other proteins which are essential for transporting them to their target membranes. VAMP721 interacts with K^+ channel at the PM and the binding site is in the longin domain. So, like the relationship between VAMP7 and AP3 in animal cells, the K^+ channels might interact with VAMP721 while the latter forms a SNARE complex and releases the longin domain from fold stage, which suggests a role for the K^+ channels also in SNARE related vesicle trafficking.

In order to get credible images of fluorescent proteins expressed in plant tissues, it is important to choose a suitable promoter in expression vector. 35S promoter of *Cauliflower mosaic* virus has long been used to drive protein expression. If the gene level is very low or the tissue-specific characteristics of expression is not important, the 35S strong promoter is the best choice. But the high level overexpression of protein rises the risk of mislocalization of target protein. So in the vector (pUBN-GFP-Dest) used for VAMP localization in these studies, *Arabidopsis* UBQ-10 promoter was used. This promoter facilitates moderate expression in nearly all tissues of *Arabidopsis* (Norris et al., 1993) and expression under the UBQ-10 promoter remains elevated for periods in excess of 2 weeks after transient transformation (Grefen et al., 2010b).

There are many techniques can be used to investigate the protein-protein interaction, such as Y2H, split-ubiquitin system, co-IP, fluorescence resonance energy transfer, and BiFC. I have used a

mating-based split-ubiquitin system to identify the interaction between VAMPs and K^+ channels. In this chapter, I chose ratiometric BiFC (rBiFC) assays to verify the results came from yeast.

BiFC is a method which has become widely used for protein-protein interaction investigation (Bracha-Drori et al., 2004; Walter et al., 2004; Honsbein et al., 2009; Grefen et al., 2010a). This method makes use of a fluorescent protein divided into two non-fluorescent parts. Provided there is interaction between A and B, then the two non-fluorescent fluorophore fragments may be brought together to reassemble a functional fluorescent protein. The most important advantages of this method are that the interaction can be detected directly in living cells and that the sub-cellular location can be assessed at the same time; it also has the advantage of a low fluorescence background in most tissues (Grefen and Blatt, 2012). However, expression level variations and lack of internal controls makes quantifying interaction results difficult. So I used the 2in1 rBiFC system. This system enables transfer of two different genes into the same vector by one step Gateway LR reaction. It gives equal gene dosage and interaction data may be directly quantified using the internal fluorescent marker (Grefen and Blatt, 2012).

As mentioned before, it was possible to tag the VAMPs only at their N termini. For consistency with the mbSUS assays, I tagged the K^+ channels at their C terminus with the C terminal half of YFP. It should be noted that, high levels of expression can lead to the mislocalization of target proteins. Nonetheless, I used 35S strong promoter in 2in1 rBiFC vector for several reasons: first, the expression level of K^+ channels under their native promoters in plant cells is generally too low for visualization (Wagner et al., 2006); second, the efficiency of BiFC complex formation is determined by the rate of fragment association, so otherwise the interaction between the two halves of the tagged proteins thus might be competed out by endogenous proteins (Kerppola et al., 2006; Kerppola et al., 2009); third, in vitro studies of BiFC complex

formation have demonstrated that many fluorescent protein fusions undergo irreversible misfolding when they do not associate with complementary fluorescent protein fragments (Hu et al., 2002), so the efficiency of BiFC complex formation under these conditions may be determined by competition between BiFC complex formation and misfolding. Thus, overexpression was expected to favour the amount of functional BiFC complexes to a detectable level, especially for interaction with the K^+ channels.

The 2in1 vector pBiFCt-2in1-NC was used in my research (the vector schematic was shown in Figure 4-2 A). The coding sequences of VAMPs and K^+ channels were cloned into the 2in1 vector system. For VAMP-KAT1 interaction, the 2in1 rBiFC constructs were transiently transformed into tobacco leaves by infiltration, as described in Chapter 2. The RFP fluorescence indicated the successful transformation and protein expression. In the controls (KAT1 alone or KAT1 with iLOV), there was almost no YFP signal, suggesting that the background fluorescence was low in tobacco leaves. After ratiometric quantification of the BiFC signal, the results of VAMP-KAT1 supported what I found by mbSUS assay. VAMP721 interacted with KAT1 while VAMP723 did not. For the single-site mutants, only VAMP721^{Y57D} yielded low rBiFC ratios similar to that of expressing KAT1 alone and together with iLOV. VAMP723^{D57Y} yielded a strong signal (Figure 4-2, Figure 4-4, and Figure 4-5). Previous reports have indicated that KAT1 is expressed in puncta form across the tobacco leaf cell surface (Sutter et al., 2006; Sutter et al., 2007). Consistent with these earlier studies, the YFP signal of interacting proteins appeared to be concentrated in punctate domains across cell surface (Figure 4-2 B). Taking the VAMP localization results and the rBiFC analysis together, delivery VAMP to the PM is likely to be a prerequisite for VAMP-K^+ channel interaction.

For VAMP-KC1 interaction, the 2in1 constructs were transiently transferred into *Arabidopsis* root epidermis by cocultivation with the

Agrobacterium. The high rBiFC ratio of control (expressed KC1 alone) and the YFP signals from coexpression of KC1 and non-interacting VAMP, could be explained by the plant derived autofluorescence, as this signal was not included in the background subtraction procedure. After analyzed the rBiFC ratios, I found strong rBiFC signal for the wild-type VAMP721 but not VAMP721^{Y57D} or VAMP723 while mutated Asp to Tyr in residue at position 57 of VAMP723 rescued the rBiFC signal (Figure 4-3 and Figure 4-6). These results verified my finding from yeast mbSUS assay in yeast.

In conclusion, the residue Tyr^{57} dependent interaction between VAMP721 and KC1 or KAT1 K^+ channels were confirmed by two different methods. The subcellular localization of rBiFC signals for VAMP-KAT1 interaction suggested that the proper delivery of VAMP721 to the PM was important for the binding. Furthermore, supported by the VAMP subcellular location results, the exchange of residue at position 57 between VAMP721 and VAMP723 affected the trafficking of these R-SNARE proteins. Interestingly, VAMP723^{D57Y} interacted with K^+ channels while wild-type VAMP723 did not. The residue at position 57 of VAMP721 and VAMP723 was like a molecular switch which determined whether the interaction happened or not.

Chapter 5. The effect of VAMP721 on KAT1 K^+ channel current depends on residue Tyr^{57}

5.1 Introduction

The combined results of the mbSUS assays and rBiFC analysis indicated that VAMP721 interacted with both the KC1 and KAT1 K^+ channels while VAMP723 did not. Furthermore, the interaction was dependent on residue 57 of the longin domain of VAMP721. In this chapter, I summarized work to investigate the functional meaning of the VAMP-K^+ channel interactions.

Previous reports had shown that interaction of the Qa-SNARE SYP121 promoted K^+ channel gating in channels assembled from KC1 and AKT1 subunits. These studies were carried out by voltage clamp analysis in *Xenopus* oocytes and *Arabidopsis* root epidermal cells (Honsbein et al., 2009). In this chapter, I performed a similar set of experiments to examine the effect of VAMP721 binding on the gating of the K^+ channels. In oocytes, KAT1 can form functional K^+ channels by itself and yield measurable K^+ currents (Sutter et al., 2006). KC1 is a 'silent' regulatory K^+ channel subunit and gives no current when expressed alone (Obrdlik et al., 2004; Duby et al., 2008). So in oocytes, KC1 was coexpressed with AKT1, CBL1, and CIPK23 as described previously (Honsbein, et al. 2009). CIPK23 is a protein kinase that requires the calcineurin-binding-like protein CBL1 to activate AKT1. In *Arabidopsis*, VAMP721 and VAMP722 are functionally redundant and *vamp721vamp722* double homozygous mutant seedlings are embryo lethal (Kwon et al., 2008; Zhang et al., 2011). Therefore, to test the function of VAMP721-K^+ channel interactions, I over expressed VAMP721, VAMP723, $VAMP721^{Y57D}$ and $VAMP721^{Y57A}$ in the root epidermis of wild-type *Arabidopsis* using the bicistronic vector

pUB-Bic-Dest (Chen et al., 2011). These electrophysiological recordings in the plant were performed by Dr. Yizhou Wang.

5.2 Results

5.2.1 VAMP721 affects KAT1 and KC1 K^+ Channels Current

To explore the functional consequences of VAMP721 interaction on K^+ channel activity, I recorded K^+ currents under voltage clamp after heterologous expression of VAMP721 and VAMP723 with the KAT1 in *Xenopus laevis* oocytes. The coding sequences for VAMP721 and VAMP723, and K^+ channels were cloned into pGT-nHA-Dest vector and pGT-cMyc-Dest vector, which added tags for Western blot analysis. After linearising and DNA purification, the cRNAs were prepared by in vitro translation and were quantified by agarose gel electrophoresis. cRNAs were manually microinjected into the cytoplasm of stage VI oocytes of *Xenopus laevis*. Then cRNAs were mixed in molar ratios as indicated below and any difference in volumes was made up with DEPC-treated water.

After 3 days incubation, cRNAs of most proteins are translated and expressed (Buckingham, 2009). To record the currents through the expressed K^+ channels, I used a classic Two-Electrode Voltage-Clamp (TEVC) system. Oocytes were impaled with two separate microelectrodes, one used to monitor the transmembrane voltage, and the other one used for current injection. The clamp circuit compared the membrane potential with the command voltage and passed a compensating current via the second electrode to control the oocytes voltage. This current was recorded as a measure of the membrane current and quantified as a function of clamp voltage. Current-voltage curves were constructed after subtracting instantaneous currents, and were used to identify the voltage-dependence and gating properties of

the K^+ channels. The entire process of clamping and the recording of the resulting data was computer-controlled via the HENRYIII software package developed by Adrian Hills (University of Glasgow).

For VAMP721, measurements were carried out on oocytes injected with KAT1 and VAMP cRNA in ratios of 1:1, 1:2, 1:4 and 1:8 (KAT1:VAMP721). Figure 5-1 presents the mean, steady-state current-voltage relations for each set of injections along with representative current traces recorded under voltage clamp. Figure 5-2, Figure 5-3 and Table 5-1 summarize the current characteristics derived from these recordings and representative Western blot analysis for KAT1 and VAMP expression. Under voltage clamp, oocytes expressing VAMP721 and VAMP723 alone, and oocytes injected with water, showed only very small background currents. Oocytes injected with KAT1 cRNA showed a substantial current that activated with halftimes around 300 ms at voltages near and negative of -100 mV, typical of KAT1 (Hoshi et al., 1995; Lefoulon et al., 2014). Co-expression with a four-fold excess of VAMP723 had no apparent effect on the KAT1 current. However, co-expressing VAMP721 yielded a dose-dependent suppression of the KAT1 current that saturated at a ratio of 1:4 KAT1:VAMP721.

To quantify the characteristics of KAT1 gating, the mean, steady-state current-voltage curves were fitted to the Boltzmann function of the form:

$$I_K = g_{\max} \frac{V - E_K}{1 + e^{\delta \frac{V - V_{\frac{1}{2}}}{RT}}} \qquad [1]$$

where g_{max} is the conductance maximum, E_K is the equilibrium voltage for K^+, $V_{1/2}$ is the voltage yielding half-maximal conductance, δ is the apparent gating charge or voltage-sensitivity coefficient (Dreyer and Blatt, 2009), V is the membrane voltage, and R and T have their usual meanings.

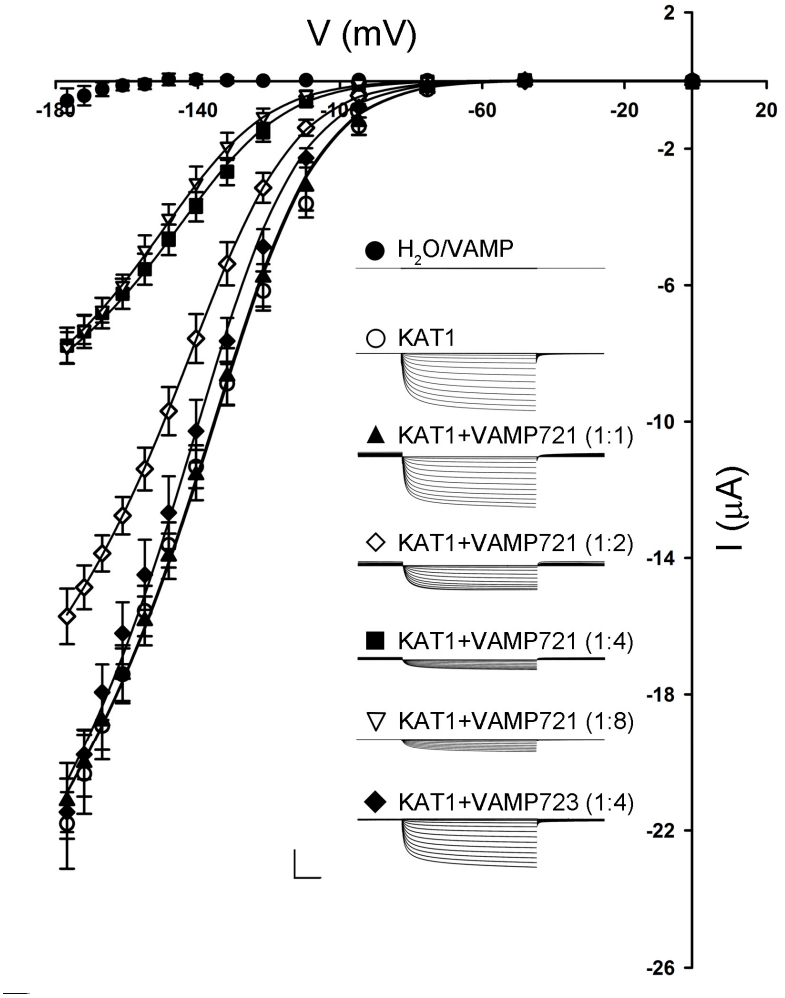

Figure 5-1. Co-expressing VAMP721 suppresses KAT1 K^+ Current and Alters Channel Gating in *Xenopus* Oocytes

Representative current traces (*insets*) recorded under voltage clamp in 30 mM K^+, and the mean steady-state current-voltage curves derived from these and similar recordings. Data are means ±SE of seven or more experiments for each set of constructs with oocytes expressing H_2O, VAMP721 and VAMP723 alone (*closed circles*), KAT1 alone (*open circles*), KAT1 and VAMP721 injected with cRNA in ratios of 1:1 (*filled triangles*), 1:2 (*open diamonds*), 1:4 (*filled squares*), and 1:8 (*open inverted triangles*), and with KAT1 and VAMP723 injected with cRNA in a ratio of 1:4 (*filled diamonds*). Clamp cycles: holding voltage, -50 mV; voltage steps, 0 to -180 mV; tail voltage -50 mV. Scale: 10 μA (*vertical*), 1 s (*horizontal*). Solid curves are the results of joint, nonlinear least-squares fitting of the K^+ currents (I_K) to the Boltzmann function (Eqn [1]). Best and visually satisfactory fittings were obtained allowing $V_{1/2}$ and g_{max} to vary between curves while holding the voltage-sensitivity coefficient (apparent gating charge) δ in common between curves. Fitted parameter values are summarized in Table 1.

To avoid substantial in determination, I applied standard methods for joint analysis with one or more selected parameters held in common between data sets. This technique is a common approach used to reduce the number of free parameters in statistical analysis (Press et al., 1992; Honsbein et al., 2009; Lefoulon et al., 2014). Statistically and visually best fittings (Figure 5-1, *solid lines*) were obtained with δ held in common while allowing g_{max} and $V_{1/2}$ to vary between data sets. These results yielded δ of -1.70±0.05 and, with KAT1 expression alone, a $V_{1/2}$ of -126±1 mV and g_{max} of 1.47±0.01 mS. With increasing VAMP721 dosage, the current trace moved to more negative voltages, while co-expression with VAMP723 had almost no effect on K^+ current. The current amplitudes at -160 mV and the value of $V_{1/2}$ are shown in Figure 5-2 and Figure 5-3. The fitted current characteristics are shown in Table 1. Like the current shown in Figure 5-1, the value of g_{max} and $V_{1/i2}$ decreased with the increasing of injection level of VAMP721 cRNA. The analysis also showed that increasing the VAMP721 dosage beyond the 1:4 ratio had little influence on either parameter. Co-expression of KAT1 with VAMP721 at ratios of 1:4 and 1:8 yielded statistically equivalent values for $V_{1/2}$ and similar current amplitudes. The expression of VAMPs and K^+ channels were verified by Western blot analysis. VAMPs linked with HA tag were analyzed by αHA antibody (1:10000), while KAT1 with the myc tag was analyzed by αMyc antibody (1:5000). Each sample showed similar expression of KAT1. The Ponceau S stain was used to normalize VAMP expression levels for lanes with VAMP721. After quantifying the band densities by ImageJ, the ratios for VAMP721 were 1: 2.06: 3.77: 6.92, which corresponded reasonably well to the injection ratio 1:1, 1:2, 1:4 and 1:8 (KAT1:VAMP721). These results indicated that VAMP721 affects both the KAT1 current amplitude and its intrinsic gating properties in a saturable and stoichiometric fashion.

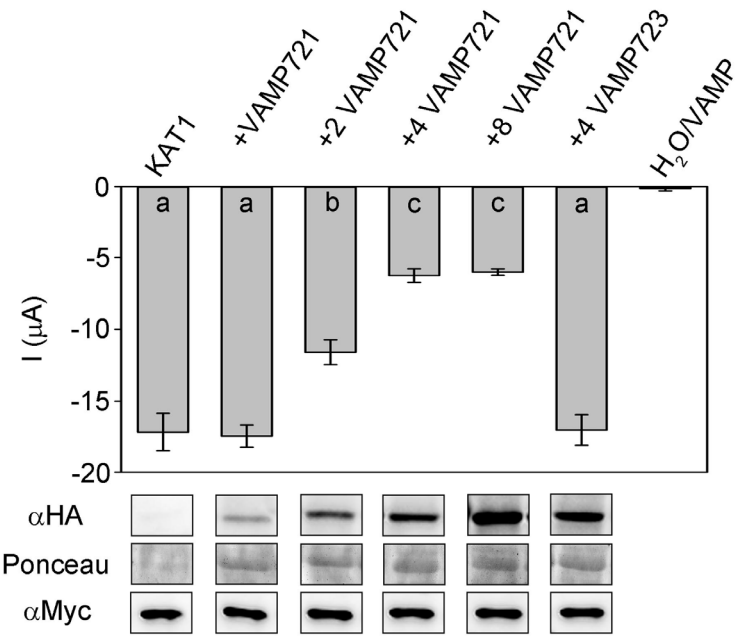

Figure 5-2. Mean KAT1 K^+ current amplitude at -160 mV and Western blot analysis results

Samples were for the data of Figure 5-1. Significance at P<0.01 is indicated by letters. Also shown (*below*) were Western blot analysis verifying VAMP (αHA antibody) and KAT1 (αmyc antibody) expression in oocytes collected after electrical recordings. Ponceau S stain was used to normalize VAMP expression levels for lanes with VAMP721 and yielded ratios of 1: 2.06: 3.77: 6.92 after quantifying band densities using ImageJ.

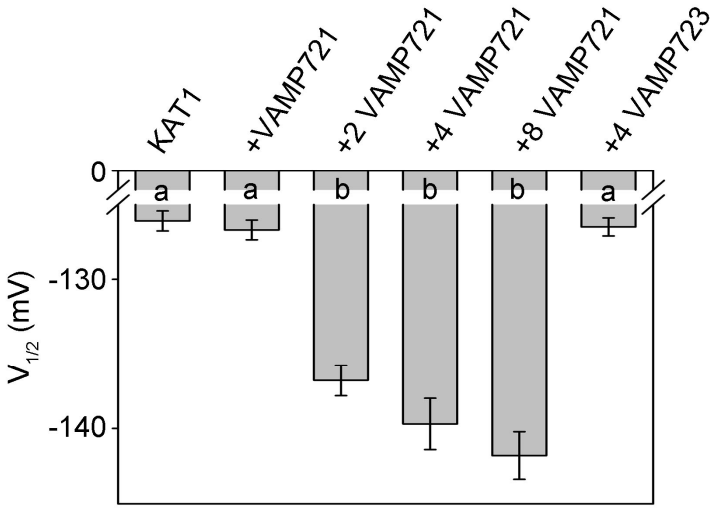

Figure 5-3. Mean values of $V_{1/2}$ derived from Figure 5-3

The value of $V_{1/2}$ derived from fittings to Boltzmann function (Eqn [1]) of the data in Figure 5-3. Significance at P<0.01 is indicated by letters .

Table 5-1. Co-expressing VAMP721 with the KAT1 K^+ Channel in *Xenopus* Oocytes Suppresses the Current Amplitude and Alters Channel Gating

	$V_{1/2}$ (mV)	g_{max} (mS)	δ
KAT1	-126.1±0.7	1.47±0.01	-1.70±0.05
KAT1+VAMP723 (1:4)	-128.5±0.6		
KAT1+VAMP721 (1:1)	-126.7±0.7		
KAT1+VAMP721 (1:2)	-136.8±1.0*	1.12±0.02	
KAT1+VAMP721 (1:4)	-139.7±1.7*	0.58±0.01	
KAT1+VAMP721 (1:8)	-141.5±1.6*		

Parameter values were results of joint, nonlinear least-squares fitting of K^+ currents in Figure 5-1. Fittings were carried out with the gating charge, δ, held in common, and values for the voltage giving half-maximal conductance $V_{1/2}$ and conductance maximum g_{max} were allowed to vary between data sets. Data for KAT1 and KAT1+VAMP721 (1:1) were visually indistinguishable and therefore g_{max} values were fitted jointly to simplify analysis; similarly g_{max} values for KAT1+VAMP721 (1:4) and KAT1+VAMP721 (1:8) were fitted jointly. Data are from seven or more separate experiments for each construct combination and are given as means ± SE. Significance as the difference from KAT1 expressed alone (*) at P<0.01.

I repeated these experiments with KC1 in oocytes. KC1 is a 'silent' K^+ channel subunit when expressed on its own; it yields substantial inward-rectifying K^+ currents only when co-expressed with other inward-rectifying K^+ channels in *Xenopus* oocytes, and in vivo it is thought to function in a complex with the AKT1 K^+ channel subunit to facilitate K^+ uptake by the root epidermis (Duby et al., 2008; Honsbein et al., 2009; Geiger et al., 2009). As before (Honsbein et al., 2009; Grefen et al., 2010a), I expressed KC1 in 1:1 ratio together with AKT1 and, to ensure activation of the channels in oocytes, I also coexpressed the protein kinase CIPK23 and calcineurin-like protein CBL1 (Xu et al., 2006). Additionally, I injected cRNAs for VAMP721 and VAMP723 constructs in a 1:4 (KC1:VAMP) ratio.

Figure 5-4 shows the current traces from representative oocytes injected with each of the combinations of cRNAs along with the mean, steady-state current-voltage curves from all of these experiments. Figure 5-5 summarized the corresponding steady-state currents at -160 mV along with Western blots validating the expression of KC1 and of the VAMP constructs. Again, the steady-state current-voltage curves were fitted jointly to the Boltzmann function (Eqn [1]), in this case holding both g_{max} and the voltage sensitivity coefficient, δ, in common between data sets (Honsbein et al., 2009; Grefen et al., 2010a). The solid lines in Figure 5-4 show the results of these fittings and values for $V_{1/2}$ derived from the analysis are summarized in Table 5-2 and Figure 5-6.

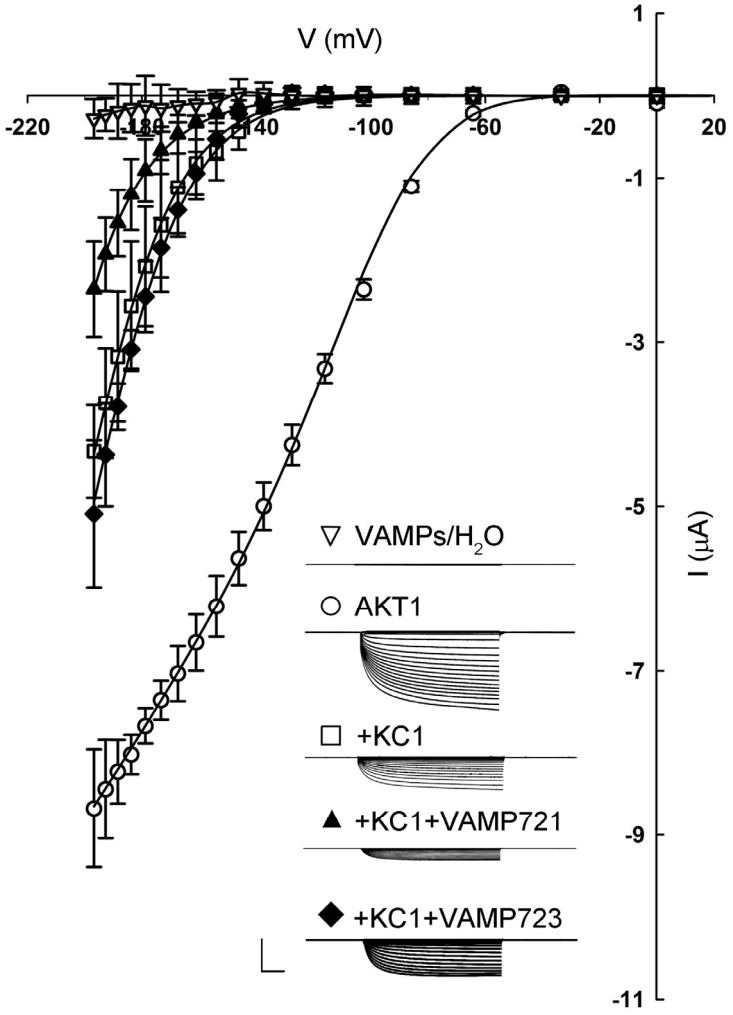

Figure 5-4. VAMP721 suppression of KC1-AKT1 K^+ Current in *Xenopus* Oocytes

Representative current traces (*insets*) recorded under voltage clamp in 30 mM K^+, and the mean steady-state current-voltage curves derived from these recordings. Data are means ±SE of seven or more experiments for each set of constructs with oocytes. Oocytes were injected with H_2O or VAMP721 or VAMP723 alone (*open inverted triangles*), AKT1 alone (*open circles*), AKT1 with KC1 (*open squares*), AKT1 and KC1 with VAMP721 (*closed triangles*), and AKT1 and KC1 with VAMP723 (*closed diamonds*). All oocytes were co-injected with CBL1 and CIPK23, essential for AKT1 function, in a 1:1:1 ratio with AKT1 (Xu et al., 2006; Honsbein et al., 2009). cRNAs were injected in a ratio of 1:1:4 for AKT1:KC1:VAMP. Clamp cycles: holding voltage, -50 mV; voltage steps, 0 to -200 mV; tail voltage -50 mV. Scale: 5 μA (*vertical*), 1 s (*horizontal*). Solid curves are the results of joint, nonlinear least-squares fitting of the K^+ currents to the Boltzmann function (Eqn [1]). Best and visually satisfactory fittings were obtained allowing $V_{1/2}$ to vary between curves while holding the voltage-sensitivity coefficient (apparent gating charge) δ and g_{max} in common between curves. Fitted parameter

values were summarized in Table 5-2.

Table 5-2. Suppressing KC1-AKT1 K^+ Current in *Xenopus* Oocytes by VAMP721.

	$V_{1/2}$ (mV)	g_{max} (mS)	δ
AKT1	-93.1±1.0	0.52±0.01	-1.45±0.03
AKT1+KC1	-186.8±2.1		
AKT1+KC1+VAMP721	-212.2±3.2*		
AKT1+KC1+VAMP723	-189.2±1.4		

Parameter values were results of joint, nonlinear least-squares fitting of K^+ currents in Figure 5-4. Fittings were carried out with the gating charge, δ, and g_{max} held in common, and values for the voltage giving half-maximal conductance $V_{1/2}$ were allowed to vary between data sets. Data are from seven or more separate experiments for each construct combination and are given as means ±SE. Significance as the difference from KC1-AKT1 expressed alone (*) at $P<0.01$.

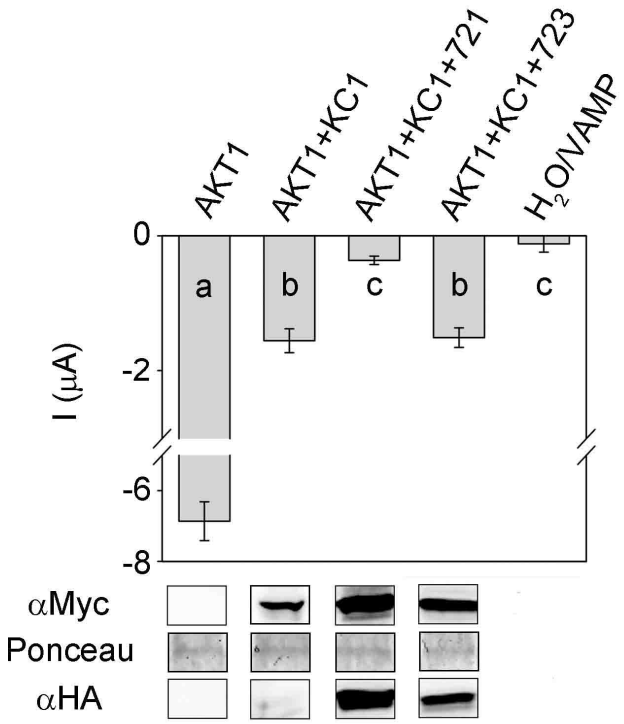

Figure 5-5. Mean KC1-AKT1 K^+ current amplitude at -160 mV and Western blot analysis results

Data and samples are from Figure 5-4. Significance is indicated by letters at P<0.01. Below are Western blot analysis verifying VAMP (αHA antibody) and KAT1 (αmyc antibody) expression in oocytes collected after electrical recordings. Ponceau S stain was used to normalize VAMP expression levels.

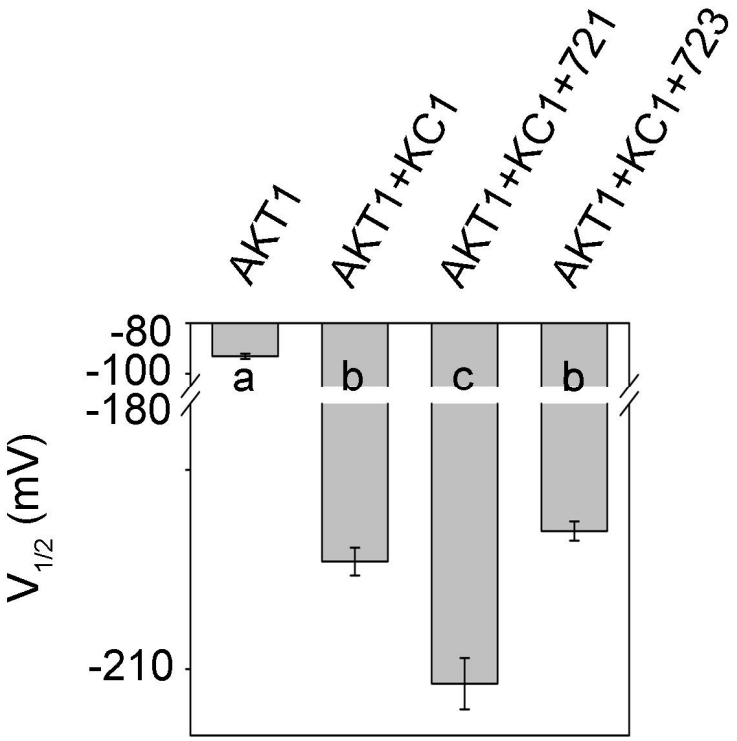

Figure 5-6. Mean values of $V_{1/2}$ derived from Figure 5-4

The value of $V_{1/2}$ derived from fittings to Boltzmann function (Eqn [1]) of the data in Figure 5-4. Significance was indicated by letters at P<0.01.

As observed previously (Duby et al., 2008; Honsbein et al., 2009), AKT1 expression on its own yielded an inward-rectifying K^+ current with $V_{1/2}$ near -100 mV; expressing AKT1 together with KC1 gave a substantive K^+ current only at voltages negative of -140 mV. AKT1 and KC1 co-expression with VAMP721 reduced the K^+ current at any one voltage, apparently displacing the steady-state current-voltage curve to the right, but co-expression with VAMP723 was without effect. Again, to avoid indetermination in our analysis, we extended fittings with Boltzmann function (Eqn [1]) to these currents asking the question whether satisfactory fittings could be obtained on holding g_{max} and δ in common so that only $V_{1/2}$ varied between data sets. The analysis yielded statistically and visually satisfactory fittings, as shown in Figure 5-6 and Table 5-2 with $V_{1/2}$ varying from -186±1 mV in the control to -212±3 mV on co-expressing VAMP721. Co-expression with VAMP723 did not have

effect on the $V_{1/2}$ for the K^+ current. These results underlined the same pattern in regulation of the KC1-AKT1 K^+ current by the VAMP constructs as we observed for the KAT1 current. The existence of K^+ current indicated there was AKT1 expressed in oocytes. The similar expression levels of KC1 and VAMPs in oocytes were verified by Western blot analysis in each case.

5.2.2 K^+ Channel activity depends on Tyr^{57} of VAMP721

Residue at position 57 of VAMP721 determined the interaction with K^+ channels in mbSUS and rBiFC analyses. Did the same mutation also affect the K^+ channel gating? To answer this question, I prepared the same single site VAMP constructs for heterologous expression in *Xenopus* oocytes, including $VAMP721^{Y57A}$, $VAMP721^{Y57D}$, and $VAMP723^{D57Y}$. Co-expression of KAT1 with VAMP721 at ratios of 1:4 and 1:8 yielded similar K^+ currents (Figure 5-1). So I injected the cRNAs of KAT1 and these single site VAMP mutants at ratio 1:4. Again, I quantified the K^+ currents under voltage clamp and analyzed the results for current relaxation, steady-state current, as well as fitting the mean steady-state current-voltage relations to the Boltzmann function (Eqn. [1]) to extract the gating parameters of $V_{1/2}$, and δ. The expression of each mutant VAMP in oocytes were verified by Western blot analysis. Figure 5-7 summarizes the mean steady-state currents recorded from seven or more independent experiments in each case. The K^+ current amplitude at -160 mV is shown in Figure 5-8. The values of δ and $V_{1/2}$ are shown in Table 5-3 and Figure 5-9.

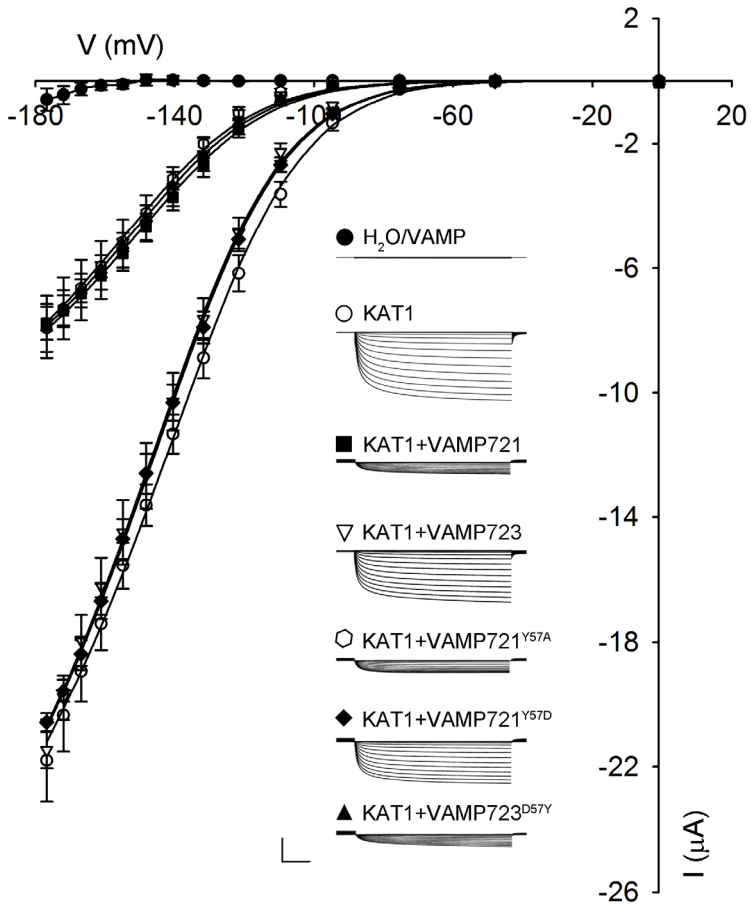

Figure 5-7. VAMP721 suppression of KAT1 K^+ Current in *Xenopus* Oocytes Depends on Tyr^{57}

Representative current traces (*insets*) recorded under voltage clamp in 30 mM K^+, and the mean steady-state current-voltage curves derived from these recordings. Data are means ±SE of seven or more experiments for each set of constructs with oocytes. VAMPs were injected in four-fold excess with KAT1. Traces are cross-referenced to the current-voltage curves and are from oocytes expressing H_2O, VAMP721 and VAMP723 alone (*closed circles*), KAT1 alone (*open circles*), KAT1 and VAMP721 (*filled squares*), KAT1 and VAMP723 (*open inverted triangles*), KAT1 and $VAMP721^{Y57A}$ (*open hexagon*), KAT1 and $VAMP721^{Y57D}$ (*filled diamond*), KAT1 and $VAMP723^{D57Y}$ (*filled triangle*). Clamp cycles: holding voltage, -50 mV; voltage steps, 0 to -180 mV; tail voltage -50 mV. Scale: 10 μA (*vertical*), 1 s (*horizontal*). Solid curves are the results of joint, nonlinear least-squares fitting of the K^+ currents to the Boltzmann function (Eqn [1]). Best and visually satisfactory fittings were obtained allowing $V_{1/2}$ and g_{max} to vary between curves while holding the voltage-sensitivity coefficient (apparent gating charge) δ in common between curves. Fitted parameter values were summarized in Table 5-3.

Table 5-3. Suppressing KAT1 K^+ Current in *Xenopus* Oocytes by VAMP721 Depends on the longin domain Residue Tyr^{57}

	$V_{1/2}$ (mV)	g_{max} (mS)	δ
KAT1	-126.7±0.7	1.47±0.01	-1.65±0.04
KAT1+VAMP721^{Y57D}	-128.5±0.6		
KAT1+VAMP723	-128.3±0.6		
KAT1+VAMP721	-139.6±1.5*	0.57±0.01	
KAT1+VAMP721^{Y57A}	-140.7±1.4*		
KAT1+VAMP723^{D57Y}	-141.5±1.6*		

Parameter values are the results of joint, nonlinear least-squares fitting of K^+ currents in Figure 5-7. Fittings were carried out with the gating charge, δ, held in common across all data sets, and values for g_{max} were held to common values between groups of three data sets as indicated. Values for the voltage giving half-maximal conductance $V_{1/2}$ and conductance maximum g_{max} were allowed to vary between all of the data sets. Data are from seven or more separate experiments for each construct combination and are given as means ±SE. Significance as the difference from KAT1 expressed alone (*) at P<0.01.

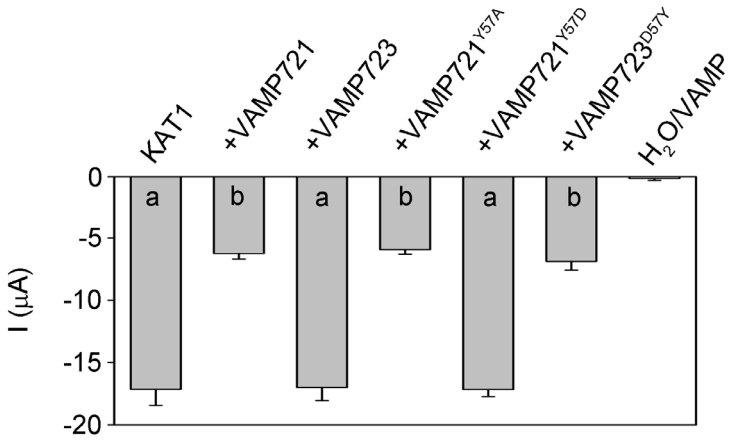

Figure 5-8. Mean KAT1 K^+ current amplitude at -160 mV

Data are from Figure 5-4. Significance is indicated by letters at P<0.01.

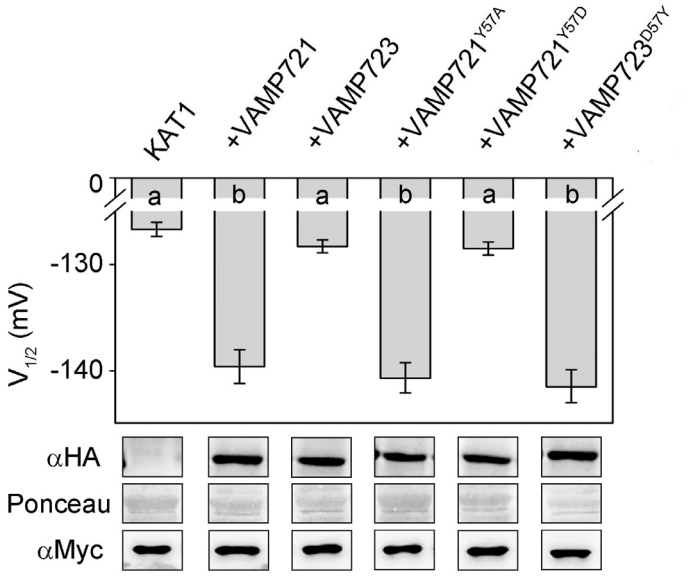

Figure 5-9. Mean values of $V_{1/2}$ and Western blot analysis results

Mean values for $V_{1/2}$ derived from fittings to Boltzmann function (Eqn [1]) of the data in Figure 5-7. Significance is indicated by letters at $P<0.01$. Also shown (*below*) are Western blot verifying VAMP (αHA antibody) and KAT1 (αmyc antibody) expression in oocytes collected after electrical recordings along with Ponceau S stain included as a loading control.

In Figure 5-7, when expressed with KAT1, VAMP721^{Y57A} and the wild-type VAMP721 yielded similar K^+ currents with reduction in current amplitude at -160 mV and a negative displacement in $V_{1/2}$, which supported that mutated Tyr^{57} to Ala had no or only a weak effect on VAMP721-KAT1 K^+ channel interaction. However, co-expression of KAT1 with the VAMP721^{Y57D} gave K^+ current characteristics similar to those for KAT1 alone and with its non-interacting partner VAMP723. KAT1 co-expression with VAMP723^{D57Y} yielded K^+ current characteristics that were statistically indistinguishable from those obtained on co-expression with wild-type VAMP721. These results were in accordance with protein-protein interaction results. Exchange of residue 57 between VAMP721 and VAMP723 affected both VAMP binding and KAT1 K^+ channel regulation. As shown in Figure 5-9, the similar expression level of KAT1 and these single site mutant VAMPs had been indicated by Western blot analysis in oocytes.

Again, the effect of single site mutants of VAMP721 on KC1-AKT1 K^+ current was performed by injection of AKT1:KC1:CIPK23:CBL1:VAMP mutant cRNA at molar ratio 1:1:1:1:4.

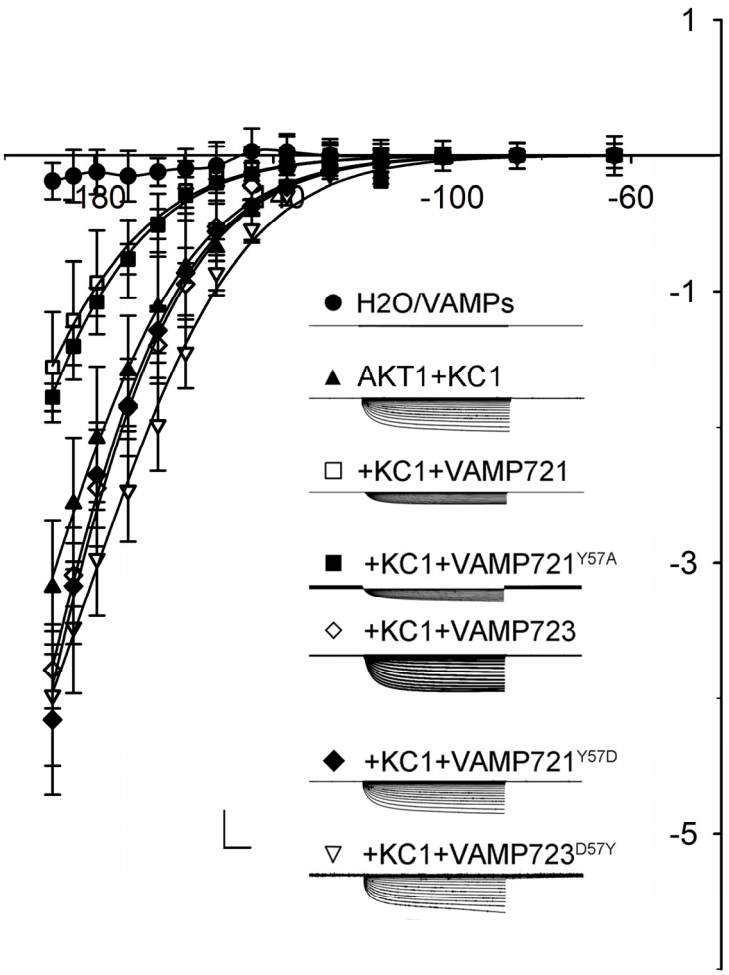

Figure 5-10. VAMP721 suppression of KC1-AKT1 K^+ Current in *Xenopus* Oocytes depends on Tyr^{57}

Representative current traces (*insets*) recorded under voltage clamp in 30 mM K^+, and the mean steady-state current-voltage curves derived from these recordings. Data are means ±SE of seven or more experiments for each set of constructs with oocytes. Oocytes were injected with H_2O or VAMP721 or VAMP723 alone (*closed circles*), AKT1 with KC1 (*closed triangles*), AKT1 and KC1 with VAMP721 (*open squares*), AKT1 and KC1 with $VAMP721^{Y57A}$ (*closed squares*), AKT1 and KC1 with VAMP723 (*open diamonds*), AKT1 and KC1 with $VAMP721^{Y57D}$ (*closed diamonds*), and AKT1 and KC1 with $VAMP723^{D57Y}$ (*open inverted triangles*). All oocytes were co-injected with CBL1 and CIPK23, essential for AKT1 function, in a 1:1:1 ratio with AKT1 (Xu et al., 2006; Honsbein et al., 2009). cRNAs were injected in a ratio of AKT1:KC1:VAMP was 1:1:4. Clamp cycles: holding voltage, -50 mV; voltage steps, 0 to -200 mV; tail

voltage -50 mV. Scale: 5 μA (*vertical*), 1 s (*horizontal*). Solid curves are the results of joint, nonlinear least-squares fitting of the K^+ currents (I_K) to the Boltzmann function (Eqn [1]). Best and visually satisfactory fittings were obtained allowing $V_{1/2}$ to vary between curves while holding the voltage-sensitivity coefficient (apparent gating charge) δ and g_{max} in common between curves. Fitted parameter values are summarized in Table 5-4.

Table 5-4. Suppressing KC1-AKT1 K^+ Current in *Xenopus* Oocytes by VAMP721 Depends on the longin domain Residue Tyr[57]

	$V_{1/2}$ (mV)	g_{max} (mS)	δ
AKT1+KC1	-186.8±2.1	0.52±0.01	-1.45±0.03
AKT1+KC1+VAMP721	-212.2±3.2*		
AKT1+KC1+VAMP721^{Y57A}	-209.7±3.1*		
AKT1+KC1+VAMP723	-189.2±1.4		
AKT1+KC1+VAMP721^{Y57D}	-187.1±2.4		
AKT1+KC1+VAMP723^{D57Y}	-190.9±1.4		

Parameter values were results of joint, nonlinear least-squares fitting of K^+ currents in Figure 5-10. Fittings were carried out with the gating charge, δ, and g_{max} held in common, and values for the voltage giving half-maximal conductance $V_{1/2}$ were allowed to vary between data sets. Data are from seven or more separate experiments for each construct combination and are given as means ± SE. Significance as the difference from KC1-AKT1 expressed alone (*) is indicated at $P<0.01$.

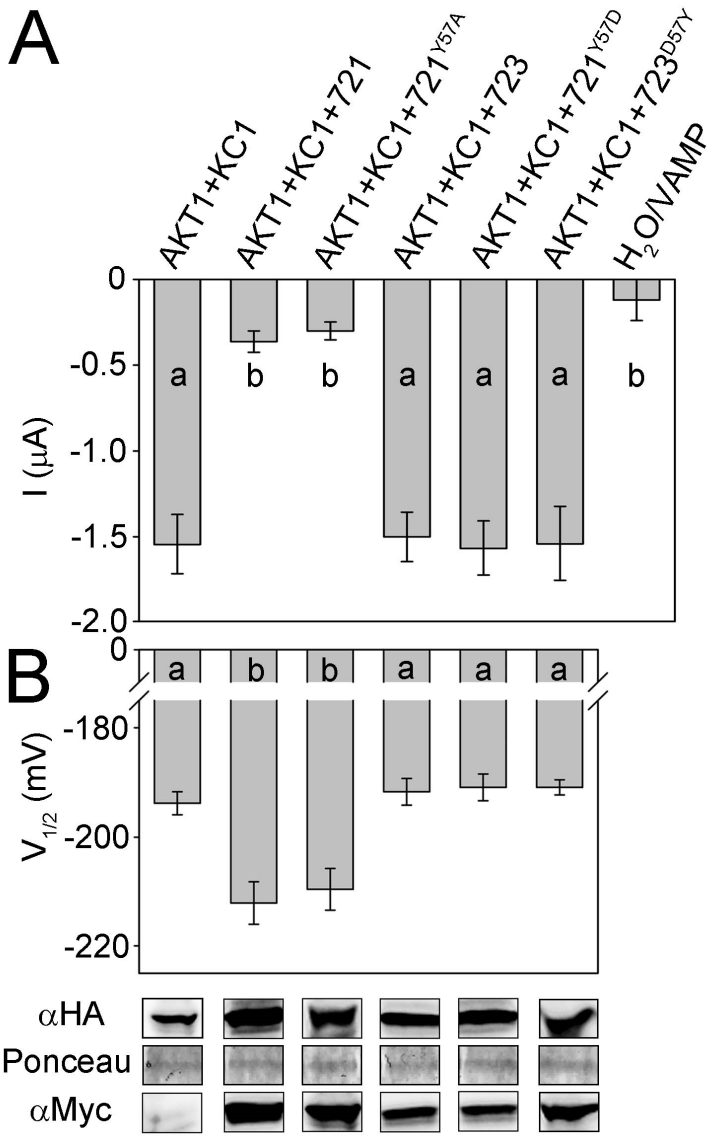

Figure 5-11. Mean values of KC1-AKT1 K^+ current amplitude at -160 mV, $V_{1/2}$, and Western blot analysis results

A: Mean KC1-AKT1 K^+ current amplitude at -160 mV, derived from Figure 5-10. Significance was indicated by letters at P<0.01.
B: Mean values for $V_{1/2}$ derived from fittings to Boltzmann function (Eqn [1]) of the data in Figure 5-10. Significance is indicated by letters at P<0.01. Also shown (*below*) are Western blots verifying VAMP (αHA antibody) and KC1 (αmyc antibody) expression in oocytes collected after electrical recordings along with Ponceau S stain included as a loading control.

The mean, steady-state current-voltage curves from all of the experiments can be found in Figure 5-10. After fitting to the Boltzmann function (Eqn[1]), only $V_{1/2}$ varied among different data sets while g_{max}

and δ were held in common (Table 5-4 and Figure 5-11). Co-expression of AKT1 and KC1 with VAMP721 or with VAMP721^{Y57A} yielded similar K^+ current and more negative value of $V_{1/2}$. Mutating Try^{57} of VAMP721 to Ala had no effect on KC1+AKT1 K^+ channel gating. The K^+ current characteristics of AKT1 and KC1 with VAMP721^{Y57D} was as that of with VAMP723 or AKT1 and KC1 alone. Interestingly, VAMP723^{D57Y} did not suppress the AKT1+KC1 K^+ current. Coexpression of VAMP723^{D57Y} with AKT1 and KC1 gave K^+ current characteristics similar to that of AKT1 and KC1 expression alone. As before, Western blot analysis showed that all single mutant VAMPs and KC1 K^+ channel expressed at similar level in oocytes in each case. These results underlined the pattern in regulation of the KC1-AKT1 K^+ current by the VAMP constructs as I observed for the KAT1 current.

5.2.3 VAMP721 and K^+ channel interaction inhibit the K^+ current in plant

VAMP721 and VAMP722 are functionally redundant and the *vamp721/vamp722* double mutant has been found to be embryo lethal (Kwon et al., 2008; Zhang et al., 2011). So it is difficult to get useful information from VAMP721 or VAMP722 single knock-out plants. In order to test the function of VAMP721-K^+ channel interaction in plant, I undertook to overexpress the VAMPs in wild type (Col-0) *Arabidopsis* using pUB-Bic-Dest vector (Chen et al., 2011) after tagging each VAMP construct N-terminally with HA tag by overlap PCR as described in Chapter 2. This bicistronic vector contains a Gateway-cassette under control of UBQ-10 promoter, a separately mGFP6 coding sequence under control of another UBQ-10 gene promoter which allows protein expression verify by GFP fluorescence, and phosphinotricin-N-acetyltransferase under control of the nopaline synthase (NOS) promoter conferring resistance to the herbicide Basta for stable transformation (Chen et al., 2011). VAMP721, VAMP723, and

VAMP721^{Y57D} each were cloned into the pUB-Bic-Dest vector, and transiently transformed into *Arabidopsis* seedlings by co-cultivation with *Agrobacterium.* In Western blot analysis, anti-HA antibody (1:10000) was used to verify the expression of each VAMP in plants.

The K^+ current of *Arabidopsis* root epidermal cells were recorded under voltage clamp by Dr. Yizhou Wang, using standard, two-electrode methods (Meharg et al., 1994; Chen et al., 2011; Honsbein et al., 2009). Measurements were carried out on 6-8 days old seedlings 3-5 days after transforming to overexpress the VAMP constructs. Mature epidermal cells in cell files lacking root hairs were chosen for recordings to avoid electrical coupling and clamp-current dissipation by root hairs and between cells (Chen et al., 2011). All recordings were analysed and leak currents subtracted using Henry III software (Adrian Hills, University of Glasgow).

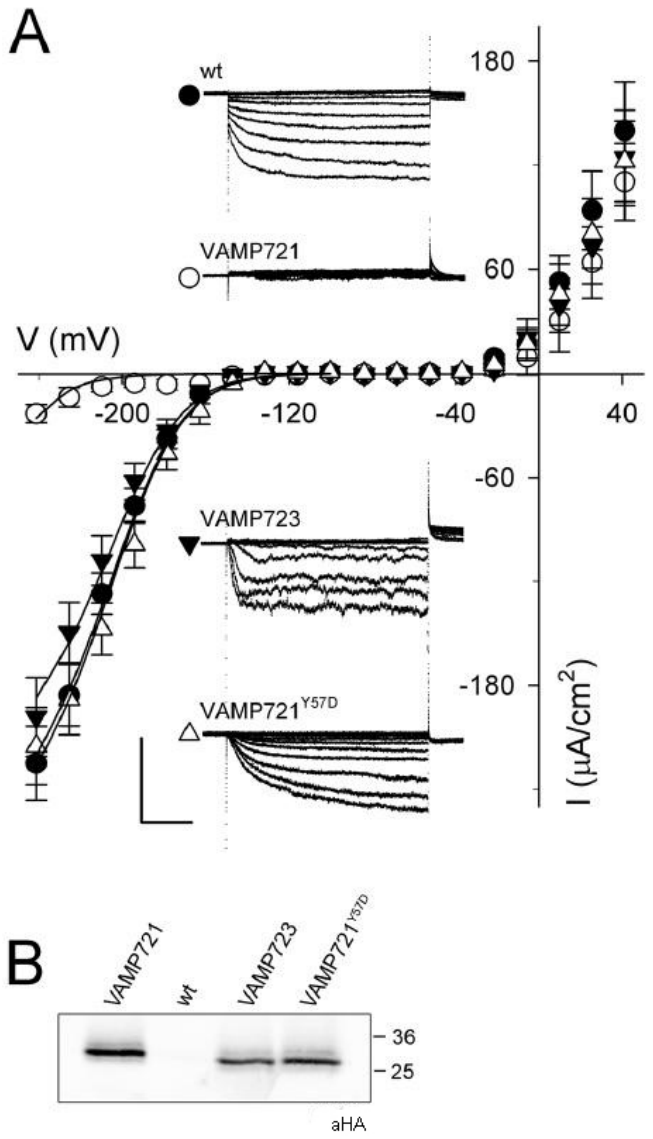

Figure 5-12.VAMP721, but not VAMP723 or VAMP721^{Y57D}, Suppresses the Inward-Rectifying K^+ Current Selectively in *Arabidopsis* Root Epidermis

(A) Representative current traces (*insets*) recorded under voltage clamp in 5 mM Ca^{2+}-MES, pH 6.1 with 10 mM K^+, and the mean steady-state current-voltage curves derived from these recordings. Data are means ±SE of five or more experiments for each set of constructs, VAMP721 (*open circles*), VAMP723 (*filled inverted triangles*) and VAMP721^{Y57D} (*open triangle*), expressed in *Arabidopsis* seedling root epidermis. Included are measurements from wild-type (untransformed) seedlings (*closed circles*). Clamp cycles: holding voltage, -50 mV; voltage steps, +40 to -240 mV; tail voltage -50 mV. Scale: 200 μA cm^{-2} (*vertical*), 1 s (*horizontal*). Solid curves are the results of joint, nonlinear least-squares fitting of the K^+ currents (I_K) to the Boltzmann function (Eqn [1]). Best and visually satisfactory fittings were obtained allowing $V_{1/2}$ to vary only for the VAMP721 data set and for g_{max} to vary between wild-type, VAMP723

and VAMP721^{Y57D} data sets while holding the voltage-sensitivity coefficient (apparent gating charge) δ in common between curves. Fitted parameter values are summarized in Table 5-5.
(B) Western blot analysis verifying VAMP transgene (αHA antibody) expression in seedlings pooled for each construct.

Table 5-5. Overexpressing VAMP721, but not VAMP723, suppresses the inward-rectifying K^+ current in *Arabidopsis* root epidermal cells

	$V_{1/2}$ (mV)	gmax (mS)	δ
Wild-type (non-transformed)	-195.7±1.4	1.38±0.04	-1.43±0.06
+VAMP723		1.27±0.04	
+VAMP721^{Y57D}		1.41±0.03	
+VAMP721	-277.2±4.9*		

Parameter values were results of joint, nonlinear least-squares fitting of K^+ currents in Figure 5-12. Fittings were carried out with the gating charge, δ held in common. Values for g_{max} were allowed to vary between data sets recorded on overexpressing VAMP721, VAMP723 and VAMP721^{Y57D}. g_{max} was held in common between the wild-type (non-transformed) and VAMP721 overexpressing roots. Voltages giving half-maximal conductance $V_{1/2}$ were allowed to vary only between data sets for the wild-type and VAMP721-overexpressing plants. Data are from five or more separate experiments for each construct combination and were given as means ± SE. Significance was as the difference from the wild-type (non-transformed) plants (*) at $P<0.01$.

Figure 5-12 included representative current traces for each of the VAMP constructs and summarized the mean steady-state currents recorded from five or more independent experiments in each case. The over expression of each VAMP in plant were verified by Western blot analysis as shown in Figure 5-12 B. As before we extracted the gating characteristics of the K^+ current by joint fittings to the Boltzmann function (Eqn[1]), holding values for δ in common between data sets. A brief inspection of the raw current traces (Figure 5-12A) and steady-state currents shows that the K^+ current was strongly suppressed when VAMP721 was expressed, yielding only a small current at all but the most

negative voltages; by contrast, currents similar to the wild-type (untransformed) plants were recorded when VAMP723 or the VAMP721^{Y57D} mutant was expressed. There was no effect on outward K^+ current when these VAMPs were over expressed, indicating that the effect is specific for the current generated by AKT1 and KC1 in vivo. Fittings to Boltzmann function (Eqn [1]) as in oocytes experiments, gave statistically and visually satisfactory results with a common value for δ, a single value for $V_{1/2}$ and with g_{max} varying only marginally between data sets for the wild-type, VAMP723 or the VAMP721^{Y57D} mutant. Incorporating the data set for VAMP721 expressing plants was best achieved by allowing only $V_{1/2}$ to differ from the wild-type. These results are summarized in Table 5-5 and the fittings are shown as the solid lines in Figure 5-12A. They concur with the analysis of the KC1-AKT1 current in oocytes, and led to the conclusion that VAMP721 acted directly on channel gating to suppress the open channel.

5.3 Discussion

A key to understanding the functional relationship between VAMP721 and the K^+ channels must be drawn from my findings of K^+ current modulation, both on heterologous expression in *Xenopus* oocytes and on overexpression in *Arabidopsis* root epidermal cells.

In the oocytes, I found that expressing VAMP721 suppressed the K^+ currents carried by KAT1 and by channels assembled from KC1 and AKT1 subunits (Figure 5-1 and 5-4). After fitting to the Boltzmann function (Eqn [1]), for KAT1 K^+ current, the effect was distributed between the ensemble channel conductance, g_{max}, and its voltage sensitivity, as evidenced by a significant negative shift in $V_{1/2}$. Furthermore, the VAMP721 action was dose-dependent, saturating near a injection cRNA ratio of 1:4 (Figure 5-1), indicating a stoichiometric relationship between the channel subunit and the VAMP. For KC1-AKT1 K^+ current, the value

of g_{max} was not affected as shown in Table 5-2. In this case, too, the currents were well-fitted with a negative shift in $V_{1/2}$ on VAMP721 co-expression. These findings demonstrate that VAMP721 has a direct effect on channel gating and that overexpression cannot be explained simply by changes in channel population at the plasma membrane.

The effect of VAMP721 on the K^+ channel gating also confirms the previous data indicating an interaction between VAMP and K^+ channel. In Chapter 3 and 4, I used mbSUS assay and rBiFC analysis to investigate the protein-protein interaction in vivo. However, these two methods are based on the reassembled effector proteins (it is ubiquitin in mbSUS, while in BiFC it is YFP fluorescent protein), which means these methods just show that the target bait and pray proteins can get close, but do not add an understanding of the consequences of interaction. The channel gating change after coexpressing with VAMP721 gives a direct evidence of VAMP-K^+ channel interaction and its effects on channel function.

Further experiments making use of coexpression of single-site mutants of VAMP721 or VAMP723 with K^+ channel in oocytes indicated that mutated Tyr^{57} to Asp of VAMP721 inhibited the VAMP dependent gating change of both KC1 and KAT1 K^+ channels (Figure 5-7 and Figure 5-10), while the single-site mutant $VAMP721^{Y57A}$ had no effect. For any one channel, changes in current amplitude, and hence in g_{max}, may be understood as the consequence either of a change in the population of channels at the membrane or of a change in channel gating. However, the mid-point voltage, $V_{1/2}$, for gating is intimately connected with the biophysical properties of the K^+ channel voltage sensor (Hille, 2001; Dreyer and Blatt, 2009; Lefoulon et al., 2014). As such, changes in this parameter is difficult to reconcile these effects with membrane traffic or changes in the number of channels at the PM. Instead, the shifts in $V_{1/2}$ are a forceful argument for a direct physical interaction with the mechanism of voltage sensing by these channels, possibly with the voltage sensor domain itself (Dreyer and Blatt, 2009; Lefoulon et al.,

2014).

It is worth noting that VAMP723^{D57Y} rescued interaction with both two K^+ channels, but only affected the K^+ current of KAT1 rather than KC1-AKT1 K^+ channel. There are two explanation for these results:

1. The regulation mechanisms of KAT1 or KC1-AKT1 are different. KAT1 can form functional K^+ channel by itself in oocyte while AKT1 form K^+ channel with KC1 silence subunit. Mutated Asp^{57} to Tyr was enough to recover the KAT1 channel gating change. For KC1-AKT1, this mutant was only rescued the interaction but did not affect the K^+ current of this two subunits formed K^+ channel.
2. The potential interaction between VAMPs and AKT1 may affect the KC1-AKT1 K^+ channel regulation. I identified the VAMP interactions with KC1 and KAT1 K^+ channels but did not test AKT1. As another K_{in} channel, AKT1 may also interact with some of the VAMPs. If so, the effects may influence interactions with AKT1 as with KC1, which leads to the lost of VAMP dependent KC1-AKT1 K^+ channel regulation.

To reveal the background to these results, details of the molecular kinetics for interaction between VAMP721 and KC1 will need to be explored. The interaction between VAMP and AKT1 and the role of the VAMPs in traffic of KC1 to form K^+ channels with AKT1 need to be investigated in the future.

These details notwithstanding, it is clear that the effects of the interactions are relevant to the physiological condition. The membrane potential range of cells is due to the ion distribution between the inside and outside of the cell. In fungi, the membrane potential can often be as negative as -250 mV and is commonly around -200 mV under most experimental conditions (Blatt and Slayman, 1983). In plant cells, typical membrane potentials range from -60 to -240 mV (Taiz and Zeiger, 2010). Recordings from *Arabidopsis* root epidermal cells yielded complementary results to that of oocytes. The dominant inward K^+ current in these cells is normally carried by channels assembled from

KC1 and AKT1 subunits (Duby et al., 2008; Dreyer and Blatt, 2009; Honsbein et al., 2009). Overexpressing of VAMP721, but not VAMP723 and VAMP721^{Y57D}, strongly suppressed the inward-rectifying K^+ current, consistent with a substantial negative shift in $V_{1/2}$ (Figure 5-12). Furthermore, the effects of VAMP721 overexpression were limited to the inward-rectifying K^+ current and were without significant effect on the outward K^+ current that was carried by the GORK channel. GORK assembles in puncta at the PM; it shows very different gating properties which are related to its channel assembly and external K^+ concentration (Eisenach et al., 2014). So I can discount a general effect of VAMP overexpression on transporter delivery to, or cycling from, the PM.

Previous reports have shown that SYP121 interacted with KC1 and promoted the gating of KC1-AKT1 K^+ channel (Honsbein et al., 2009; Grefen et al., 2010a). After injection of AKT1, KC1, and SYP121 at cRNA molar ratio 1:1:4, the K^+ current moved to more positive values and the value of $V_{1/2}$ was increased in oocytes (Honsbein et al., 2009). Additionally, Eisenach et al. (2012) found that KAT1 K^+ current and conductance were reduced by 50% or more in guard cells of the *Arabidopsis syp121* mutant when compared with the currents in the guard cells of wild-type plants. While the latter observations may reflect, in part, a suppression in channel traffic to the PM, the explanation is clearly not the case for SYP121 binding with KC1 (Eisenach et al. 2012). The role of SYP121 in these two examples were opposite to the action of VAMP721 on K^+ current as I have demonstrated above. Indeed, the effect of the syp121 mutant on the inward-rectifying K^+ current may arise from the imbalance between VAMP721/VAMP722 and SYP121 in this mutant. SYP121 and VAMP721 can form a SNARE complex at the PM (Kwon et al., 2008). The opposite effect of these two SNAREs on channel gating suggests that there is a K^+ channel regulation system which is coordinated with the assembly of the SNAREs during the vesicle fusion cycle.

In previous reports, the interaction between SYP121 and K^+ channels could be understood as a mechanism for their mutual control, coordinating the rates of solute uptake and of surface area expansion as the cell grows (as described in Chapter 1 section 1.6 or in these papers: Grefen and Blatt, 2008; Honsbein et al., 2009; Grefen et al., 2010a). My finding about VAMP721 in K^+ channel regulation anticipates a sequence in which channel binding alternately with one SNARE and then the other. When K^+ channel binding proceeds from SYP121 to VAMP721, the gating is switched off. While in reverse order (from VAMP721 to SYP121), the channel is open. The periodic switching might serve to regulate the K^+ flux while engaging the SNAREs for assembly. How might these alternatives be distinguished? In order to reveal the relationship between VAMP721 and SYP121 in K^+ channel regulation, it will be necessary to identify the binding site of VAMP721 on K^+ channel protein. This is work that will need to be undertaken in the future.

Chapter 6. VAMPs and the effects of their domains on traffic

6.1 Introduction

In last several chapters, I reported that VAMP721 interacted with K^+ channels and this binding was dependent on Tyr^{57} in the longin domain of VAMP721. What is the function of this interaction? I found VAMP721 regulated K^+ channel gating. Yet, as a SNARE protein, VAMP721 is known to be involved in membrane vesicle traffic. So this fact alone raises the question of whether K^+ channel binding might also affect traffic. The aim of work outlined in this chapter was to explore whether the K^+ channel interaction affected VAMP721-dependent vesicle traffic. To explore the role of the R-SNARE in vesicle traffic, I cloned the coding sequences of VAMP721, VAMP723, $VAMP721^{\Delta C}$, $VAMP723^{\Delta C}$, $VAMP721^{Y57D}$, and, as control, $SYP121^{\Delta C}$ in the tetracistronic vector pTecG-2in1-NC (Karnik et al., 2013b) and performed the traffic analysis in *Arabidopsis* seedlings and tobacco leaves. I carried out similar experiment, testing the role for VAMP-K^+ channel interactions in vesicle traffic by including KC1 in the same vector and transforming *Arabidopsis* seedlings.

It should be noted that the data in this chapter are preliminary; most of the experiments were carried out only once or twice and there are no supporting Western blot data to verify protein expression. So these results should be accepted with caution.

6.2 Results

6.2.1 Overexpression of VAMP721 and VAMP723 blocks vesicle traffic in tobacco leaves.

As shown in Figure 6-1, the pTecG-2in1-NC vector incorporates a set of independent, Gateway-compatible cassettes, each with a 35S promoter, an Omega Enhancer, and tags for Western blot analysis (HA and myc tags). In order to monitor traffic to the PM, two cassettes are given to expression of secretory marker secYFP and GFP-HDEL. GFP-HDEL is included as a transformation marker and ratiometric reference. Because expression of secYFP leads to its secretion, little or no YFP fluorescence is recovered within the tissue. If secretory is blocked at the PM, secYFP will accumulate within the ER and the secretory pathway, which yields YFP fluorescence associated with these endomembrane compartments. As in rBiFC analysis, I used a ratiometric method to quantify secYFP/GFP-HDEL fluorescence as a measure of secretory traffic and its block.

Previous reports (Geelen et al., 2002; Sutter et al., 2006; Tyrrell et al., 2007; Karnik et al., 2013b) indicated that SYP121$^{\Delta C}$, the so-called Sp2 fragment of SYP121, selectively blocked secretory traffic to the PM. In order to investigate the role of VAMP721 in vesicle traffic, the full length coding sequences for VAMP721, VAMP723, VAMP721$^{\Delta C}$, and VAMP723$^{\Delta C}$ were cloned into pTecG-2in1-NC. The latter two constructs lack the transmembrane domain and were used as soluble R-SNAREs, like the Sp2 fragment of SYP121. The native VAMP incorporated a C-terminal membrane anchor, hence, I cloned them in the R3R2 Gateway cassette to add a HA tag to the N terminus of the protein. As a positive control, I cloned SYP121$^{\Delta C}$ in R1R4 Gateway cassette. The background control expressing secYFP and GFP-HDEL alone is referred to as “control” from here on.

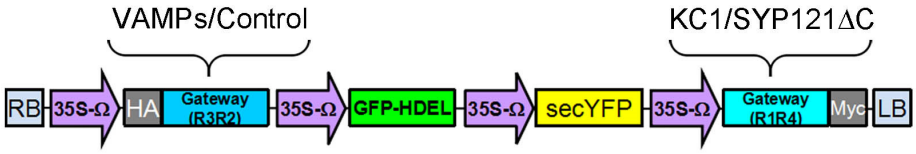

Figure 6-1. Schematic of the pTecG-2in1-NC vector

Figure 6-2 summarizes the results of traffic rescue analysis from two independent experiments with confocal images collected at random across 10-20 leaf surfaces for each construct. The fluorescence of GFP in leaf cells indicated successful transformation and expression of proteins from the pTecG constructs. I found, as reported before (Tyrrell et al., 2007; Karnik et al., 2013b), that expressing SYP121$^{\Delta C}$ led to a significant block of traffic and retention of the secYFP signal relative to the cellular marker GFP-HDEL. Expressing VAMP723 yielded a similar YFP/GFP ratio as that of SYP121$^{\Delta C}$, indicating overexpression of VAMP723 blocked vesicle traffic. Interestingly, expressing VAMP721 gave ratio of YFP/GFP 62% higher than that of SYP121$^{\Delta C}$, suggesting overexpression of VAMP721 strongly inhibited secYFP traffic to the PM. Overexpressing VAMP721$^{\Delta C}$ and VAMP723$^{\Delta C}$, without transmembrane domain, also led to retention of the secYFP marker, but less than I observed with the native VAMPs. The secYFP signal I observed with VAMP721$^{\Delta C}$ was not distributed uniformly. I show a typical YFP image of VAMP721$^{\Delta C}$ in Figure 6-1 A, where some cells had strong expression while the other cells did not. But this non-uniformity in fluorescence should not affect the calculation of traffic level, because the ratiometric approach based on the pTecG-2in1-NC vector corrects for variations in transgene load (Karnik, et al. 2013b).

Because VAMP721$^{\Delta C}$ and VAMP723$^{\Delta C}$ did not block the traffic as strongly as the native R-SNAREs, I chose to use the full-length VAMP721 and VAMP723 in further experiments.

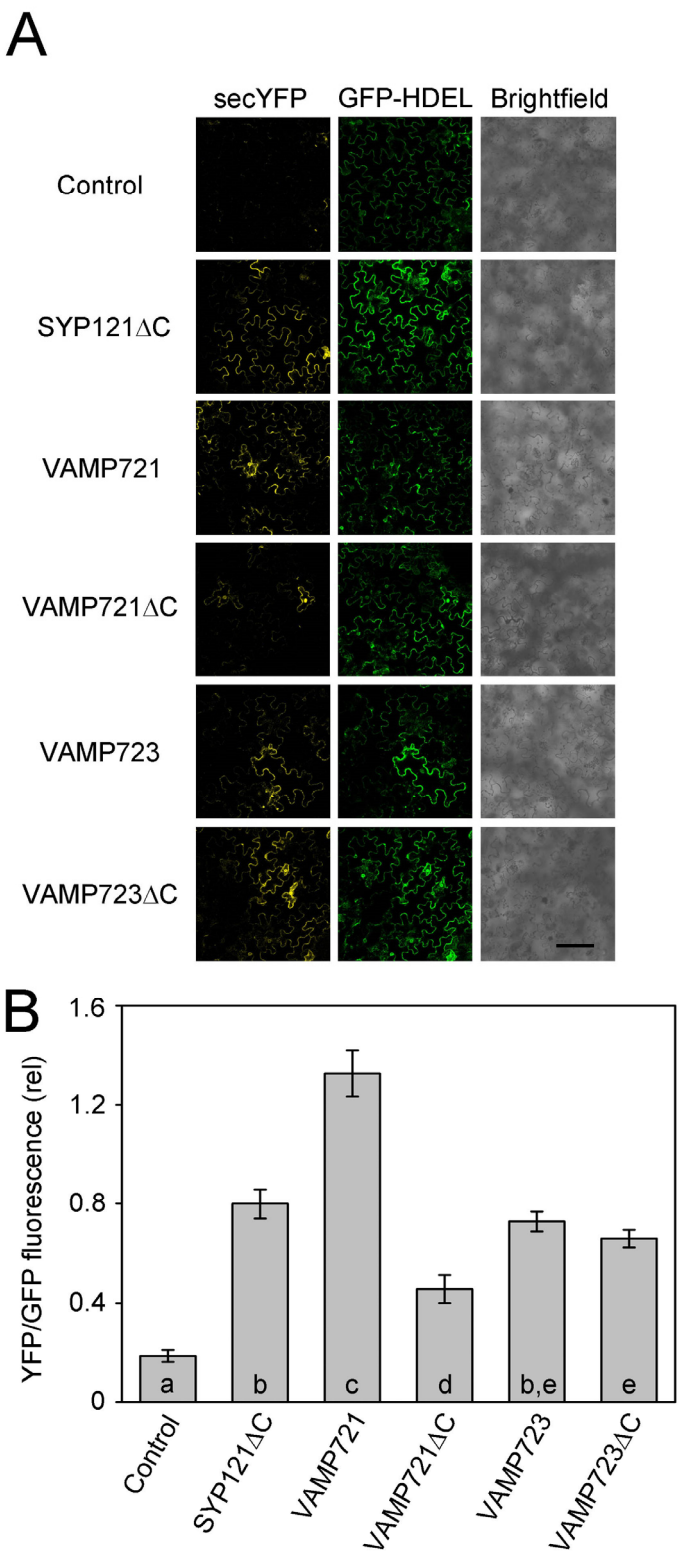

Figure 6-2. Both VAMP721 and VAMP723 blocks vesicle traffic in tobacco leaves

A. Confocal images (left to right) of the secretory marker (secYFP), cellular marker (GFP-HDEL) fluorescence, and brightfield signals from tobacco epidermis after transformation. The construct expressing secYFP and GFP-HDEL alone was used as background control and

SYP121$^{\Delta C}$ was included as positive control. Scare bar: 50 μm.
B. Means ± SE of relative secYFP retention (=YFP fluorescence/GFP fluorescence) as a measure of secretory block. Fluorescence ratios were calculated from the mean fluorescence intensities determined from image pairs collected at random over 10-20 leaf surfaces in each of two independent experiments after correction for background. Significance of differences is indicated by letters ($P < 0.05$).

6.2.2 Coexpression of KC1 and VAMP721 rescues the VAMP721-dependent traffic block.

As mentioned before, KC1 is mislocalized in tobacco. Therefore, I carried out transient transformations of constructs including the channel in *Arabidopsis* seedings. In order to explore the role of VAMP-K^+ channel binding in vesicle traffic, I cloned both VAMPs and KC1 in pTecG-2in1-NC vector and generated constructs including VAMP721+KC1, VAMP723+KC1, and VAMP721^{Y57D}+KC1. These constructs, and those expressing the corresponding VAMPs alone were also transformed in *Arabidopsis* seedings. SYP121$^{\Delta C}$ and KC1 alone were used as positive and negative controls along with the construct expressing secYFP and GFP-HDEL alone as background control.

Confocal images of these constructs is shown in Figure 6-3. The ratios between YFP and GFP from 5-7 roots per experiment of two independent experiments was present in Figure 6-4. In *Arabidopsis* roots, overexpressing SYP121$^{\Delta C}$ or VAMP721 alone yielded significant block of traffic. But the YFP/GFP ratio of VAMP721 was lower than that of SYP121$^{\Delta C}$, which was different to the results from tobacco. Expression of KC1 alone gave a YFP/GFP ratio indistinguishable from that of background control, indicating overexpression of the channel alone did not affect the secYFP traffic. Expressing VAMP723 alone also blocked traffic and yielded high YFP/GFP ratio, which has no significant difference compared to that of VAMP721. Mutating Try^{57} to Asp led to an inhibition of the interaction between VAMP721 and KC1. But this single

site mutant did not affect the VAMP721 dependent traffic block. Coexpressing KC1 with VAMP721 gave a reduced YFP/GFP ratio compared to VAMP721 alone, indicating a partial rescue of secYFP traffic. VAMP723 and VAMP721^{Y57D} do not interact with the KC1 K^+ channel. Coexpressing these VAMP constructs with KC1 yielded similar level of YFP/GFP ration as expressing the corresponding VAMP alone, suggesting that KC1 did not rescue the traffic block related to these two R-SNAREs. Thus these results indicate that the interaction between VAMP721 and KC1 affects the ability of overexpressed VAMP721 to inhibit secretion.

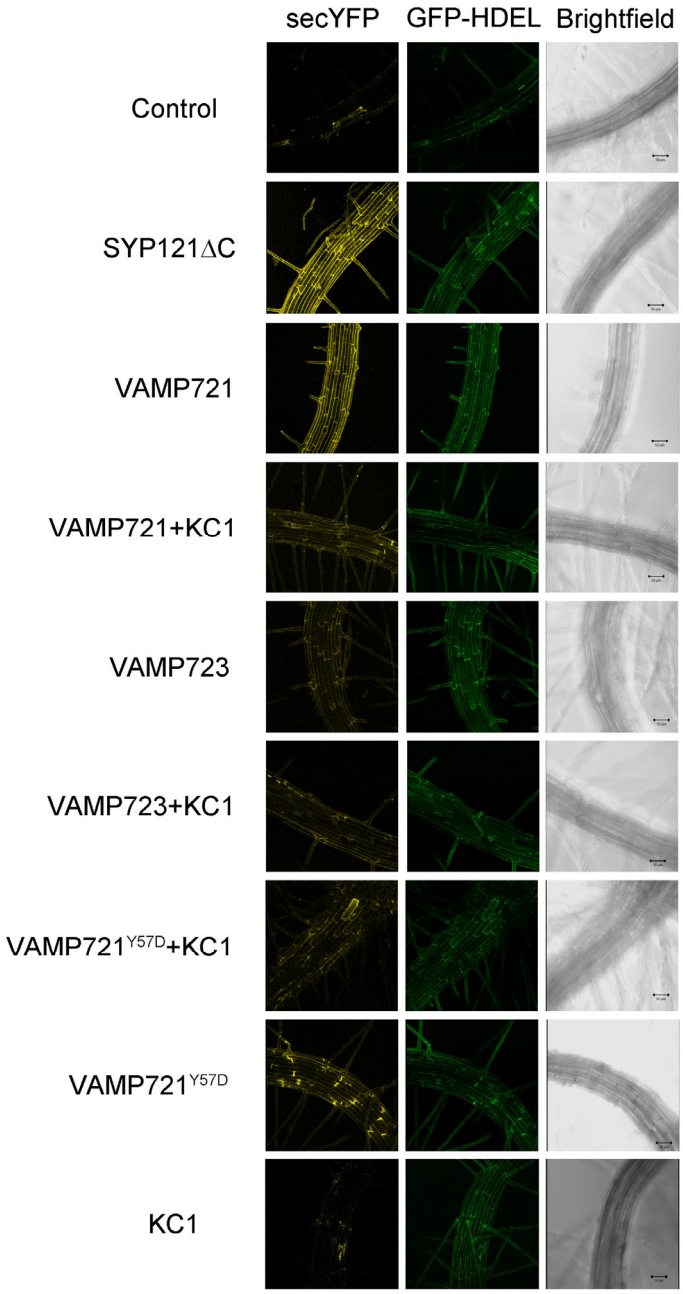

Figure 6-3. Secretory traffic block in vivo by VAMP721 is rescued by coexpressing with KC1

Confocal images (left to right) of the secretory marker (secYFP), cellular marker (GFP-HDEL) fluorescence, and brightfield signals from *Arabidopsis* roots after transformation. The construct expressing secYFP and GFP-HDEL alone was used as background control. The sample expressing SYP121$^{\Delta C}$ were used as positive control. Scare bar: 50 μm.

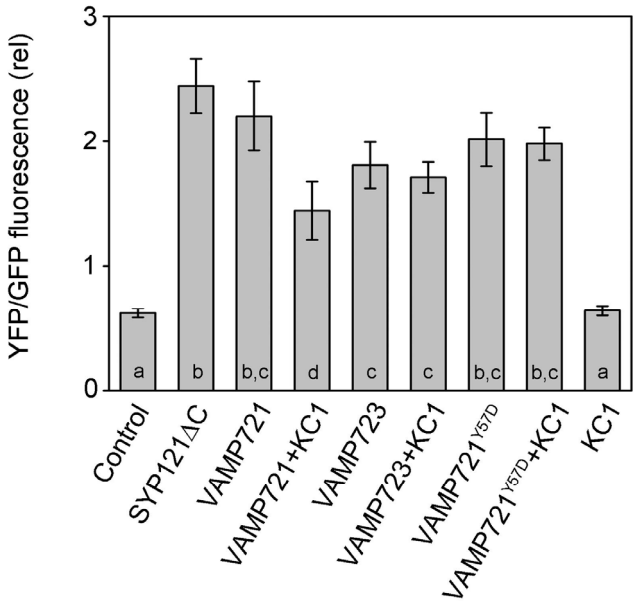

Figure 6-4. Interaction between VAMP721 and KC1 rescues the traffic block

The results was corresponding to Figure 6-3. Means ± SE of relative secYFP retention (=YFP fluorescence/GFP fluorescence) as a measure of secretory block. Fluorescence ratios were calculated from the mean fluorescence intensities determined from images of 5-7 random roots of transient transformed *Arabidopsis* per construct in each of two independent experiments after correction for background. Significance of difference was indicated by letters ($P < 0.05$).

6.2.3 VAMP711, VAMP721, and VAMP723 block the secYFP secretion

The results outlined above show that both VAMP721 and VAMP723 affected secYFP secretion. I was puzzled by this finding. A previous report (Uemura et al., 2004) and my results in Chapter 4 indicate that VAMP721 is expressed at the PM, but VAMP723 is normally found at the ER. Why did VAMP723 block secYFP traffic as VAMP721? I reasoned that different VAMPs might be involved in different steps of protein traffic along the pathway to the PM and overexpression any one of them could affect normal protein traffic. I discuss this point in later.

To test this hypothesis, I cloned VAMP711, which is known to be targeted to the vacuolar membrane (Uemura et al., 2004), into

pTecG-2in1-NC vector and performed another traffic analysis in *Arabidopsis* seedings. Again, SYP121$^{\Delta C}$ was used as positive control, while the construct expressing secYFP and GFP-HDEL alone was used as a background control. The confocal images from one experiment and the analysis of secYFP retention is summarized in Figure 6-5. As before, SYP121$^{\Delta C}$, VAMP721, and VAMP723 expression alone led to secYFP retention. Expressing VAMP711 alone gave a similar level of YFP/GFP ratio as that of VAMP723, indicating overexpression of VAMP711 also affected traffic of secYFP. These results suggest that overexpression of the VAMPs influences vesicle traffic to the PM, even when they are normally localized elsewhere in the cell.

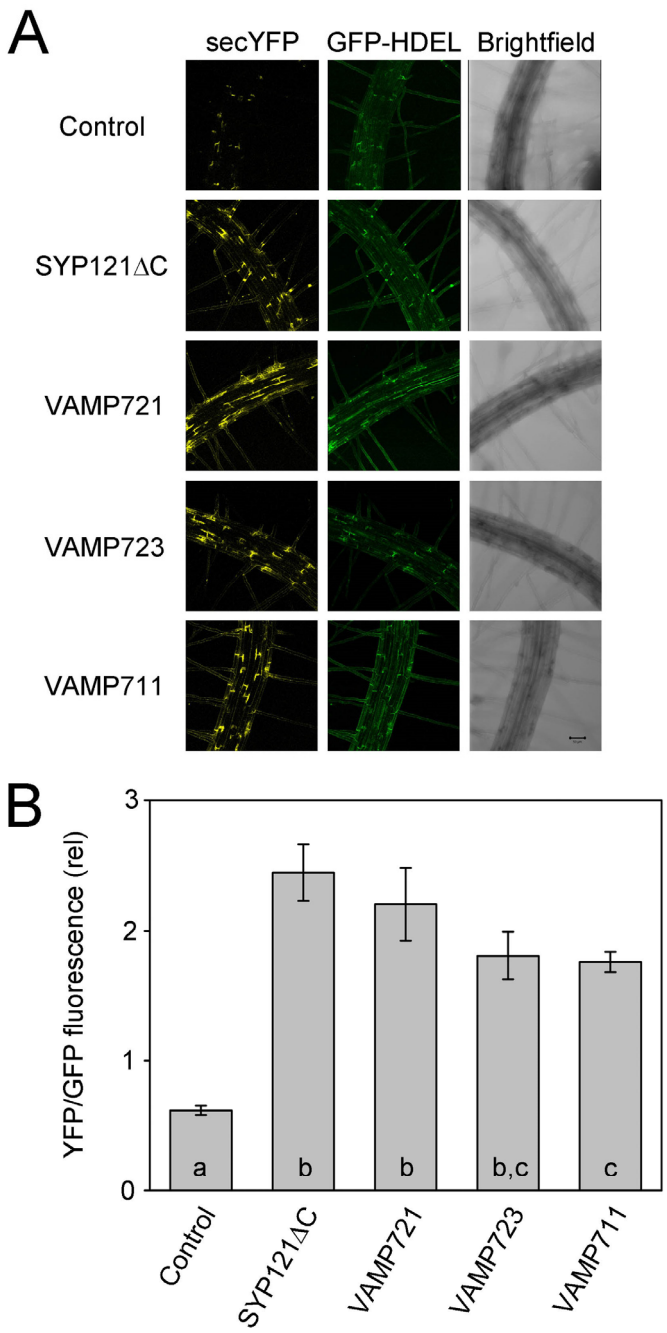

Figure 6-5. The secYFP secretion is blocked be different VAMPs

A. Confocal images (left to right) of the secretory marker (secYFP), cellular marker (GFP-HDEL) fluorescence, and brightfield signals from *Arabidopsis* roots after transformation. The construct expressing secYFP and GFP-HDEL alone was used as background control and addition of SYP121$^{\Delta C}$ was used as positive control. Scale bar, 50 μm.

B. Means ± SE of relative secYFP retention (=YFP fluorescence/GFP fluorescence) as a measure of secretory block. Fluorescence ratios were calculated from the mean fluorescence intensities determined from images of 5-7 random roots of transient transformed *Arabidopsis* per construct in each of two independent experiments after correction for background. Significance of difference was indicated by letters (P <

0.05).

6.3 Discussion

In Chapter 3 and Chapter 4, I found that VAMP721 interacted with KC1 and KAT1 K^+ channels and this interaction was dependent on the residue 57 of R-SNARE longin domain. Further research indicated that the interaction between VAMP721 and the K^+ channels KC1 and KAT1 regulated the gating of the channels. Previous reports have showed that the Qa-SNARE SYP121 interacts with these K^+ channels and promotes their gating (Honsbein et al., 2009; Honsbein et al., 2011; Grefen and Blatt, 2008). The interaction between SYP121 and the K^+ channels is associated with a FxRF motif of SYP121 (Grefen et al., 2010a) and overlaps with the binding site for the SM protein SEC11. It has been suggested that these proteins take part in a handover of the Qa-SNARE between K^+ channel and SEC11 which releases SYP121 for SNARE complex assembly (Karnik et al., 2013b). Such a mechanism would indicate a role for K^+ channel binding in SNARE-related vesicle traffic. In plant cells, VAMP721 can form a SNARE complex with SYP121 at the PM (Kwon et al., 2008). In animal cells, phosphorylation of residue 45 of TI-VAMP longin domain increased the binding with its t-SNARE partners (Burgo et al., 2013), suggesting longin domain of mammalian VAMP was important for SNARE complex forming. These observations raised the question if the interaction between VAMP721 and K^+ channel affected the SNARE complex formation, which would indicate the role of SNARE-K^+ channel interaction in vesicle traffic from R-SNARE side.

In order to test this hypothesis, I performed the traffic rescue analysis by overexpressing VAMP721, VAMP723, VAMP721^{Y57D} in *Arabidopsis* seedlings via the pTecG-2in1-NC vector. In this system, secYFP is used to monitor the vesicle traffic and export at the plasma membrane, and the ratio between secYFP and GFP-HDEL is used as a

quantitative measure of secretion. As a positive control, I used SYP121$^{\Delta C}$. Previous studies (Geelen et al., 2002; Sutter et al., 2006; Tyrrell et al., 2007) had shown that SYP121$^{\Delta C}$ selectively blocks the secretory traffic to the PM. This traffic block was thought to result from the ability of the soluble SYP121$^{\Delta C}$ to assemble in complex with its SNARE partners but not to facilitate fusion. In other words, SYP121$^{\Delta C}$ was proposed as a dominant-negative inhibitor by competing with the native Qa-SNARE for binding partners.

As shown in Figure 6-2 and Figure 6-3, I found expressing VAMP721 alone yielded strong traffic block, while VAMP723, the soluble VAMP721$^{\Delta C}$, and VAMP723$^{\Delta C}$ also inhibited secYFP traffic. The two soluble fragments gave YFP/GFP ratios that were not as high as that of native VAMP721. How can we understand these findings? The ability of VAMP721$^{\Delta C}$ and VAMP723$^{\Delta C}$ to block traffic can be understood if, like SYP121$^{\Delta C}$, they bind with and compete for the cognate partner proteins, in this case the Qa-SNAREs. A model is shown in Figure 6-6. The Qa-SNARE, in this case SYP121, is thought to form 'icebergs' at the PM in which much of the protein is held inactive (Sieber et al., 2007; Murray et al., 2009; Honsbein et al., 2011). Binding with the soluble, non-functional R-SNAREs, might be thought to compete with native VAMPs for binding and thereby affect the secretion of secYFP.

Previous reports have indicated that overexpression of many full-length SNAREs inhibits vesicle traffic. Chatre et al. (2005) found that overexpression of R-SNARE SEC22 and Qb-SNARE MEMB11 block secYFP secretion in tobacco leaf epidermal cells. Foresti et al. (2006) reported that overexpressing the full-length Qa-SNARE SYP21 inhibited the traffic from the prevacuolar compartment to the vacuole. In my research, I found overexpressing of full length VAMP blocked traffic. How did this happen? Several possible explanations can be put forward for these observations.

First, the excess of VAMPs may lead to non-function SNARE

complexes assembly by self-interaction, which blocks the normal secretion. Many SNAREs can bind with the same SNARE protein and form homodimers, which is often called “self-interaction”. In animal cells and yeast, previous reports have indicated many SNAREs, like synaptobrevin/VAMP II (Laage and Langosch, 1997; Roy et al., 2004), syntaxin 1A (Laage et al., 2000), Sso1p (Zhang et al., 2006b), and Vam3p (Hofmann et al., 2006), can form homodimers and their self-interaction is dependent on the transmembrane domain. During membrane fusion, SNAREs appear to exist in different forms - as monomers, as homodimers, and as forms bound to other SNAREs (Pennuto et al., 2002). In normal conditions, the existence of SNARE homodimers affects the interconversion among these forms and regulates the SNARE complex formation speed (Roy et al., 2004). My results are consistent with this idea. Thus, overexpressing native VAMPs may increase the proportion of R-SNAREs in a homodimer form at the vesicle membrane (See Figure 6-6 C) which affects their interaction with the cognate Q-SNAREs and SNARE complex formation. Finally, as a consequence, secretion of secYFP might be blocked.

Secondly, overexpression of the native VAMP might cause the production of non-functional SNARE complexes with only one or two of their SNARE partners, leading to titration by forming incomplete complexes which then also affect vesicle traffic. This explanation supports the i-SNARE (inhibitory or interfering SNARE) model, which predicts that in addition to a role in driving membrane fusion, some SNAREs have additional non-fusogenic roles and are able to inhibit fusion by substituting for or binding to a subunit of SNARE complex. Foresti et al. (2006) found SYP21 overexpression specifically inhibited vesicle traffic from the PVC. In 2012, De Benedictis et al. also found that SYP51 and SYP52 have dual localization and associated functional characteristics. When targeted to TGN, SYP51 and SYP52 behaved like normal Q-SNAREs and facilitated the membrane fusion. However, when

they were sorted to the tonoplast, their behaved in a non-fusogenic manner. Furthermore, both functions of SYP51 and SYP52 appeared to play structural roles in tonoplast formation by regulating the arrival of new vesicles.

Thirdly, overexpressing the VAMPs may consume more Q-SNAREs than is normal, which in turn may block traffic by tying up other SNARE components. As shown in Figure 6-6 C with VAMP721 as an example, overexpression of this R-SNARE might lead to more density in the distribution of the proteins on the surface of vesicle. During membrane fusion, these high concentrations of VAMP721 might then bind to more Q-SNAREs than normal. In other words, overexpression of VAMP721 might increase the requirement for the corresponding Q-SNARE at the target membrane, which then disrupts the balance between R-SNAREs and Q-SNAREs and finally affects the traffic of secYFP to the PM.

There are other explanations too. For example, overexpressing the VAMPs may affect the expression of other SNAREs. Shanks et al. (2012) found that SM protein Vps45p regulates cellular levels of its SNARE binding partners, the syntaxin Tlg2p and the v-SNARE Snc2p in yeast. Yeast lacking Vps45p reduced cellular levels of both Tlg2p and Snc2p and showed the phenotype of growth defects. Selectively restoring Snc2p levels in *vps45* mutant yeast rescued this growth phenotype. This result also suggests the SNARE population balance is important for the vesicle traffic and the expression level of one SNARE can be affected by other SNARE.

In Chapter 4, I explored the localization of GFP tagged VAMP721 and VAMP723 in *Arabidopsis* root hairs. I found VAMP721 was expressed at the PM while VAMP723 was at the ER, which supported previous report (Uemura et al., 2004). These results raised a question why overexpressing VAMP723 also blocked the secYFP traffic. To answer this question, I cloned VAMP711, a vacuolar target R-SNARE (Uemura et al., 2004) in pTecG-2in1-NC vector and tested its effect on

traffic. As shown in Figure 6-5, like that of VAMP721 or VAMP723, expressing of VAMP711 also blocked secYFP secretion. Previous report have shown that overexpression of the Golgi apparatus localized SNAREs, SEC22 and MEMB11, block secretion of secYFP (Chatre et al., 2005). These results indicated that overexpressing differently localized SNAREs affects the secretion.

How might we explain these results? Each functional SNARE complex requires three Q-SNAREs and one R-SNARE to generate a fusogenic complex (Katz & Brennwald, 2000; Ossig et al., 2000; Graf et al., 2005). After membrane fusion, the SNARE complex needs to dissociate again, which is mediated by regulatory factors like N-ethylmaleimide-sensitive factor (NSF) and soluble NSF attachment protein (α-SNAP) that require ATP to dissociate the complex (Whiteheart et al., 2001). The overexpression of a VAMP might form a excess of non-functional SNARE complexes which consume NSF and α-SNAP that are otherwise needed for normal SNARE related secretion. In this case SNARE recycling becomes limiting and the fusogenic complexes can not dissociate, which finally blocks the secretion of secYFP.

However, to reveal the role of full length VAMPs in traffic block, some more experiments will need to be done in the future, including coexpressing VAMP721 and SYP121 together to test whether rebalancing the ratio between R-SNARE and Qa-SNARE might rescue the VAMP721-related traffic block.

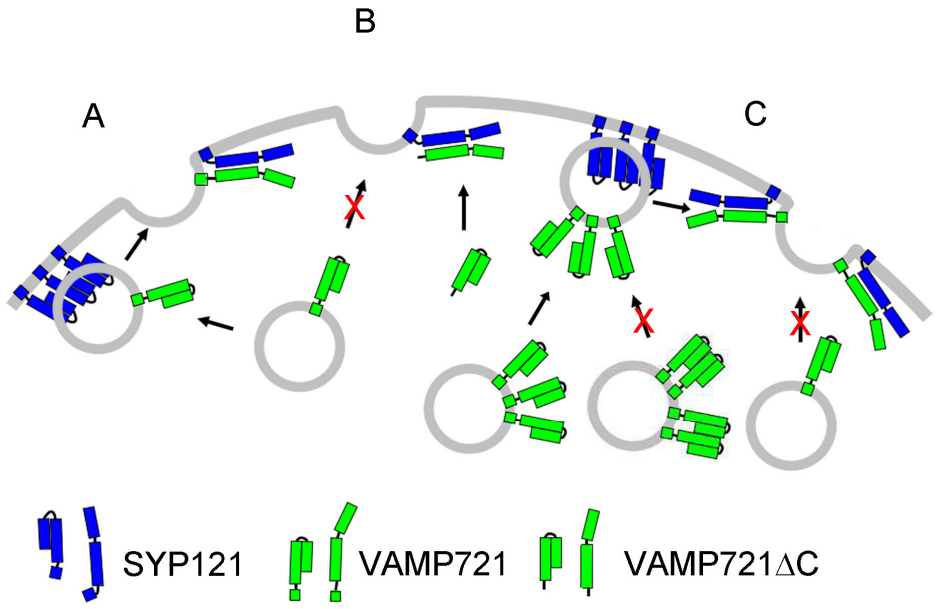

Figure 6-6. Overexpression of VAMP721 or VAMP721ΔC block secretion to the PM

For clarity, only the SNAREs SYP121 and VAMP721 are shown. The Q-SNARE SYP121 form a 'icebergs' at the PM (Sieber et al., 2007; Murray et al., 2009; Honsbein et al., 2011).
A. The assembly of SNARE complex drives the membrane fusion at the PM.
B. The soluble VAMP721$^{\Delta C}$ blocks the traffic to the PM by competition with the native VAMP721.
C. Overexpressing VAMP721 blocks traffic to the PM. On one hand, more VAMP721 expressed at the surface of vesicle membrane, which consumes more SYP121 at the PM and leads to traffic block. On the other hand, VAMP721 self interaction (or interact with other SNAREs to form non-functional complex, which is not shown in figure) at the surface of vesicle membrane affects their binding with SYP121, which blocks the secretion.

To explore the role of VAMP721-K^+ channel interaction in vesicle trafficking, I cloned VAMP721, VAMP723, and VAMP721^{Y57D} with KC1 in pTecG-2in1-NC vector and performed the traffic rescue analysis in *Arabidopsis* seedlings. The results were summarized in Figure 6-3 and 6-4. Expressing KC1 alone did not affect the expression of GFP and yielded the YFP/GFP ratio at similar level as that of the control, indicating overexpressing of KC1 had no effect on secYFP secretion. Expressing

VAMP721^{Y57D} alone also inhibited the secYFP secretion. In Chapter 4, I indicated that this single site VAMP mutant expressed at the ER or on other endomembrane systems. So this traffic block might arise because VAMP721^{Y57D} is mislocalized in plant cells and interrupted the function of other R-SNAREs. But this explanation requires more experiments to investigate the predict interaction between different SNARE pairs. Compared to R-SNARE expression alone, coexpressing KC1 with VAMP721 reduced the YFP/GFP ratio, while there was no significant change of KC1 with VAMP723 or KC1 with VAMP721^{Y57D}. As I noted in the results of Chapter 3 and chapter 4, VAMP721 interacted with KC1 while VAMP723 and VAMP721^{Y57D} did not. These results suggest VAMP721-K^+ channel interaction is involved in vesicle traffic, which supports previous reports in animal cells. The Kv2.1 K^+ channel direct interacts with Q-SNARE syntaxin 1A in mammalian cells (Michaelevski et al., 2003). These interactions facilitate dense core vesicle-mediated norepinephrine secretion in PC12 neuronal cells and insulin secretion in rodent and human islets, which are independent of K^+ currents (Singer-Lahat et al., 2007; Singer-Lahat et al., 2008; Dai et al., 2012). VAMP2, the SNARE partner of syntaxin 1A, also directly interacts with Kv2.1 (Lvov et al., 2008). Syntaxin 1A interacts with Kv2.1 in a Q-SNARE complex containing syntaxin 1A and SNAP25, but not in the SNARE complex containing syntaxin 1A, SNAP25 and VAMP2, suggests Kv2.1 stabilizes complexes of Q-SNAREs before forming the functional SNARE complex (Tsuk et al., 2008). However, the role of VAMP2 in Kv2.1 related secretion is still unknown. In plant cells, both SYP121 and VAMP721 interact with K^+ channels, while the interaction between K^+ channel and R-SNAREs rescues the traffic blocks. To reveal the relationship among these three proteins, more work need to do in the future.

Figure 6-7 brings together a hypothetical sequence based on our understanding of SYP121 and VAMP721. Here SYP121 is recruited by the K^+ channels from larger ‘icebergs’ of the Qa-SNARE at the PM

(Sieber et al., 2007; Murray et al., 2009; Honsbein et al., 2011). During membrane fusion, the first possibility is that the interaction between K^+ channel and VAMP may release VAMP from homodimer form and lead to the normal secretion. The second possibility is that the overexpressed R-SNAREs interact with K^+ channels, instead of interaction with Q-SNAREs, which rebalance the ratio between R-SNAREs and Q-SNAREs and finally rescue the traffic block. In other word, it may be reasonable to assume that normally K^+ channels like KC1 interact with VAMP721 and affect the R-SNARE related traffic block.

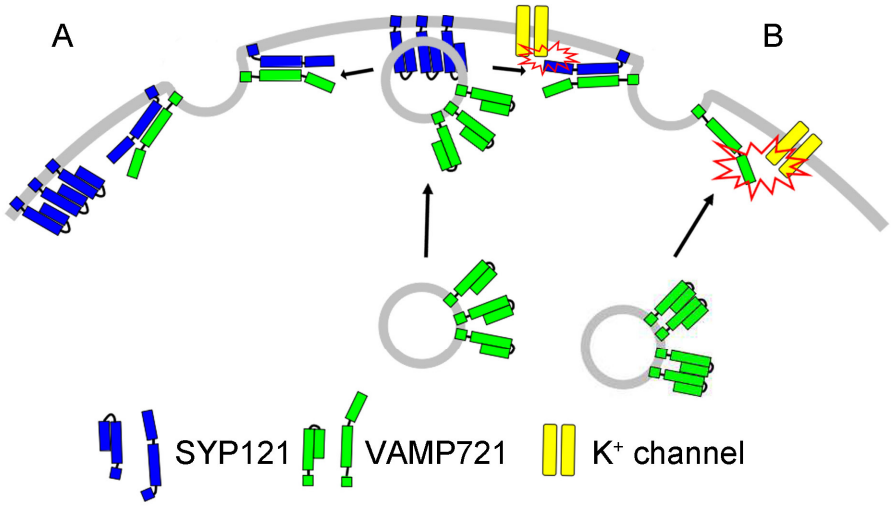

Figure 6-7. The interaction between VAMP721 and KC1 rescues the R-SNARE overexpression related traffic block

For clarity, only the SNAREs SYP121 and VAMP721 are shown. The Q-SNARE SYP121 form a 'icebergs' at the PM, which helped the vesicle target to the PM (Sieber et al., 2007; Murray et al., 2009; Honsbein et al., 2011).

A. Overexpressing of VAMP721 blocks traffic to the PM.

B. The interaction between VAMP721 and K^+ channel rescues the traffic block. The binding with K^+ channel releases the R-SNARE from homodimer form or consumes some over expressed VAMP721 in the vesicle membrane and balanced the cost of R-SNARE and Q-SNARE during membrane fusion, which rescue the secretion.

Previous reports have proposed a molecular governor model for SYP121-K^+ channel interactions to keep channel-mediated uptake of the

osmotically active K^+ in check and to coordinate its transport with changes in cell volume (Grefen and Blatt, 2008; Honsbein et al., 2009). My results in chapter 5 and this chapter gives a new set of supporting data for this idea. I found VAMP721 interacted with K^+ channels and suppressed their channel gating. The same interaction also affected VAMP721 related vesicle traffic, demonstrating a potential action of VAMP-K^+ channel interaction on secretory traffic. These results add to understanding the interaction between SNARE and K^+ channels that link membrane traffic with osmotically active solute transport in the plant.

Chapter 7. General Discussion and Outlook

7.1 Summary

There is now a substantial body of information for Qa-SNAREs in *Arabidopsis* and other plants of their roles in cell division and polarization, endomembrane and secretory traffic (Lipka et al., 2007; Bassham et al., 2008). These proteins contribute to a number of related physiological activities, notably in osmotic homeostasis (Zhu et al., 2002; Drakakaki et al., 2012), tropic growth (Kato et al., 2002; Morita et al., 2002), and pathogen defense (Collins et al., 2003; Kwon et al., 2008; Zhang et al., 2007; Kalde et al., 2007), each of which relies on the mechanics of vesicle traffic. A subset of Qa-SNAREs has proven important also in controlling K^+ and other solute uptake through mechanisms that are unrelated to SNARE complex forming. Previous reports identified the Qa-SNARE SYP121 (=SYR1/PEN1) of tobacco and *Arabidopsis* through its activity in hormonal regulation of K^+ and Cl^- channels that facilitate solute flux for stomatal movements and cellular expansion (Leyman et al., 1999; Leyman et al., 2000; Geelen et al., 2002). Subsequent studies demonstrated that SYP121 binds directly with two inward-rectifying K^+ channels, KC1 and KAT1, altering channel gating and channel-mediated K^+ uptake (Honsbein et al., 2009; Grefen et al., 2010a; Honsbein et al., 2011). Recent work has extended these findings to the interaction of SYP121 with a subset of aquaporins at the PM of *Arabidopsis* and maize (Besserer et al., 2012; Hachez et al., 2014), implying a role in coordinating both solute and water uptake for growth.

Much less is known of the physiology and functional associations that pertain to the cognate SNARE partners of Q-SNAREs in plants, notably the VAMPs. VAMPs have been implicated in endosomal biogenesis (Ueda et al., 2004), gravitropism (Kato et al., 2002; Yano et al., 2003), nodulation (Mai et al., 2006), pathogen defense (Kwon et al.,

2008; Yun et al., 2013), salt and drought tolerance (Leshem et al., 2006; Zhu et al., 2002), and cytokinesis (Zhang et al., 2011; El Kasmi et al., 2013), again with the expectation that they act through SNARE-driven vesicle fusion to affect these processes. The near-identical homologs VAMP721 and VAMP722 are known to assemble SNARE core complexes with SYP121 to drive vesicle fusion at the PM in *Arabidopsis* (Kwon et al., 2008; Karnik et al., 2013b). Thus, the non-canonical functions of SYP121 raises the possibility that these VAMPs interact with the same K^+ channels that bind SYP121. In this thesis, I have explored this possibility to define the characteristics of VAMP interactions with the K^+ channels, KAT1 and KC1, previously shown to bind with SYP121. I found that:

1. VAMP721 and VAMP722, but not VAMP723, interacted with KC1 and KAT1 K^+ channels by mbSUS assay and rBiFC analysis. The selective binding of these R-SNAREs was associated with the longin domain of the VAMP721, specifically with Tyr^{57}.
2. VAMP721 affected K^+ channel gating and suppressed the K^+ current within the physiological voltage range when recorded in *Xenopus* oocytes. In *Arabidopsis*, overexpression of VAMP721 strongly suppressed inward K^+ current. This K^+ channel regulation was also dependent on $Tyr^{57}$of VAMP721.
3. The exchange of residue 57 between VAMP721 and VAMP723 was sufficient to switch on or off the VAMP-K^+ channel binding and channel gating regulation. This substitution also affected the localization of VAMP721 and VAMP723.
4. The interaction between VAMP721 and the KC1 K^+ channel affected R-SNARE-related traffic block. Overexpressing VAMP721 or VAMP723 blocked secretion traffic in plants and the coexpression of VAMP721 with KC1 partially rescued this traffic block.

7.2 The K^+ channels KAT1 and KC1 associate with a subset of R-SNAREs

In *Arabidopsis*, there are twelve genes that belong to VAMP family, four in the VAMP71 group and eight in the VAMP72 group (as shown in Table 1-1). Both KC1 and KAT1 K^+ channels interacted with all four VAMP71 group proteins and VAMP721, VAMP722, VAMP724, VAMP726, and VAMP727 in VAMP72 group (Figure 3-1 and Figure 3-2 in Chapter 3).

The VAMP71 group proteins are known to associate with endosomal traffic (Sanderfoot et al., 2007). Previous reports (Leshem et al., 2006; Leshem et al., 2010) have indicated that VAMP711 is involved in the transport of vesicles containing ROS, and the silencing of VAMP711 suppresses ABA related stomatal closure. For VAMP712, VAMP713, and VAMP714, the function is still uncertain. The only reports about localization of these R-SNAREs have shown that VAMP711, VAMP712 and VAMP713 are localized to the vacuolar membrane, while VAMP714 is localized to the Golgi apparatus (Uemura et al., 2004). KC1 and KAT1 K^+ channels were localized at the PM. So it's difficult to explain the reason why there are interactions between VAMP71 group with K^+ channels. However, it should be noted that Uemura and colleagues (Uemura et al., 2004) made use of overexpression with GFP-tagged proteins; as a result of this approach, the subcellular distributions may not always show the true locations of the proteins.

Of eight proteins in the VAMP72 subgroup, both K^+ channels selectively interacted with only a subset, including VAMP721, VAMP722, VAMP724, and VAMP726, which are known to facilitate traffic to the PM (Uemura et al., 2004), and VAMP727 which has been localized to the endosome (Uemura et al., 2004). VAMP723, which localizes on the ER (Uemura et al., 2004), did not interact with the K^+ channels, either SUS assay or rBiFC analysis. Previous reports indicated that SYP121

interacts with KC1 and KAT1 K^+ channels and regulated their channel gating (Honsbein et al., 2009; Honsbein et al., 2011). VAMP721 and VAMP722 are SNARE partners of SYP121 at the PM (Kwon et al., 2008). VAMP727 co-localizes with SYP22 on early endosome and pre-vacuolar compartment membranes (Ebine et al., 2008), but it has also been shown to relocate to the PM and bind with SYP121 (Ebine et al., 2011). Little is known of the cognate SNAREs that interact with VAMP724 and VAMP726. Most of the members of VAMPs which interacted with K^+ channels were SNARE partners of SYP121. Thus, these results suggest a potential regulation system of K^+ channels which work together with the SNAREs.

7.3 Implications of the interaction between VAMP721 and K^+ channels and its dependence on residue 57

The amino acid sequences of VAMP721 and VAMP722 show greater than 97% identity (as shown in Figure 3-3) and these two R-SNAREs appear functionally redundant in vivo (Kwon et al., 2008; Zhang et al., 2011; El Kasmi et al., 2013). Therefore, I focused on VAMP721 in my research. To explore the domain essential for VAMP721-K^+ channel interaction, I exchanged domains between VAMP721 and the non-interacting VAMP723, and generated several chimeric constructs. I found that VAMP721 binding to the channels was dependent on the longin domain of this R-SNARE (Figure 3-4 and Figure 3-5 for mbSUS assay; Figure 4-4 for rBiFC analysis). Further experiments showed that VAMP721 binding was associated with the single amino-acid residue Tyr^{57}, located centrally within the longin domain (Figure 3-8 and 3-9 in SUS assay; Figure 4-5 and 4-6 in rBiFC analysis). Exchange of residues between VAMP721 and VAMP723 generated the $VAMP721^{Y57D}$ and $VAMP723^{D57Y}$ mutant constructs. The former inhibited the interaction while the latter was sufficient to engineer

channel interaction in non-interacting VAMP723. To investigate the role of Tyr^{57} in VAMP721-K^+ channel binding, I also mutated this residue to Asn and Phe. The results showed that $VAMP721^{Y57A}$ and $VAMP721^{Y57F}$ mutations had little effect on channel association in yeast. $VAMP721^{Y57D}$ and $VAMP721^{Y57N}$ suppressed yeast growth (Figure 3-8, Figure 3-9, and Figure 3-10), indicating there was no interaction. These results suggest the negative charge introduced by Asp had little or no importance in VAMP-K^+ channel interaction, but the physical size was important.

Apart from the importance of residue 57 of the VAMPs, these results do not rule out contributions from other residues. Further experiments targeted amino acids around residue 57 and indicated that Gly^{52} to Asn^{56}, Leu^{58} to Glu^{60}, Gly^{62}, Tyr^{65}, Val^{67} and VAl^{68} of VAMP721 were also important for the VAMP-channel binding (Figure 3-11 and Figure 3-12). From structural predictions using Phyre2, I found the residues around Tyr^{57} (from Gly^{52} to Glu^{60}) formed a beta-strand in the longin domain of VAMP721, which is predicted to be exposed and therefore is probably an interaction surface involved in the interaction with K^+ channel. Mutating residue at position 57 of VAMP721 from Tyr to Asp can be predicted to change the structure of this beta-strand structure within the longin domain and therefore affects the channel binding.

In animals, several SNAREs have been identified to interact directly with K^+ channels. Qa-SNARE syntaxin 1A, which mediates in traffic at the neuronal PM, binds with Kv2.1 K^+ channels in vitro and has been shown to subtly modulate channel activity when expressed in *Xenopus* oocytes (Tsuk et al., 2005). Tl-VAMP/VAMP7 is the cognate partner of syntaxin 1A in mammalian cells. It also binds with the Kv2.1 in vitro and enhances channel inactivation when expressed in oocytes (Lvov et al., 2008). However, channel binding by syntaxin 1A is associated with the H3 domain of the Qa-SNARE (Bezprozvanny et al., 2000; Cui et al., 2004; Tsuk et al., 2005). Kv2.1 binding to Tl-VAMP/VAMP7 is lost on assembly of the SNARE core complex in vitro (Tsuk et al., 2008), suggesting that

the channel also binds with the SNARE domain of Tl-VAMP/VAMP7. By contrast, selective binding of VAMP721 with the KAT1 and KC1 K^+ channels in *Arabidopsis* is localized to the longin domain, well separated from the R-SNARE motif residues that assemble with SYP121 in the SNARE core complex (Lipka et al., 2007; Bassham et al., 2008). This finding parallels earlier discovery that SYP121 binds the channels through its N-terminal FxRF motif, again well-removed from the H_c domain (Grefen et al., 2010a; Honsbein et al., 2011).

In animal cells, the residue Tyr^{45} of the neuronal Tl-VAMP/VAMP7 plays a crucial role in maintaining the VAMP in a closed conformation and unavailable for binding in a SNARE core complex with syntaxin 1A and SNAP25 (Vivona et al., 2010). The residue is phosphorylated by the *c-Src* kinase in vitro and in vivo the phosphomimetic Tl-$VAMP^{Y45E}$ mutant activates exocytosis and increases the VAMP binding affinity with the cognate SNAREs (Burgo et al., 2013).

In the plants, VAMP localization has been suggested to be determined by the longin domain of R-SNAREs (Uemura et al., 2005). These findings raised the question whether the residue at position 57 was important for VAMP localization. I performed a set of localization analyses by fusing the VAMPs with a GFP tag at the N terminus, transiently transformed them into *Arabidopsis* seedlings, and imaged the fluorescence signals in root hairs. I found VAMP721 expressed at the PM while VAMP723 was on the ER (as shown in Figure 4-1), which supported the previous reports (Uemura et al., 2004; Uemura et al., 2005). Mutating residue 57 of VAMP721 from Tyr to Asp resulted in a relocation of this R-SNARE to the ER, while the mutant $VAMP723^{D57Y}$ was relocated to the PM. These results supported the role of longin domain in R-SNARE localization and especially the residue at position 57, as important for determining the location of these VAMPs when expressed in vivo. Because previous results showed that $VAMP723^{D57Y}$ interacted with K^+ channel at the PM, while $VAMP721^{Y57D}$ did not, the

simple explanation is that changing the location of the VAMP is important for binding. These findings also rule out an effect of fluorophore (nYFP-cYFP) annealing in determining the location of the VAMP-channel complex.

Again, it is useful to compare these finding to work with animals. TI-VAMP/VAMP7, mentioned above, is known to interact with AP3 through its longin domain. AP3 is one of the of heterotetrameric clathrin adaptors which deliveries proteins to late endosomes/lysosomes. This VAMP7-AP3 interaction is important to deliver the R-SNARE to its target, the late endosomes (Martinez-Arca et al., 2003; Pryor et al., 2008). By analogy, I can imagine that residue at position 57 plays a role in R-SNARE localization, possibly as a potential binding site for some proteins which are essential to transport the VAMPs to their targets. Residue at position 57 was essential also for K^+ channel interaction, suggesting that the K^+ channels might play a role in SNARE related traffic, which I return to later.

7.4 The functional implications of interaction between VAMP721 and K^+ channels

To explore the function of the VAMP721-K^+ channel interaction, I coexpressed the VAMPs and the K^+ channels in oocytes and performed electrophysiology analysis similar to that of previous reports about SYP121 (Honsbein et al., 2009; Grefen et al., 2010a). In oocytes, I found that expressing VAMP721 suppressed the K^+ currents carried by KAT1 or by channels assembled from KC1 and AKT1 subunits (Figures 5-1 and Figure 5-4). For KAT1, the effect was distributed between the ensemble channel conductance, g_{max}, and its voltage sensitivity, as evidenced by a significant negative shift in $V_{1/2}$. VAMP721 action was dose-dependent, saturating near a ratio of 1:4, indicating a stoichiometric relationship between the channel and VAMP. For KC1, the current is commonly

visible only near the most negative voltages that can be recorded in oocytes. So I assumed that g_{max} was not affected, in line with previous analysis of the channel and its association with AKT1 and SYP121 (Duby et al., 2008; Honsbein et al., 2009; Grefen et al., 2010a). I found that these currents were well-fitted with a negative shift in $V_{1/2}$ on VAMP721 co-expression. This regulation of the gate, again, was sensitive to the residue at position 57 of VAMP721.

I also examined the currents in the plant. Single mutants of VAMP721 and VAMP722 are apparently without phenotype but the *vamp721/vamp722* double mutant is embryo lethal, consistent with their (near) complete functional redundancy (Kwon et al., 2008; Zhang et al., 2011). So to investigate the role of VAMP721-K^+ channel interaction in plants, I overexpressed VAMP721, VAMP723, and VAMP721^{Y57D} in wild type Col-0 *Arabidopsis* seedlings and performed the electrophysiology analysis with help of Dr. Yizhou Wang. Recordings from *Arabidopsis* root epidermal cells yielded complementary results to the oocytes. The dominant inward K^+ current in these cells was normally carried by channels assembled from KC1 and AKT1 subunits (Duby et al., 2008; Honsbein et al., 2009; Dreyer et al., 2009). I found that overexpressing VAMP721, but not VAMP723 and VAMP721^{Y57D}, strongly suppressed the inward-rectifying K^+ current, consistent with a substantial shift in $V_{1/2}$ (Figure 5-12). Furthermore, the effects of VAMP721 overexpression were limited to the inward-rectifying K^+ current and were without significant effect on the outward K^+ current which was carried by the GORK channel. So I can discount a general effect of VAMP overexpression on the channel population and activity at the plasma membrane.

How can the effects on the K^+ currents be understood? Changes in current amplitude, and hence in g_{max}, arise as the consequence either of a change in the population of channels at the membrane or of a change in channel gating. However, the mid-point voltage, $V_{1/2}$, for gating is

connected with the biophysical properties of the K^+ channel voltage sensor (Hille et al., 2001; Dreyer et al., 2009; Lefoulon et al., 2014). So it is difficult to understand the effects of VAMP721 (and VAMP723^{D57Y}) as arising from membrane traffic or changes in the population of channels at the PM. For the same reason, the observations cannot be explained as a result of binding and titration of the channels by the R-SNARE so that the channels are no longer functional. Again, simply altering the number of channels available for activation at negative voltages could be expected to affect current amplitude, but not its intrinsic gating characteristics. Instead, the shifts in $V_{1/2}$ are a forceful argument for a direct, physical interaction with the mechanism of voltage sensing by these channels, possibly with the voltage sensor domain itself (Dreyer et al., 2009; Lefoulon et al., 2014).

In previous reports, SYP121 was shown to interact directly with KC1 and KAT1 K^+ channels (Honsbein et al., 2009; Honsbein et al., 2011). This interaction promoted channel gating of the AKT1-KC1 channel assembly in oocytes and in *Arabidopsis* root epidermal cells (Honsbein et al., 2009). Eisenach et al. (2012) found that basal KAT1 currents were reduced by 50% or more in guard cells of the *Arabidopsis syp121* mutant when compared with the currents in the guard cells of wild-type plants, which suggested SYP121 also regulated KAT1. What is important is that in both cases SYP121 interaction with the channels promoted channel activities and enhanced K^+ uptake. The interaction between VAMP721 and the K^+ channels thus appears to have the opposite effect: gating of AKT1-KC1 and KAT1 in each case was suppressed by VAMP721.

This functional juxtaposition between VAMP721 and SYP121 in their actions on K^+ channel gating raises a question whether the control of K^+ channel gating might be woven together with the roles of VAMP721, VAMP722 and SYP121 in vesicle fusion. At least part of an answer to this question comes from my trafficking studies outlined in Chapter 6. Previous reports indicated that SYP121$^{\Delta C}$, which was SYP121 without

transmembrane domain, blocked secretory traffic to the PM, while native SYP121 did not (Geelen et al., 2002; Sutter et al., 2006; Tyrrell et al., 2007). This traffic block was understood to arise because the soluble SYP121$^{\Delta C}$ competed with the native Qa-SNARE for binding partners. My results with the VAMPs were different to that of SYP121, even without considering the channels. I found that overexpressing native VAMP711, VAMP721, and VAMP723 blocked the secretion of secYFP (Figure 6-5). VAMP721$^{\Delta C}$ and VAMP723$^{\Delta C}$, corresponding to the soluble domains of these VAMPs, were also able to block the secretion, but the relative secYFP retention (YFP/GFP ratio) was not as high as was observed with the native VAMPs (Figure 6-1 and 6-2).

In interpreting these findings, it is necessary to consider two different mechanisms. VAMPs are normally located on the vesicle membrane while Qa-SNAREs are found at the target membranes. The traffic block of soluble VAMPs was thought to occur because overexpression of these non-functional R-SNAREs blocked traffic via competing with native VAMPs like that of SYP121$^{\Delta C}$ (As explained in Figure 6-6 B). For the full-length R-SNAREs, I considered principally three main explanations for the traffic block, self-interaction, titration/imbalance with the SNARE partners, and effect on the expression of other SNAREs.

The first possibility is that overexpression of VAMPs leads to formation of R-SNARE homodimers, which block traffic. In animal cells and yeast, during membrane fusion, many SNAREs appear to undergo self-interaction, which affects their binding with other SNAREs and regulates the speed of SNARE complex formation (Pennuto et al., 2002; Roy et al., 2004). The existence of SNARE homodimers has been shown to depend on their transmembrane domain (Laage and Langosch, 1997; Roy et al., 2004; Laage et al., 2000; Zhang et al., 2006b; Hofmann et al., 2006). As shown in Figure 6-6 C, overexpression of VAMPs may form homodimers on the vesicle membrane by transmembrane domain-dependent self-interaction, which then might affect their binding

with Q-SNAREs and block secretion.

Another possibility is that the overexpression of VAMPs consumes their corresponding Q-SNAREs and disrupts the population balance between R-SNAREs and Q-SNAREs, which finally blocks, or at least slows, secYFP secretion. Previous report have indicated that the population balance of SNAREs, Tlg2 and Snc2, is important for vesicle traffic in yeast (Shanks et al., 2012). Again, overexpression might lead to more R-SNARE proteins present in vesicles. During membrane fusion of the vesicle, these additional R-SNAREs then tie up more Q-SNAREs on target membrane, which thereby disrupts the SNARE population balance. The exist of more VAMPs may also lead to binding with one or two SNARE partners and formation of non-functional SNARE complexes, which also affects the SNARE population balance.

The third possibility is that the overexpressing the VAMPs may affect the expression of other SNAREs, which finally blocks traffic. The SM protein Vps45p in yeast, for example, regulates the expression level of its SNARE binding partners, the syntaxin Tlg2p and the v-SNARE Snc2p (Shanks et al., 2012). In the plants, the excess of VAMP721 may affect the cellular levels of SYP121 or other SNAREs involved in SNARE complex forming, which blocks the secYFP secretion.

VAMP711 is expressed on the vacuolar membrane, while VAMP723 is expressed on the endoplasmic reticulum (Uemura et al., 2004). Why does the overexpression of VAMP711 and VAMP723 also block the secretion of secYFP? If overexpression of different localized VAMPs can block secretion, there must be a common factor that associates with all (or at least many) VAMP-related processes. Then the excess of any of the VAMPs leads to an imbalance of the factor needed for traffic. NSF and α-SNAP are obvious potential members of these common factors. NSF is an AAA ATPase, broadly required for membrane fusion. NSF functions as a SNARE chaperone which binds to SNARE complexes through α-SNAP and utilizes the energy of ATP hydrolysis to

disassemble the SNARE complex thus facilitating SNARE recycling (Whiteheart et al., 2001). There are a lot of SNARE proteins in an eukaryote, which form different SNARE complexes (Jahn et al., 2006; as shown in Table 1-1 and Table 1-2 for plant cells). But there are only a few SNAP and very few NSF species present in plants (Sanderfoot et al., 2001; Bitto et al., 2008; Vivona et al., 2013). A recent report has investigated the structures of NSF, and the NSF/SNAP/SNARE (20S) supercomplex (Zhao et al., 2015). It suggests that one NSF/SNAP species can disassemble most, if not all SNARE complexes using shape and characteristic electrostatic pattern recognition of SNARE complexes by SNAPs. As mentioned above, the overexpression of any VAMP leads to more non-functional or functional SNARE complexes forming. In the former, the VAMP binds with one or two SNARE partners, while in the latter it forms a fusogenic SNARE complex with corresponding SNARE partners. The excess of SNARE complexes formed might be seen to consume NSF and α-SNAP from the same pool that could have been used for SNARE related secretion, in which case SNARE recycling could be affected. If so, then overexpression of any VAMP would then affect many trafficking pathways.

Another possible explanation is that SNAREs can interact with each other even they have different subcellular localizations. Fujiwara et al. (2014) have investigated the Qa-SNARE-interacting proteins by immunoprecipitation and mass spectrometric. Their results show that SYP22, one of Qa-SNARE located on the tonoplasts, is immunoprecipitated with the PM localized VAMP721, suggesting SYP22 interacts with VAMP721 and generate a SNARE complex with the R-SNARE. Given the possible cross-interaction between different localized SNAREs, the excess of one VAMP like VAMP721 and VAMP723 may bind with other unrelated SNAREs and affect the normal secretion.

Most important, when coexpressing KC1 with VAMP721, but not

VAMP723 or VAMP721^{Y57D}, the block of secYFP secretion was partially rescued (See Figure 6-4), indicating a role for the VAMP-K^+ channel interaction in vesicle traffic. Again, in mammalian cells, the Kv2.1 channel directly interacts with VAMP2 (Lvov et al., 2008). However, the role of this R-SNARE in Kv2.1 related secretion is still unknown. As shown in Figure 6-7, traffic rescue in the plant might arise because the interaction between KC1 and VAMP721 releases the R-SNARE from a homodimer or it may titrate out the overexpressed VAMP721 and rebalance the ratio between the R-SNARE and its cognate Q-SNARE. Of course, these explanations raised more questions. For example, we will want to know what is the role of SYP121 and K^+ channel interaction in plant vesicle traffic? What is the relationship between SYP121 and VAMP721 in binding the K^+ channels? And is there a specific order to binding?

7.5 A model of VAMP721-K^+ channel interaction in plant cells

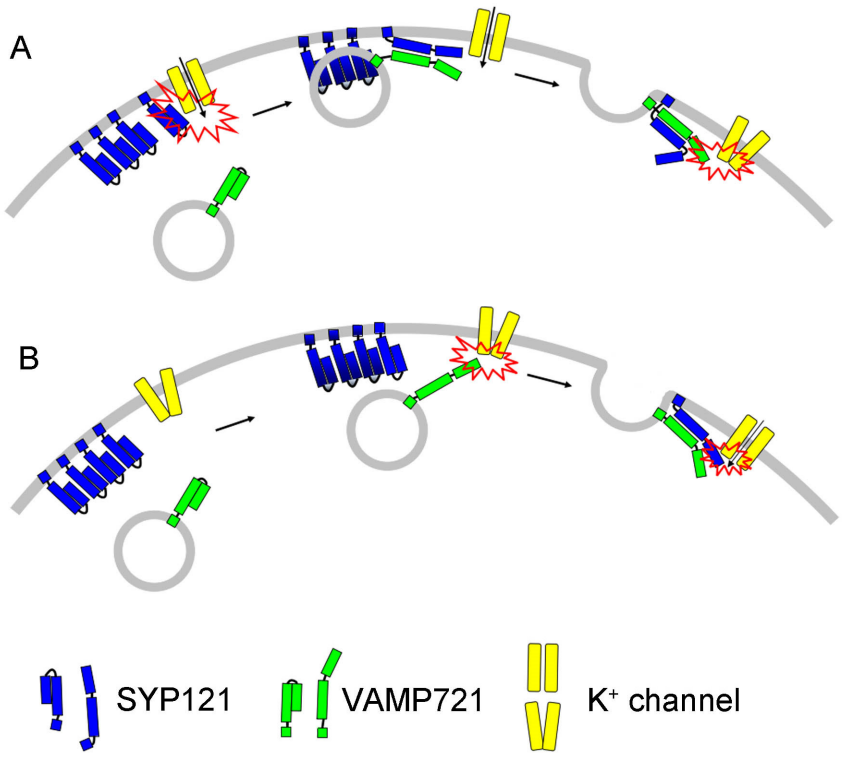

Figure 7-1. Two potential models of vesicle membrane fusion associated with K^+ channel binding and control by SYP121 and its

cognate R-SNAREs VAMP721

For clarity, only the SNAREs SYP121 and VAMP721 are shown. The Q-SNARE SYP121 form a 'icebergs' at the PM (Sieber et al., 2007; Murray et al., 2009; Honsbein et al., 2011).

A. SYP121 interacts with K^+ channel and promotes its channel gating. The K^+ channel recruits this Q-SNARE from the 'icebergs'. During membrane fusion, R-SNARE and Q-SNARE form the SNARE complex and transfer the K^+ channel from One SNARE to the other. Then K^+ channel interacts with VAMP721, which inhibits the channel gating and close the channel.

B. VAMP721 interacts with K^+ channel and inhibits the channel gating. During membrane fusion, R-SNARE and Q-SNARE form the SNARE complex and transfer the K^+ channel from One SNARE to the other. The interaction between SYP121 and K^+ channel promote the channel gating and open the channel.

How does this new discovery of an interaction between K^+ channel and VAMP721 fit into the current model of SNARE-K^+ channel system in plants? So far, previous reports suggested that SYP121 interaction with the K^+ channels could be understood as a mechanism for their mutual control, coordinating the rates of solute uptake and of surface area expansion as the cell grows. This hypothesis satisfies a number of experimental observations, including the uncoupling of solute uptake from cell expansion and runaway solute accumulation in cells expressing a soluble fragment of SYP121 (Geelen et al., 2002; Sokolovski et al., 2008; Honsbein et al., 2009). The findings about the VAMPs in this thesis anticipate a sequence in which channel binding, alternately with one SNARE and then the other, periodically activates and inactivates the channel to regulate K^+ flux while engaging the SNAREs for assembly. Two hypothetical sequences were illustrated in Figure 7-1, which bring together our understanding of the channels as focal points for vesicle traffic (Sutter et al., 2006; Sutter et al., 2007), and of SYP121 recruitment by the K^+ channels - a variation of the so-called 'icebreaker' model (Sieber et al., 2007; Murray et al., 2009; Honsbein et al., 2011) - leading up to vesicle fusion.

1. The first possibility is that VAMP721 and SYP121 assemble the

SNARE complex, and this process includes transfer of the K^+ channel from the Q-SNARE to the R-SNARE during membrane fusion. SYP121 binds with K^+ channel and promotes its gating (Honsbein et al., 2009; Honsbein et al., 2011), while interaction between VAMP721 and K^+ channel inhibits the channel gating. So in this case, the K^+ channel transfer between SNAREs closes the channel in conjunction with the SNARE related membrane fusion.

2. The second hypothetical sequence proposes that when the vesicle is brought close to the PM, VAMP721 interacts with K^+ channel and inhibits its opening. During membrane fusion, the K^+ channel is passed from VAMP721 to SYP121. This process on one hand recruits SYP121 from the Qa-SNARE 'icebergs'; on the other hand, it promotes K^+ influx and activates both SNAREs for their assembly in the core complex to drive the final stages of membrane fusion.

Considering the other proteins known to be involved in membrane fusion, the second hypothesis seems more likely. As introduced in Chapter 1, the exocyst is a complex of proteins mediating the tethering between secretory vesicles and the target membrane (Zarsky et al., 2013). It is easy to imagine that vesicle approach and tethering by the exocyst complex leads to docking when VAMP721 binds with the K^+ channel to bring the vesicle within 8-10 nm of the plasma membrane surface. Once docked via the VAMP longing domain, the K^+ channel-VAMP complex recruits SYP121 leading to an exchange of binding. SEC11 is also involved in membrane fusion. Karnik et al. (2013b) have reported that SEC11 interact with N-terminus of SYP121, which stabilizes the closed state of the Qa-SNARE. The binding between SYP121 and K^+ channel is dependent on the same site (Grefen et al., 2010a). So in the second hypothesis, when K^+ channel is passed from VAMP721 to SYP121, the same process dislodges SEC11 and allows SYP121 change to the open state. Together with these events, the K^+ channel is activated and the SNAREs are brought together for their

assembly in the core complex to drive the final stages of membrane fusion. Clearly these are just conjecture for now. More work need to be done in the future, for example to identify the R-SNARE binding sites on the K^+ channel proteins. This work and investigating the sequence of gating changes with VAMP721, SYP121, and channel protein binding will be important to place the SNARE - channel interactions in a role with channel regulation and cell expansion.

Appendix I. Primers which were designed to construct the clones used in this study

No.	Primer sequence 5'-3'
1	AAGTTAACCACCTGGTTACCACTAAACCAG
2	AAATACGTACCAAAGTTGAGCGTTTATTCTGAG
3	AGTTTAAACATGTACCCATACGATGTTCCTGACTATGC
4	TGTTAACCCGCCACCACCAACCACTTTGT
5	attB1-TAATGGCGATTCTGTACGCC
6	attB2-TTAAATGCAAGATGGTAGAGTAGG
7	attB1-TAATGTCGATATTATACGCGTTGGT
8	attB2-TTAAACGCAAGAGGGTAGAGTTG
9	attB1-TAATGGCGATCATATTTGCGTT
10	attB2-TTACTTGAAACAAGAAGGAAGACTTG
11	attB1-TAATGGCGATTGTCTATGCTGTTG
12	attB2-TTAAGATCTGCATGATGGTAAAGTGA
13	attB1-TAATGGCGCAACAATCGTTGAT
14	attB2-TTAACACTTAAACCCATGGCAAAC
15	attB1-TAATGGCGCAACAATCGTTGA
16	attB2-TTATTTACCGCAGTTGAATCC
17	attB1-TAATGGCGCAACAATCGTTGT
18	attB2-TTATTTACCGCAGTTGAATCCC
19	attB1-TAATGGGTCAAGAATCGTTTATCTATAG
20	attB2-TCAATCCGTGCAATTAAATCC
21	attB1-TAATGGATCGCAGCGTCGTC
22	attB2-TTAGGTACACTTGAATCCCCCG
23	attB1-TAATGGGACAACAATCGTTGATCTAC
24	attB2-TTAAGTACACTTGAAGCCATGGC
25	attB1-TAATGAGTCAAAAGGGTTTGATATATAGC
26	attB2-TCATGATGAGCATTTGAAACCTC
27	attB1-TAATGGTGGTGGATAGGAATGGC
28	attB2-TTATGATATCTTCTTGACCTTTGAACG
29	attB3-TAATGGCGCAACAATCGTTGAT
30	attB3-TAATGGCGCAACAATCGTTGT
31	attB1-TAATGATTAATCGTATTAAGGGTGAAATG
32	attB2-TTACCTATCGGCATTAGGATCAT
33	attB1-TAATGGAGATTAGCAAGCTTGC
34	attB2-TTAATCAGGATGATCCATGCAAT
35	attB1-TAATGGAGATTAGCAACCTTGCT

36	attB2-TTAATCCATGCAATACTGCAT
37	attB1-TAATGTCGATCTCTTGGACTCGA
38	attB2-GATTTGATGAAAAATACAAATGATCACC
39	attB1-TAATGTCTACGACGACTACTGAGGC
40	attB2-GGAAAATATATAAATGATCGTTTTCTC
41	attB4-GATTTGATGAAAAATACAAATGATC
42	attB4-GGAAAATATATAAATGATCGTTTTCTCG
43	ATCAGGATGATCCATGCAATACTGCAT
44	GACAATGAGTTTTATCTTCATGTTCTG
45	CACTATGAGTTTTATCTTCATGTTCTG
46	TGCATGGATCATCCTGATGAGATTAGC
47	AAGATAAAACTCATTGTCCTTGCAATT
48	AAGATAAAACTCATAGTGCTCGCCATC
49	AAGCTTCCGTCCTCGAACAACAAGTTT
50	AATCTTCCTTCTTCGAACAACAAGTTC
51	GTTCGAGGACGGAAGCTTCTGGAGGCA
52	GTTCGAAGAAGGAAGATTCTCAAGGTA
53	CCCATGTCCTTCTTGGAACGCGTGAAG
54	CCTATGGCTTTTTTGGAAAGAGTAAAA
55	TTCCAAGAAGGACATGGGAATTTGCCT
56	TTCCAAAAAAGCCATAGGAATCTCCCT
57	TGCGATGGCCATACCTTCAATGCCCTTGTCGAAGATG GATT
58	ACAAGGGCATTGAAGGTATGGCCATCGCAGTTGTAG GTGA
59	CAAGGTCATTGAAGGTATGGCCATCGCAGTTGTAGGT G
60	CTGCGATGGCCATACCTTCAATGACCTTGTCGAAGAT G
61	CTGCGATGGCCATACCTTCAATTTCCTTGTCGAAGAT
62	ACAAGGAAATTGAAGGTATGGCCATCGCAGTTGTAG
63	TGTCGAAGCTGGATTTACGTATTGTGTTGTTG
64	CAACACAATACGTAAATCCAGCTTCGACAAGGTA
65	GTCGAAAATGGATTTACGTATTGTGTTGTTGCGGT
66	ACAATACGTAAATCCATTTTCGACAAGGTAATTG
67	ATTCTGCCGGCAGGGCAATTCCCATGTCCTTTTT
68	GGGAATTGCCCTGCCGGCAGAATCAACCGCAACAAC
69	TTCTGCCGGCAGGGAAATTCCCATGTCC
70	GAATTTCCCTGCCGGCAGAATCAACCG
71	CCCATGGCCTTTCTAGAAAGAGTAAAAGAAGATTT
72	CTCTTTCTAGAAAGGCCATGGGAATTTGCCTCCCA

73	CAAGTTCACTTATAACGCGGATGGCCATACC
74	TGGCCATCCGCGTTATAAGTGAACTTGTTGTTC
75	CAACTGCGCCGGCCATACCTTC
76	GGTATGGCCGGCGCAGTTGTAGGT
77	CTGCGATGCGCATACCTTCAATGCC
78	AAGGTATGCGCATCGCAGTTGTAGG
79	GATGGCGCCACCTTCAATGCCCTTGTC
80	GAAGGTGGCGCCATCGCAGTTGTAG
81	CGATGGGCATGCTTTCAATGCCCTT
82	CATTGAAAGCATGCCCATCGCAGTTG
83	CATACCGCCAATGCATTAGTCGAAGATGGA
84	TTCGACTAATGCATTGGCGGTATGGCCATC
85	TACCTTCGCTGCACTAGTCGAAGATGGAT
86	TTCGACTAGTGCAGCGAAGGTATGGCC
87	CAATGCCGCGGTCGAAGATGGAT
88	TTCGACCGCGGCATTGAAGGT
89	CAATGCATTAGCCGAAGATGGATTCACC
90	TCTTCGGCTAATGCATTGAAGGTATGG
91	CAATGCACTAGTCGCTGATGGATTCACC
92	TCCATCAGCGACTAGTGCATTGAAGGTA
93	GAAGATGCATTCACCTATTGT
94	GGTGAATGCATCTTCGACAAG
95	CAATGCACTAGTCGAAGATGGAGCCACCTATTGTGT
96	TAGGTGGCTCCATCTTCGACTAGTGCATTGAAGGTA
97	GATTCGCCTATTGTGTTGTTGCGGTCGACTCTGCTGGGAGG
98	GCAGAGTCGACCGCAACAACACAATAGGCGAATCCATCTTCG
99	TTCACCGCTTGTGTTGTTGCGGTCGACTCTGCTGGGAGG
100	AGCAGAGTCGACCGCAACAACACAAGCGGTGAATCCATC
101	TGGATTTACGTATGCTGTTGTTGCGGT
102	ACAACAGCATACGTAAATCCATCTTCGAC
103	ATTGTGCTGTTGCGGTCGACTCTGCTGGGAGG
104	AGCAGAGTCGACCGCAACAGCACAATAGGTGA
105	TTGTGTTGCCGCGGTTGATTCTGC
106	AATCAACCGCGGCAACACAATAGGTG
107	CGATGGCCATACGTTCAACTACCTCGTCGAAAATG
108	CGAGGTAGTTGAACGTATGGCCATCGCAGTTGTAGG
109	CCGGACTATGCAGCGCAACAATCG

110	CGATTGTTGCGCTGCATAGTCCGG
111	attB1-TAATGTACCCTTATGATGTTCCTG

In this table, attB1 stands for GGGGACAAGTTTGTACAAAAAAGCA GGCT; attB2 stands for GGGGACCACTTTGTACAAGAAAG CTGGGT; attB3 stands for GGGGACAACTTTGTATAATAAAGTTG; attB4 stands for GGGGACAACTTTGTATAGAAAAGTTGGGT.

List of References

Allan, B.B., Moyer, B.D., and Balch, W.E. (2000). Rab1 recruitment of p115 into a cis-SNARE complex: programming budding COPII vesicles for fusion. Science. **289**: 444-448.

Apel, K., and Hirt, H. (2004). Reactive oxygen species: metabolism, oxidative stress, and signal transduction. Annual Review of Plant Biology. **55**: 373-399.

Assaad, F.F., Huet, Y., Mayer, U., and Jürgens, G. (2001). The cytokinesis gene KEULE encodes a Sec1 protein that binds the syntaxin KNOLLE. Journal of Cell Biology. **152**: 531-543.

Baizabal-Aguirre, V.M., Clemens, S., Uozumi, N. and Schroeder, J.I. (1999). Suppression of inward-rectifying K^+ channels KAT1 and AKT2 by dominant negative point mutations in the KAT1 a-subunit. Journal of Membrane Biology. **167**: 119-125.

Balch, W., Dunphy, W., Braell, W., and Rothman, J. (1984). Reconstitution of the transport of protein between successive compartments of the Golgi measured by the coupled incorporation of N-acetylglucosamine. Cell. **39**: 405-416.

Barnard, R.J., Morgan, A., and Burgoyne, R.D. (1997). Stimulation of NSF ATPase activity by alpha-SNAP is required for SNARE complex disassembly and exocytosis. Journal of Cell Biology. **139**: 875-883.

Bassham, D.C., Sanderfoot, A.A., Kovaleva, V., Zheng, H., and Raikhel, N.V. (2000). AtVPS45 complex formation at the trans-Golgi network. Molecular Biology of the Cell. **11**: 2251-2265.

Bassham, D.C., Brandizzi, F., Otegui, M.S., and Sanderfoot, A.A. (2008a). The Secretory System of Arabidopsis. The Arabidopsis Book. **6**:e0116.

Bassham, D.C. and Blatt, M.R. (2008b). SNAREs-cogs or coordinators in signalling and development? Plant Physiology. **147**: 1504-1515.

Becker, D., Geiger, D., Dunkel, M., Roller, A., Bertl, A., Latz, A., Carpaneto, A., Dietrich, P., Roelfsema, M.R., Voelker, C., Schmidt, D., Mueller-Roeber, B., Czempinski, K., and Hedrich, R. (2004). AtTPK4, an Arabidopsis tandem-pore K^+ channel, poised to control the pollen membrane voltage in a pH- and Ca^{2+}-dependent manner. Proceedings of

the National Academy of Sciences of United States of America. **101**: 15621-15626.

Bennett, M.K., Calakos, N., and Scheller, R.H. (1992). Syntaxin: a synaptic
protein implicated in docking of synaptic vesicles at presynaptic active zones. Science. **257**: 255-259.

Bennett-Lovsey, R.M., Herbert, A.D., Sternberg, M.J.E., and Kelley, L.A. (2008). Exploring the extremes of sequence/structure space with ensemble fold recognition in the program Phyre. Proteins. **70**: 611-625.

Berkowitz, G., Zhang, X., Mercie, R., Leng, Q., and Lawton, M. (2000). Co-expression of calcium-dependent protein kinase with the inward rectified guard cell K^+ channel KAT1 alters current parameters in *Xenopus laevis* oocytes. Plant cell and physiology. 41: 785-790.

Besserer, A., Burnotte, E., Bienert, G.P., Chevalier, A.S., Errachid, A., Grefen, C., Blatt, M.R., and Chaumont, F. (2012). Selective Regulation of Maize Plasma Membrane Aquaporin Trafficking and Activity by the SNARE SYP121. Plant Cell. **24**: 3463-3481.

Betz, A., Okamoto, M., Benseler, F., and Brose, N. (1997). Direct interaction of the rat unc-13 homologue Munc13-1 with the N terminus of syntaxin. Journal of Biological Chemistry. **272**: 2520-2526.

Bezprozvanny, I., Zhong, P.Y., Scheller, R.H., and Tsien, R.W. (2000). Molecular determinants of the functional interaction between syntaxin and N-type Ca^{2+} channel gating. Proceedings Of The National Academy Of Sciences Of The United States Of America. **97**: 13943-13948.

Bitto, E., Bingman, C.A., Kondrashov, D.A., McCoy, J.G., Bannen, R.M., Wesenberg, G.E., and Phillips, G.N. (2008). Structure and dynamics of gamma-SNAP: insight into flexibility of proteins from the SNAP family. Proteins. **70**: 93-104.

Blatt, M.R. and Slayman, C.L. (1983). KCl leakage from microelectrodes and its impact on the membrane parameters of a nonexcitable cell. The Journal of Membrane Biology. **72**: 223-234.

Blatt, M.R. and Teiel, G. (1993). Hormonal control of ion channel gating. Annual Review of Plant Physiology and Plant Molecular Biology. **44**: 543-567.

Blatt, M.R. and Gradmann, D. (1997). K^+-sensitive gating of the K^+ outward rectifier in Vicia guard cells. Journal of Membrane Biology. **158**:

241-256.

Blatt, M.R. (1999). Reassessing roles for Ca^{2+} in guard cell signalling. Journal of Experimental Botany. **50**: 989-999.

Blatt, M.R. (2000). Cellular signaling and volume control in stomatal movements in plants. Annual Review of Cell and Developmental Biology. **16**: 221-241.

Blatt, M.R. (2004). Membrane Transport in Plants. In Membrane Transport in Plants, M.R. Blatt, ed (Oxford: Blackwell), pp. 1-256.

Blatt, M.R., and Grefen, C. (2014). Applications of Fluorescent Marker Proteins in Plant Cell Biology. In Arabidopsis Protocols, J.J. Sanchez-Serrano and J. Salinas, eds, pp. 487-507.

Boevink, P., Santa Cruz, S., Hawes, C., Harris, N., and Oparka, K.J. (1996). Virus-mediated delivery of the green fluorescent protein to the endoplasmic reticulum of plant cells. Plant Journal. **10**: 935-941.

Boevink, P., Martin, B., Oparka, K., Cruz, S.S., and Hawes, C. (1999). Transport of virally expressed green fluorescent protein through the secretory pathway in tobacco leaves is inhibited by cold shock and brefeldin A. Planta. **208**: 392-400.

Bowen, M.E., Weninger, K., Brunger, A.T., and Chu, S. (2004). Single molecule observation of liposome-bilayer fusion thermally induced by soluble N-ethyl maleimide sensitive-factor attachment protein receptors (SNAREs). Biophysical Journal. **87**: 3569-3584.

Batoko, H., Zheng, H.Q., Hawes, C., and Moore, I. (2000). A Rab1 GTPase is required for transport between the endoplasmic reticulum and Golgi apparatus and for normal Golgi movement in plants. Plant Cell. **12**: 2201-2217.

Brownlee, C., Goddard, H., Hetherington, A.M., and Peake, L.A. (1999). Specificity and integration of responses: Ca as a signal in polarity and osmotic regulation. Journal of Experimental Botany. **50**: 1001-1011.

Bruggemann, L., Dietrich, P., Becker, D., Dreyer, I., Palme, K., & Hedrich, R. (1999). Channel-mediated high-affinity K^+ uptake into guard cells from Arabidopsis. Proceedings of the National Academy of Sciences of the United States of America. **96**: 3298-3302.

Brunger, A.T. (2005). Structure and function of SNARE and SNARE-interacting proteins. Quarterly Reviews of Biophysics. **38**: 1-47.

Buckingham, S.D. (2009). Ten tips for better oocyte recordings. Lab

Times: Methods. 1-2009.

Burgo, A., Casano, A.M., Kuster, A., Arold, S.T., Wang, G., Nola, S., Verraes, A., Dingli, F., Loew, D., and Galli, T. (2013). Increased activity of the Vesicular Soluble N-Ethylmaleimide-sensitive Factor Attachment Protein Receptor TI-VAMP/VAMP7 by Tyrosine Phosphorylation in the Longin Domain. Journal of Biological Chemistry. **288**: 11960-11972.

Bushman, W., Thompson, J. F., Vargas, L., and Landy, A. (1985). Control of Directionality in Lambda Site Specific Recombination. Science. **230**: 906-911.

Catterall, W.A. (1999). Interactions of presynaptic Ca^{2+} channels and snare proteins in neurotransmitter release. Annals of the New York Academy of Sciences. **868**: 144-159.

Cameron, A.J., Escribano, C., Saurin, A.T., Kostelecky, B., and Parker, P.J. (2009). PKC maturation is promoted by nucleotide pocket occupation independently of intrinsic kinase activity. Nature Structural and Molecular Biology. **16**: 624-630.

Campanoni, P., Sutter, J.U., Davis, C.S., Littlejohn, G.R., and Blatt, M.R. (2007). A generalized method for transfecting root epidermis uncovers endosomal dynamics in Arabidopsis root hairs. Plant Journal. **51**: 322-330.

Cano-Delgado, A., Yin, Y., Yu, C., Vafeados, D., Mora-Garcia, S., Cheng, J.C., Nam, K.H., Li, J., and Chory, J. (2004). BRL1 and BRL3 are novel brassinosteroid receptors that function in vascular differentiation in Arabidopsis. Development. **131**: 5341-5351.

Carr, C.M., Grote, E., Munson, M., Hughson, F.M., and Novick, P.J. (1999). Sec1p binds to SNARE complexes and concentrates at sites of secretion. Journal of Cell Biology. **146**: 333-344.

Carroll, K.S., Hanna, J., Simon, I., Krise, J., Barbero, P., and Pfeffer, S.R. (2003). Role of Rab9 GTPase in facilitating receptor recruitment by TIP47. Science. **292**: 1373-1376.

Chatre, L., Brandizzi, F., Hocquellet, A., Hawes, C., and Moreau, P. (2005). Sec22 and Memb11 are v-SNAREs of the anterograde endoplasmic reticulum-Golgi pathway in tobacco leaf epidermal cells. Plant Physiology. **139**: 1244-1254.

Chapman, S., Faulkner, C., Kaiserli, E., Garcia-Mata, C., Savenkov, E.I., Roberts, A.G., Oparka, K.J., and Christie, J.M. (2008). The photoreversible fluorescent protein iLOV outperforms GFP as a reporter

of plant virus infection. Proceedings Of The National Academy Of Sciences Of The United States Of America. **105**: 20038-20043.

Chen, Z.H., Grefen, C., Donald, N., Hills, A., and Blatt, M.R. (2011). A bicistronic, Ubiquitin-10 promoter-based vector cassette for transient transformation and functional analysis of membrane transport demonstrates the utility of quantitative voltage clamp studies on intact Arabidopsis root epidermis. Plant Cell And Environment. **34**: 554-564.

Cheong, Y.H., Pandey, G.K., Grant, J.J., Batistic, O., Li, L., Kim, B.G., Lee, S.C., Kudla, J., and Luan, S. (2007). Two calcineurin B-like calcium sensors, interacting with protein kinase CIPK23, regulate leaf transpiration and root potassium uptake in Arabidopsis. Plant Journal. **52**: 223-239.

Cheung, A.Y., Chen, C.Y., Glaven, R.H., de Graaf, B.H., Vidali, L., Hepler, P.K., and Wu, H.M. (2000). Rab2 GTPase regulates vesicle trafficking between the endoplasmic reticulum and the Golgi bodies and is important to pollen tube growth. Plant Cell. **14**:945-962.

Chinchilla, D., Bauer, Z., Regenass, M., Boller, T., and Felix, G. (2006). The Arabidopsis receptor kinase FLS2 binds flg22 and determines the specificity of flagellin perception. Plant Cell. **18**: 465-476.

Clouse, S.D. and Sasse, J.M. (1998). BRASSINOSTEROIDS: Essential Regulators of Plant Growth and Development. Annual Review of Plant Physiology and Plant Molecular Biology. **49**: 427-451.

Cole, N.B., Smith, C.L., Sciaky, N., Terasaki, M., Edidin, M., and Lippincott-Schwartz, J. (1996). Diffusional mobility of Golgi proteins in membranes of living cells. Science. **273**: 797-801.

Cole, C., Barber, J.D., and Barton, G.J. (2008). The Jpred 3 secondary structure prediction server. Nucleic Acids Research. **36**: W197-W201.

Collins, N.C., Thordal-Christensen, H., Lipka, V., Bau, S., Kombrink, E., Qiu, J.L., Hückelhoven, R., Stein, M., Freialdenhoven, A., Somerville, S.C., and Schulze-Lefert, P. (2003). SNARE-protein mediated disease resistance at the plant cell wall. Nature. **425**: 973-977.

Cosgrove, D.J. (1997). Assembly and enlargement of the primary cell wall in plants. Annual review of cell and developmental biology. **13**: 171-201.

Cuff, J.A. and Barton, G.J. (1999). Application of enhanced multiple

sequence alignment profiles to improve protein secondary structure prediction. Proteins. **40**: 502-511.

Cui, N.G., Kang, Y.H., He, Y., Leung, Y.M., Xie, H.L., Pasyk, E.A., Gao, X.D., Sheu, L., Hansen, J.B., Wahl, P., Tsushima, R.G., and Gaisano, H.Y. (2004). H3 domain of syntaxin 1A inhibits K-ATP channels by its actions on the sulfonylurea receptor 1 nucleotide-binding folds-1 and -2. Journal of Biological Chemistry. **279**: 53259-53265.

Dai, X.Q., Manning Fox, J.E., Chikvashvili, D., Casimir, M., Plummer, G., Hajmrle, C., Spigelman, A.F., Kin, T., Singer-Lahat, D., Kang, Y., Shapiro, A.M., Gaisano, H.Y., Lotan, I., and Macdonald, P.E. (2012). The voltage-dependent potassium channel subunit Kv2.1 regulates insulin secretion from rodent and human islets independently of its electrical function. Diabetologia. 55: 1709-1720.

D'Angelo, C., Weinl, S., Batistic, O., Pandey, G.K., Cheong, Y.H., Schültke, S., Albrecht, V., Ehlert, B., Schulz, B., Harter, K., Luan, S., Bock, R., and Kudla, J. (2006). Alternative complex formation of the Ca-regulated protein kinase CIPK1 controls abscisic acid-dependent and independent stress responses in Arabidopsis. Plant Journal. **48**: 857-872.

De Benedictis, M., Bleve, G., Faraco, M., Stigliano, E., Grieco, F., Piro, G., Dalessandro, G., Di Sansebastiano, G.P. (2013). AtSYP51/52 functions diverge in the post-Golgi traffic and differently affect vacuolar sorting. Molecular Plant. **6**: 916-930.

Demidchik, V., Bowen, H.C., Maathuis, F.J., Shabala, S.N., Tester, M.A., White, P.J., and Davies, J.M. (2002). Arabidopsis thaliana root non-selective cation channels mediate calcium uptake and are involved in growth. Plant Journal. **32:** 799-808.

Demidchik, V., Shabala, S.N., Coutts, K.B., Tester, M.A., and Davies, J.M. (2003). Free oxygen radicals regulate plasma membrane Ca^{2+}- and K^{+}-permeable channels in plant root cells. Journal of Cell Science. **116**: 81-88.

Demidchik, V., Cuin, T.A., Svistunenko, D., Smith, S.J., Miller, A.J., Shabala, S., Sokolik, A., and Yurin, V. (2010). Arabidopsis root K^{+}-efflux conductance activated by hydroxyl radicals: single-channel properties, genetic basis and involvement in stress-induced cell death. Journal of Cell Science. **123**: 1468-1479.

Delhaize, E., Ryan, P.R., and Randall, P.J. (1993). Aluminum tolerance in wheat (*Triticum aestivum* L.). II. Aluminum-stimulated excretion of malic acid from root apices. Plant Physiology. **103**: 695-702.

Delhaize, E., Gruber, B.D., Ryan, and P.R. (2007). The roles of organic anion permeases in aluminium resistance and mineral nutrition. FEBS Letter. **581**: 2255-2262.

Dietrich, L.E., Boeddinghaus, C., LaGrassa, T.J., and Ungermann, C. (2003). Control of eukaryotic membrane fusion by N-terminal domains of SNARE proteins. Biochimica et Biophysica Acta. **1641**: 111-119.

Doolittle, R.F. (1995). The origins and evolution of eukaryotic proteins. Philosophical Transactions of the Royal Society B: Biological. **349**: 235-240.

Drakakaki, G., van de Ven, W., Pan, S., Miao, Y., Wang, J., Keinath, N.F., Weatherly, B., Jiang, L., Schumacher, K., Hicks, G., and Raikhel, N. (2012). Isolation and proteomic analysis of the SYP61 compartment reveal its role in exocytic trafficking in Arabidopsis. Cell Research. **22**: 413-424.

Dreyer, I., Antunes, S., Hoshi, T., Müller-Röber, B., Palme, K., Pongs, O., Reintanz, B., and Hedrich, R. (1997). Plant K^+ channel alpha-subunits assemble indiscriminately. Biophysical Journal. **72**: 2143-2150.

Dreyer, I., and Blatt, M.R. (2009). What makes a gate? The ins and outs of Kv-like K^+ channels in plants. Trends In Plant Science. **14**: 383-390.

Dreyer, I., Michard, E., Lacombe, B., and Thibaud, J.B. (2001). A plant Shaker-like K^+ channel switches between two distinct gating modes resulting in either inward-rectifying or "leak" current. FEBS Letter. **505**: 233-239.

Dreyer, I., Porée, F., Schneider, A., Mittelstädt, J., Bertl, A., Sentenac, H., Thibaud, J.B., and Mueller-Roeber, B. (2004). Assembly of plant Shaker-like K-out channels requires two distinct sites of the channel alpha-subunit. Biophysical Journal. **87**: 858-872.

Duby, G., Hosy, E., Fizames, C., Alcon, C., Costa, A., Sentenac, H., and Thibaud, J.B. (2008). AtKC1, a conditionally targeted Shaker-type subunit, regulates the activity of plant K^+ channels. Plant Journal. **53**: 115-123.

Dulubova, I., Yamaguchi, T., Wang, Y., Südhof, T.C., and Rizo, J. (2001). Vam3p structure reveals conserved and divergent properties of syntaxins. Nature Structural Biology. **8**: 258-264.

Dulubova, I., Yamaguchi, T., Gao, Y., Min, S.W., Huryeva, I., Südhof, T.C., and Rizo, J. (2002). How Tlg2p/syntaxin 16 'snares' Vps45. EMBO Journal. **21**: 3620-3631.

Ebine, K., Okatani, Y., Uemura, T., Goh, T., Shoda, K., Niihama, M., Morita, M.T., Spitzer, C., Otegui, M.S., Nakano, A., and Ueda, T. (2008). A SNARE complex unique to seed plants is required for protein storage vacuole biogenesis and seed development of Arabidopsis thaliana. Plant Cell **20**: 3006-3021.

Ebine, K., Fujimoto, M., Okatani, Y., Nishiyama, T., Goh, T., Ito, E., Dainobu, T., Nishitani, A., Uemura, T., Sato, M.H., Thordal-Christensen, H., Tsutsumi, N., Nakano, A., and Ueda, T. (2011). A membrane trafficking pathway regulated by the plant-specific RAB GTPase ARA6. Nature Cell Biology. **13**: 853-859.

Ebine, K., Uemura, T., Nakano, A., and Ueda, T. (2012). Flowering time modulation by a vacuolar SNARE via FLOWERING LOCUS C in Arabidopsis thaliana. PLoS ONE. **7**: e42239.

Eisenach, C., Chen, Z.H., Grefen, C., and Blatt, M.R. (2012). The trafficking protein SYP121 of Arabidopsis connects programmed stomatal closure and K^+ channel activity with vegetative growth. Plant Journal. **69**: 241-251.

Eisenach, C., Papanatsiou, M., Hillert, E.K., and Blatt, M.R. (2014). Clustering of the K^+ channel GORK of Arabidopsis parallels its gating by extracellular K^+. Plant Journal. **78**: 203-214.

Elias, M., Drdova, E., Ziak, D., Bavlnka, B., Hala, M., Cvrckova, F., Soukupova, H., and Zarsky, V. (2003). The exocyst complex in plants. Cell Biology International. **27**: 199-201.

El Kasmi, F., Krause, C., Hiller, U., Stierhof, Y.D., Mayer, U., Conner, L., Kong, L., Reichardt, I., Sanderfoot, A.A., and Jürgens, G. (2013). SNARE complexes of different composition jointly mediate membrane fusion in Arabidopsis cytokinesis. Molecular Biology of the Cell. **24**: 1593-1601.

Fasshauer, D., Sutton, R., Brunger, A.T., and Jahn, R. (1998). Conserved structural features of the synaptic fusion complex: SNARE proteins reclassified as Q- and R-SNAREs. Proceedings of the National Academy of Sciences of United States of America. **95**: 15781-15786.

Felix, G., Duran, J.D., Volko, S., and Boller, T. (1999). Plants have a sensitive perception system for the most conserved domain of bacterial

flagellin. Plant Journal. **18**: 265-276.

Fendrych, M., Synek, L., Pecenková, T., Toupalová, H., Cole, R., Drdová, E., Nebesárová, J., Sedinová, M., Hála, M., Fowler, J.E., and Zársky, V. (2010). The Arabidopsis exocyst complex is involved in cytokinesis and cell plate maturation. Plant Cell. **22**: 3053-3065.

Fendrych, M., Synek, L., Pecenková, T., Drdová, E.J., Sekeres, J., de Rycke, R., Nowack, M.K., and Zársky, V. (2013). Visualization of the exocyst complex dynamics at the plasma membrane of *Arabidopsis thaliana*. Molecular Biology of the Cell. **24**: 510-520.

Fernandez, I., Ubach, J., Dulubova, I., Zhang, X., Südhof, T.C., and Rizo, J. (1998). Three-dimensional structure of an evolutionarily conserved N-terminal domain of syntaxin 1A. Cell. **94**: 841-849.

Fields, S. and Song, O. (1989). A novel genetic system to detect protein-protein interactions. Nature. **340**: 245-246.

Fili, O., Michaelevski, I., Bledi, Y., Chikvashvili, D., Singer-Lahat, D., Boshwitz, H., Linial, M. and Lotan, I. (2001). Direct interaction of a brain voltage-gated K^+ channel with syntaxin 1A: functional impact on channel gating. Journal of Neuroscience. **21**: 1964-1974.

Foresti, O., daSilva, L.L., and Denecke, J. (2006). Overexpression of the Arabidopsis syntaxin PEP12/SYP21 inhibits transport from the prevacuolar compartment to the lytic vacuole in vivo. Plant Cell. **18**: 2275-2293.

Freidit Frey, N. and Robatzek, S. (2009). Trafficking vesicles: pro or contra pathogens? Current Opinion in Plant Biology. **12**: 437-443.

Frietsch, S., Wang, Y.F., Sladek, C., Poulsen, L.R., Romanowsky, S.M., Schroeder, J.I., and Harper, J.F. (2007). A cyclic nucleotide-gated channel is essential for polarized tip growth of pollen. Proceedings of the National Academy of Sciences of United States of America. **104**: 14531-14536.

Furst, J., Sutton, R.B., Chen, J., Brunger, A.T., and Grigorieff, N. (2003). Electron cryomicroscopy structure of N-ethyl maleimide sensitive factor at 11 A resolution. EMBO Journal. **22**: 4365-4374.

Fujimoto, M., and Ueda, T. (2012). Conserved and plant-unique mechanisms regulating plant post-Golgi traffic. Frontiers in Plant Science. **3**: 197.

Fujiwara, M., Uemura, T., Ebine, K., Nishimori, Y., Ueda, T., Nakano, A., Sato, M.H., and Fukao, Y. (2014). Interactomics of Qa-SNARE in *Arabidopsis thaliana*. Plant Cell and Physiology. **55**: 781-789.

Furuichi, T., Cunningham, K.W., and Muto, S. (2001). A putative two pore channel AtTPC1 mediates Ca^{2+} flux in Arabidopsis leaf cells. Plant Cell Physiology. **42**: 900-905.

Gall, L., Stan, R.C., Kress, A., Hertel, B., Thiel, G., and Meckel, T. (2010). Fluorescent detection of fluid phase endocytosis allows for in vivo estimation of endocytic vesicle sizes in plant cells with sub-diffraction accuracy. Traffic. **11**: 548-559.

Gapper, C. and Dolan, L. (2006). Control of plant development by reactive oxygen species. Plant Physiology. **141**: 341-345.

Garcia-Mata, C., Wang, J., Gajdanowicz, P., Gonzalez, W., Hills, A., Donald, N., Riedelsberger, J., Amtmann, A., Dreyer, I., and Blatt, M.R. (2010). A minimal cysteine motif required to activate the SKOR K^+ channel of Arabidopsis by the reactive oxygen species H_2O_2. Journal of Biological Chemistry. **285**: 29286-29294.

Gaymard, F., Pilot, G., Lacombe, B., Bouchez, D., Bruneau, D., Boucherez, J., Michaux-Ferrière, N., Thibaud, J.B., and Sentenac, H. (1998). Identification and disruption of a plant shaker-like outward channel involved in K^+ release into the xylem sap. Cell. **94**: 647-655.

Geelen, D., Leyman, B., Batoko, H., Di Sansabastiano, G.P., Moore, I., and Blatt, M.R. (2002). The abscisic acid-related SNARE homolog NtSyr1 contributes to secretion and growth: Evidence from competition with its cytosolic domain. Plant Cell. **14**: 387-406.

Geiger, D., Scherzer, S., Mumm, P., Stange, A., Marten, I., Bauer, H., Ache, P., Matschi, S., Liese, A., Al-Rasheid, K.A., Romeis, T., and Hedrich, R. (2009). Activity of guard cell anion channel SLAC1 is controlled by drought-stress signaling kinase-phosphatase pair. Proceedings of the National Academy of Sciences of United States of America. **106**: 21425-21430.

Geiger, D., Maierhofer, T., Al-Rasheid, K.A., Scherzer, S., Mumm, P., Liese, A., Ache, P., Wellmann, C., Marten, I., Grill, E., Romeis, T., and Hedrich, R. (2011). Stomatal closure by fast abscisic acid signaling is mediated by the guard cell anion channel SLAH3 and the receptor RCAR1. Science Signal. **4**: ra32.

Geldner, N., Hyman, D.L., Wang, X., Schumacher, K., and Chory, J.

(2007). Endosomal signaling of plant steroid receptor kinase BRI1. Genes and Development. **21**: 1598-1602.

Gelli, A. and Blumwald, E. (1997). Hyperpolarization-activated Ca^{2+}-permeable channels in the plasma membrane of tomato cells. Journal of Membrane Biology. 1**55**: 35-45.

Gietz, R.D., Schiestl, R.H., Willems, A.R., and Woods, R.A. (1995). Studies on the transformation of intact yeast cells by the LiAc/SS-DNA/PEG procedure. Yeast. **11**: 355-360.

Gobert, A., Isayenkov, S., Voelker, C., Czempinski, K., and Maathuis, F.J. (2007). The two-pore channel TPK1 gene encodes the vacuolar K^+ conductance and plays a role in K^+ homeostasis. Proceedings of the National Academy of Sciences of United States of America. **104**: 10726-10731.

Gonzalez, L.C. Jr., Weis, W.I., and Scheller, R.H. (2001). A novel snare N-terminal domain revealed by the crystal structure of Sec22b. Journal of Biological Chemistry. **276**: 24203-24211.

Grant, J.J. and Loake, G.J. (2000). Role of reactive oxygen intermediates and cognate redox signaling in disease resistance. Plant Physiology. **124**: 21-29.

Graf, C.T., Riedel, D., Schmitt, H.D., and Jahn, R. (2005). Identification of functionally interacting SNAREs by using complementary substitutions in the conserved '0' layer. Molecular Biology of the Cell. **16**: 2263-2274.

Grefen, C., Lalonde, S., and Obrdlik, P. (2007). Split-ubiquitin system for identifying protein-protein interactions in membrane and full-length proteins. Current Protocols Neuroscience. **5**: 5-27.

Grefen, C., and Blatt, M.R. (2008). SNAREs - molecular governors in signalling and development. Current Opinion In Plant Biology. **11**: 600-609.

Grefen, C., Obrdlik, P., and Harter, K. (2009). The determination of protein-protein interactions by the mating-based split-ubiquitin system (mbSUS). Methods in Molecular Biology. **479**: 1-17.

Grefen, C., Chen, Z.H., Honsbein, A., Donald, N., Hills, A., and Blatt, M.R. (2010 a). A Novel Motif Essential for SNARE Interaction with the K^+ Channel KC1 and Channel Gating in Arabidopsis. Plant Cell. **22**: 3076-3092.

Grefen, C., Donald, N., Hashimoto, K., Kudla, J., Schumacher, K., and Blatt, M.R. (2010 b). A ubiquitin-10 promoter-based vector set for fluorescent protein tagging facilitates temporal stability and native protein distribution in transient and stable expression studies. Plant Journal. **64**: 355-365.

Grefen, C., and Blatt, M.R. (2012). A 2in1 cloning system enables ratiometric bimolecular fluorescence complementation (rBiFC). Biotechniques. **53**: 311-314.

Grosshans, B.L., Ortiz, D., and Novick, P. (2006). Rabs and their effectors: achieving specificity in membrane traffic. Proceedings of the National Academy of Sciences of United States of America. **103**: 11821-11827.

Guo, Y., Halfter, U., Ishitani, M., and Zhu, J.K. (2001). Molecular characterization of functional domains in the protein kinase SOS2 that is required for plant salt tolerance. Plant Cell. **13**: 1383-1400.

Hachez, C., Veselov, D., Ye, Q., Reinhardt, H., Knipfer, T., Fricke, W., and Chaumont, F. (2012). Short-term control of maize cell and root water permeability through plasma membrane aquaporin isoforms. Plant Cell Environment. **35**: 185-198.

Hachez, C., Besserer, A., Chevalier, A.S., and Chaumont, F. (2013). Insights into plant plasma membrane aquaporin trafficking. Trends in Plant Science. **18**: 344-352.

Hachez, C., Laloux, T., Reinhardt, H., Cavez, D., Degand, H., Grefen, C., De Rycke, R., Inzé, D., Blatt, M.R., Russinova, E., Chaumont, F. (2014). Arabidopsis SNAREs SYP61 and SYP121 Coordinate the Trafficking of Plasma Membrane Aquaporin PIP2;7 to Modulate the Cell Membrane Water Permeability. Plant Cell. **26**: 3132-3147.

Hala, M., Cole, R., Synek, L., Drdová, E., Pecenková, T., Nordheim, A., Lamkemeyer, T., Madlung, J., Hochholdinger, F., Fowler, J.E., and Zárský, V. (2008). An exocyst complex functions in plant cell growth in Arabidopsis and tobacco. Plant Cell. **20**: 1330-1345.

Hamilton, D.W., Hills, A., Kohler, B., and Blatt, M.R. (2000). Ca^{2+} channels at the plasma membrane of stomatal guard cells are activated by hyperpolarization and abscisic acid. Proceedings of the National Academy of Sciences of United States of America. **97**: 4967-4972.

Han, X., Wang, C.T., Bai, J., Chapman, E.R., and Jackson, M.B. (2004). Transmembrane segments of syntaxin line the fusion pore of

Ca^{2+}-triggered exocytosis. Science. **304**: 289-292.

Harper, J.F., Sussman, M.R., Schaller, G.E., Putnam-Evans, C., Charbonneau, H., and Harmon, A.C. (1991). A calcium-dependent protein kinase with a regulatory domain similar to calmodulin. Science. **252**: 951-954.

Harper, J.F. and Harmon, A. (2005). Plants, symbiosis and parasites: a calcium signalling connection. Nature Reviews Molecular Cell Biology. **6**: 555-566.

Hara-Nishimura, I., Shimada, T., Hatano, K., Takeuchi, Y., and Nishimura, M. (1998). Transport of storage proteins to protein storage vacuoles is mediated by large precursor-accumulating vesicles. Plant Cell **10**: 825-836.

Haseloff, J. and Amos, B. (1995). GFP in plants. Trends in Genetics. **11**: 328-329.

He, Z., Wang, Z.Y., Li, J. Zhu, Q., Lamb, C., Ronald, P., and Chory, J. (2000). Perception of brassinosteroids by the extracellular domain of the receptor kinase BRI1. Science. **288**: 2360-2363.

Helms, J.B. and Rothman, J.E. (1992). Inhibition by brefeldin A of Golgi membrane enzyme that catalyzes exchange of guanine nucleotide bound to ARF. Nature (Lond.). **360**: 352-354.

Heim R., Cubitt A.B. and Tsien R.Y. (1995). Improved green fluorescence. Nature. **373**: 663-664.

Hedrich, R., Marten, I., Lohse, G., Dietrich, P., Winter, H., Lohaus, G., and Heldt, H. (1994). Malate-sensitive anion channels enable guard cells to sense changes in the ambient CO_2 concentration. Plant Journal, 6: **741-748.**

Hedrich, R., and Neher, E. (1987). Cytoplasmic calcium regulates voltage dependent ion channels in plant vacuoles. Nature. **329**: 833-835.

Hepler, P.K., Vidali, L., and Cheung, A.Y. (2001) Polarized cell growth in higher plants. Annual review of cell and developmental biology. **17**: 159-187.

Hille, B. (2001). Ionic Channels of Excitable Membranes. (Sunderland, Mass.: Sinauer Press).

Hoekenga, O.A., Maron, L.G., Piñeros, M.A., Cançado, G.M., Shaff, J.,

Kobayashi, Y., Ryan, P.R., Dong, B., Delhaize, E., Sasaki, T., Matsumoto, H., Yamamoto, Y., Koyama, H., and Kochian, L.V. (2006). AtALMT1, which encodes a malate transporter, is identified as one of several genes critical for aluminum tolerance in Arabidopsis. Proceedings of the National Academy of Sciences of United States of America. **103**: 9738-9743.

Hofmann, M.W., Peplowska, K., Rohde, J., Poschner, B.C., Ungermann, C., and Langosch, D. (2006). Self-interaction of a SNARE transmembrane domain promotes the hemifusion-to-fusion transition. Journal of Molecular Biology. **364**: 1048-1060.

Hong, W. (2005). SNAREs and traffic. Biochimica et Biophysica Acta. **1744**: 120-144.

Honsbein, A., Blatt, M.R., and Grefen, C. (2011). A molecular framework for coupling cellular volume and osmotic solute transport control. Journal Of Experimental Botany. **62**: 2363-2370.

Honsbein, A., Sokolovski, S., Grefen, C., Campanoni, P., Pratelli, R., Paneque, M., Chen, Z.H., Johansson, I., and Blatt, M.R. (2009). A Tripartite SNARE-K^+ Channel Complex Mediates in Channel-Dependent K^+ Nutrition in Arabidopsis. Plant Cell. **21**: 2859-2877.

Hosy, E., Vavasseur, A., Mouline, K., Dreyer, I., Gaymard, F., Porée, F., Boucherez, J., Lebaudy, A., Bouchez, D., Very, A.A., Simonneau, T., Thibaud, J.B., and Sentenac, H. (2003). The Arabidopsis outward K^+ channel GORK is involved in regulation of stomatal movements and plant transpiration. Proceedings of the National Academy of Sciences of United States of America. **100**: 5549-5554.

Hoshi, T. (1995). Regulation of voltage-dependence of the KAT1 channel by intracellular factors. Journal of General Physiology. **105**: 309-328.

Hu, C,D., Chinenov, Y., and Kerppola, T.K. (2002). Visualization of Interactions among bZIP and Rel Family Proteins in Living Cells Using Bimolecular Fluorescence Complementation. Molecular Cell. **9**: 789-798.

Irani, N.G., Di Rubbo, S., and Russinova, E. (2014). In vivo imaging of brassinosteroid endocytosis in Arabidopsis. Methods in Molecular Biology. **1209**: 107-117.

Isayenkov, S., Isner, J.C., and Maathuis, F.J. (2011). Membrane localisation diversity of TPK channels and their physiological role. Plant Signal Behavior. **6:** 1201-1204.

Ishitani, M., Liu, J., Halfter, U., Kim, C.S., Shi, W., and Zhu, J.K. (2000). SOS3 function in plant salt tolerance requires N-myristoylation and calcium binding. Plant Cell. **12**: 1667-1678.

Ivanov, S., Fedorova, E.E., Limpens, E., De Mita, S., Genre, A., Bonfante, P., and Bisseling, T. (2012). Rhizobium-legume symbiosis shares an exocytotic pathway required for arbuscule formation. Proceedings of the National Academy of Sciences of United States of America. **109**: 8316-8321.

Jahn, R. and Scheller, R.H. (2006). SNAREs-engines for membrane fusion. Nature Reviews Molecular Cell Biology. **7**: 631-643.

Jessing, K.K., Cedergreen, N., Mayer, P., Libous-Bailey, L., Strobel, B.W., Rimando, A., and Duke, S.O. (2013). Loss of artemisinin produced by *Artemisia annua* L. to the soil environment. Industrial Crops and Products. **43**: 132-140.

Johnsson, N. and Varshavsky, A. (1994). Split ubiquitin as a sensor of protein interactions in vivo. Proceedings of the National Academy of Sciences of United States of America. **91**: 10340-10344.

Johansson, I., Wulfetange, K., Porée, F., Michard, E., Gajdanowicz, P., Lacombe, B., Sentenac, H., Thibaud, J.B., Mueller-Roeber, B., Blatt, M.R., Dreyer, I. (2006). External K^+ modulates the activity of the Arabidopsis potassium channel SKOR via an unusual mechanism. Plant Journal. **46**: 269-281.

Jurgens, G. and Geldner,. N. (2002) Protein secretion in plants: from the trans-Golgi network to the outer space. Traffic. **3**: 605-613.

Kaether, C. and Gerdes, H.H. (1995). Visualization of protein transport along the secretory pathway using green fluorescent protein. FEBS Letter. **369**: 267-271.

Kalde, M., Nuhse, T.S., Findlay, K., and Peck, S.C. (2007). The syntaxin SYP132 contributes to plant resistance against bacteria and secretion of pathogenesis-related protein 1. Proceedings of the National Academy of Sciences of United States of America. **104**: 11850-11855.

Katz, L. and Brennwald, P. (2000). Testing the 3Q:1R "rule": mutational analysis of the ionic "zero" layer in the yeast exocytic SNARE complex reveals no requirement for arginine. Molecular Biology of the Cell. **11**: 3849-3858.

Kato, T., Morita, M.T., Fukaki, H., Yamauchi, Y., Uehara, M., Niihama,

M., and Tasaka, M. (2002). SGR2, a phospholipase-like protein, and ZIG/SGR4, a SNARE, are involved in the shoot gravitropism of Arabidopsis. Plant cell. **14**: 33-46.

Karnik, A., Karnik, R., and Grefen, C. (2013a). SDM-Assist software to design sitedirected mutagenesis primers introducing "silent" restriction sites. Bmc Bioinformatics. **14**: 105.

Karnik, R., Grefen, C., Bayne, R., Honsbein, A., Koehler, T., Kioumourtzoglou, D., Williams, M., Bryant, N.J., and Blatt, M.R. (2013b). Arabidopsis Sec1/Munc18 Protein SEC11 Is a Competitive and Dynamic Modulator of SNARE Binding and SYP121-Dependent Vesicle Traffic. Plant Cell. **25**: 1368-1382.

Keiper, B.D. (2003). Translation of mRNAs in *Xenopus* Oocytes. eLS.
Kelley, L.A. and Sternberg, M.J. (2009). Protein structure prediction on the Web: a case study using the Phyre server. Nature Protocols. **4**: 363-371.

Kent, H.M., Evans, P.R., Schafer, I.B., Gray, S.R., Sanderson, C.M., Luzio, J.P., Peden, A.A., and Owen, D.J. (2012). Structural basis of the intracellular sorting of the SNARE VAMP7 by the AP3 adaptor complex. Development Cell. **22**: 979-988.

Kerppola, T. K. (2006). Visualization of molecular interactions by fluorescence complementation. Nature Reviews Molecular Cell Biology. **7**: 449-456.

Kerppola, T.K. (2009). Visualization of molecular interactions using bimolecular fluorescence complementation analysis: Characteristics of protein fragment complementation. Chemical Society Reviews. **38**: 2876-2886.

Kinoshita, T., Cano-Delgado, A., Seto, H., Hiranuma, S., Fujioka, S., Yoshida, S., and Chory, J. (2005). Binding of brassinosteroids to the extracellular domain of plant receptor kinase BRI1. Nature. **433**: 167-171.

Kotzer, A.M., Brandizzi, F., Neumann, U., Paris, N., Moore, I., and Hawes, C. (2004). AtRabF2b (Ara7) acts on the vacuolar trafficking pathway in tobacco leaf epidermal cells. Journal of Cell Science. **117**: 6377-6389.

Kulich, I., Pečenková, T., Sekereš, J., Smetana, O., Fendrych, M., Foissner, I., Höftberger, M., and Zárský, V. (2013). Arabidopsis exocyst subcomplex containing subunit EXO70B1 is involved in the

autophagy-related transport to the vacuole. Traffic. **14:** 1155-1165.

Kudla, J., Xu, Q., Harter, K., Gruissem, W., and Luan, S. (1999). Genes for calcineurin B-like proteins in Arabidopsis are differentially regulated by stress signals. Proceedings of the National Academy of Sciences of United States of America. **96**: 4718-4723.

Kwon, C., Neu, C., Pajonk, S., Yun, H.S., Lipka, U., Humphry, M., Bau, S., Straus, M., Kwaaitaal, M., Rampelt, H., El Kasmi, F., Jurgens, G., Parker, J., Panstruga, R., Lipka, V., and Schulze-Lefert, P. (2008). Co-option of a default secretory pathway for plant immune responses. Nature. **451**: 835-840.

Laage, R. and Langosch, D. (1997). Dimerization of the synaptic vesicle protein synaptobrevin (vesicle-associated membrane protein) II depends on specific residues within the transmembrane segment. European Journal of Biochemistry. **249**: 540-546.

Laage, R., Rohde, J., Brosig, B., and Langosch, D. (2000). A conserved membrane-spanning amino acid motif drives homomeric and supports heteromeric assembly of presynaptic SNARE proteins. Journal of Biology Chemistry. **275**: 17481-17487.

Latz, A., Becker, D., Hekman, M., Müller, T., Beyhl, D., Marten, I., Eing, C., Fischer, A., Dunkel, M., Bertl, A., Rapp, U.R., and Hedrich, R. (2007). Plant Journal. **52**: 449-459.

Lan, W.Z., Lee, S.C., Che, Y.F., Jiang, Y.Q., and Luan, S. (2011). Mechanistic analysis of AKT1 regulation by the CBL-CIPK-PP2CA interactions. Molecular Plant. **4**: 527-536.

Lebaudy, A., Hosy, E., Simonneau, T., Sentenac, H., Thibaud, J.B., and Dreyer, I. (2008). Heteromeric K^+ channels in plants. Plant Journal. **54**: 1076-1082.

Lebaudy, A., Pascaud, F., Véry, A.A., Alcon, C., Dreyer, I., Thibaud, J.B., and Lacombe, B. (2010). Preferential KAT1-KAT2 heteromerization determines inward K^+ current properties in Arabidopsis guard cells. Journal of Biological Chemistry. 285: 6265-6274.

Lee, S.Y., Voronov, S., Letinic, K., Nairn, A.C., Di Paolo, G., and De Camilli, P. (2005). Regulation of the interaction between PIPKI gamma and talin by proline-directed protein kinases. Journal of Cell Biology. **168**: 789-799.

Lee, S.C., Lan, W.Z., Kim, B.G., Li, L., Cheong, Y.H., Pandey, G.K., Lu,

G., Buchanan, B.B., and Luan, S. (2007). A protein phosphorylation/ dephosphorylation network regulates a plant potassium channel. Proceedings of the National Academy of Sciences of United States of America. **104**: 15959-15964.

Lee, S.C., Lan, W., Buchanan, B.B., and Luan, S. (2009). A protein kinase-phosphatase pair interacts with an ion channel to regulate ABA signaling in plant guard cells. Proceedings of the National Academy of Sciences of United States of America. **106**: 21419-21424.

Lefoulon, C., Gutla, P.V., Honsbein, A., Wang, Y., Grefen, C., Riedelsberger, J., Karnik, R., Gonzalez, W., and Blatt, M.R. (2014). Voltage-sensor transitions of the inward-rectifying K^+ channel KAT1 indicate a closed-to-open latching mechanism that is biased by hydration around the S4 alpha-helix. Plant Physiology. **166**: 960-975.

Lehming, N. (2002). Analysis of protein-protein proximities using the split-ubiquitin system. Briefings in functional genomics and proteomics. **1**: 230-238.

Leubner-Metzger, G. (2001). Brassinosteroids and gibberellins promote tobacco seed germination by distinct pathways. Planta. **213**: 758-763.

Leyman, B., Geelen, D., and Blatt, M.R. (2000). Localization and control of expression of Nt-Syr1, a tobacco SNARE protein. Plant Journal. **24**: 369-381.

Leshem, Y., Melamed-Book, N., Cagnac, O., Ronen, G., Nishri, Y., Solomon, M., Cohen, G., and Levine, A. (2006). Suppression of Arabidopsis vesicle-SNARE expression inhibited fusion of H_2O_2-containing vesicles with tonoplast and increased salt tolerance. Proceedings of the National Academy of Sciences of United States of America. **103**: 18008-18013.

Leshem, Y., Golani, Y., Kaye, Y., and Levine, A. (2010). Reduced expression of the v-SNAREs AtVAMP71/AtVAMP7C gene family in Arabidopsis reduces drought tolerance by suppression of abscisic acid-dependent stomatal closure. Journal of Experimental Botany. **61**: 2615-2622.

Leyman, B., Geelen, D., Quintero, F.J., and Blatt, M.R. (1999). A tobacco syntaxin with a role in hormonal control of guard cell ion channels. Science. **283**: 537-540.

Li, J., Lee, Y.R., and Assmann, S.M. (1998). Guard cells possess a calcium-dependent protein kinase that phosphorylates the KAT1

potassium channel. Plant Physiology. **116**: 785-795.

Lipka, V., Kwon, C., and Panstruga, R. (2007). SNARE-Ware: The role of SNARE Domain proteins in plant biology. Annual Review Of Cell And Developmental Biology. **23**: 147-174.

Lin, C.Y., Trinh, N.N., Fu, S.F., Hsiung, Y.C., Chia, L.C., Lin, C.W., and Huang, H.J. (2013). Comparison of early transcriptome responses to copper and cadmium in rice roots. Plant Molecular Biology. **81**: 507-522.

Luan, S., Kudla, J., Rodriguez-Concepcion, M., Yalovsky, S., and Gruissem, W. (2002). Calmodulins and calcineurin B-like proteins: Calcium sensors for specific signal response coupling in plants. Plant Cell. **14** (suppl.): S389-S400.

Lvov, A., Chikvashvili, D., Michaelevski, I., and Lotan, I. (2008). VAMP2 interacts directly with the N terminus of Kv2.1 to enhance channel inactivation. Pflugers Archiv-European Journal of Physiology. **456**: 1121-1136.

McBride, H.M., Rybin, V., Murphy, C., Giner, A., Teasdale, R., and Zerial, M. (1999). Oligomeric complexes link Rab5 effectors with NSF and drive membrane fusion via interactions between EEA1 and syntaxin 13. Cell. **98**: 377-386.

Mai, H.T., Nomura, M., Takegawa, K., Asamizu, E., Sato, S., Kato, T., Tabata, S., and Tajima, S. (2006). Identification of a Sed5-like SNARE gene LjSYP32-1 that contributes to nodule tissue formation of Lotus japonicus. Plant and Cell Physiology. **47**: 829-838.

Markham K.R., Gould K.S., Winefield C.S., Mitchell K.A., Bloor S.J., and Boase M.R. (2000). Anthocyanic vacuolar inclusions - Their nature and significance in flower colouration. Phytochemistry. **55**: 327-336.

Marquardt, D. (1963). An algorithm for least-squares estimation of nonlinear parameters. Journal of the Society for Industrial and Applied Mathematics. **11**: 431-441.

Martinez-Arca, S., Rudge, R., Vacca, M., Raposo, G., Camonis, J., Proux-Gillardeaux, V., Daviet, L., Formstecher, E., Hamburger, A., Filippini, F., D'Esposito, M., and Galli, T. (2003). A dual mechanism controlling the localization and function of exocytic v-SNAREs. Proceedings of the National Academy of Sciences of United States of America. **100**: 9011-9016.

Maser, P., Thomine, S., Schroeder, J.I., Ward, J.M., Hirschi, K., Sze,

H., Talke, I.N., Amtmann, A., Maathuis, F.J., Sanders, D., Harper, J.F., Tchieu, J., Gribskov, M., Persans, M.W., Salt, D.E., Kim, S.A., Guerinot, M.L. (2001). Phylogenetic relationships within cation transporter families of Arabidopsis. Plant Physiology. **126**: 1646-1647.

Marten, I., Hoth, S., Deeken, R., Ache, P., Ketchum, K.A., Hoshi, T., and Hedrich, R. (1999). AKT3, a phloem-localized K^+ channel, is blocked by protons. Proceedings of the National Academy of Sciences of United States of America. **96**: 7581-7586.

McGuffin, L.J., Bryson, K., and Jones, D.T. (2000). The PSIPRED protein structure prediction server. Bioinformatics. **16**: 404-405.

McBride, H.M., Rybin, V., Murphy, C., Giner, A., Teasdale, R., and Zerial, M. (1999). Oligomeric complexes link Rab5 effectors with NSF and drive membrane fusion via interactions between EEA1 and syntaxin 13. Cell. **98**: 377-386.

Meckel, T., Hurst, A.C., Thiel, G., and Homann, U. (2005). Guard cells undergo constitutive and pressure-driven membrane turnover. Protoplasma. **226**: 23-29.

Meharg, A.A, Maurousset, L., and Blatt, M.R. (1994). Cable correction of membrane currents recorded from root hairs of *Arabidopsis thaliana* L. Journal of Experimental Botany. **45**: 1-6.

Meyer, S., Mumm, P., Imes, D., Endler, A., Weder, B., Al-Rasheid, K.A., Geiger, D., Marten, I., Martionia, E., and Hedrich, R. (2010). AtALMT12 represents an R-type anion channel required for stomatal movement in Arabidopsis guard cells. Plant Journal. **63**: 1054-1062.

Michaelevski, I., Chikvashvili, D., Tsuk, S., Fili, O., Lohse, M.J., Singer-Lahat, D., and Lotan, I. (2002). Modulation of a brain voltage-gated K^+ channel by syntaxin 1A requires the physical interaction of Gbetagamma with the channel. Journal of Biology Chemistry. **277**: 34909-34917.

Michaelevski, I., Chikvashvili, D., Tsuk, S., Singer-Lahat, D., Kang, Y.H., Linial, M., Gaisano, H.Y., Fili, O., and Lotan, I. (2003). Direct interaction of target SNAREs with the Kv2.1 channel - Modal regulation of channel activation and inactivation gating. Journal of Biology Chemistry. **278**: 34320-34330.

Michard, E., Lima, P.T., Borges, F., Silva, A.C., Portes, M.T., Carvalho, J.E., Gilliham, M., Liu, L.H., Obermeyer, G., and Feijo, J.A. (2011). Glutamate receptor-like genes form Ca^{2+} channels in pollen tubes and

are regulated by pistil D-serine. Science. **332:** 434-437.

Misura, K.M.S., Scheller, R.H., and Weis, W.I. (2000). Three-dimensional structure of the neuronal-Sec1-syntaxin 1a complex. Nature. **404**: 355-362.

Miwa, K., Takano, J., Omori, H., Seki, M., Shinozaki, K., and Fujiwara, T. (2007). Plants tolerant of high boron levels. Science. **318**: 1417.

Morita, M.T., Kato, T., Nagafusa, K., Saito, C., Ueda, T., Nakano, A., and Tasaka, M. (2002). Involvement of the vacuoles of the endodermis in the early process of shoot gravitropism in Arabidopsis. Plant cell. **14**: 47-56.

Moyer, B.D., Allan, B.B., and Balch, W.E. (2001). Rab1 interaction with a GM130 effector complex regulates COPII vesicle *cis*-Golgi tethering. Traffic. **2**: 268-276.

Muller, J. and Johnsson, N. (2008). Split-ubiquitin and the split-protein sensors: chessman for the endgame. Chembiochem. **9**: 2029-2038.

Munson, M., Chen, X., Cocina, A.E., Schultz, S.M., and Hughson, F.M. (2000). Interactions within the yeast t-SNARE Sso1p that control SNARE complex assembly. Nature Structural and Molecular Biology. **7**: 894-902.

Murray, D.H., and Tamm, L.K. (2009). Clustering of syntaxin-1A in model membranes is modulated by phosphatidylinositol 4,5-bisphosphate and cholesterol. Biochemistry. **48**: 4617-4625.

Negi, J., Matsuda, O., Nagasawa, T., Oba, Y., Takahashi, H., Kawai-Yamada, M., Uchimiya, H., Hashimoto, M., and Iba, K. (2008). CO2 regulator SLAC1 and its homologues are essential for anion homeostasis in plant cells. Nature. **452:** 483-486.

Nemhauser, J.L., Mockler, T.C., and Chory, J. (2004). Interdependency of brassinosteroid and auxin signaling in Arabidopsis. PLoS Biology. **2**: E258.

Norris, S.R., Meyer, S.E. and Callis, J. (1993). The intron of Arabidopsis thaliana polyubiquitin genes is conserved in location and is a quantitative determinant of chimeric gene expression. Plant Molecular Biology. **21**: 895-906.

Novick, P., Field, C., and Schekman, R. (1980). Identification of 23 complementation groups required for posttranslational events in the yeast secretory pathway. Cell. **21**: 205-215.

Nuhse, T., Boller, T., and Peck, S. (2003). A plasma membrane syntaxin is phosphorylated in response to the bacterial elicitor flagellin. Journal of Biological Chemistry. **278**: 45248-45254.

Obrdlik, P., El-Bakkoury, M., Hamacher, T., Cappellaro, C., Vilarino, C., Fleischer, C., Ellerbrok, H., Kamuzinzi, R., Ledent, V., Blaudez, D., Sanders, D., Revuelta, J.L., Boles, E., André, B., and Frommer, W.B. (2004). K^+ channel interactions detected by a genetic system optimized for systematic studies of membrane protein interactions. Proceedings of the National Academy of Sciences of United States of America. **101**: 12242-12247.

Ossig, R., Schmitt, H.D., de Groot, B., Riedel, D., Keränen, S., Ronne, H., Grubmüller, H., and Jahn, R. (2000). Exocytosis requires asymmetry in the central layer of the SNARE complex. EMBO Journal. **19**: 6000-6010.

Otegui, M.S. (2014). Preface. In: Methods and Protocols: Plant Endosomes. Humana Press.

Pecenkova, T., Hala, M., Kulich, I., Kocourková, D., Drdová, E., Fendrych, M., Toupalová, H., and Zársky, V. (2011). The role for the exocyst complex subunits Exo70B2 and Exo70H1 in the plant-pathogen interaction. Journal of Experimental Botany. **62**: 2107-2116.

Pei, Z.M., Ward, J.M., and Schroeder, J.I. (1999). Magnesium sensitizes slow vacuolar channels to physiological cytosolic calcium and inhibits fast vacuolar channels in fava bean guard cell vacuoles. Plant Physiology. **121**: 977-986.

Peiter, E., Maathuis, F.J., Mills, L.N., Knight, H., Pelloux, J., Hetherington, A.M., and Sanders, D. (2005). The vacuolar Ca^{2+}-activated channel TPC1 regulates germination and stomatal movement. Nature. **434**: 404-408.

Pennuto, M., Dunlap, D., Contestabile, A., Benfenati, F., and Valtorta, F. (2002). Fluorescence resonance energy transfer detection of synaptophysin I and vesicle-associated membrane protein 2 interactions during exocytosis from single live synapses. Molecular Biology of the Cell. **13**: 2706-2717.

Phillips, G.D., Preshaw, C., and Steer, M.W. (1988). Dictyosome vesicle production and plasma-membrane turnover in auxin-stimulated outer epidermal-cells of coleoptile segments from *avena-sativa* (L). Protoplasma, **145**: 59-65.

Philippar, K., Fuchs, I., Luthen, H., Hoth, S., Bauer, C.S., Haga, K., Thiel, G., Ljung, K., Sandberg, G., Bottger, M., Becker, D., and Hedrich, R. (1999). Auxin-induced K^+ channel expression represents an essential step in coleoptile growth and gravitropism. Proceedings of the National Academy of Sciences of United States of America. **96**: 12186-12191.

Pilot, G., Lacombe, B., Gaymard, F., Cherel, I., Boucherez, J., Thibaud, J.B. and Sentenac, H. (2001). Guard cell inward K^+ channel activity in Arabidopsis involves expression of the twin channel subunits KAT1 and KAT2. Journal of Biology Chemistry. **276**: 3215-3221.

Pineros, M.A. and Kochian, L.V. (2001). A patch-clamp study on the physiology of aluminum toxicity and aluminum tolerance in maize. Identification and characterization of Al^{3+}-induced anion channels. Plant Physiology. **125**: 292-305.

Pollastri, G., Przybylski, D., Rost, B. and Baldi, P.(2002).Improving the prediction of protein secondary structure in three and eight classes using recurrent neural networks and profiles. Proteins. **47**: 228-235.

Pratelli, R., Sutter, J.U., and Blatt, M.R. (2004). A new catch in the SNARE. Trends in Plant Science. **9**: 187-195.

Press, W., Flannerly, B., Teukolsky, S., and Vetterling, W. (1992). Numerical Recipies: The Art of Scientific Computing. (Cambridge: Cambridge University Press).

Pryor, P.R., Jackson, L., Gray, S.R., Edeling, M.A., Thompson, A., Sanderson, C.M., Evans, P.R., Owen, D.J., and Luzio, J.P. (2008). Molecular basis for the sorting of the SNARE VAMP7 into endocytic clathrin-coated vesicles by the ArfGAP Hrb. Cell. **134**: 817-827.

Ptashne, M. (1992). A Genetic Switch: Phage (Lambda) and Higher Organisms, Cell Press, Cambridge, MA

Randazzo, P.A., Yang, Y.C., Rulka, C., and Kahn, R.A. (1993). Activation of ADP-ribosylation factor by Golgi membranes. Evidence for a brefeldin A- and protease-sensitive activating factor on Golgi membranes. Journal of Biological Chemistry. **268**: 9555-9563.

Rehman, R.U. and Sansebastiano, G.D. (2014). SNARE Proteins as Signaling Elements. In Hakeem, K.R., Rehman, R.U., and Tahir, I. (eds). Plant signaling: Understanding the molecular crosstalk. Springer India. pp 39-49.

Reintanz, B., Szyroki, A., Ivashikina, N., Ache, P., Godde, M., Becker, D., Palme, K., and Hedrich, R. (2002). AtKC1, a silent Arabidopsis potassium channel alpha -subunit modulates root hair K^+ influx. Proceedings of the National Academy of Sciences of United States of America. **99**: 4079-4084.

Robert, S., Chary, S.N., Drakakaki, G., Li, S., Yang, Z., Raikhel, N.V., and Hicks, G.R. (2008). Endosidin1 defines a compartment involved in endocytosis of the brassinosteroid receptor BRI1 and the auxin transporters PIN2 and AUX1. Proceedings of the National Academy of Sciences of United States of America. **105**: 8464-8469.

Robatzek, S., Chinchilla, D., and Boller, T. (2006). Ligand induced endocytosis of the pattern recognition receptor FLS2 in Arabidopsis. Genes & Development. **20**: 537-542.

Rojo, E., Zouhar, J., Kovaleva,V., Hong, S., and Raikhel, N.V. (2005). The AtC-VPS protein complex is localized to the tonoplast and the prevacuolar compartment in Arabidopsis. Molecular Biology of the Cell. **14**: 361-369.

Rossi, V., Banfield, D., Vacca, M., Dietrich, L., Ungermann, C., D'Esposito, M., Galli, T., and Filippini, F. (2004). Longins and their longin domains: regulated SNAREs and multifunctional SNARE regulators. Trends in Biochemical Sciences. **29**: 682-688.

Roy, R., Laage, R., and Langosch, D. (2004). Synaptobrevin transmembrane domain dimerization - revisited. Biochemistry. **43**: 4964-4970.

Russinova, E., Borst, J.W., Kwaaitaal, M., Cano-Delgado, A., Yin, Y., Chory, J., and de Vries, S.C. (2004). Heterodimerization and endocytosis of Arabidopsis brassinosteroid receptors BRI1 and AtSERK3 (BAK1). Plant Cell. **16**: 3216-3229.

Saito, C. and Ueda, T. (2009). Chapter 4 functions of RAB and SNARE proteins in plant life. International Review of Cell and Molecular Biology. **274**: 183-233.

Saji, S., Bathula, S., Kubo, A., Tamaoki, M., Kanna, M., Aono, M., Nakajima, N., Nakaji, T., Takeda, T., Asayama, M. and Saji, H. (2008). Disruption of a gene encoding C4-dicarboxylate transporter-like protein increases ozone sensitivity through deregulation of the stomatal response in *Arabidopsis thaliana*. Plant Cell Physiology. **49**: 2-10.

Sanderfoot, A.A. (2007). Increases in the number of SNARE genes parallels the rise of multicellularity among the green plants. Plant Physiology. **144**: 6-17.

Sanderfoot, A.A., Assaad, F.F., and Raikhel, N.V. (2000). The Arabidopsis genome. An abundance of soluble N-ethylmaleimide-sensitive factor adaptor protein receptors. Plant Physiology. **124**: 1558-1569.

Sato, T.K., Rehling, P., Peterson, M.R., and Emr, S.D. (2000). Class C Vps protein complex regulates vacuolar SNARE pairing and is required for vesicle docking/fusion. Molecular Cell. **6**: 661-671.

Sasaki, T., Yamamoto, Y., Ezaki, B., Katsuhara, M., Ahn, S.J., Ryan, P.R., Delhaize, E., and Matsumoto, H. (2004). A wheat gene encoding an aluminum-activated malate transporter. Plant Journal. **37**: 645-653.

Sasaki, T., Mori, I.C., Furuichi, T., Munemasa, S., Toyooka, K., Matsuoka, K., Murata, Y., and Yamamoto, Y. (2010). Closing plant stomata requires a homolog of an aluminum-activated malate transporter. Plant Cell Physiology. **51**: 354-365.

Schmidt, C. and Schroeder, J.I. (1994). Anion selectivity of slow anion channels in the plasma membrane of guard cells (large nitrate permeability). Plant Physiology. **106**: 383-391.

Schramek, N., Wang, H., Römisch-Margl, W., Keil, B., Radykewicz, T., Winzenhörlein, B., Beerhues, L., Bacher, A., Rohdich, F., Gershenzon, J., Liu, B., and Eisenreich, W. (2010). Artemisinin biosynthesis in growing plants of *Artemisia annua*. A $^{13}CO_2$ study. Phytochemistry. **71**: 179-187.

Schultz, J., Doerks, T., Ponting, C.P., Copley, R.R., and Bork, P. (2000).More than 1,000 putative new human signalling proteins revealed by EST data mining. Nature Genet. **25**: 201-204.

Shanks, S.G., Carpp, L.N., Struthers, M.S., McCann, R.K., and Bryant, N.J. (2012). The Sec1/Munc18 protein Vps45 regulates cellular levels of its SNARE binding partners Tlg2 and Snc2 in *Saccharomyces cerevisiae*. PLoS One. **7**: e49628.

Shen, J.S., Tareste, D.C., Paumet, F., Rothman, J.E., and Melia, T.J. (2007). Selective activation of cognate SNAREpins by Sec1/Munc18 proteins. Cell. **128**: 183-195.

Shi, J., Geshi, N., Takahashi, S., Kiyonaka, S., Ichikawa, J., Hu, Y.,

Mori, Y., Ito, Y., and Inoue, R. (2013). Molecular determinants for cardiovascular TRPC6 channel regulation by Ca^{2+}/calmodulin-dependent kinase II. The Journal of Physiology. **591**: 2851-2866.

Shin, R. and Schachtman, D.P. (2004). Hydrogen peroxide mediates plant root cell response to nutrient deprivation. Proceedings of the National Academy of Sciences of United States of America. **101**: 8827-8832.

Shirakawa, M., Ueda, H., Shimada, T., Nishiyama, C., and Hara-Nishimura, I. (2009). Vacuolar SNAREs function in the formation of the leaf vascular network by regulating auxin distribution. Plant Cell Physiology. **50**: 1319-1328.

Shope, J.C., DeWald, D.B. and Mott, K.A. (2003). Changes in surface area of intact guard cells are correlated with membrane internalization. Plant Physiology. **133**: 1-8.

Sieber, J.J., Willig, K.I., Heintzmann, R., Hell, S.W., and Lang, T. (2006). The SNARE motif is essential for the formation of syntaxin clusters in the plasma membrane. Biophysical Journal. **90**: 2843-2851.

Sigel, E. (2010). Microinjection into *Xenopus* Oocytes. eLS.

Singer-Lahat, D., Sheinin, A., Chikvashvili, D., Tsuk, S., Greitzer, D., Friedrich, R., Feinshreiber, L., Ashery, U., Benveniste, M., Levitan, E. S., and Lotan, I. (2007). K^+ channel facilitation of exocytosis by dynamic interaction with syntaxin. Journal of Neuroscience. **27**: 1651-1658.

Singer-Lahat, D., Chikvashvili, D., and Lotan, I. (2008). Direct interaction of endogenous Kv channels with syntaxin enhances exocytosis by neuroendocrine cells. PloS One. **3**: e1381.

Sollner, T., Bennett, M.K., Whiteheart, S.W., Scheller, R.H. and Rothman, J.E. (1993). A protein assembly-disassembly pathway in vitro that may correspond to sequential steps of synaptic vesicle docking, activation, and fusion. Cell. **75**: 409-418.

Sottocornola, B., Visconti, S., Orsi, S., Gazzarrini, S., Giacometti, S., Olivari, C., Camoni, L., Aducci, P., Marra, M., Abenavoli, A., Thiel, G., and Moroni, A. (2006). The potassium channel KAT1 is activated by plant and animal 14-3-3 proteins. Journal of Biological Chemistry. **281**: 35735-35741.

Sokolovski, S., Hills, A., Gay, R., and Blatt, M.R. (2008). Functional interaction of the SNARE protein NtSyp121 in Ca^{2+} channel gating, Ca^{2+}

transients and ABA signalling of stomatal guard cells. Molecular Plant. **1**: 347-358.

Stiekema, W.J., Heidekamp, F., Dirkse, W.G., van Beckum, J., de Haan, P., Bosch, C.T., and Louwerse, J.D. (1988). Molecular cloning and analysis of four potato tuber mRNAs. Plant Molecular Biology. **11**: 255-269.

Stael, S., Wurzinger, B., Mair, A., Mehlmer, N., Vothknecht, U.C., and Teige, M. (2012). Plant organellar calcium signalling: an emerging field. Journal of Experimental Botany. **63**: 1525-1542.

Steber, C.M. and McCourt, P. (2001). A role for brassinosteroids in germination in Arabidopsis. Plant Physiology. **125**: 763-769.

Stegmann, M., Anderson, R.G., Ichimura, K., Pecenkova, T., Reuter, P., Žársky, V., McDowell, J.M., Shirasu, K., and Trujillo, M. (2012). The ubiquitin ligase PUB22 targets a subunit of the exocyst complex required for PAMP-triggered responses in Arabidopsis. Plant Cell. **24**: 4703-4716.

Stoelzle, S., Kagawa, T., Wada, M., Hedrich, R., Dietrich, P. (2003). Blue light activates calciumpermeable channels in Arabidopsis mesophyll cells via the phototropin signaling pathway. Proceedings of the National Academy of Sciences of United States of America. **100**: 1456-1461.

Stone, J.R. and Yang, S. (2006). Hydrogen peroxide: a signaling messenger. Antioxidants & Redox Signaling. **8**: 243-270.

Sudhof, T.C. (1995). The synaptic vesicle cycle: a cascade of protein-protein interactions. Nature. **375**: 645-653.

Sutter, J.U., Homann, U., and Thiel, G. (2000). Ca^{2+}-stimulated exocytosis in maize coleoptile cells. Plant Cell. **12**: 1127-1136.

Sutter, J.U., Campanoni, P., Tyrrell, M., and Blatt, M.R. (2006). Selective mobility and sensitivity to SNAREs is exhibited by the Arabidopsis KAT1 K^+ channel at the plasma membrane. Plant Cell. **18**: 935-954.

Sutter, J.U., Sieben, C., Hartel, A., Eisenach, C., Thiel, G., and Blatt, M.R. (2007). Abscisic acid triggers the endocytosis of the Arabidopsis KAT1 K^+ channel and its recycling to the plasma membrane. Current Biology. **17**: 1396-1402.

Surpin, M., Zheng, H., Morita, M.T., Saito, C., Avila, E., Blakeslee, J.J., Bandyopadhyay, A,, Kovaleva, V., Carter, D., Murphy, A., Tasaka, M.,

and Raikhel, N. (2003). The VTI family of SNARE proteins is necessary for plant viability and mediates different protein transport pathways. Plant Cell. **15**: 2885-2899.

Synek, L., Schlager, N., Eliás, M., Quentin, M., Hauser, M.T., and Zárský, V. (2006). AtEXO70A1, a member of a family of putative exocyst subunits specifically expanded in land plants, is important for polar growth and plant development. Plant Journal. **48:** 54-72.

Szekeres, M., Németh, K., Koncz-Kálmán, Z., Mathur, J., Kauschmann, A., Altmann, T., Rédei, G.P., Nagy, F., Schell, J., and Koncz, C. (1996). Brassinosteroids rescue the deficiency of CYP90, a cytochrome P450, controlling cell elongation and de-etiolation in Arabidopsis. Cell. **19**: 171-182.

Szyroki, A., Ivashikina, N., Dietrich, P., Roelfsema, M.R., Ache, P., Reintanz, B., Deeken, R., Godde, M., Felle, H., Steinmeyer, R., Palme, K., and Hedrich, R. (2001). KAT1 is not essential for stomatal opening. Proceedings of the National Academy of Sciences of United States of America. **98**: 2917-2921.

Takahashi, Y. and Ito, T. (2011). Structure and Function of CDPK: A Sensor Responder of Calcium. In: Luan, S. (eds) Coding and Decoding of Calcium Signals in Plants. Springer-Verlag Berlin Heidelberg. pp 129-146.

Takano, J, Miwa, K., Yuan, L., von Wirén, N., and Fujiwara, T. (2005). Endocytosis and degradation of BOR1, a boron transporter of Arabidopsis thaliana, regulated by boron availability. Proceedings of the National Academy of Sciences of United States of America. **102**: 12276-12281.

Tapken, D. and Hollmann, M. (2008). Arabidopsis thaliana glutamate receptor ion channel function demonstrated by ion pore transplantation. Journal of Molecular Biology. **383**: 36-48.

Taiz, L. and Zeiger, E. (2010). Plant physiology, Fifth edition. Sinauer.

Tochio, H., Tsui, M.M., Banfield, D.K. and Zhang, M. (2001). An autoinhibitory mechanism for nonsyntaxin SNARE proteins revealed by the structure of Ykt6p. Science **293**: 698-702.

TerBush, D.R., Maurice, T., Roth, D., and Novick, P. (1996). The Exocyst is a multiprotein complex required for exocytosis in *Saccharomyces cerevisiae*. EMBO Journal. **15**: 6483-6494.

Toonen, R.F. and Verhage, M. (2003) Vesicle trafficking: pleasure and pain from SM genes. Trends in Cell Biology. **13**: 177-186.

Towler, M.J. and Weathers, P.J. (2007). Evidence of artemisinin production from IPP stemming from both the mevalonate and the nonmevalonate pathways. Plant Cell Reports. **26**: 2129-2136.

Tran, D., Rossi, M., Biligui, B., Kawano, T., Mancuso, S., and Bouteau, F. (2013). Ozone-induced caspase-like activities are dependent on early ion channel regulations and ROS generation in Arabidopsis thaliana cells. Plant Signaling and Behavior. **8**: e25170.

Tsuk, S., Michaelevski, I., Bentley, G.N., Joho, R.H., Chikvashvili, D., and Lotan, I. (2005). Kv2.1 channel activation and inactivation is influenced by physical interactions of both syntaxin 1A and the syntaxin 1A/soluble N-ethylmaleimide-sensitive factor-25 (t-SNARE) complex with the C terminus of the channel. Molecular Pharmacology. **67**: 480-488.

Tsuk, S., Lvov, A., Michaelevski, I., Chikvashvili, D., and Lotan, I. (2008). Formation of the full SNARE complex eliminates interactions of its individual protein components with the Kv2.1 channel. Biochemistry. **47**: 8342-8349.

Tuskan, G.A., Difazio, S., Jansson, S. et al. (2006). The genome of black cottonwood, *Populus trichocarpa* (Torr. & Gray). Science. **313**: 1596-1604.

Tyrrell, M., Campanoni, P., Sutter, J.U., Pratelli, R., Paneque-Corralles, M., and Blatt, M.R. (2007). Selective targeting of plasma membrane and tonoplast traffic by inhibitory (dominant-negative) SNARE fragments. Plant Journal. **51**: 1099-1115.

Uemura, T., Kim, H., Saito, C., Ebine, K., Ueda, T., Schulze-Lefert, P., and Nakano, A. (2012). Qa-SNAREs localized to the trans-Golgi network regulate multiple transport pathways and extracellular disease resistance in plants. Proceedings of the National Academy of Sciences of United States of America. **109**: 1784-1789.

Uemura, T. and Ueda, T. (2014). Plant vacuolar trafficking driven by RAB and SNARE proteins. Current Opinion in Plant Biology. **22**: 116-121.

Vahisalu, T., Kollist, H., Wang, Y.F., Nishimura, N., Chan, W.Y., Valerio, G., Lamminmaki, A., Brosche, M., Moldau, H., Desikan, R., Schroeder, J.I., and Kangasjarvi, J. (2008). SLAC1 is required for plant guard cell S-type anion channel function in stomatal signalling. Nature. **452:** 487-491.

Vahisalu, T., Puzõrjova, I., Brosché, M., Valk, E., Lepiku, M., Moldau,

H., Pechter, P., Wang, Y.S., Lindgren, O., Salojärvi, J., Loog, M., Kangasjärvi, J., and Kollist, H. (2010). Ozone-triggered rapid stomatal response involves the production of reactive oxygen species, and is controlled by SLAC1 and OST1. Plant Journal. **62**: 442-453.

van den Wijngaard, P.W., Sinnige, M.P., Roobeek, I., Reumer, A., Schoonheim, P.J., Mol, J.N., Wang, M., and De Boer, A.H. (2005). Abscisic acid and 14-3-3 proteins control K channel activity in barley embryonic root. Plant journal. **41**: 43-55.

Veit, M., Sollner, T.H. and Rothman, J.E. (1996). Multiple palmitoylation of synaptotagmin and the t-SNARE SNAP-25. FEBS Letter. **385**: 119-123.

Verret, F., Wheeler, G., Taylor, A.R., Farnham, G., and Brownlee, C. (2010). Calcium channels in photosynthetic eukaryotes: implications for evolution of calcium-based signalling. New Phytologist. **187**: 23-43.

Viotti, C. (2014). ER and vacuoles: never been closer. Frontiers in Plant Science. **5**: 20.

Vivona, S., Liu, C.W., Strop, P., Rossi, V., Filippini, F., and Brunger, A.T. (2010). The Longin SNARE VAMP7/TI-VAMP Adopts a Closed Conformation. Journal of Biological Chemistry. **285**: 17965-17973.

Vivona, S., Cipriano, D.J., O'Leary, S., Li, Y.H., Fenn, T.D., and Brunger, A.T. (2013). Disassembly of all SNARE complexes by N-ethylmaleimidesensitive factor (NSF) is initiated by a conserved 1:1 interaction between a-soluble NSF attachment protein (SNAP) and SNARE complex. Journal of Biology Chemistry. **288**: 24984-24991.

Wang, S.Y. and Jiao, H. (2000). Scavenging capacity of berry crops on superoxide radicals, hydrogen peroxide, hydroxyl radicals, and singlet oxygen. Journal of Agricultural and Food Chemistry. **48**: 5677-5684.

Wang, X., Wang, X., Deng, L., Chang, H., Dubcovsky, J., Feng, H., Han, Q., Huang, L., and Kang, Z. (2014). Wheat TaNPSN SNARE homologues are involved in vesicle-mediated resistance to stripe rust (*Puccinia striiformis f. sp. tritici*). Journal of Experimental Botany. **65**: 4807-4820.

Waizenegger, I., Lukowitz, W., Assaad, F., Schwarz, H., Jürgens, G., and Mayer, U. (2000). The Arabidopsis KNOLLE and KEULE genes interact to promote vesicle fusion during cytokinesis. Current Biology. **10**: 1371-1374.

Walter, M., Chaban, C., Schutze, K., Batistic, O., Weckermann, K., Nake, C., Blazevic, D., Grefen, C., Schumacher, K., Oecking, C., Harter, K., & Kudla, J. (2004). Visualization of protein interactions in living plant cells using bimolecular fluorescence complementation. Plant Journal. **40**: 428-438.

Wagner, S., Bader, M.L., Drew, D., and de Gier, J.W. (2006). Rationalizing membrane protein overexpression. Trends in Biotechnology. **24**: 364-371.

Walter, M., Chaban, C., Schutze, K., Batistic, O., Weckermann, K., Nake, C., Blazevic, D., Grefen, C., Schumacher, K., Oecking, C., Harter, K., and Kudla, J. (2004). Visualization of protein interactions in living plant cells using bimolecular fluorescence complementation. Plant Journal. **40**: 428-438.

Wellhausen, A. and Lehming, N. (1999). Analysis of the in vivo interaction between a basic repressor and an acidic activator. FEBS Letter. **453**: 299-304.

Wheeler, G.L. and Brownlee, C. (2008). Ca^{2+} signalling in plants and green algae--changing channels. Trends in Plant Science. **13**: 506-514.
Whiteheart, S.W., Schraw, T., and Matveeva, E.A. (2001). N-ethylmaleimide sensitive factor (NSF) structure and function. International Review of Cytology. **207**: 71-112.

Wick, P., Gansel, X., Oulevey, C., Page, V., Studer, I., Durst, M., and Sticher, L. (2003). The expression of the t-SNARE AtSNAP33 is induced by pathogens and mechanical stimulation. Plant Physiology. **132:** 343-351.

Woollard, A.A. and Moore, I. (2008). The functions of Rab GTPases in plant membrane traffic. Current Opinion in Plant Biology. **11**: 610-619.

Wu, W., Wang, Y., Lee, S.C., Lan, W., and Luan, S. (2010). Regulation of Ion Channels by the Calcium Signaling Network in Plant Cells. In: Demidchik, V. and Maathuis, F. (eds) Ion Channels and Plant Stress Responses. Springer-Verlag Berlin Heidelberg. *pp* 111-135.

Xicluna, J., Lacombe, B., Dreyer, I., Alcon, C., Jeanguenin, L., Sentenac, H., Thibaud, J.B., and Chérel, I. (2007). Increased functional diversity of plant K^+ channels by preferential heteromerization of the shaker-like subunits AKT2 and KAT2. Journal of Biology Chemistry. **282**: 486-494.

Xu, J., Li, H.D., Chen, L.Q., Wang, Y., Liu, L.L., He, L., and Wu, W.H.

(2006). A protein kinase, interacting with two calcineurin B-like proteins, regulates K^+ transporter AKT1 in Arabidopsis. Cell. **125**: 1347-1360.

Xu, Y., Su, L., and Rizo, J. (2010). Binding of Munc18-1 to synaptobrevin and to the SNARE four-helix bundle. Biochemistry. **49**: 1568-1576.

Yamaguchi, T., Dulubova, I., Min, S.W., Chen, X., Rizo, J., and Südhof, T.C. (2002). Sly1 binds to Golgi and ER syntaxins via a conserved N-terminal peptide motif. Development Cell. **2**: 295-305.

Yang, L., Dun, A.R., Martin, K.J., Qiu, Z., Dunn, A., Lord, G.J., Lu, W., Duncan, R.R., and Rickman, C. (2012). Secretory vesicles are preferentially targeted to areas of low molecular SNARE density. PLoS One. **7**: e49514.

Yano, D., Sato, M., Saito, C., Sato, M.H., Morita, M.T., and Tasaka, M. (2003). A SNARE complex containing SGR3/AtVAM3 and ZIG/VTI11 in gravity-sensing cells is important for Arabidopsis shoot gravitropism. Proceedings of the National Academy of Sciences of United States of America. **100**: 8589-8594.

Yi, C., Park, S., Yun, H.S., and Kwon C. (2012). Vesicle-associated membrane proteins 721 and 722 are required for unimpeded growth of Arabidopsis under ABA application. Journal of Plant Physiology. **170**: 529-533.

Yun, H.S., Kwaaitaal, M., Kato, N., Yi, C., Park, S., Sato, M.H., Schulze-Lefert, P., and Kwon, C. (2013). Requirement of vesicle-associated membrane protein 721 and 722 for sustained growth during immune responses in Arabidopsis. Molecules and Cells. **35**: 481-488.

Zárský, V., Kulich, I., Fendrych, M., and Pečenková, T. (2013). Exocyst complexes multiple functions in plant cells secretory pathways. Current Opinion in Plant Biology. **16**: 726-733.

Zhang, H., Wang, L., Deroles, S., Bennett, R., and Davies, K. (2006a). New insight into the structures and formation of anthocyanic vacuolar inclusions in flower petals. BMC Plant Biology. **6**: 29.

Zhang, Y. and Shin, Y.K. (2006b). Transmembrane organization of yeast syntaxin-analogue Sso1p. Biochemistry. **45**: 4173-4181.

Zhang, Z., Feechan, A., Pedersen, C., Newman, M.A., Qiu, J.L., Olesen, K.L., and Thordal-Christensen, H. (2007). A SNARE-protein

has opposing functions in penetration resistance and defence signalling pathways. Plant Journal. **49**: 302-312.

Zhang, Z., Lenk, A., Andersson, M.X., Gjetting, T., Pedersen, C., Nielsen, M.E., Newman, M.A., Hou, B.H., Somerville, S.C., and Thordal-Christensen, H. (2008). A lesion-mimic syntaxin double mutant in Arabidopsis reveals novel complexity of pathogen defense signaling. Molecular Plant. **1**: 510-527.

Zhang, Y., Liu, C.M., Emons, A.M., and Ketelaar, T. (2010). The plant exocyst. Journal of Integrative Plant Biology. **52**: 138-146.

Zhang, L., Zhang, H., Liu, P., Hao, H., Jin, J.B., and Lin, J. (2011). Arabidopsis R-SNARE proteins VAMP721 and VAMP722 are required for cell plate formation. PLoS one. **6**: e26129.

Zhang, B., Zheng, L.P., Li, W.Y., and Wang,J.W. (2013). Stimulation of Artemisinin Production in Artemisia annua Hairy Roots by Ag-SiO_2 Core-shell Nanoparticles. Current Nanoscience. **9**: 363-370.

Zhao, M., Wu, S., Zhou, Q., Vivona, S., Cipriano, D.J., Cheng, Y., and Brunger, A.T. (2015). Mechanistic insights into the recycling machine of the SNARE complex. Nature. doi:10.1038/nature14148.

Zhu, J., Gong, Z., Zhang, C., Song, C.P., Damsz, B., Inan, G., Koiwa, H., Zhu, J.K., Hasegawa, P.M., and Bressan, R.A. (2002). OSM1/SYP61: a syntaxin protein in Arabidopsis controls abscisic acid-mediated and non-abscisic acid-mediated responses to abiotic stress. Plant cell. **14**: 3009-3028.

Zouhar, J., Rojo, E., and Bassham, D.C. (2009). AtVPS45 is a positive regulator of the SYP41/SYP61/VTI12 SNARE complex involved in trafficking of vacuolar cargo. Plant Physiology. **149**: 1668-1678.

Zwickl, P., Seemüller, E., Kapelari, B., Baumeister, W. (2001). The proteasome: a supramolecular assembly designed for controlled proteolysis. Advances in Protein Chemistry. **59**: 182-222.

Appendix II.

Zhang, B., Karnik, R., Wang, Y., Wallmeroth, N., Blatt, M.R. and Grefen, C. (2015). The R-SNARE VAMP721 Interacts with KAT1 and KC1 K^+ Channels to Moderate K^+ Current at the Plasma Membrane. (Submitted to Plant Cell, under review)

To this paper I contributed the mbSUS data (Chapter 3: Figure 3-1 to Figure 3-10), the rBiFC data (Chapter 4: Figure 4-2 to Figure 4-6), the electrophysiological measurements after heterologous expression in *Xenopus* oocytes (Chapter 5: Figure 5-1 to Figure 5-11, Table 5-1 to Table 5-4), and the transient expression and localisation of VAMPs in Arabidopsis root cells (Chapter 4: Figure 4-1).

Karnik, R., Zhang, B., Waghmare, S., Aderhold, C., Grefen, C., and Blatt, M.R. (2015). Binding of SEC11 indicates its role in SNARE recycling after vesicle fusion and identifies two pathways for vesicular traffic to the plasma membrane. Plant Cell. doi: http://dx.doi.org/10.1105/tpc.114.134429

Wang, Y., Chen, Z.H., Zhang, B., Hills, A., and Blatt, M.R. (2013). PYR/PYL/RCAR abscisic acid receptors regulate K^+ and Cl^- channels through reactive oxygen species-mediated activation of Ca^{2+} channels at the plasma membrane of intact Arabidopsis guard cells. Plant Physiology. **163**: 566-577.